Enhancing sustainability in cross-linkable block copolymer formulations

ANISHA PATEL

Doctor of Philosophy

ASTON UNIVERSITY

December 2024

Abstract: Enhancing sustainability in cross-linkable block copolymer formulations

Anisha Patel

Thesis presented for the degree of Doctor of Philosophy

2024

This research showcases the use of ionic liquid as a more sustainable and effective solvent for the synthesis of poly(2-hydroxyethyl methacrylate)-*b*-poly(*n*-butyl methacrylate) (PHEMA-*b*-PBuMA) diblock copolymers, developing the first emulsion polymerisation-induced self-assembly (PISA) formulation in ionic liquid in the process. Also, the viability of suitable candidates to introduce ultraviolet (UV) cross-linking functionality to poly(2-hydroxyethyl methacrylate) (PHEMA) was investigated, showcasing potential for use in applications such as inkjet printing.

1-Ethyl-3-methyl-imidazolium ethylsulfate, [EMIM][$EtOSO_3$], *N*,*N*-dimethylformamide (DMF) and an ethanol/water mixture were used as reaction solvents for the chain extension of PHEMA macromolecular chain transfer agents (macro-CTAs) with *n*-butyl methacrylate (BuMA) via reversible addition-fragmentation chain transfer (RAFT) polymerisation to yield PHEMA-*b*-PBuMA diblock copolymers. Reactions conducted in [EMIM][$EtOSO_3$] yielded high monomer conversions (> 86%) and diblock copolymers with molar mass dispersity values as low as 1.15 in shorter reaction times compared to other solvent systems. Subsequently, a series of diblock copolymers with PBuMA DPs varying from 50 to 1000 were synthesised in [EMIM][$EtOSO_3$] via RAFT-mediated PISA under emulsion conditions. This yielded highly transparent dispersions, even at nanoparticle diameters >100 nm, due to the closely matched refractive index values of the [EMIM][$EtOSO_3$] solvent and PBuMA nanoparticle core. The presence of spherical nanoparticles was confirmed by small-angle X-ray scattering (SAXS) and transmission electron microscopy (TEM).

4-Methylumbelliferone (4MU), cinnamic acid (CA), 9-anthracenecarboxylic acid (9ACA) and 3-(2-furyl)acrylic acid (FAA) were explored as UV cross-linkable monomer precursors. ^{1}H nuclear magnetic resonance (NMR) and Fourier-transform infrared (FTIR) spectroscopy were used to confirm dimerization success, where CA was found to be the only precursor to not dimerize successfully. Subsequently, 4MU was converted into polymerisable 7-acryloyloxy-4-methylcoumarin (AOMC), whereas 9ACA and FAA were esterified with PHEMA, forming poly(9-anthrancenylethyl methacrylate) (P9AEMA) and poly(ethylfurfurylideneacetate methacrylate) (PEFMA), respectively. Overall, FAA was deemed the most suitable precursor due to easier purification and successful UV cross-linking before and after functionalisation.

Key words: ionic liquids; reversible addition-fragmentation chain transfer; polymerisation-induced self-assembly; block copolymers; emulsion; isorefractive; nanoparticles; cross-linking

Acknowledgements

I would like to start by expressing my deepest gratitude for the endless encouragement and constant support from my family, friends, and colleagues throughout the course of this PhD.

I cannot begin to describe the rollercoaster of a journey I have encountered throughout this PhD, but I was lucky enough to have two supervisors who were always there for me. Firstly, I would like to thank Dr. Matthew Derry for having the utmost belief in my potential, throughout all of my moments of doubt and lack of self-confidence. Secondly, I would like to thank Professor Paul Topham for providing me with encouragement and motivation in times of need throughout this process. Thank you for the opportunity to travel to different countries, as well as visiting and conducting experiments at UK's national synchrotron (Diamond Light Source), which was hands down my favourite trip, the countless laughs and light-hearted moments along the way really kept me going. I feel that it has been an absolute privilege work with you both, and I will always cherish your belief, confidence and motivation that not only inspired me to grow as a researcher, but also as a person, I truly cannot thank you both enough.

My fellow PhD colleagues have made this journey unforgettable. Ben, I will never forget all of the JetPunk quizzes during times of procrastination. Snook, I am grateful for all of your kindness and support, especially towards the end of my journey. Amit, thank you for all of the early morning conversations and thoughtful advice, I am so appreciative for your help and support throughout your time at Aston. Alice, thank you for being such a great climbing buddy, I am so grateful for your encouragement and motivation, and I hope we will continue to climb together in the future. Nawal, thank you for helping keep my sanity, listening to all of my problems, and introducing me to crochet, I hope that we will continue to be craft buddies. To Bridget and Georgia, I could not have asked for two better people to have started my PhD journey with. Bridget, you have never let me down, early mornings to late evenings you've been there constantly. Georgia, you never failed to always brighten my day, I will never forget our giggles at the absolute silliest things. I am so lucky to have met you both, we have shared so many memories together I know we will continue to do so in the future, I love you both so much. Lauren, from the moment you joined we instantly formed a friendship, we have seen each other through such big ups and downs, and I am thankful for your presence in my life. And last but definitely not least, Joseph. I will never forget all of the times you sat and listened in frustration at my somewhat questionable decisions and dilemmas. You were there for me at the very start, and even after you left Aston, continued to be there. Thank you for picking up the pieces and keeping me calm after all of my tears and tantrums. Your patience, love and encouragement kept me motivated, and your presence reminded me of what truly matters.

I would also like to thank my family, especially mum and dad. Thank you for supporting my decision to pursue a PhD and being there for me through the most difficult times. I appreciate all the late-night meals and listening to my frustrations. Thank you to the rest of my family, all who have which provided me with the endless support and comfort when needed.

Table of contents

Abbreviations

AIBN	2, 2'-Azoisobutyronitrile
ATRP	Atom transfer radical polymerisation
BuMA	*n*-Butyl methacrylate
CA	Cinnamic acid
CMC	Critical micelle concentration
CPTP	4-Cyano-4-(phenylcarbonothioylthio)pentanoic acid
CTA	Chain transfer agent
D	Diffusion coefficient
DCC	*N,N'*-Dicyclohexylcarbodiimide
D_h	Hydrodynamic diameter
DLS	Dynamic light scattering
$Đ_M$	Molar mass dispersity
DMAP	4-Dimethylaminopyridine
DMF	*N,N*-Dimethylformamide
DP	Degree of polymerisation
DTRP	Degenerative-transfer radical polymerisation
EtOH	Ethanol
FAA	3-(2-Furyl)acrylic acid
FRP	Free radical polymerisation
GPC	Gel permeation chromatography
HEMA	2-Hydroxyethyl methacrylate
IL	Ionic liquid
LAM	Less activated monomer

LCA	Life cycle assessment
Macro-CTA	Macromolecular chain transfer agent
MAM	More activated monomer
M_n	Number-average molar mass
M_r	Molecular mass
M_w	Weight-average molar mass
NMP	Nitroxide-mediated polymerisation
NMR	Nuclear magnetic resonance
PILs	Poly(ionic liquid)s
PISA	Polymerisation-induced self-assembly
PLF	Polymers in liquid formulations
PMMA	Poly(methyl methacrylate)
q	Scattering vector
q*	Primary Bragg peak
RAFT	Reversible addition-fragmentation chain transfer
RDRP	Reversible-deactivation radical polymerisation
RI	Refractive index
SAXS	Small-angle X-ray scattering
SEC	Size exclusion chromatography
TEM	Transmission electron microscopy
V_h	Hydrodynamic volume
χ	Flory-Huggins interaction parameter
[EMIM][EtOSO$_3$]	1-Ethyl-3-methyl-imidazolium ethylsulfate
4MU	4-Methylumbelliferone

9ACA	9-Anthracenecarboxylic acid

List of figures

List of tables

List of schemes

1. Introduction

The excessive use of synthetic polymers has raised concerns due to their potential negative environmental impact. Typically, traditional block copolymer formulations use petroleum-derived monomers which are easier to access, however result in resource depletion as well as an accumulation of non-biodegradable waste. Due to this, there is an increasing interest in enhancing the sustainability of such block copolymer formulations, which can be achieved by changing conditions and/or the reagents involved. This research specifically explores the synthesis of block copolymers using an ionic liquid as a more sustainable solvent system, and the potential incorporation of monomers which can be derived from renewable resources, such as coumarins and furfurals, with the added benefit of adding cross-linkability due to their functionality. Cross-linkable block copolymers are useful due to their enhanced durability and properties, making them effective for use in a broader range of applications[1, 2]. This research has potential for applications such as polymeric additives for inkjet printing, which have previously used thermal treatment to induce cross-linking[3], whereas this project focuses on ultraviolet (UV) light triggerable compounds as an attempt to further improve the sustainability by reducing energy requirements.

1.1 Polymers

Polymers play a fundamental role in our everyday lives, from use in coatings[4] and cosmetics[5], to packaging[6] and medicine[7], amongst many others[8]. A polymer can be defined as a macromolecule formed from the bonding of smaller repeating units, often referred to as monomers. When a single monomer is used as the repeating unit, a homopolymer is formed, whereas when two different monomers are polymerised, a copolymer is formed. The number of repeat units per polymer chain, more formally known as the degree of polymerisation (DP), is one of the ways in which the size of a polymer can be defined. The mean DP can be calculated by dividing the number-average molecular mass (M_n) by the relative molar mass (M_r) of the monomer repeating unit (Equation 1.1).

$$DP = \frac{M_{n(polymer)}}{M_{r(monomer)}} \qquad \textbf{1.1}$$

Polymers cannot be allocated one specific molar mass value, instead they have a molecular mass distribution (Figure 1.1) with an associated number-average molar mass (M_n) and a weight-average

molar mass (M_w). The M_n can be defined as an average which reflects the mean molecular weight of polymer chains, that is based on the number of polymer molecules in the sample (Equation 1.2)[9].

$$M_n = \frac{\sum N_i M_i}{\sum N_i} \qquad \textbf{1.2}$$

N_i is term representing the number of polymer chains containing 'i' repeat units, and M_i is a term representing the molar mass of polymer chains with 'i' repeat units[9]. M_w can be defined as an average which also reflects the mean molecular weight of polymer chains, however takes the weights of the chains as well as the number of chains into consideration. (Equation 1.3).

$$M_w = \frac{\sum N_i {M_i}^2}{\sum N_i M_i} \qquad \textbf{1.3}$$

These two values determine the breadth of the distribution, more formally known as the dispersity ($Đ_M$) of the polymer (Equation 1.4)[9].

$$Đ_M = \frac{M_w}{M_n} \qquad \textbf{1.4}$$

A dispersity value of 1.00 would indicate a perfectly monodisperse polymer, where M_n and M_w are of equal value, i.e. when all polymer molecules in a sample have the same molar mass. Proteins are examples of such polymers[10]. A dispersity value below 1.5 is considered to be low and therefore has a 'narrow' distribution, compared to that of a polymer with a dispersity value greater than 1.5, which is considered to be higher, and would hence have a much broader distribution[11].

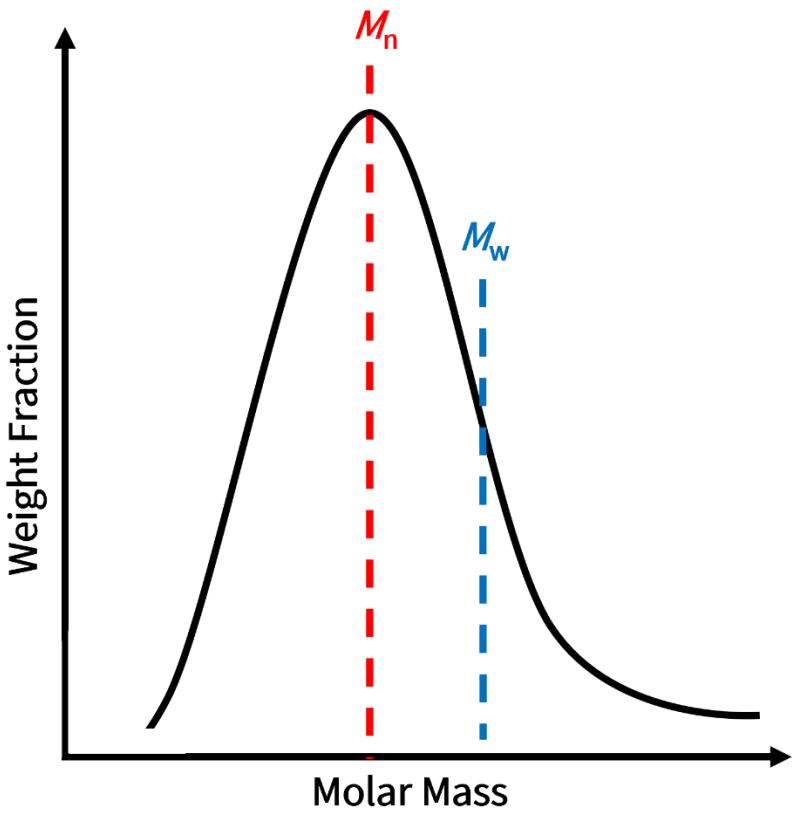

Figure 1.1. *Representative molar mass distribution displaying the M_n and M_w for a polymer.*

1.2 Polymer molecular characterisation

1.2.1 Gel permeation chromatography (GPC)

There are various analytical techniques which can be used to characterise polymers, with one of the most frequently employed methods of analysis being gel permeation chromatography (GPC), also known as size exclusion chromatography (SEC)[12].

This analytical technique generates a molecular weight distribution by separating the polymer chains according to size, specifically using their hydrodynamic volume (V_h) as shown in Figure 1.2. Typically, this is achieved by dissolving the polymer in a solvent in which the polymer adopts an overall spherical coil-like confirmation. The size of the 'coil' is primarily dependant on the molecular weight of the polymer, with lower molecular weight polymers being smaller than larger molecular weight polymers. The polymer solution is then injected into the system and pumped through at a constant flow rate. The stationary phase, a column typically composed of tightly packed, porous cross-linked polystyrene beads, causes the polymer sample to be separated based on 'coil' size. Larger coils cannot travel through many of the pores within the beads, therefore bypass them and

are eluted at a much faster rate than the smaller coils, which are able to travel through much smaller pores. A detector, the most common being a refractive index (RI) detector, then detects the elution of the polymer at specific elution times based on the difference in RI values between the solvent and the polymer. The elution volume is then converted into retention time, which can be defined as the time taken for a fraction to travel and elute from the column[9, 13].

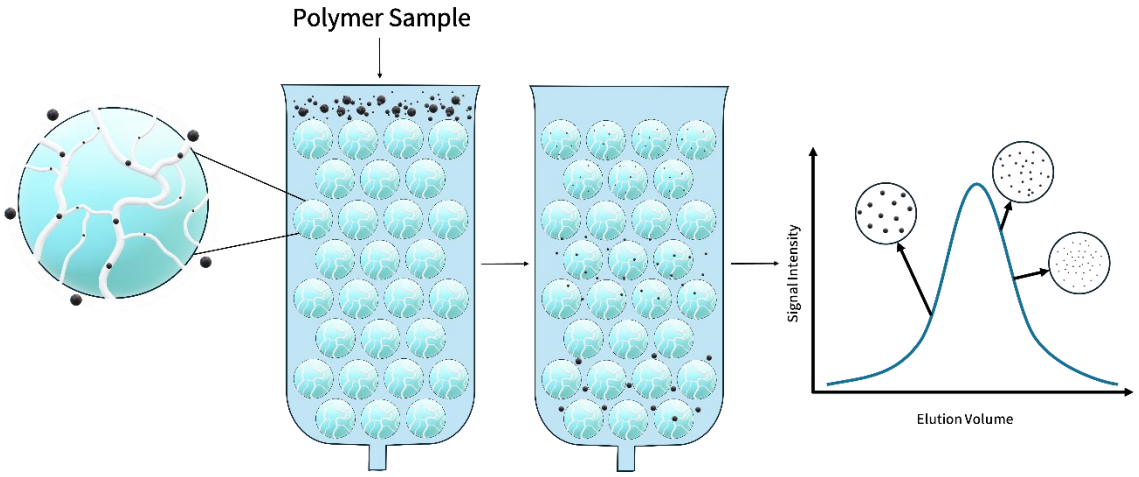

Figure 1.2. *A diagram depicting the separation of a polymer sample through a GPC column and the resulting chromatogram.*

This data is compared to a calibration curve generated from a series of polymers with narrow molecular weight distributions and known molecular weight values. From relating the retention time to the molar mass of the calibrants, the molecular weight distribution of the unknown sample can be quantified. As mentioned briefly in section 1.1, there are a range of distribution types possible, from narrow (low $Đ_M$), to broad (high $Đ_M$). Bimodal distributions can also be observed when there are two populations within a sample with sufficiently different molecular weights present[9, 13].

This analytical technique offers many advantages, including its ability to generate a molecular weight distribution for a polymer sample, relatively simple sample preparation and readily available equipment. However, it should be noted that the reliability of the molecular weight averages provided is dependent on the calibration standard used – species with more similar chemical structures to the calibration standard produce more reliable results, as there would be more similarities between their behaviours and interactions with the GPC solvent.

1.2.2 Nuclear magnetic resonance (NMR)

Nuclear magnetic resonance (NMR) spectroscopy is a widely used analytical technique that utilises the magnetic properties of the nucleus of an atom. From this, the molecular structure and content of a molecule can be determined[14].

NMR is also commonly used for polymer analysis[15]. The monomer conversion and DP (and therefore molecular weight) of polymer synthesis reactions can be calculated based on NMR spectra. Monomer conversion is calculated by first assigning all peaks in the monomer spectrum to their corresponding protons. From this, the corresponding polymer peaks in the polymer spectrum can be assigned. Often, and in the most straightforward cases, the monomer and its corresponding polymer peaks are chosen to calculate conversion (depending on factors such as any overlapping peaks). The monomer peak is integrated and calibrated to its set value (i.e. a peak representing one proton would be set to 1), the polymer peak is then integrated and the value obtained is noted. These values can then be substituted into Equation 1.5, from which the conversion can be obtained. It should be noted that this method is only valid when the number of protons represented by the monomer and polymer peaks is the same.

$$\text{conversion (\%)} = \frac{\text{integration of polymer}}{\text{integration of polymer + integration of monomer}} \times 100 \qquad \textit{1.5}$$

There are some cases where a peak for a distinctive proton environment on an end-group of the polymer (such as a chain-transfer agent) can be used and calibrated to a set value (the number of protons in the proton environment). From this, the polymer peaks can be integrated and the DP of the polymer can be determined, also enabling the molecular weight to be calculated. Internal standards can also be used to help calculate conversions (i.e. the reduction in vinylic peaks can be monitored by integrating the peak(s) compared to the internal standard peak calibrated to a set value of 1). Overall NMR is a reliable, readily available instrument which can be used to characterise polymers; however it should be noted that complications can arise with more complex solutions which can make calculating conversion, DP and molecular weight more difficult (e.g. due to no visible distinct peaks caused from the overlap with other peaks from different components within the sample).

1.3 Polymerisation methods

Polymer synthesis typically proceeds via one of two general mechanisms: step and chain polymerisation.

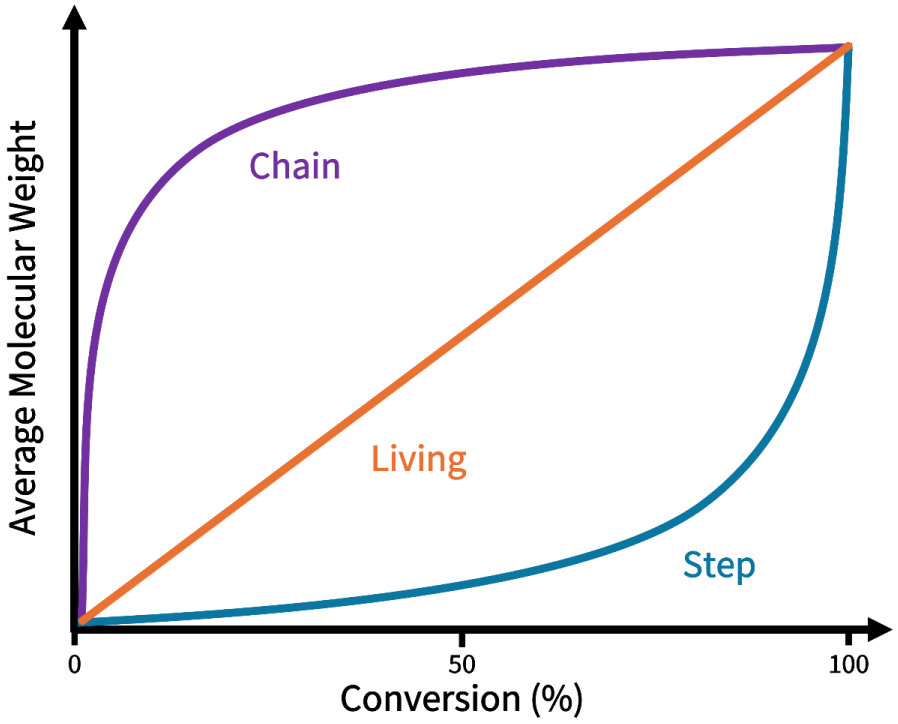

Figure 1.3. *A graph depicting the difference in polymer average molecular weight growth against conversion for chain (purple), living (orange) and step (blue) polymerisation methods.*

Step polymerisation is the process by which polymers are formed through the joining of bi-functional/multifunctional monomers which combine in multiple steps; firstly forming oligomers (such as dimers and trimers) which can subsequently join to form longer chain polymers[13]. As seen in Figure 1.3, there is slow growth of the polymer chains, therefore high molecular weight polymers are only obtained once higher conversions are reached. This method can be further split into two sub-categories: polycondensation and polyaddition. Polycondensation reactions involve the elimination of a small molecule, such as water. An example of this is an esterification reaction by which a diacid and a diol react to form a polyester chain, eliminating a water molecule in the process (Figure 1.4a). Polyesters are abundant in our everyday lives, most frequently being used in clothing, home furnishings and food/drink packaging, however they are also used in biomedical applications, such as in tissue scaffolds and bone screws[16]. Polyaddition reactions are similar, however have no expulsion of a small molecule, polyurethanes and polyamides are an example of this (Figure 1.4b

and c). Polyamides are widely used in food packaging and clothing, with two notable examples including Kevlar[17], used in body armour and protective textiles, and nylon used in fabrics and in the medical field, with use in dental implants and skin dressings[18]. In addition to this, polyurethanes are also a group of frequently used polymers, with applications in coatings, adhesives, textiles and medical science, just to name a few[19].

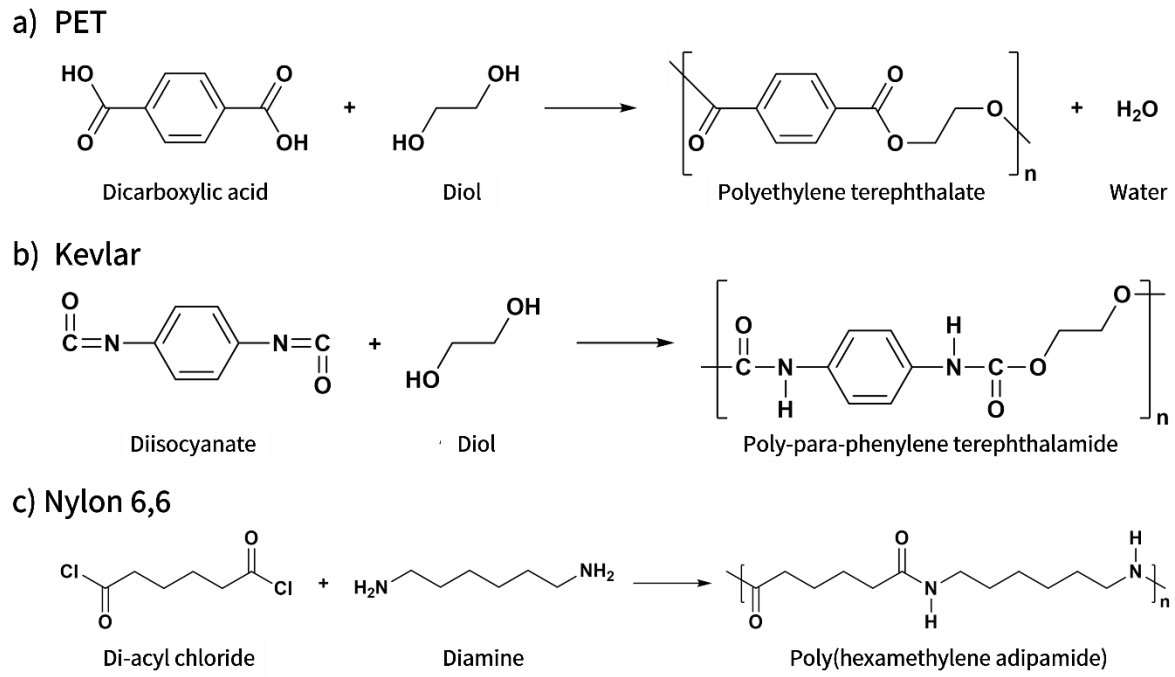

Figure 1.4. *Example polymer syntheses for a) PET, a polyester (via a polycondensation reaction), b) Kevlar, a polyurethane (via a polyaddition reaction) and c) nylon 6,6, a poly(amide) (via a polyaddition reaction).*

Chain polymerisation is the main focus of this research, and therefore will be discussed in further detail. A chain-growth polymerisation typically requires an unsaturated monomer and initiator to initiate the polymerisation process. Typically, the three principal steps involved are initiation, propagation, and termination. As seen in Figure 1.3, high molecular weight polymers can be obtained at lower conversions compared to step polymerisation, depending on the conditions of the syntheses.

Living polymerisations (a form of chain polymerisation) involve polymer chains growing simultaneously in the absence of chain transfer and termination, resulting in a linear increase of molecular weight with conversion (Figure 1.3), and therefore allowing for more control over the molecular weight and dispersity[20].

1.3.1 Free radical polymerisation (FRP)

Free radical polymerisation (FRP) is a popular chain polymerisation technique that has been used since 1910[21] to synthesise commercial polymers such as poly(methyl methacrylate) (PMMA) and poly(acrylamide) (PAM)[22].

The first stage involves the decomposition of an initiator to form an active radical species, which can be achieved via various methods such as thermal or photochemical decomposition. Figure 1.5 shows 2,2'-azobis(isobutyronitrile) (AIBN), a commonly used thermal initiator which can decompose into two active radical species.

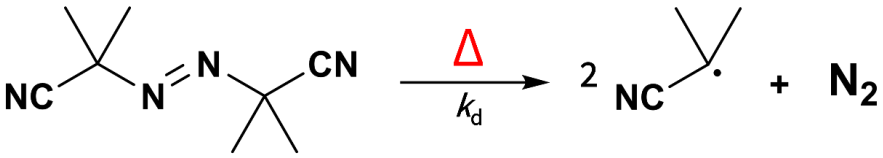

Figure 1.5. *Thermal decomposition of AIBN yielding two active radical species and expelling nitrogen in the process.*

The rate of decomposition can be denoted by R_d, which can be defined as:

$$R_d = k_d[In] \qquad \textbf{1.6}$$

Where k_d is the rate constant for initiator decomposition and [In] is the concentration of initiator. The addition of the first monomer unit (Figure 1.6) produces the first initiating polymer chain.

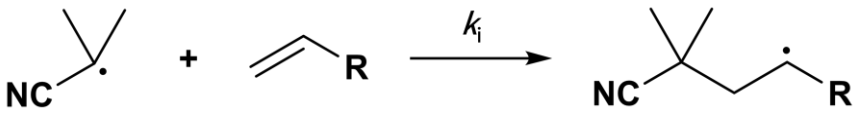

Figure 1.6. *The addition of the first monomer unit onto the active radical species (AIBN-derived) to create a new radical species which can undergo further reactions with added monomer.*

It should be noted that not all of the radicals generated will react with the added monomer. The actual efficiency of the initiator (f) can be calculated using Equation 1.7:

$$f = \frac{k_i}{k_i + k_c + k_{c'} \ldots} \qquad \textit{1.7}$$

Where k_i is the rate constant for the desired initiation and k_c and $k_{c'}$ are the rate constants for combination, examples of these possible reactions can be seen in Figure 1.7.

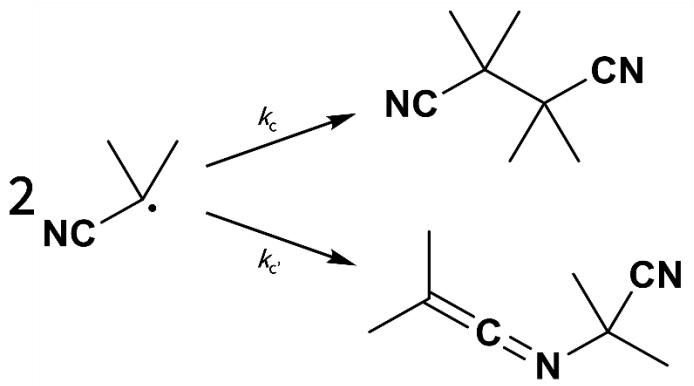

Figure 1.7. *Possible side reactions which may occur during initiation, specifically the combination of AIBN-derived radical species.*

Ideal FRP reaction conditions are selected so that k_i is much greater than k_d, thus the rate-determining step is the initial step of the decomposition of the initiator molecule. From this, the overall rate of initiation (R_i) can be defined as:

$$R_i = 2 k_d f [In] \qquad \textit{1.8}$$

The next step is propagation, where there is additional growth of the polymer chain as more monomer is sequentially added (Figure 1.8).

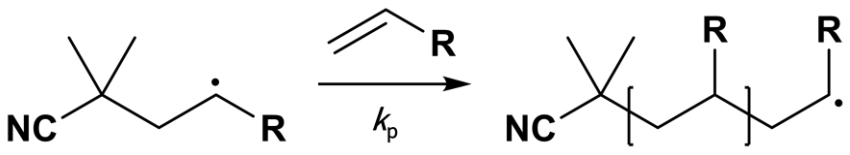

Figure 1.8. *The addition of additional monomer to create a growing polymer chain with an active radical end, which can continue propagation or undergo termination.*

The rate of propagation (R_p) can be defined by:

$$R_p = k_p[M][M^{\bullet}] \qquad \textit{1.9}$$

Where k_p is the rate constant for propagation, [M] is the concentration of monomer and [M•] is the concentration of growing polymer chains. R_p is proportional to $[M][In]^{1/2}$, meaning that if the concentration of monomer is doubled, the rate will be doubled. However, if the amount of initiator is doubled, there will be no increase in the rate.

The final stage of termination occurs when the growing polymer loses its active centre, therefore cannot continue to undergo further polymerisation. This can occur via two different pathways, namely, combination or disproportionation (Figure 1.9).

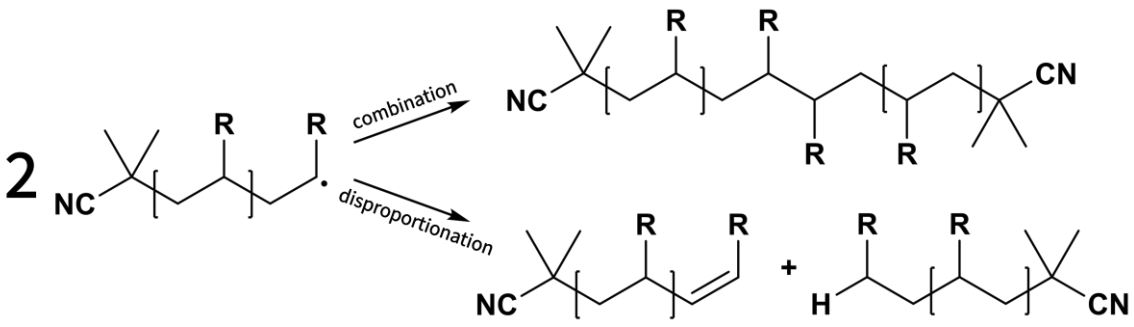

Figure 1.9. *Possible routes for termination, specifically via combination (top) and disproportionation (bottom).*

The rate of termination, R_t can be defined as:

$$R_t = 2k_t[M^{\bullet}]^2 \qquad \textit{1.10}$$

Where the rate constant for termination is denoted as k_t. Termination by combination involves the direct coupling of the radical ends of two growing polymer chains, which prevents any further growth. Disproportionation occurs from the transfer of an atom, such as hydrogen, from one growing polymer chain to another, again producing a dead polymer chain[9, 13].

1.3.2 Reversible-deactivation radical polymerisation (RDRP)

FRP is a versatile technique which can be used to polymerise a wide range of monomers, producing high conversions and molar masses compared to step polymerisation methods. However, higher dispersity values are often obtained due to its uncontrolled nature. Reversible-deactivation radical polymerisation (RDRP) is a living polymerisation technique which involves the incorporation of an added species, resulting in a more controlled process, and therefore enables the production of polymers with more defined structures[13] (Figure 1.10).

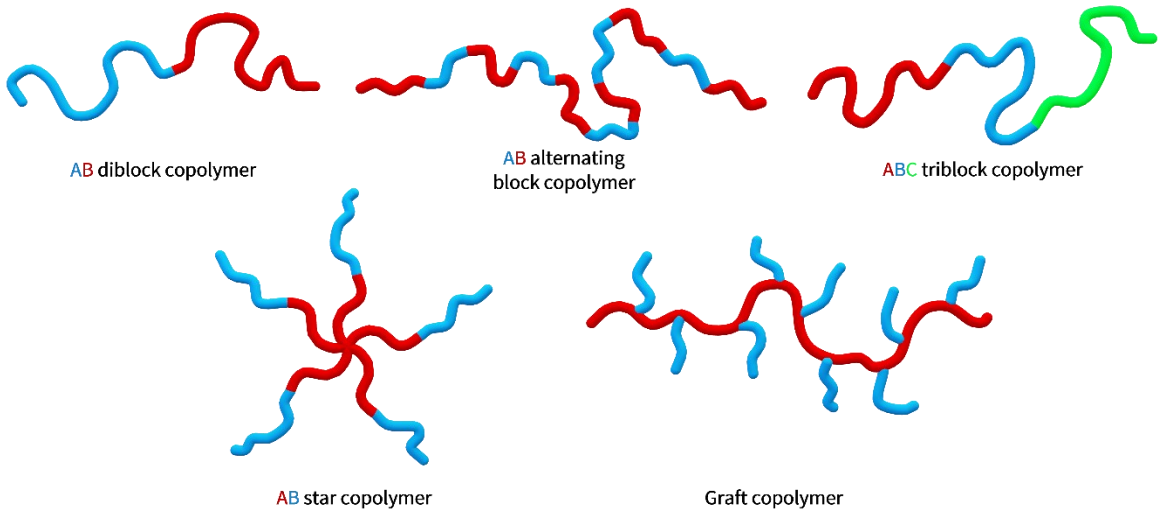

Figure 1.10. *Different architectures which can be obtained from reversible-deactivation radical polymerisation (RDRP) techniques.*

In RDRP, since the rate of termination cannot fully be eliminated, it is decreased by the rate of propagation being directly proportional to [M•]; a lower [M•] results in a lower chance of termination occurring.

This is achieved by controlling the reaction by using an added species which induces the activation and deactivation of the active radicals on the growing polymer chains. The dynamic equilibrium between the active and dormant species therefore decreases the possibility of termination occurring, and since each chain has an equal chance of propagating, produces polymers with lower molecular weight distributions (Figure 1.11)[23, 24].

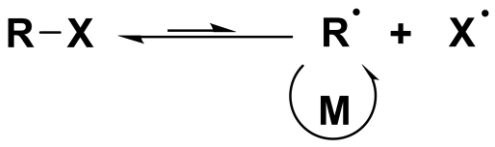

Figure 1.11. *The equilibrium between active and dormant states which occurs in RDRP polymerisation.*

There are many examples of RDRP in the literature, including involvement in the synthesis of degradable and recyclable polymers[25] and the synthesis of sequence-controlled polymers[26]. Although RDRP can provide more control, produce polymers with narrower molecular weight distributions and complex architectures, it does require more specific reaction conditions and sometimes longer reaction times.

Reversible addition-fragmentation chain transfer (RAFT) polymerisation is an example of RDRP which will be discussed in further detail due to its utilisation in this thesis. However, it should be noted that there are other examples of RDRP including nitroxide-mediated polymerisation (NMP), which uses a nitroxide radical as the controlling species[27], and atom transfer radical polymerisation (ATRP), which uses a halide initiator and a transition metal complex [28].

1.3.2.1 Reversible addition-fragmentation chain transfer (RAFT) polymerisation

In 1998, the Commonwealth Scientific and Industrial Research Organisation (CSIRO) discovered a revolutionary living-controlled polymerisation technique, known now as RAFT polymerisation. This versatile method offers advantages such as the ability to use a wide range of monomers and reaction conditions, producing polymers with narrow molecular weight distributions and controlled molecular weights[29, 30].

RAFT can be defined as a degenerative transfer radical polymerisation (DTRP) technique that uses a chain transfer agent (CTA) to control the polymerisation process. A CTA is typically chosen based on the monomer being polymerised. Monomers for RAFT polymerisations can be classified as either more activated monomers (MAMs) or less activated monomers (LAMs). MAMs, as indicated by the name, are more reactive towards radicals as they generate a more stable propagating radical species, whilst LAMs on the other hand generate a less propagating radical species. Depending on if the monomer of choice is a MAM or LAM, the most appropriate R- and Z-groups for the CTA can be

selected (Figure 1.12). The Z-group is responsible for the stability of the dormant radical species as it modifies the addition and fragmentation reaction rates. This implies that the Z-group should be able to moderately stabilise the dormant radical species, but not excessively as this would result in the molecule being in a continuous dormant state. Conversely, the R-group is responsible for reinitiating the polymerisation reaction, this implies that it should be a relatively good radical leaving group that is also not highly stabilising. Again, too much stability would result in dormancy[31, 32].

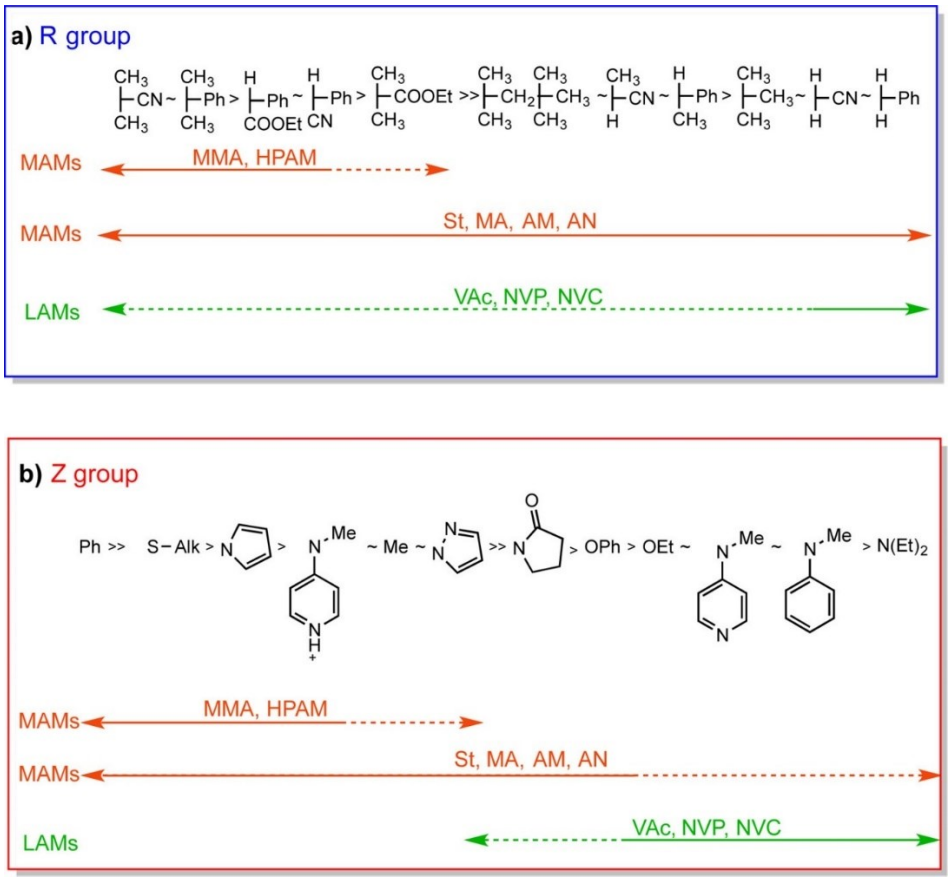

Figure 1.12. *Guidelines for deciding the most appropriate R- and Z-groups for a RAFT agent to use with different monomers (grouped into MAMs and LAMs). Reproduced with permission from Perrier et al.[30, 33].*

The mechanism for a RAFT polymerisation still involves the three main stages of initiation, propagation and termination, however the propagation stage is split to show the formation of equilibrium during the addition-fragmentation process.

The first step of initiation involves the generation of radicals, typically from the decomposition of an initiator, this is also denoted as the rate-determining step (I). The addition of monomer creates the first growing polymer chains, which are now also the active radical species (II) (Figure 1.13).

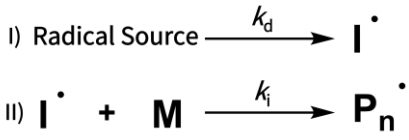

Figure 1.13. *The initiation mechanism for a typical RAFT polymerisation, where k_d and k_i are the rate constant for decomposition and initiation, respectively.*

Propagation begins with the RAFT pre-equilibrium step (III). The addition occurs first, this is when the polymer active radical species ($P_n^{\bullet}$) rapidly adds to the CTA and the equilibrium is established, generating the dormant state radical intermediate. The fragmentation step occurs after this where the R-group radical ($R^{\bullet}$) is expelled and therefore able to undergo reinitiation (IV). $R^{\bullet}$ then initiates the growth of new polymer chains and creates a new polymeric active radical species ($P_m^{\bullet}$). This brings us to the main RAFT equilibrium step, which is considered to be the most important step in the mechanism as this is where there is an equal distribution of radicals amongst the growing polymer chains. Both $P_n^{\bullet}$ and $P_m^{\bullet}$ are able to undergo further polymerisation when not attached to the CTA in the dormant state – meaning there is a constant reversible attachment and detachment (V) (Figure 1.14).

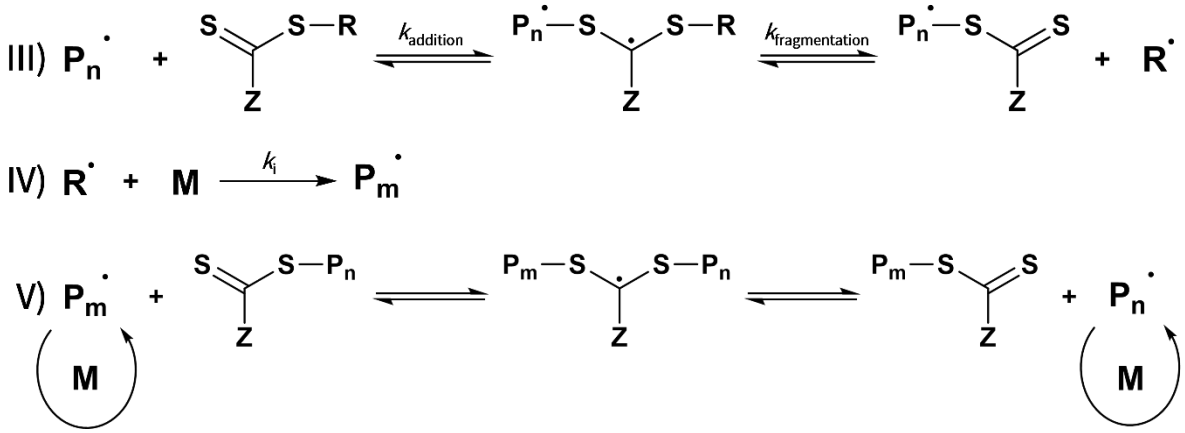

Figure 1.14. *The propagation mechanism for a typical RAFT polymerisation, where III) displays the reversible chain transfer, IV) displays reinitiation and V) displays chain equilibrium.*

The final step of termination occurs when the radicals combine and form a dormant species (VI)(Figure 1.15).

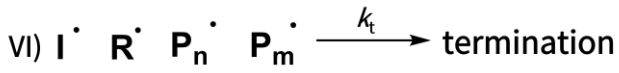

Figure 1.15. *The termination of a RAFT polymerisation by which the combination of radicals results in dead polymer chains.*

RAFT as a polymerisation technique has been used continually throughout literature over the past 20 years due to its ability to create well-defined block copolymers[34] and different molecular architectures[35]. It also has use in many biological applications[36], as well as every-day applications such as in inks[3] and optoelectrics[37]. End-group modification or removal is also possible, which may be desirable for many other applications. Both Willcock *et al.*[38] and Moad *et al.*[39] have provided an insight into the ways in which either end (α- and ω-ends) of a RAFT synthesised polymer can be modified, using methods such as thermolysis, or be completely removed. Although the many advantages of RAFT have been highlighted, the process does have some disadvantages such as costly CTAs and sometimes difficulty in finding compatibility with certain monomers.

1.4 Self-assembly

Self-assembly is ubiquitous in nature and is more often referred to as molecular self-assembly, which can be described as a spontaneous organisation of molecules into an ordered arrangement without the need for any external interactions[40]. A few examples of molecularly self-assembled systems in nature include the phospholipid bilayer in cells[41] and shell, coral and pearl formed from the self-assembly of proteins and peptides[42].

1.4.1 Block copolymer self-assembly

Block copolymers are macromolecules made up of two or more polymer 'blocks', which can be synthesised via RAFT from the extension of a macromolecular chain transfer agent (macro-CTA) using a different monomer. They can be arranged in various formations as seen in Figure 1.16. If the different polymer 'blocks' have opposing characteristics, such as different hydrophilicities, it can cause microphase separation to occur. This phenomenon occurs to minimise any unfavourable interactions; macrophase separation cannot occur due to the covalent bonding between the molecules[43, 44].

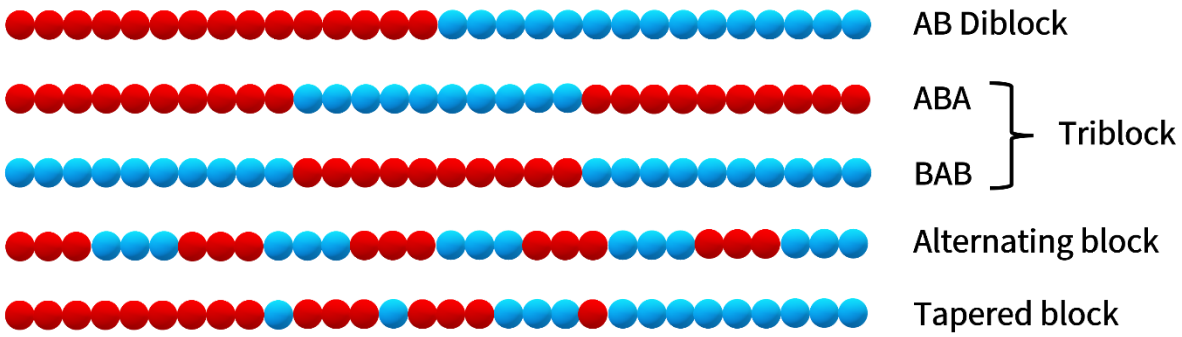

Figure 1.16. *Example structures for polymers containing two different blocks, A (red) and B (blue). Adapted with permission from Mai et al.*[45]*.*

1.4.1.1 Bulk microphase separation

Microphase separation can either occur in the bulk[46] or in solution[47]. The Flory-Huggins theory is used to understand how the block copolymers undergo microphase separation into different structures. Typically, chi (χ) denotes the Flory-Huggins interaction parameter, which represents the incompatibility between the constituent blocks of a block copolymer. For further discussion, the simplest form of block copolymer, an AB diblock copolymer, will be used as the example.

In the bulk, there are four common morphologies which can form as a result of microphase separation, these are spheres (S), cylinders (C), gyroid (G) or lamellae (L)[45, 48] (Figure 1.17).

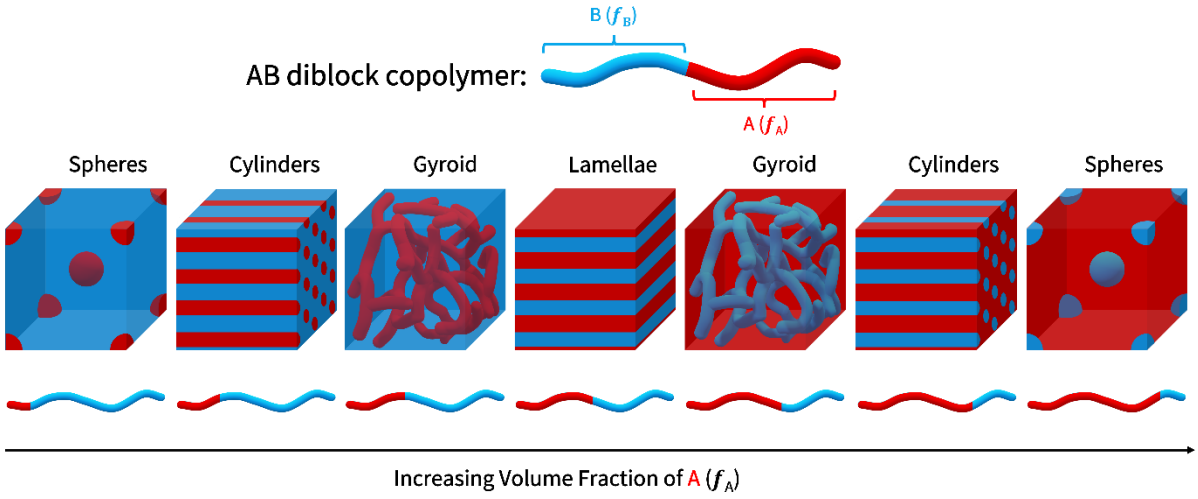

Figure 1.17. *The four possible morphologies obtained from the microphase separation of an AB diblock copolymer in the bulk, where f_A represents the volume fraction of block A and f_B represents the volume fraction of block B. Adapted with permission from Mai et al.*[45, 49]*.*

The formation of these structures depends on three main parameters. The first is the volume fractions of each block, denoted as f_A and f_B, where $f_A+f_B=1$; the second is χ_{AB}; and the third is the total degree of polymerisation of the polymer, in this case denoted as N_A and N_B, where $N_A+N_B=N$. The equation below incorporates the Flory-Huggins parameter and temperature, which can also act as a determining factor in the structure of the block copolymer (Equation 1.11)[49, 50].

$$X_{AB} = \left(\frac{z}{k_B T}\right)\left[\varepsilon_{AB} - \frac{1}{2}(\varepsilon_{AA} + \varepsilon_{BB})\right] \qquad \textbf{1.11}$$

The term z represents the number of nearest neighbours present per repeat unit (coordination number) in the polymer, k_B represents the Boltzmann constant and T represents the temperature. The remaining terms ε_{AA}, ε_{BB} and ε_{AB} represent the interaction energies of A-A, B-B and A-B, respectively. A phase diagram can also be used to predict the morphology of the block copolymer (Figure 1.18).

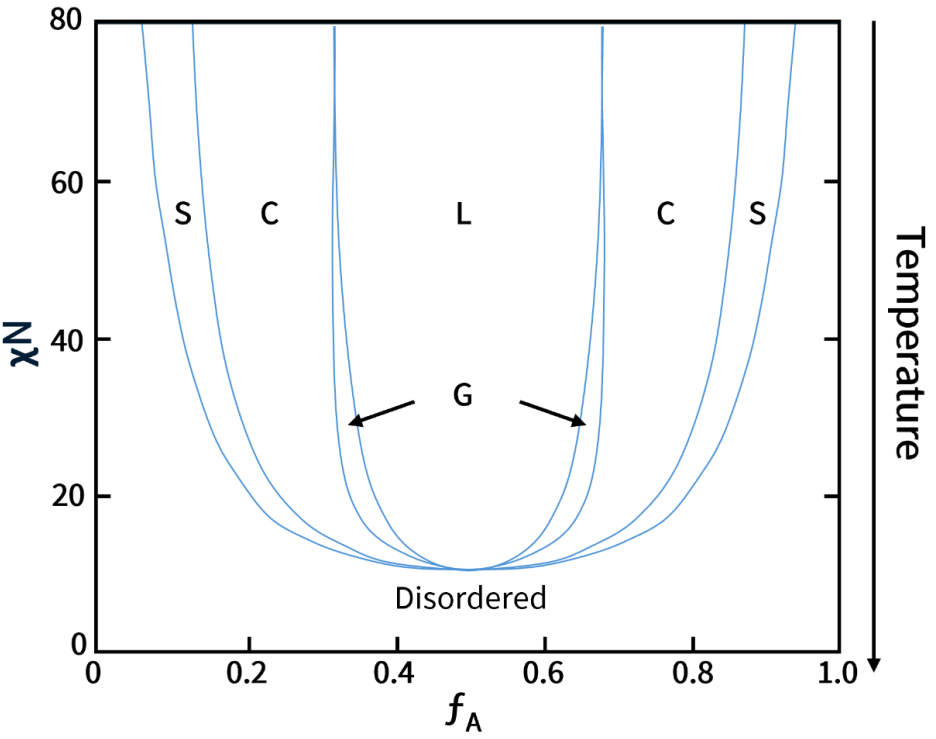

Figure 1.18. *Theoretical phase diagram of the Flory–Huggins segment–segment interaction multiplied by the degree of polymerisation (χN) against the increasing volume fraction of block A (f_A), with a decreasing temperature trend at lower χN values, which can be used to predict the morphologies obtained from the bulk self-assembly of an AB diblock copolymer. S represents body-centred cubic spheres, C represents hexagonally packed cylinders, G represents bicontinuous gyroids and L represents lamellae Adapted with permission from Mai et al.*[45, 49].

It can be observed that χN is inversely proportional to temperature. Processes such as annealing can impact self-assembly, where heating the sample to higher temperatures results in complete disorder, however as there is a slow decrease in temperature, more order begins to appear. This process is often used to achieve well-defined morphologies.

When there are more than two different blocks, e.g. a triblock copolymer such as ABC, there are even more parameters which need to be considered. There total degree of polymerisation stands as it is, however, there would now be three volume fractions (f_A+f_B+f_C=1) and three χ parameters (χ_{AB},χ_{AC},χ_{BC}). Due to this, the number of possible morphologies within the system drastically increases (Figure 1.19), with literature suggesting that there are thirty experimentally discovered structures[45, 51].

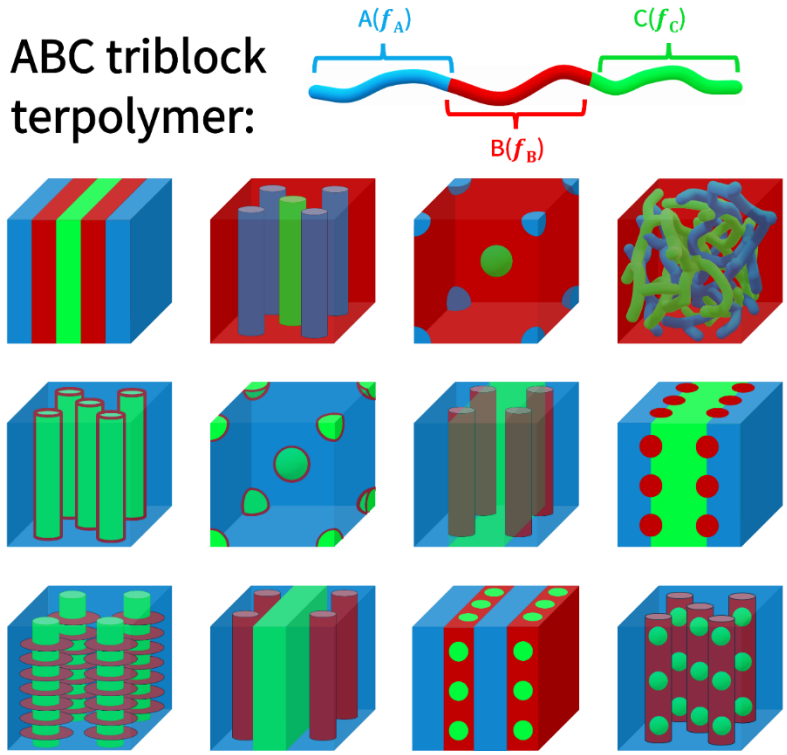

Figure 1.19. *Some of the possible morphologies that could be obtained from the bulk microphase separation of an ABC triblock terpolymer, where f_A represents the volume fraction of block A, f_B represents the volume fraction of block B and f_C represents the volume fraction of block C. Adapted with permission from Park et al.*[49, 52-54].

1.4.1.2 Solution self-assembly

Microphase separation of block copolymers in solution adds even more complexity to the Flory-Huggins theory; the interactions of the block copolymer and the solvent must also be considered. For an AB diblock copolymer, there are now six χ parameters to consider ($\chi_{AB}, \chi_{AS}, \chi_{BS}, \chi_{AA}, \chi_{BB}, \chi_{SS}$), with new interactions of the solvent (denoted as S) with both blocks.

The concentration of the system and the hydrophilicity of the block copolymer would also have an impact upon the resulting morphology. For example, if a block copolymer containing a very small hydrophobic block and a large hydrophilic block was dissolved in water, no self-assembly would occur due to the polymer chains happily dissolving in the solvent. However, as the size of the hydrophobic block increases, there would be an increase in incompatibility with the solvent, hence self-assembly occurring into different structures.

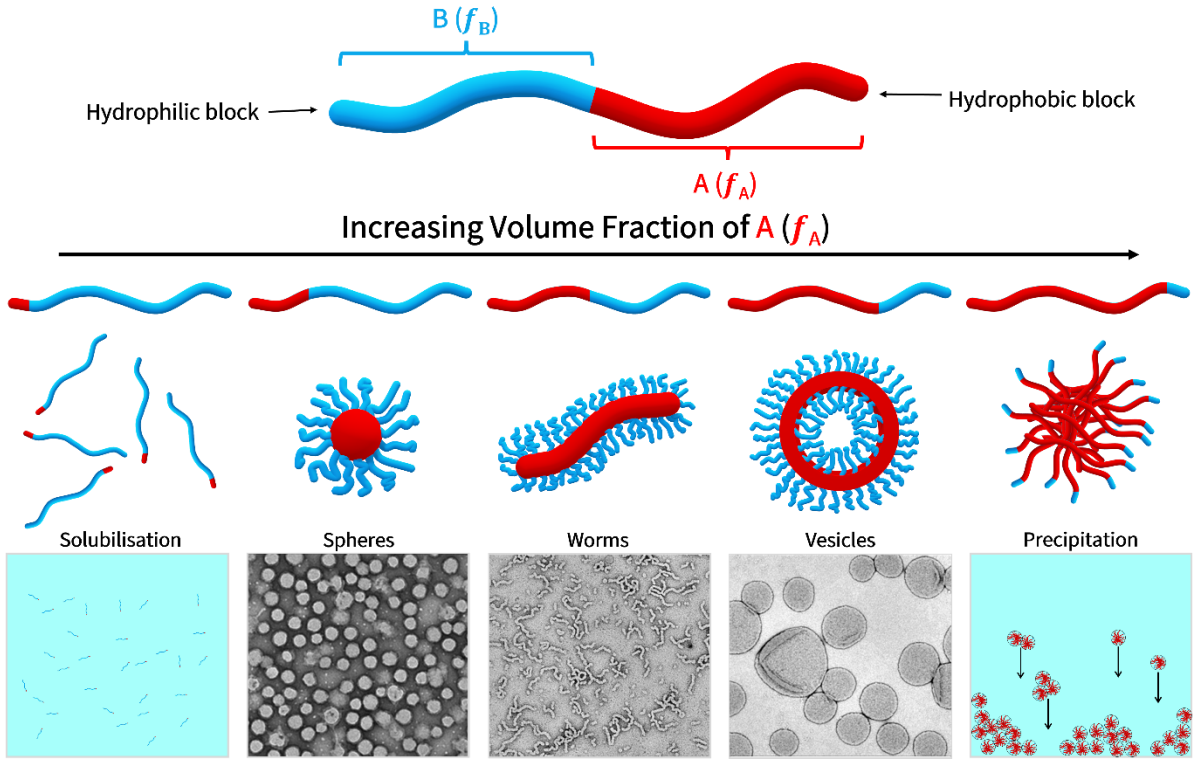

Figure 1.20. *The formation of different morphologies in solution for the self-assembly of an amphiphilic AB diblock copolymer (where f_A represents the volume fraction of block A and f_B represents the volume fraction of block B), which is dependent upon the fraction of hydrophobicity (f_A). TEM images reproduced with permission from Semsarilar et al.[55] (spheres) and Blanazs et al.[56] (worms and vesicles).*

It can be observed from Figure 1.20 that spherical micelle-like structures are formed when there is more hydrophilicity in the block copolymer, however there is enough hydrophobicity for the chains to orient in a way which conceals the hydrophobic block, hence creating a micellular structure. Worm-like micelles (cylinders) are created when there are similar amounts of each block and vesicles (low curvature lamellae-like structures) are created when there is more of the hydrophobic block. After this, any more hydrophobicity will cause the polymer to separate completely form the solvent. The polymer concentration must be equal to or more than the critical micelle concentration (CMC), for self-assembled structures to begin to form. The CMC can be defined as the concentration at which micelles start to form[57].

1.5 Polymerisation-induced self-assembly (PISA)

Polymerisation-induced self-assembly (PISA) can be defined as a process by which a solvophilic polymer is chain extended with a monomer to form ordered block copolymer nanostructures via

self-assembly[58]. Traditional block copolymer self-assembly requires the need for post-polymerisation processing such as solvent annealing[59], pH switching[60] or thin-film rehydration[61]. PISA does not require these additional steps as the synthesis of the block copolymer and self-assembly occurs simultaneously in one process. PISA can also be conducted at much higher solids concentrations (up to 50% w/w)[58, 62] rather than low concentrations of less than 1% w/w[63]. The most popular technique for facilitating PISA syntheses is RAFT polymerisation[64].

The process of PISA begins with a macromolecular precursor, often referred to as the stabilising block, which is soluble in the reaction solvent. The added monomer, which polymerises to form an insoluble polymer block, is either miscible or immiscible in the reaction solvent, giving rise to dispersion or emulsion conditions, respectively. This results in microphase separation during the polymerisation process and hence the self-assembly of the block copolymer into an ordered structure, such as spheres, worms or vesicles[47, 65]. Similarly to solution self-assembly, the formation of these morphologies depends on the ratio between both blocks (for an amphiphilic AB diblock copolymer). As the length of the second block increases, the change in morphology from spheres (lower order) to vesicles (higher order) occurs (Figure 1.21).

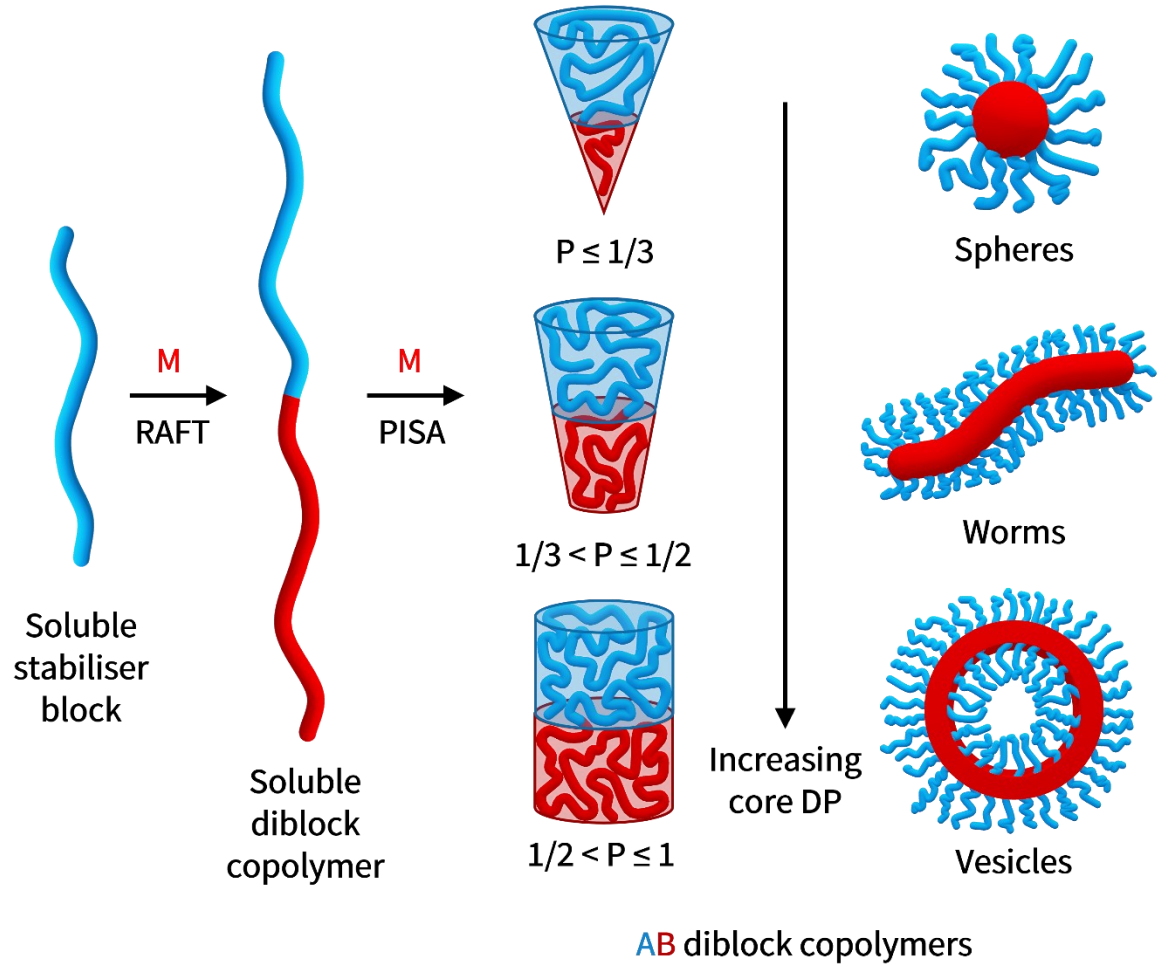

Figure 1.21. *The process of PISA, where the added monomer can be miscible (dispersion) or immiscible (emulsion), resulting in possible sphere, worm or vesicle morphologies. Adapted with permission from Canning et al.*[65]*.*

As mentioned briefly, PISA can occur via dispersion[66-69] or emulsion[70-73], depending of the miscibility of the added monomer in the reaction solvent. RAFT dispersion PISA has been shown in literature to have good efficiency in producing a wide range of morphologies[74] and be used with a number of aqueous[67, 74] and non-aqueous solvents[75]. However, RAFT emulsion PISA also has advantages as a wider selection of monomers are available to utilise, as immiscibility within the starting solution is possible.

1.5.1 Aqueous RAFT dispersion PISA

Aqueous RAFT dispersion PISA has been more extensively explored in the literature compared to non-aqueous systems. This can be suggested to be due to its potential in greener chemical

processes, as well as its ability to produce a wide range of morphologies[74]. Since the solvent system will have an aqueous component, it is a requirement that the chosen monomer is water-miscible, but forms a water-insoluble polymer, therefore monomer choice can be somewhat limited[67].

The first report of such a system was reported by An *et al.*[76], who produced nanoparticles, which could be transformed into thermo-responsive nanogels by adding a suitable cross-linker. Two different macro-CTAs with different hydrophilicities were synthesised, using 2-(dodecylthiocarbonothioylthio)-2-methylpropionic acid (DDMAT) (hydrophobic) and *S*-3-(propionic acid)-*S*'-2-(2,2'-dimethylacetic acid)trithiocarbonate (hydrophilic) as the RAFT agents providing end-group functionality. The CTAs were extended with *N*-isopropylmethacrylamide (NIPAm), with water as the reaction solvent at 70 °C and microwave irradiation, from which novel core–shell nanostructures were discovered post-polymerisation. Further work showed the addition of *N,N*'-methylenebisacrylamide (BIS) as a cross-linker. It was found that the continuation of polymerisation with BIS resulted in the same micellular morphologies obtained before the addition, however in a more swollen state. On the other hand, without the presence of BIS, the nanoparticles were found to dissociate into double hydrophilic block copolymers, losing their morphology. Thermo-responsive nanogels have been investigated by Grazon *et al.*[77] and Liu *et al.*[78]. Ethylene oxide, *N,N*-dimethylacrylamide and *N,N*'-methylene bisacrylamide (MBA) were used by Grazon *et al.*[77] to synthesise a cross-linkable block copolymer. Self-assembly into star-shaped micelles were observed from light scattering and fluorescence spectroscopy studies. Other interesting, related work demonstrates the transition of spherical to worm to vesicular morphologies, via a 'one pot' RAFT-mediated aqueous PISA syntheses. Blanazs *et al.*[56] used a poly(glycerol monomethacrylate) (PGMA) macro-CTA which was chain extended using 2-hydroxypropyl methacrylate (HPMA), reaching almost 100% conversion in 2 hours. TEM images displayed that there are intermediate morphologies present through the transition from spheres to vesicles, including "octopi" and "jellyfish" labelled structures.

1.5.2 Non-aqueous RAFT dispersion PISA

Non-aqueous solvents have been used to synthesise a range of different block copolymers with varying morphologies[75]. Examples in the literature have shown the use of polar[79-82], non-polar[83-86] and other organic media[87] (e.g ionic liquids[88-92]) as suitable solvent systems[74].

The first synthesis of RAFT-mediated PISA forming micelles in an organic solvent was reported by Zheng *et al.*[83], using tetrahydrofuran (THF) and cyclohexane. Dithiobenzoate-functionalised

polystyrene macromolecular chain transfer agents (macro-CTAs) were synthesised with very low dispersities ranging from 1.03 to 1.11, as determined from GPC. 4-Vinylpyridine was used as the extending monomer, where THF was shown to achieve better conversions than cyclohexane. Although this synthesis was successful, low conversions were obtained, with the highest conversions achieved being below 40%. In addition to this, the reaction kinetics were observed to plateau after around 10 hours[93]. Semsarilar *et al.*[79] reported the synthesis of diblock copolymers yielding spheres, worms and vesicles in an alcohol-based solvent system. Four different macro-CTAs were synthesised using 4-cyano-4-(phenylcarbonothioylthio)pentanoic acid (PETTC) as the selected RAFT agent and glycerol monomethacrylate (GMA), 2-(methacryloyloxy)ethyl phosphorylcholine (MPC), 2-(dimethylamino)ethyl methacrylate (DMA) or methacrylic acid (MAA) as the chosen monomer. All were chain extended with benzyl methacrylate in either ethanol or methanol, where high conversions above 93% and low dispersities (ranging between 1.09 and 1.30) were obtained within 24 hours. All three types of morphologies were found to be present when using each macro-CTA, as confirmed by TEM. Another example from the literature includes work conducted by Pei *et al.*[80] who presented the synthesis of spheres, worms and vesicles. This was achieved by using 2-phenylethyl methacrylate (PEMA) to chain extend poly[2-(dimethylamino)ethyl methacrylate] (PDMAEMA) macro-CTAs. This RAFT-mediated dispersion polymerisation was conducted in ethanol at 70 °C for 18 hours, which resulted in higher conversions (89 -97%) for the lower targeted DPs (50 – 250) and a lower conversion (43%) for the higher targeted DP (800).

1.5.3 Emulsion PISA

RAFT-mediated emulsion PISA can occur in an aqueous or non-aqueous solvent, depending on the nature of the starting monomer. As previously mentioned, emulsion polymerisations are considered to be versatile, due to the wide range of monomers which are able to be used in syntheses reactions.

The first report of an emulsion polymerisation under these condition was by Ferguson *et al.*[94, 95], by which an acrylic acid macro-CTA was synthesised, using 2-[(butylsulfanyl)carbonothioyl]sulfanyl]propanoic acid as the RAFT agent, which was subsequently chain extended with *n*-butyl acrylate. This resulted in the formation of micelles, however it was found that latex particles (dispersed polymer particle suspended in a medium) could be created as the polymerisation was continued by adding further hydrophobicity. Most of the examples in literature for RAFT aqueous emulsion formulations result in kinetically-trapped spheres, regardless of the ratio between hydrophilic and hydrophobic blocks[65]. Further research showed that it is

possible to achieve other morphologies through optimised reaction conditions. Khor *et al.*[73], demonstrated for the first time that by manipulating the concentration of initiator radicals and the hydrophobicity of the macro-CTA, different morphologies can be obtained. The chosen RAFT agent, 4-cyano-4-(ethylthiocarbonothioylthio)pentanoic acid (ECT), was modified to replace the carboxylic end-group functionality with a methyl ester, hence increasing its hydrophobicity. The original RAFT agent and the newly modified version were then used to synthesise a macro-CTA comprising of *N*-hydroxyethyl acrylamide (HEAA) and poly(ethylene glycol) methyl ether acrylate (PEGA). Both macro-CTAs were extended using styrene in water, with initiator concentrations at an approximate 1:1 molar ratio with respect to macro-CTA, resulting in the formation of spherical micelles, whilst increasing initiator concentrations by a factor of 2-3 created vesicle structures instead. This work demonstrated that there is the potential to synthesise specific morphologies using this manipulation.

Worms, vesicles and lamellae were synthesised by Truong *et al.*[96], who then tested their surfactant tolerance and reported no change at room temperature. Styrene was added to a P(DEGMA-*co*-HPMA) macro-CTA under RAFT emulsion conditions yielding spheres, which upon cooling transformed into a range of different morphologies. TEM images were used to show the changes in morphologies, as well as the maintenance of morphologies after being added to concentrated surfactant solutions. This demonstrated the stability of the thermoresponsive copolymers synthesised, providing potential for use as surfactant-tolerant nanomaterials.

1.5.4 Isorefractive PISA formulations

The phenomenon of isorefractivity occurs when materials have the same refractive index values, which then results in optical transparency. The refractive index of a material can be defined as the ratio of velocity of light in a vacuum relative to its velocity passing through the material[97], this can be determined using a refractometer. Isorefractivity is desirable for applications such as lenses and optical coatings, it can also can be observed in everyday applications such as fibre optics and even food.

As mentioned previously, isorefractivity can also be observed during syntheses, and of more relevance to this thesis, in the synthesis of nanoparticles in solution. Thompson *et al.*[98] and Rymaruk *et al.*[70] have demonstrated the isorefractivity of Pickering emulsions (emulsions stabilised by colloidal particles) containing anisotropic and spherical morphologies, respectively (Figure 1.22). Poly(lauryl methacrylate)-*b*-poly(benzyl methacrylate) diblock copolymer worms were synthesised

by Thompson *et al.*[98] and used in an ethylene glycol and an *n*-alkane solvent mixture, acting as the stabilising component. The refractive index value of *n*-tetradecane more closely matches that of ethylene glycol than *n*-dodecane, resulting in more transparency (up to 81% transmittance) of the resulting *n*-tetradecane solutions compared to the resulting *n*-dodecane solutions. Rymaruk *et al.*[70] reported much higher transmittance values of up to 96% using a range of different solvent mixtures and block copolymers. Specifically, sucrose and glycerol were added to dispersed poly(glycerol monomethacrylate)–poly(2,2,2-trifluoroethyl methacrylate) diblock copolymer nanoparticles in *n*-dodecane. The resulting Pickering emulsions had varied transparencies, with a sucrose concentration of around 50% resulting in the most highly transparent system.

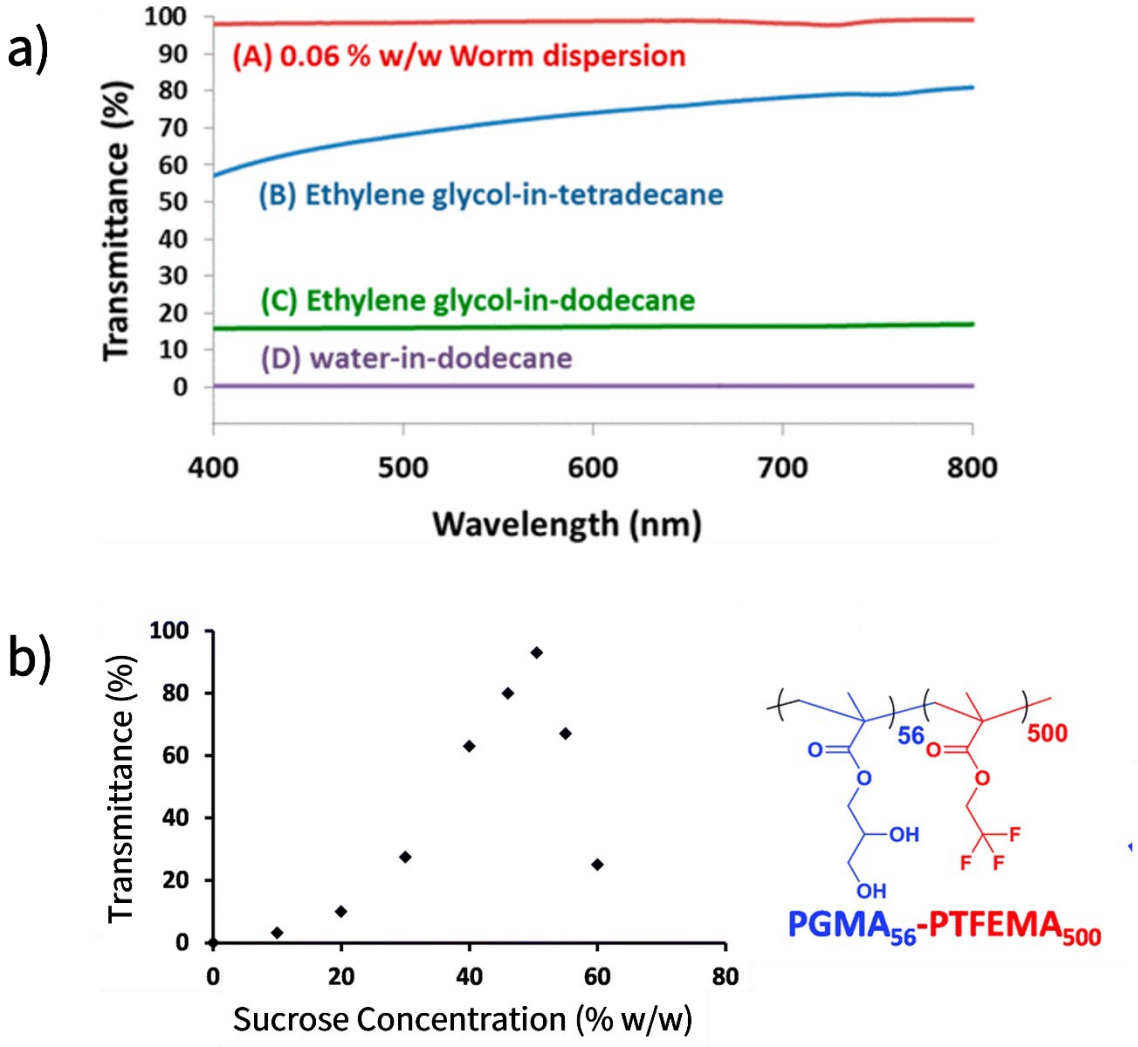

Figure 1.22. *The reported transmittance of Pickering emulsions, reproduced with permission from a) Thomson et al.*[98] *and b) Rymaruk et al.*[70]*.*

The presence of vesicles in a highly transparent dispersion was observed by György *et al.*[99] In this work, poly(stearyl methacrylate) (PSMA) was synthesised as a macro-CTA which was chain extended with 2,2,2-trifluoroethyl methacrylate (TFEMA) under RAFT-mediated dispersion PISA conditions in an *n*-alkane, yielding different morphologies (spheres, worms and vesicles). It was discovered that temperature affected the isorefractivity of the block copolymer in different solvents, where highly transparent solutions were obtained at 25 °C in *n*-dodecane, 50 °C in *n*-tetradecane and 90 °C in *n*-hexadecane (Figure 1.23).

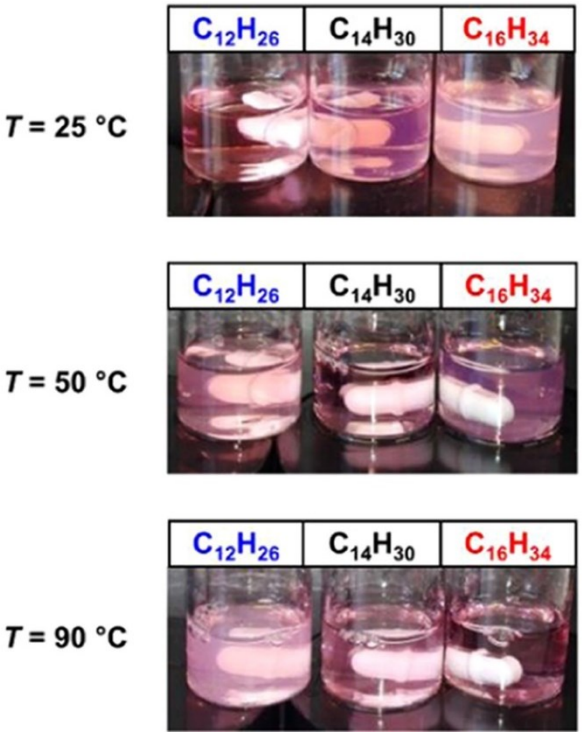

***Figure 1.23**. The different transparencies of nanoparticle-containing solutions prepared in different solvents and at different temperatures. Reproduced with permission from György et al.[69].*

1.6 Polymer nanostructure characterisation

1.6.1 Dynamic light scattering

Dynamic light scattering (DLS) can be defined as a monochromatic light-scattering technique, which can generate a distribution of particle size for a given sample. This distribution is created from the monitoring of fluctuation in intensity from the scattered light[100].

Due to Brownian motion in the sample, the particles move in a random motion and direction, with smaller particles typically able to move faster than larger ones, therefore meaning they diffuse much more quickly. The fluctuation in scattered light arises from this random movement, which is measured and used to create an autocorrelation function. From this, the diffusion coefficient (D) can be extracted and used in the Stokes-Einstein equation (Equation 1.12)[101] to calculate the hydrodynamic size (D_h) of the particles within the sample [102].

$$D_h = \frac{k_B T}{3\pi\eta D} \qquad \textit{1.12}$$

The term k_B represents the Boltzmann constant, T represents the absolute temperature and η represents the viscosity of the solvent used to prepare the sample. Although a distribution can be generated for the sample, the hydrodynamic size is calculated based on a spherical model which diffuses at the same rate as the particles within the sample. This indicates that the presence of any other morphologies, such as worms or vesicles, would not have accurately determined particle sizes[102], representing a limitation of the technique.

1.6.2 Transmission electron microscopy

Transmission electron microscopy, more often referred to as TEM, is used to provide clarity on the nano-structural arrangement within materials / samples[103]. In polymer chemistry, TEM is often used to help assign morphologies to particles within a sample, whether that be achieved via bulk (Figure 1.24) or solution microphase separation (Figure 1.25). This analytical technique involves an electron beam passing through the prepared sample, resulting in an image being formed based on the electron densities present, showing lighter and darker areas representing highly and less dense areas in the sample (depending on the type of TEM used). The image is then magnified to be visible using a magnifying lens.

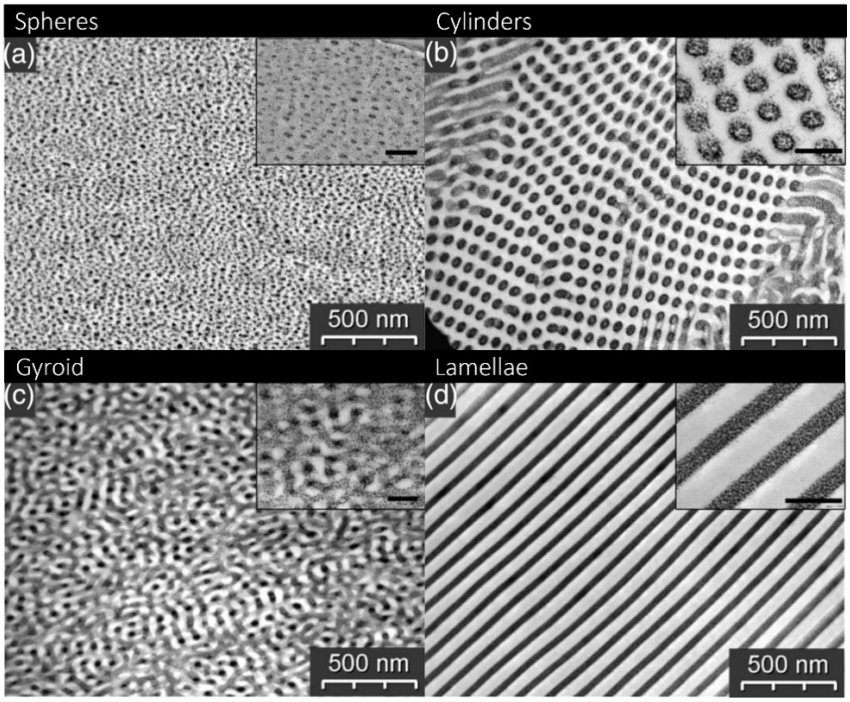

Figure 1.24. *The bulk microphase separation of block copolymers forming (a) spherical, (b) cylindrical, (c) gyroid and (d) lamellae morphologies. Reproduced with permission from Fahmi et al.* [104].

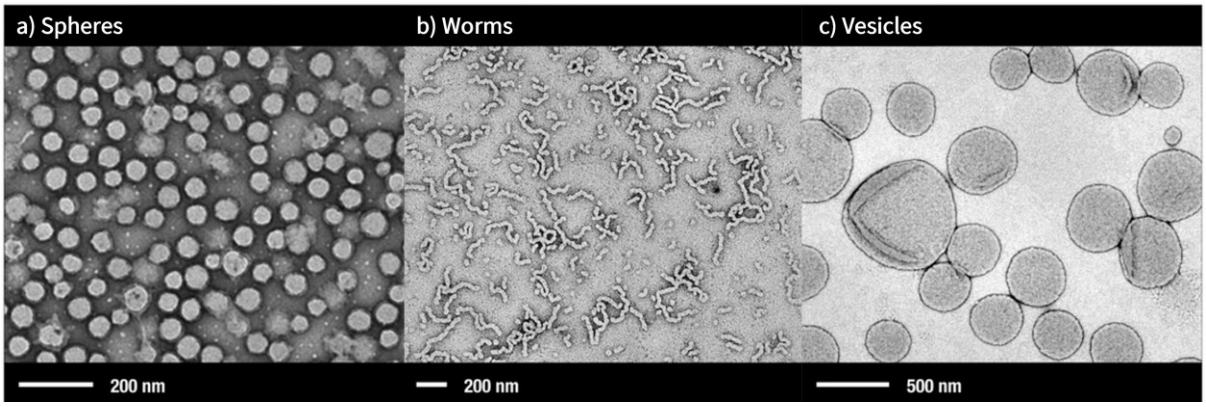

Figure 1.25. *The solution microphase separation of block copolymers forming a) spherical, b) worm and c) vesicular morphologies*[65]*. Reproduced with permission from Semsarilar et al.*[55] *(spheres) and Blanazs et al.*[56] *(worms and vesicles).*

TEM is considered to be a good characterisation technique as the self-assembly of block copolymers can be observed and the equipment is relatively accessible. However, it should be noted that the TEM sample is only a small region of the whole sample, and sometimes it can be difficult to see the difference between certain morphologies depending on the resolution of the image, which may subsequently require some interpretation.

1.6.3 Small-angle X-ray scattering

Small-angle X-ray scattering, also known as SAXS, is a technique that has been used to characterise nanoparticles since the 1950s[105]. The X-ray scattering pattern produced can be used to help determine the size, shape and structure of nanoparticles[106].

The scattering pattern is produced as a result of the X-ray beam irradiating electrons in the sample and being scattered at different angles. This process is an example of elastic scattering, occurring when the X-ray has the same wavelength before and after interacting with an electron. The scattering pattern emerges based on the distances between regions with the same electron density, these are considered to be like-domains. The angle of scattering (θ) and domain spacing (d) can be linked by Bragg's law (Equation 1.13).

$$n\lambda = 2d\sin\theta \qquad \textit{1.13}$$

Where n is an integer value representing the order of diffraction and λ is the wavelength of the X-rays. From this, the scattering vector (q) can be calculated using Equation 1.14 (Figure 1.26).

$$q = \frac{4\pi}{\lambda}\sin\theta \qquad \textit{1.14}$$

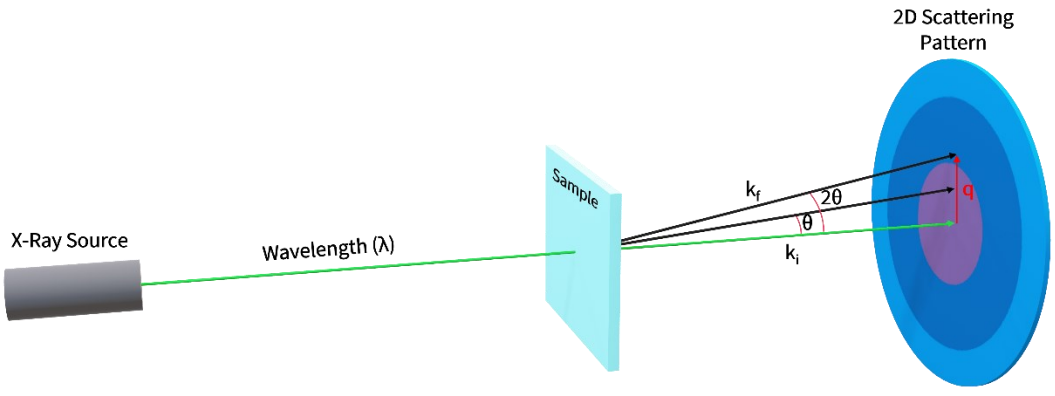

Figure 1.26. *A diagram depicting the principles of SAXS and the values used to calculate q, where k_f and k_i represent the length of a scattered x-ray and the x-ray beam, respectively and θ is the angle of scattering.*

The 2D scattering pattern obtained can be integrated to obtain intensity values, which can be plotted against q to generate a graph (Figure 1.27).

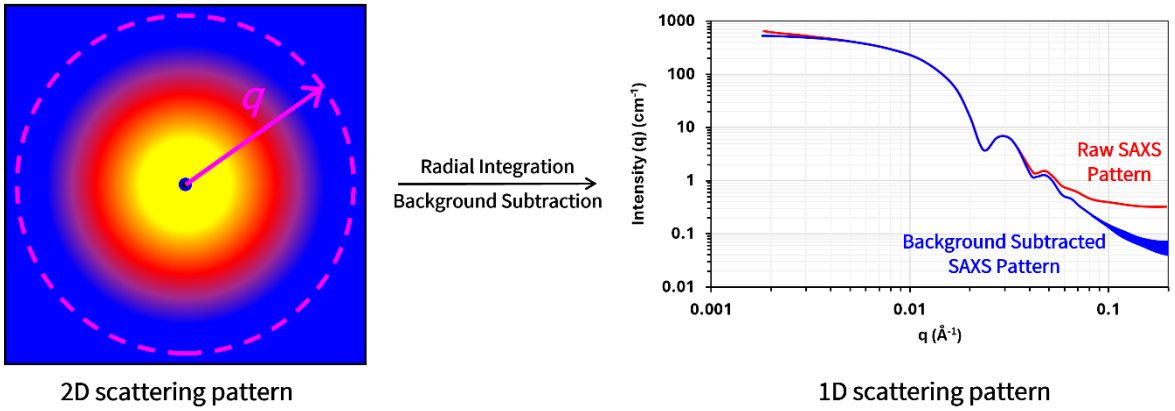

Figure 1.27. *The transition from a 2D scattering pattern to a 1D scattering pattern.*

This can then be fitted to a specific model (depending on the morphology present) and hence used to characterise the sample. For the bulk microphase separation of block copolymers, intensity plotted against the ratio of q to q^* (primary Bragg peak) can be used to determine the morphologies present in a given sample, being lamellae (LAM), hexagonally-packed cylinders (HEX), body-centred cubic spheres (BCC), face-centred cubic spheres (FCC) or gyroid (GYR) (Figure 1.28). For the solution microphase separation of block copolymers, the formation of spheres, worms and vesicles and their relative size can be noted from intensity plotted against q (Figure 1.29).

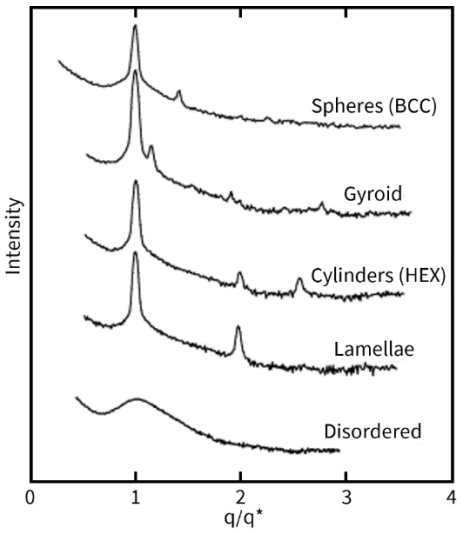

Figure 1.28. *A visual representation of the formation of spheres (body-centred cubic - BCC), cylinders (hexagonally packed - HEX), gyroid and lamellae determined from SAXS data for the bulk microphase separation of block copolymers, for comparison a sample showing complete disorder has been shown (bottom). Adapted with permission from Hamley et al.*[107]*.*

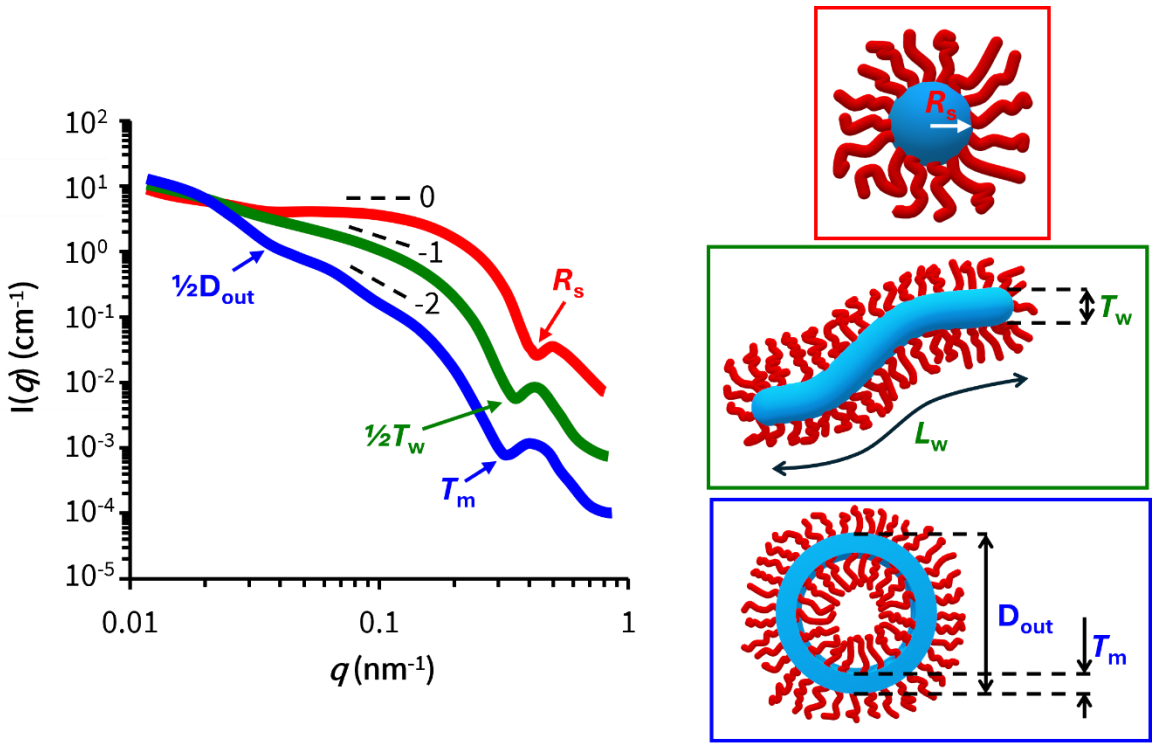

Figure 1.29. *A visual representation of the formation and respective size of spheres (R_s = radius of sphere), worms (T_w = mean worm thickness, L_w = worm length) and vesicles (D_{out} = outer vesicle diameter, T_m = vesicle membrane thickness) determined from SAXS data for the microphase separation of block copolymer in solution. The gradient of the graph depicts the specific morphology present: 0 indicates spheres (red), -1 indicates worms (green) and -2 indicates vesicles (blue). The feature for the worm length, L_w, is not shown.*

SAXS is a good analytical technique for confirming the morphology present in a sample as, unlike TEM, the whole sample is taken into consideration and a dried sample is not mandatory, making it more advantageous, especially for solution self- assembly. However, for the morphology to be accurately determined, there must be a distinct order of the particles within the sample. It should also be noted that SAXS instruments is not typically readily available and can be costly compared to other analytical instruments. Also, in order to access a synchrotron, a research proposal is usually required, after which access may be granted, however this may require long waiting times.

1.7 Sustainable polymerisation formulations

Sustainability in our current world is a highly significant factor that plays an essential role in the protective maintenance of our planet, without it devastation to our environment is inevitable. As mentioned previously, polymers contribute to our everyday lives and a large sub-section of these are polymers in liquid formulations, more commonly known as PLFs. These are used globally in a wide range of industries, such as food and packaging, building protection, infrastructure/transport and consumer products (as part of health and wellbeing)[108, 109]. Approximately 36 million tonnes of PLFs are generated each year and the global PLF market is estimated at over $1 trillion, thus it is undeniable that we have a considerable amount of reliance upon them[110].

1.7.1 Renewable monomers

PLFs are mostly created using synthetic monomers, however there is a drive to make use of natural monomers to improve their sustainability[110]. The synthesis of renewable monomers is prevalent throughout literature. Gandini[111-115] has provided extensive research on the synthesis of monomers from renewable resources, with more specific focus on polysaccharides, furans and vegetable oils. This work includes a review article, by which the synthesis of monomers from biomass and natural resources is discussed in-depth[113]. Other relevant reviews include the synthesis of useful polymers using precursor monomers generated from sustainable feedstocks[116], including the synthesis of frequently used synthetic polymers such as nylons and polyacrylates[117]. Of specific interest, Hatton[118] provided a minireview displaying precursor molecules derived from renewable resources which can be polymerised via RAFT polymerisation (Figure 1.30). Although there are many options available to create monomers from renewable resources, the actual sustainability of their synthesis

reactions has not yet been quantified. Hatton[118] has implied that a life cycle assessment (LCA) of the synthesised monomers is challenging as there are many other external factors to consider.

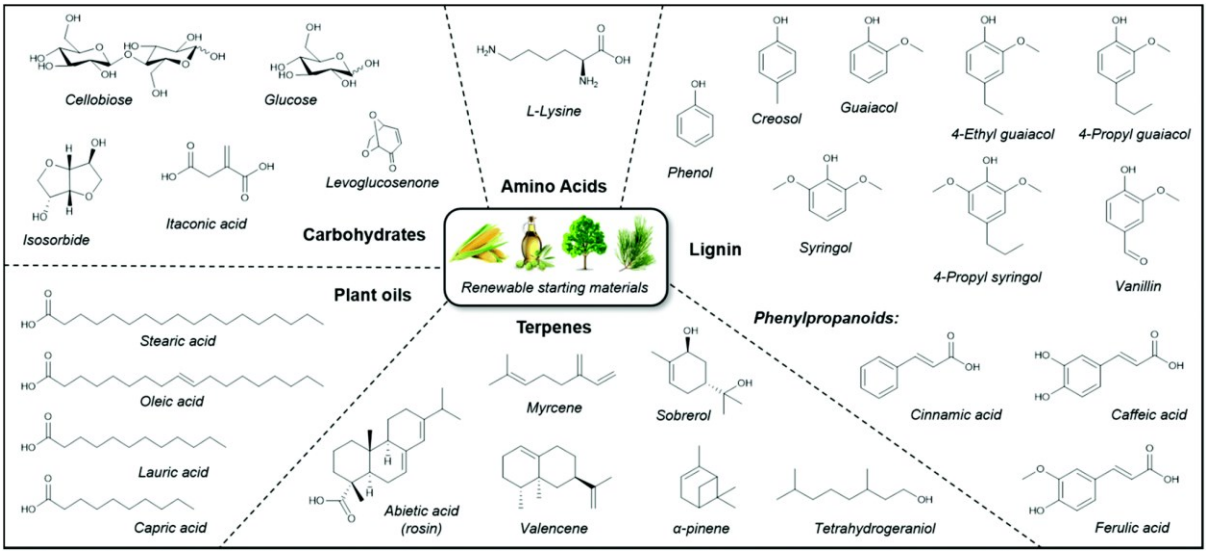

Figure 1.30. *Potential monomer precursor molecules derived from renewable resources. Reproduced with permission from Hatton [118].*

1.7.1.1 Cross-linkable monomers

Different monomers tend to have different properties, making them useful for specific applications. In this thesis, the cross-linkability of different monomers has been researched to add extra functionality to the synthesised block copolymer which would enable use in a broader range of applications, such as inkjet printing. Some polymers can be thermally or photo responsive[119], although the use of photo-responsive polymers are the focus of this thesis, in an attempt to increase the sustainability of the system. Photo-responsive polymers have been used in many applications[120], including drug delivery[121, 122] and light-healing materials[123, 124]. Pyrenylmethyl, *o*-nitro-benzyl and coumarin are all examples of photo-triggerable groups[121], coumarin is of particular interest due to its natural abundance in renewable feedstocks. Other photo-triggerable monomers that can be derived from renewable resources have been reported by Wang *et al.*[125], who provided an extensive list of naturally derived reagents which have been modified into biomaterials (hydrogels) and have the ability to be cross-linked using either visible or ultraviolet light. In addition to this, Pezzana *et al.*[126] have conducted promising research which shows how waste by-products, from the pulp and paper industry, can be used to obtain UV cross-linkable monomer precursor molecules. Hughes *et al.*[127] provided a useful list of photo-formable and photo-reversible

compounds via a [2+2] cycloaddition process, some of which can be derived from renewable resources (coumarin and cinnamic acid). These, along with other compounds, namely anthracene[127] and furan derivatives[128], are investigated in this thesis.

1.7.2 Sustainable polymer synthesis

As mentioned previously, RAFT is used continually to synthesise many different block copolymers that are used in many different applications. The use of this, combined with a desire to have an increase in sustainability for synthesis reactions is prevalent in the literature. Atkinson *et al.*[129] demonstrated that renewable terpene meth(acrylates) can be used to synthesise block copolymers via RAFT polymerisation. In addition to this, Hillmyer *et al.*[130] successfully synthesised aliphatic polyesters for use as sustainable, renewable and degradable thermoplastic elastomers. Woods *et al.*[131] reported the synthesis of temperature-responsive nanoparticles using bio-based monomers (synthesised from biobased feedstocks) and water as the reaction solvent.

Sustainable block copolymer synthesis has also been demonstrated from the use of greener solvents. Solvents can be categorised as being preferred, unusable and undesirable, with preferred being the more 'greener' choice (e.g. water), unusable being the worst choice (e.g. 1,4-dioxane) and undesirable being mid-range between the two (e.g. tetrahydrofuran)[132]. An example of this from the literature is from Coumes *et al.*[133], who have used a green solvent mixture of ethanol and water to further increase the sustainability of their reaction. In addition to this, Cyrene™, a solvent derived from biomass which has been noted to be biodegradable, non-mutagenic and non-toxic[134], can also be used as a green solvent alternative[135-138]. Harris *et al.*[139] have used RAFT, with Cyrene™ as the reaction solvent, for the first time to polymerise a bio-based lactone monomer, specifically γ-methyl-αmethylene-γ-butyrolactone (γMeMBL). Previously, the polymerisation of hydrophilic[135] and hydrophobic[135, 136] monomers were found to be successful in Cyrene™ using other polymerisation methods. More recently, the use of alternative greener solvents to replace commonly used organic solvents is preferred, and several alternatives to hazardous solvents have been previously employed (Figure 1.31)[140-143]. It should be noted that although there are bio-based solvent options, better sustainability can still be achieved by taking other factors (such as the renewability of feedstocks) into consideration[144].

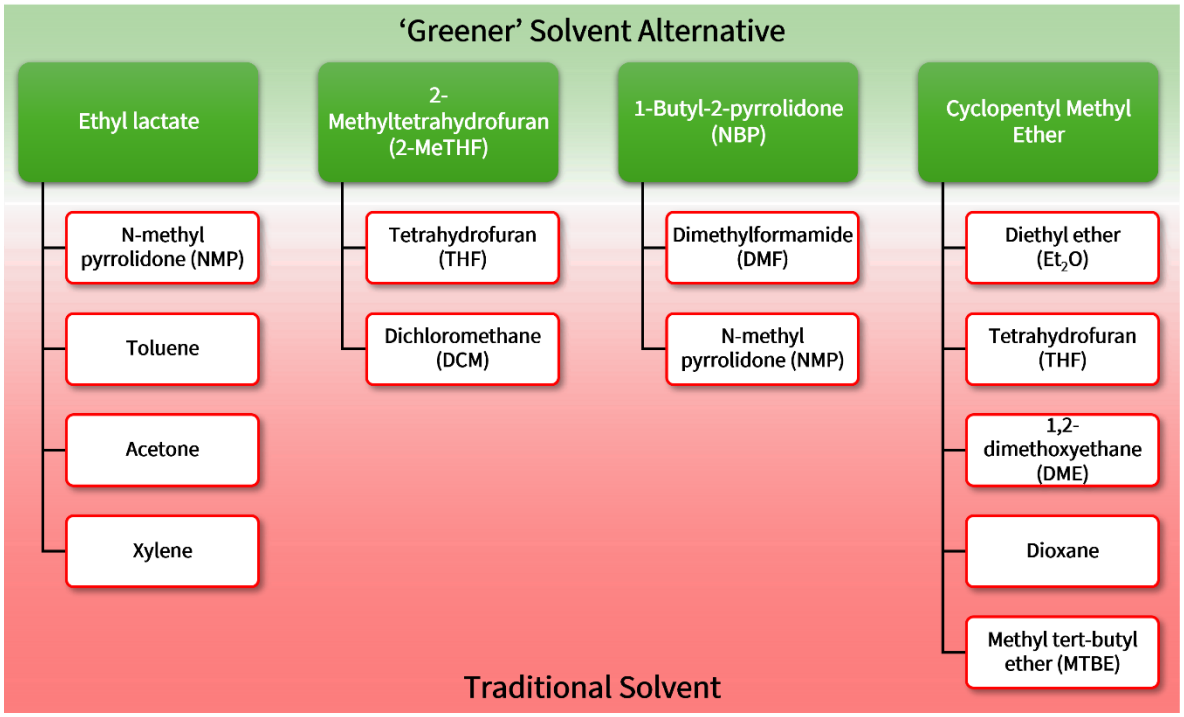

Figure 1.31. *'Greener' solvent choices and the traditional solvents they can replace*[140-143].

Of particular interest, ionic liquids have been shown to be much more advantageous than traditional solvents, also due to their less hazardous and toxic nature[145, 146]. Ionic liquids are noted to have low vapour pressure and high thermal stability, which allows them to be stored and sometimes recovered and recycled[147].

1.8 Ionic liquids

During the past couple of decades, the interest in ionic liquids has grown considerably. An ionic liquid (IL) can be defined as a salt with a melting point below 100 °C, which is composed entirely of ions[148]. Some traditional organic solvents often used in chemical syntheses are problematic due to their high volatility and potential to damage health and the environment. ILs have been shown to successfully replace such conventional solvents, in applications such as batteries[149] and CO_2 capturing[150], and eliminating most of the concerns due to their low vapour pressure[151, 152].

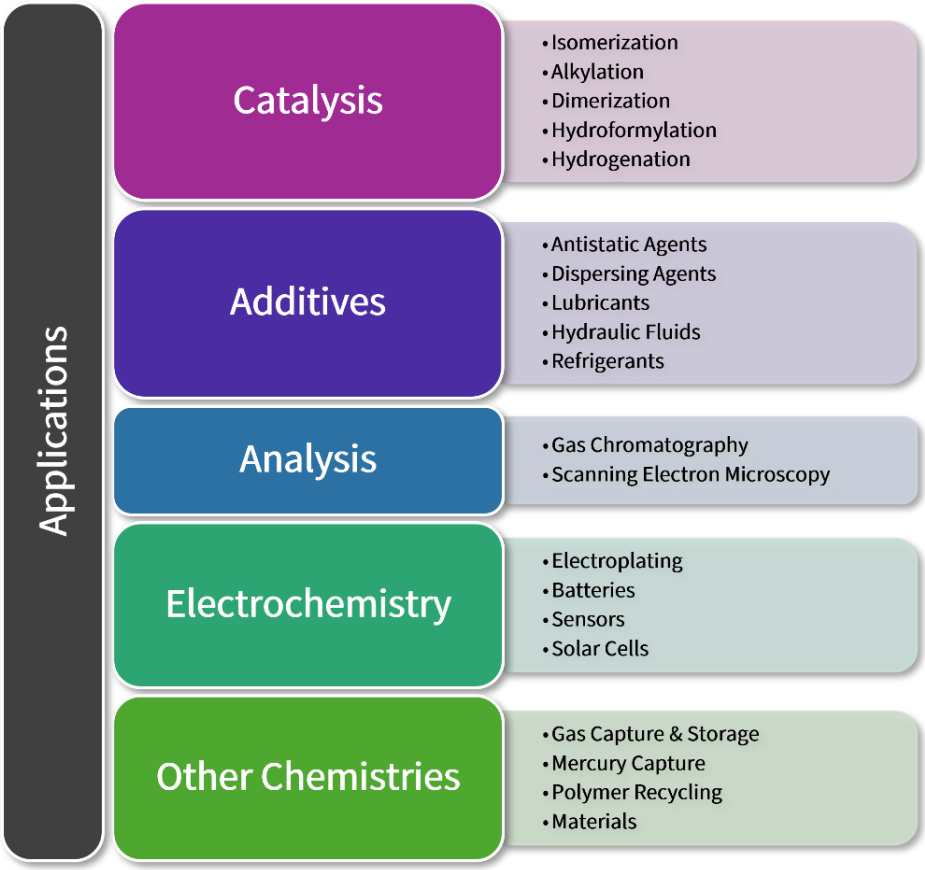

Figure 1.32. *The various areas in which ionic liquids can be used, alongside more specific applications. Adapted from Greer et al.*[153]*.*

Another advantage of ILs is the fact that there are an almost inexhaustible number of anions and cations that can be combined to prepare ILs with tuneable properties, such as varied hydrophilicities[154]. This can be particularly useful if there are problems with solvent compatibility for certain reactions. Other favoured properties of ILs include their high ionic conductivity, low flammability, thermal and electrochemical stability, and commercial availability. Due to this, the application of ionic liquids is not limited to use as solvents, they are also commonly used in catalysis[155, 156], additives[157-161], analysis[162, 163], electrochemistry[164-167] and other chemistries[153, 168-173] (Figure 1.32). ILs have also shown to be recyclable[174-176], as demonstrated by Kumar *et al.*[176] who showed that the ionic liquid used for a RAFT polymerisation was successfully recycled and used for three successive polymerisations, all of which proceeded to have high monomer conversions (ranging from 92 to 96%) and high subsequent IL solvent recovery (ranging from 92 to 95%)[176].

1.8.1 Polymers in ionic liquids

Since the first report of polymerisation in IL in 1990[177], there has been a growing interest in polymer synthesis conducted in ILs and their effects, if any[178, 179]. An example of this in literature is from Strehmel *et al.*[180], who investigated the polymerisation of *n*-butyl methacrylate (BuMA) in a wide range of ILs and discovered that imidazolium-based salts are better for this particular monomer, resulting in higher PBuMA DPs than when conducted in other solvents, such as toluene, and when conducted in the bulk. In addition to this, Kubisa[181, 182] showcased in a review that polymerisations in ionic liquids lead to faster rates of reactions and higher monomer conversions compared to when conducted in traditional organic solvents such as benzene. ILs have also been used to create poly(ionic liquids) (PILs), which have potential in applications as ionic conductors[183] and the ability to act as precursors for the synthesis of carbonaceous materials[184], due to them being able to exhibit properties of both ionic liquids and macromolecular structures[185].

1.8.1.1 Block copolymer self-assembly in ionic liquids

The synthesis of block copolymers in ionic liquids is also popular throughout the literature, predominantly due to the ability to form nanostructures resulting from self-assembly[186-188]. He *et al.*[188] demonstrated that the synthesis of four block copolymers, comprising of different compositions of poly((1,2-butadiene)-block-ethylene oxide) (PB−PEO), in an imidazolium-based IL, 1-butyl-3-methylimidazolium hexafluorophosphate ([BMIM][PF_6]), yielded spherical micelle, wormlike micelle, and bilayered vesicle structures. It was found that these morphologies also formed when conducted in other solvents (such as water), however when conducted in IL, the morphologies were temperature-independent (maintained stable) between 25 and 100 °C. The self-assembly of nanostructures in IL ca also result in the formation of gels[189, 190]. He *et al.*[189] also reported the synthesis of a triblock copolymer ,poly(styrene-block-ethylene oxide-block-styrene) (SOS), in [BMIM][PF_6] – a room-temperature ionic liquid. This was discovered to form a transparent gel, offering new routes to develop highly conductive materials.

1.8.1.2 PISA in ionic liquids

The differences between traditional block copolymer self-assembly and PISA have previously been discussed. Of more relevance to this thesis, the literature of PISA conducted in ionic liquids will be

discussed in more detail. To date, there are only a few examples of RAFT-mediated PISA syntheses conducted in IL solvent.

The first system reported by Zhang *et al.*[91] was a dispersion polymerisation leading to the formation of nanoaggregates with varied morphologies (Figure 1.33). Specifically, a poly(ethylene glycol) (PEG) macro-CTA with trithiocarbonate functionality was chain extended using three different monomers, namely styrene (St), BuMA and 2-hydroxyethyl methacrylate (HEMA) in [BMIM][PF_6]. All three block copolymers were chain extended using the same macro-CTA and were shown for form vesicular nanostructures. However, another PEG macro-CTA synthesised with a lower DP was used to chain extend St, targeting a higher and lower DP, yielding different morphologies. Resulting TEM images displayed the formation of spherical, vesicular, stretched vesicular, large compound vesicular, rod-like and other complex (not-defined) morphologies within the polymeric sample. It should be noted that although the formation of different morphologies was successful, the structures were mainly spherical and vesicular.

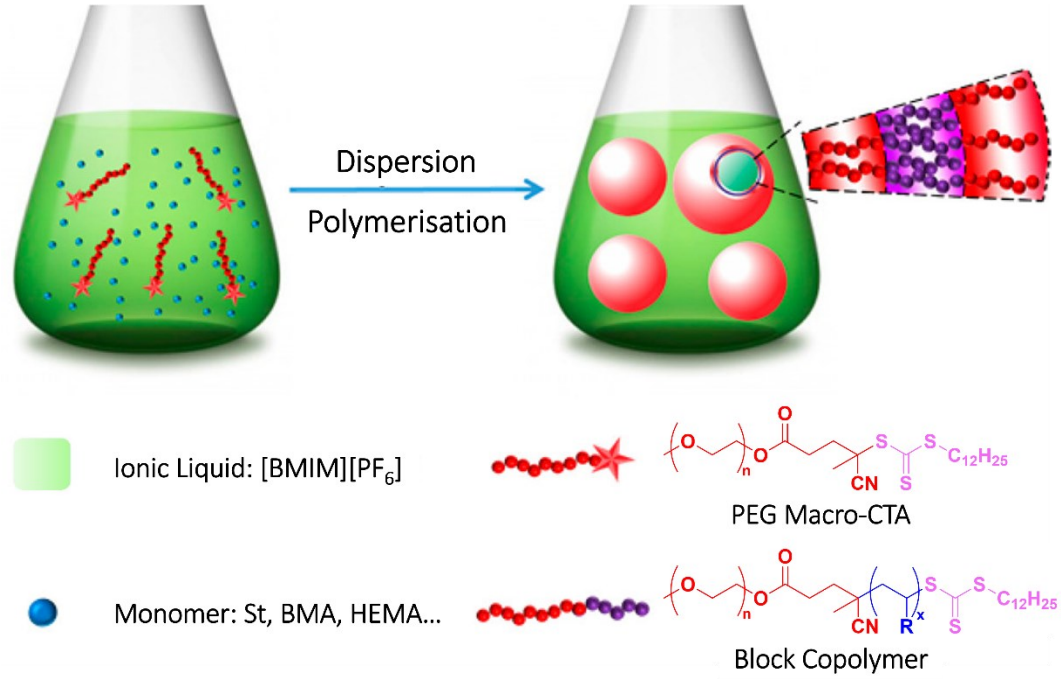

Figure 1.33. *The synthesis of block copolymers in 1-butyl-3-methylimidazolium hexafluorophosphate [BMIM][PF_6] yielding spherical morphologies. Adapted with permission from Zhang et al.*[91]*.*

Zhou *et al.*[92] used a very similar system, composing a PEG macro-CTA that was chain extended in [BMIM][PF_6] using St via RAFT-mediated dispersion PISA. It was found that the reaction proceeded

faster and yielded higher monomer conversions (~95% at 10 hours) in the IL than in methanol (~65% at 10 hours) and a methanol/water (4:1, w:w) solvent system (~17% at 10 hours). Narrow molecular weight distributions (≤1.22) were obtained and there was a linear increase of molecular weight with monomer conversion for all systems, indicating good control in these RAFT polymerisations. Again, nanospheres and vehicles were the morphologies obtained, which were confirmed using TEM (Figure 1.34).

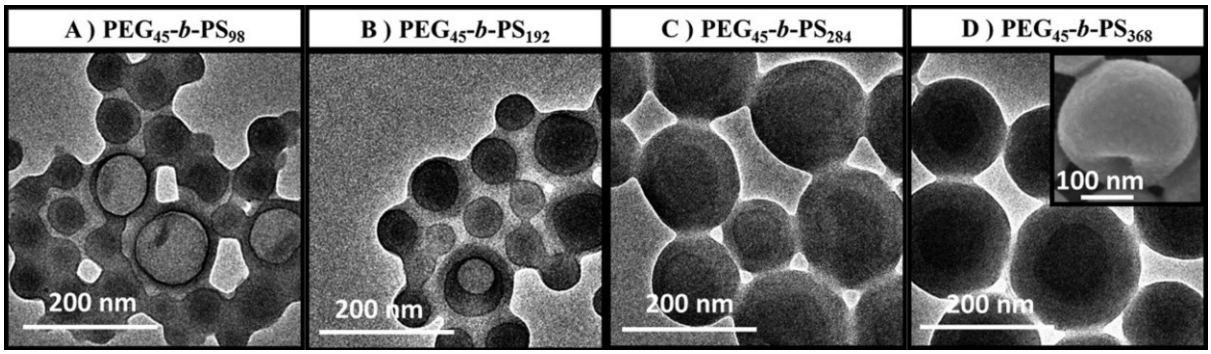

Figure 1.34. *TEM images of the PEG_{45}-b-PS block copolymers synthesised via RAFT-mediated dispersion PISA in 1-butyl-3-methylimidazolium hexafluorophosphate [BMIM][PF_6]. Reproduced with permission from Zhou et al.*[92]*.*

For the first time, SAXS and oscillatory rheology were used by Yamanaka *et al.*[89] to monitor PISA and the gelation process of BAB triblock copolymers in ionic liquid (Figure 1.35), where HEMA was used to chain extend a pre-synthesised PEG macro-CTA in [BMIM][PF_6]. It has previously been noted that PEG-PHEMA block copolymers self-assemble into vesicular morphologies[91], however in this case where a triblock copolymer is synthesised, spherical morphologies were obtained. This was thought to be due to the constriction formed from the interconnected network of the two blocks. The point of gelation during the reaction was noted to occur directly after the induction period and the time at which self-assembly occurred increased when PISA syntheses were conducted at lower concentrations. Although gelation was shown to occur for 50, 30 and 10% w/w, it did not occur at 5% w/w, implying that there is a limitation if lower concentrations are required.

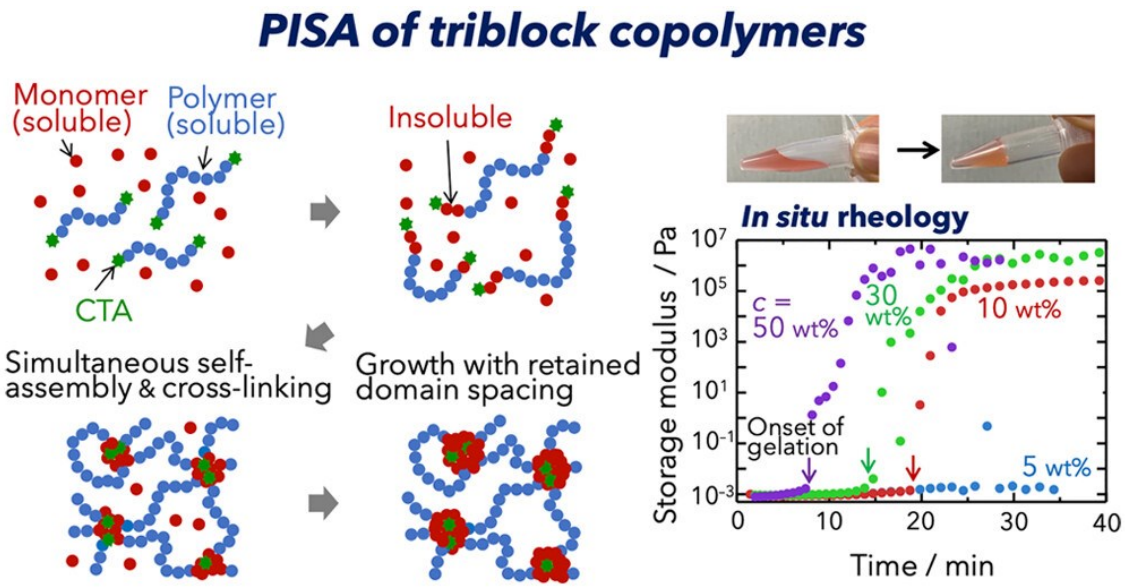

Figure 1.35. *The monitoring of the synthesis of triblock copolymers in 1-butyl-3-methylimidazolium hexafluorophosphate [BMIM][PF_6] to yield a gel material. Reproduced with permission from Yamanaka et al.*[89]*.*

More recently, the synthesis of gels via RAFT dispersion polymerisation in IL was further investigated by Maitland *et al.*[88], who reported the first successful synthesis of worm morphologies via PISA in IL, in addition to spherical and vesicular nanoparticles (Figure 1.36). A PHEMA macro-CTA was chain extended using benzyl methacrylate (BzMA) in 1-ethyl-3-methyl imidazolium dicyanamide, [EMIM][DCA]. High conversions (>89%) were achieved within 2 hours and the gel formation was observed in dispersions with copolymer concentrations above 4%. Electrochemical properties of the gels were analysed using electrochemical impedance spectroscopy (EIS), which showed promise for potential application as gel electrolytes.

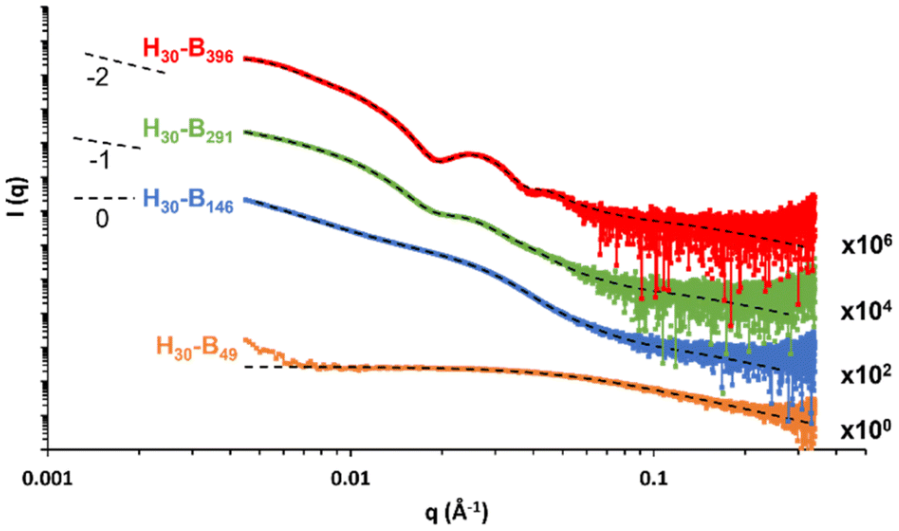

Figure 1.36. *SAXS data indicating the successful synthesis of spheres (red), worms (green) and vesicles (blue) alongside a disordered sample (orange), from the block copolymer self-assembly of PHEMA-b-PBzMA in 1-ethyl-3-methyl imidazolium dicyanamide, [EMIM][DCA]. Reproduced with permission from Maitland et al.*[88]*.*

Another more recent example in the literature is from Yamanaka *et al.*[90], where the synthesis of different architectures (stars) was explored. St was added to PEG macro-CTAs with two, four and eight arms in [BMIM][PF_6] and, as expected, self-assembly and gelation occurred as the polymerisation proceeded. It was discovered that hexagonally packed cylinders were formed from the linear two arm PEG-Ps and hexagonally close-packed/disordered spheres were formed from the star four and eight arm PEG-Ps polymers, with low dispersities below 1.15 also obtained (Figure 1.37). From this research, it was concluded that the molecular structure of polymers is a controlling factor of the resulting morphology and mechanical properties of the polymer. Again, this is an example of a dispersion polymerisation, it can be observed that the use of emulsion polymerisation has been less explored.

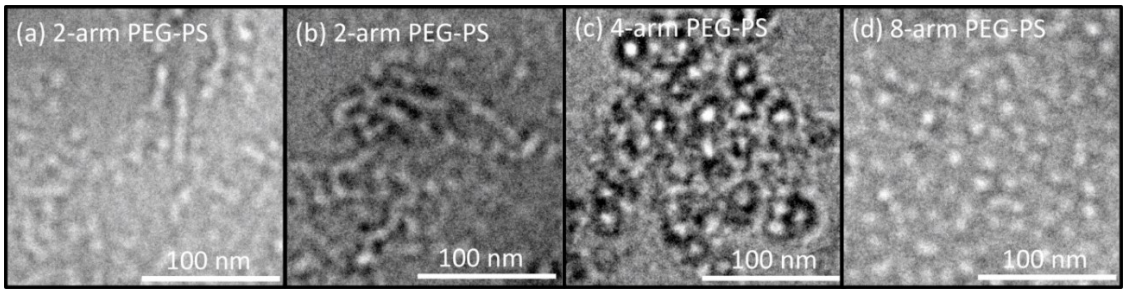

Figure 1.37. *TEM images of the star PEG_{45}-b-PS block copolymers with a)/b) 2-arms, c) 4-arms and d) 8-arms, synthesised in 1-butyl-3-methylimidazolium hexafluorophosphate [BMIM][PF_6]. Reproduced with permission from Yamanaka et al.*[90]*.*

1.9 Outline and aims

The overall aim for this thesis is to investigate the more sustainable synthesis of block copolymers in ionic liquid (as a more sustainable solvent) and potential cross-linkable molecules which could be relatively easily added into the block copolymer to add more functionality. The synthesis of block copolymers in IL is prevalent in the literature, however the RAFT PISA synthesis of block copolymer in ILs is not as widely researched. To this date, there are few publications to demonstrate this, all of which report on RAFT dispersion PISA specifically. Chapter 2 reports on the synthesis of PHEMA-*b*-PBuMA block copolymers synthesised via emulsion PISA, by extending a PHEMA macro-CTA with BuMA in a commercially available ionic liquid, specifically 1-ethyl-3-methyl-imidazolium ethylsulfate ([EMIM][$EtOSO_3$]). The synthesis of the amphiphilic PHEMA-*b*-PBuMA is also conducted in other solvents, namely DMF and an EtOH/H_2O (4:1 w:w) solvent mixture to compare reaction control and conversion. The isorefractivity of the solutions and formation of any nanostructures is also investigated, using a range of analytical techniques including UV-Vis spectroscopy, DLS, TEM and SAXS. Chapter 3 reports on the testing and modification of a range of cross-linkable compounds, namely 4-methylumbelliferone (4MU), cinnamic acid (CA), 9-anthracenecarboxylic acid (9ACA) and 3-(2-furyl)acrylic acid (FAA). The dimerization ability of the molecules alone is tested using exposure to the relevant wavelength of light which would trigger the breaking of two double bonds to form a cyclobutane ring. From these results, the most promising compounds are selected and modified using a pre-existing PHEMA macro-CTA or acryloyl chloride, depending on if the compound has carboxylic acid or alcohol functionality, respectively. Chapter 4 discusses the conclusions made and any potential future work. Overall, this research aims to open additional avenues for accelerated polymerisation techniques not previously demonstrated, and present novel routes to nanoparticle formation, as well as building on these through exploration of potential candidates for cross linking to demonstrate the potential for use in applications such as inkjet printing.

1.10 References

1. A. X. Chen, J. D. Hilgar, A. A. Samoylov, S. S. Pazhankave, J. A. Bunch, K. Choudhary, G. L. Esparza, A. Lim, X. Luo and H. Chen, *Advanced Materials Interfaces*, 2023, **10**, 2202053.
2. J. W. Rumer and I. McCulloch, *Materials Today*, 2015, **18**, 425-435.
3. G. E. Parkes, H. J. Hutchins-Crawford, C. Bourdin, S. Reynolds, L. J. Leslie, M. J. Derry, J. L. Harries and P. D. Topham, *Polymer Chemistry*, 2020, **11**, 2869-2882.
4. A. Kausar, *Journal of Macromolecular Science, Part A*, 2018, **55**, 440-448.
5. R. Y. Lochhead, in *Cosmetic Nanotechnology*, American Chemical Society, 2007, vol. 961, ch. 1, pp. 3-56.

6. C. Silvestre, D. Duraccio and S. Cimmino, *Progress in Polymer Science*, 2011, **36**, 1766-1782.
7. M. F. Maitz, *Biosurface and Biotribology*, 2015, **1**, 161-176.
8. F. W. Harris, *Journal of Chemical Education*, 1981, **58**, 837.
9. J. M. G. Cowie and V. Arrighi, *Polymers: Chemistry and Physics of Modern Materials, Third Edition*, CRC Press, 2007.
10. J. Yang, I. Gitlin, V. M. Krishnamurthy, J. A. Vazquez, C. E. Costello and G. M. Whitesides, *Journal of the American Chemical Society*, 2003, **125**, 12392-12393.
11. P. C. Hiemenz and T. P. Lodge, *Polymer Chemistry*, CRC Press, 2007.
12. S. Balke, A. Hamielec, B. LeClair and S. Pearce, *Industrial & Engineering Chemistry Product Research and Development*, 1969, **8**, 54-57.
13. T. P. Lodge and P. C. Hiemenz, *Polymer Chemistry*, CRC Press, 2020.
14. M. Kaliva and M. Vamvakaki, in *Polymer Science and Nanotechnology*, ed. R. Narain, Elsevier, 2020, pp. 401-433.
15. K. Hatada, T. Kitayama and K. Ute, in *Annual Reports on NMR Spectroscopy*, ed. G. A. Webb, Academic Press, 1993, vol. 26, pp. 99-210.
16. I. Manavitehrani, A. Fathi, H. Badr, S. Daly, A. Negahi Shirazi and F. Dehghani, *Polymers*, 2016, **8**, 20.
17. T. J. Singh and S. Samanta, *Materials Today: Proceedings*, 2015, **2**, 1381-1387.
18. M. Shakiba, E. Rezvani Ghomi, F. Khosravi, S. Jouybar, A. Bigham, M. Zare, M. Abdouss, R. Moaref and S. Ramakrishna, *Polymers for advanced technologies*, 2021, **32**, 3368-3383.
19. A. Das and P. Mahanwar, *Advanced Industrial and Engineering Polymer Research*, 2020, **3**, 93-101.
20. R. B. Grubbs and R. H. Grubbs, *Macromolecules*, 2017, **50**, 6979-6997.
21. D. Braun, *International Journal of Polymer Science*, 2009, **2009**, 893234.
22. H. A. Pearce, Y. S. Kim, L. Diaz-Gomez and A. G. Mikos, in *Biomaterials Science (Fourth Edition)*, eds. W. R. Wagner, S. E. Sakiyama-Elbert, G. Zhang and M. J. Yaszemski, Academic Press, 2020, pp. 1317-1334.
23. D. A. Shipp, *Polymer Reviews*, 2011, **51**, 99-103.
24. N. Corrigan, K. Jung, G. Moad, C. J. Hawker, K. Matyjaszewski and C. Boyer, *Progress in Polymer Science*, 2020, **111**, 101311.
25. M. R. Martinez and K. Matyjaszewski, *CCS Chemistry*, 2022, **4**, 2176-2211.
26. M. Ouchi and M. Sawamoto, *Polymer Journal*, 2018, **50**, 83-94.
27. H. R. Lamontagne and B. H. Lessard, *ACS Applied Polymer Materials*, 2020, **2**, 5327-5344.
28. F. Lorandi, M. Fantin and K. Matyjaszewski, *J Am Chem Soc*, 2022, **144**, 15413-15430.
29. J. Chiefari, Y. K. Chong, F. Ercole, J. Krstina, J. Jeffery, T. P. T. Le, R. T. A. Mayadunne, G. F. Meijs, C. L. Moad, G. Moad, E. Rizzardo and S. H. Thang, *Macromolecules*, 1998, **31**, 5559-5562.
30. S. Perrier, *Macromolecules*, 2017, **50**, 7433-7447.
31. D. J. Keddie, *Chemical Society Reviews*, 2014, **43**, 496-505.
32. D. J. Keddie, C. Guerrero-Sanchez, G. Moad, R. J. Mulder, E. Rizzardo and S. H. Thang, *Macromolecules*, 2012, **45**, 4205-4215.
33. D. J. Keddie, G. Moad, E. Rizzardo and S. H. Thang, *Macromolecules*, 2012, **45**, 5321-5342.
34. P. Relógio, M.-T. Charreyre, J. P. S. Farinha, J. M. G. Martinho and C. Pichot, *Polymer*, 2004, **45**, 8639-8649.
35. A. Gregory and M. H. Stenzel, *Progress in Polymer Science*, 2012, **37**, 38-105.
36. C. Boyer, V. Bulmus, T. P. Davis, V. Ladmiral, J. Liu and S. Perrier, *Chemical Reviews*, 2009, **109**, 5402-5436.
37. G. Moad, M. Chen, M. Häussler, A. Postma, E. Rizzardo and S. H. Thang, *Polymer Chemistry*, 2011, **2**, 492-519.
38. H. Willcock and R. K. O'Reilly, *Polymer Chemistry*, 2010, **1**, 149-157.

39. G. Moad, E. Rizzardo and S. H. Thang, *Polymer International*, 2011, **60**, 9-25.
40. G. M. Whitesides and M. Boncheva, *Proc Natl Acad Sci U S A*, 2002, **99**, 4769-4774.
41. P. Dey, S. Ray and P. Chattopadhyay, in *Design and Applications of Theranostic Nanomedicines*, eds. S. Ray and A. K. Nayak, Woodhead Publishing, 2023, pp. 345-366.
42. A. Solomonov and U. Shimanovich, *Israel Journal of Chemistry*, 2020, **60**, 1152-1170.
43. L. Leibler, *Macromolecules*, 1980, **13**, 1602-1617.
44. D. J. Lohse and N. Hadjichristidis, *Current Opinion in Colloid & Interface Science*, 1997, **2**, 171-176.
45. Y. Mai and A. Eisenberg, *Chemical Society Reviews*, 2012, **41**, 5969-5985.
46. J. K. Kim, J. I. Lee and D. H. Lee, *Macromolecular Research*, 2008, **16**, 267-292.
47. M. Karayianni and S. Pispas, *Journal of Polymer Science*, 2021, **59**, 1874-1898.
48. S. B. Darling, *Progress in Polymer Science*, 2007, **32**, 1152-1204.
49. F. S. Bates and G. H. Fredrickson, *Physics Today*, 1999, **52**, 32-38.
50. F. S. Bates, *Science*, 1991, **251**, 898-905.
51. V. Abetz and R. Stadler, *Macromolecular Symposia*, 1997, **113**, 19-26.
52. A. B. Chang and F. S. Bates, *Macromolecules*, 2020, **53**, 2765-2768.
53. C. Park, J. Yoon and E. L. Thomas, *Polymer*, 2003, **44**, 6725-6760.
54. W. Zheng and Z.-G. Wang, *Macromolecules*, 1995, **28**, 7215-7223.
55. M. Semsarilar, V. Ladmiral, A. Blanazs and S. Armes, *Langmuir*, 2013, **29**, 7416-7424.
56. A. Blanazs, J. Madsen, G. Battaglia, A. J. Ryan and S. P. Armes, *Journal of the American Chemical Society*, 2011, **133**, 16581-16587.
57. C. Jungnickel, J. Łuczak, J. Ranke, J. F. Fernández, A. Müller and J. Thöming, *Colloids and Surfaces A: Physicochemical and Engineering Aspects*, 2008, **316**, 278-284.
58. L. Qiu, X. Han, C. Xing and U. Glebe, *Small*, 2023, **19**, 2207457.
59. C. K. Wong, X. Qiang, A. H. E. Müller and A. H. Gröschel, *Progress in Polymer Science*, 2020, **102**, 101211.
60. V. Bütün, S. P. Armes and N. C. Billingham, *Polymer*, 2001, **42**, 5993-6008.
61. J. R. Howse, R. A. Jones, G. Battaglia, R. E. Ducker, G. J. Leggett and A. J. Ryan, *Nature materials*, 2009, **8**, 507-511.
62. N. J. W. Penfold, J. Yeow, C. Boyer and S. P. Armes, *ACS Macro Letters*, 2019, **8**, 1029-1054.
63. U. Tritschler, S. Pearce, J. Gwyther, G. R. Whittell and I. Manners, *Macromolecules*, 2017, **50**, 3439-3463.
64. S. P. Armes, S. Perrier and P. B. Zetterlund, *Polymer Chemistry*, 2021, **12**, 8-11.
65. S. L. Canning, G. N. Smith and S. P. Armes, *Macromolecules*, 2016, **49**, 1985-2001.
66. J.-T. Sun, C.-Y. Hong and C.-Y. Pan, *Polymer Chemistry*, 2013, **4**, 873-881.
67. N. J. Warren and S. P. Armes, *Journal of the American Chemical Society*, 2014, **136**, 10174-10185.
68. X. Wang and Z. An, *Macromolecular Rapid Communications*, 2019, **40**, 1800325.
69. C. György, M. J. Derry, E. J. Cornel and S. P. Armes, *Macromolecules*, 2021, **54**, 1159-1169.
70. M. J. Rymaruk, K. L. Thompson, M. J. Derry, N. J. Warren, L. P. Ratcliffe, C. N. Williams, S. L. Brown and S. P. Armes, *Nanoscale*, 2016, **8**, 14497-14506.
71. A. Takashima, Y. Maeda and S. Sugihara, *ACS Omega*, 2022, **7**, 26894-26904.
72. M. Zeng, X. Li, Y. Zhang, X. Chen, X. Sui and J. Yuan, *Polymer*, 2020, **206**, 122853.
73. S. Y. Khor, N. P. Truong, J. F. Quinn, M. R. Whittaker and T. P. Davis, *ACS Macro Letters*, 2017, **6**, 1013-1019.
74. D. Ikkene, J.-L. Six and K. Ferji, *European Polymer Journal*, 2023, **188**, 111848.
75. M. J. Derry, L. A. Fielding and S. P. Armes, *Progress in Polymer Science*, 2016, **52**, 1-18.
76. Z. An, Q. Shi, W. Tang, C.-K. Tsung, C. J. Hawker and G. D. Stucky, *Journal of the American Chemical Society*, 2007, **129**, 14493-14499.
77. C. Grazon, J. Rieger, N. Sanson and B. Charleux, *Soft Matter*, 2011, **7**, 3482-3490.

78. G. Liu, Q. Qiu and Z. An, *Polymer Chemistry*, 2012, **3**, 504-513.
79. M. Semsarilar, E. R. Jones, A. Blanazs and S. P. Armes, *Advanced Materials*, 2012, **24**, 3378-3382.
80. Y. Pei and A. B. Lowe, *Polymer Chemistry*, 2014, **5**, 2342-2351.
81. W. Zhao, G. Gody, S. Dong, P. B. Zetterlund and S. Perrier, *Polymer Chemistry*, 2014, **5**, 6990-7003.
82. D. Das, D. Gerboth, A. Postma, S. Srinivasan, H. Kern, J. Chen, D. M. Ratner, P. S. Stayton and A. J. Convertine, *Polymer Chemistry*, 2016, **7**, 6133-6143.
83. G. Zheng and C. Pan, *Macromolecules*, 2006, **39**, 95-102.
84. B. Darmau, M. J. Rymaruk, N. J. Warren, R. Bening and S. P. Armes, *Polymer Chemistry*, 2020, **11**, 7533-7541.
85. L. A. Fielding, M. J. Derry, V. Ladmiral, J. Rosselgong, A. M. Rodrigues, L. P. Ratcliffe, S. Sugihara and S. P. Armes, *Chemical Science*, 2013, **4**, 2081-2087.
86. Y. Kang, A. Pitto-Barry, H. Willcock, W.-D. Quan, N. Kirby, A. M. Sanchez and R. K. O'Reilly, *Polymer Chemistry*, 2015, **6**, 106-117.
87. C. Gao, H. Zhou, Y. Qu, W. Wang, H. Khan and W. Zhang, *Macromolecules*, 2016, **49**, 3789-3798.
88. G. L. Maitland, M. Liu, T. J. Neal, J. Hammerton, Y. Han, S. D. Worrall, P. D. Topham and M. J. Derry, *Chemical Science*, 2024, **15**, 4416-4426.
89. R. Yamanaka, A. Sugawara-Narutaki and R. Takahashi, *Macromolecules*, 2023, **56**, 4354-4361.
90. R. Yamanaka, A. Sugawara-Narutaki and R. Takahashi, *ACS Macro Letters*, 2024, **13**, 1050-1055.
91. Q. Zhang and S. Zhu, *ACS Macro Letters*, 2015, **4**, 755-758.
92. H. Zhou, C. Liu, C. Gao, Y. Qu, K. Shi and W. Zhang, *Journal of Polymer Science Part A: Polymer Chemistry*, 2016, **54**, 1517-1525.
93. J.-T. Sun, C.-Y. Hong and C.-Y. Pan, *Soft Matter*, 2012, **8**, 7753-7767.
94. C. J. Ferguson, R. J. Hughes, B. T. T. Pham, B. S. Hawkett, R. G. Gilbert, A. K. Serelis and C. H. Such, *Macromolecules*, 2002, **35**, 9243-9245.
95. C. J. Ferguson, R. J. Hughes, D. Nguyen, B. T. T. Pham, R. G. Gilbert, A. K. Serelis, C. H. Such and B. S. Hawkett, *Macromolecules*, 2005, **38**, 2191-2204.
96. N. P. Truong, C. Zhang, T. A. H. Nguyen, A. Anastasaki, M. W. Schulze, J. F. Quinn, A. K. Whittaker, C. J. Hawker, M. R. Whittaker and T. P. Davis, *ACS Macro Letters*, 2018, **7**, 159-165.
97. C. Raymond and S. Ronca, in *Brydson's Plastics Materials (Eighth Edition)*, ed. M. Gilbert, Butterworth-Heinemann, 2017, pp. 103-125.
98. K. L. Thompson, J. A. Lane, M. J. Derry and S. P. Armes, *Langmuir*, 2015, **31**, 4373-4376.
99. C. György, M. J. Derry, E. J. Cornel and S. P. Armes, *Macromolecules*, 2021, **54**, 1159-1169.
100. M. Mohammadi, H. Zargartalebi, R. Salahandish, R. Aburashed, K. W. Yong and A. Sanati-Nezhad, *Biosensors and Bioelectronics*, 2021, **183**, 113176.
101. C. C. Miller, *Proceedings of the Royal Society of London. Series A, Containing Papers of a Mathematical and Physical Character*, 1924, **106**, 724-749.
102. A. Wishard and B. C. Gibb, *Supramol Chem*, 2019, **31**, 608-615.
103. L. E. Franken, E. J. Boekema and M. C. Stuart, *Advanced Science*, 2017, **4**, 1600476.
104. A. Fahmi, T. Pietsch, C. Mendoza and N. Cheval, *Materials Today*, 2009, **12**, 44-50.
105. A. Guinier, G. Fournet, C. B. Walker and K. L. Yudowitch, *Small-angle Scattering of X-rays*, Wiley New York, 1955.
106. T. Li, A. J. Senesi and B. Lee, *Chemical Reviews*, 2016, **116**, 11128-11180.
107. I. W. Hamley and V. Castelletto, *Progress in Polymer Science*, 2004, **29**, 909-948.
108. *Polymers in liquid formulations - Opportunities for a sustainable future*, Royal Society of Chemistry, 2021.

109. *Polymers in liquid formulations - Technical report: A landscape view of the global PLFs market*, Royal Society of Chemistry, 2021.
110. C. L. Kelly, *Chemical Science*, 2023, **14**, 6820-6825.
111. A. Gandini, *Macromolecules*, 2008, **41**, 9491-9504.
112. A. Gandini, *Green Chemistry*, 2011, **13**, 1061-1083.
113. A. Gandini and T. M. Lacerda, *Progress in Polymer Science*, 2015, **48**, 1-39.
114. A. Gandini, T. M. Lacerda, A. J. F. Carvalho and E. Trovatti, *Chemical Reviews*, 2016, **116**, 1637-1669.
115. A. Gandini, A. J. Silvestre, C. P. Neto, A. F. Sousa and M. Gomes, *Journal of Polymer Science: Part A: Polymer Chemistry*, 2009, **47**, 295.
116. Y. Zhu, C. Romain and C. K. Williams, *Nature*, 2016, **540**, 354-362.
117. G. Hayes, M. Laurel, D. MacKinnon, T. Zhao, H. A. Houck and C. R. Becer, *Chemical Reviews*, 2023, **123**, 2609-2734.
118. F. L. Hatton, *Polymer Chemistry*, 2020, **11**, 220-229.
119. S. Dai, P. Ravi and K. C. Tam, *Soft Matter*, 2009, **5**, 2513-2533.
120. O. Bertrand and J.-F. Gohy, *Polymer Chemistry*, 2017, **8**, 52-73.
121. J.-F. Gohy and Y. Zhao, *Chemical Society Reviews*, 2013, **42**, 7117-7129.
122. Y. Huang, R. Dong, X. Zhu and D. Yan, *Soft Matter*, 2014, **10**, 6121-6138.
123. L. Li, J. M. Scheiger and P. A. Levkin, *Advanced Materials*, 2019, **31**, 1807333.
124. I. Tomatsu, K. Peng and A. Kros, *Advanced Drug Delivery Reviews*, 2011, **63**, 1257-1266.
125. Y. Wang, S. Zhang and J. Wang, *Chinese Chemical Letters*, 2021, **32**, 1603-1614.
126. L. Pezzana, E. Malmström, M. Johansson and M. Sangermano, *Polymers*, 2021, **13**, 1530.
127. T. Hughes, G. P. Simon and K. Saito, *Materials Horizons*, 2019, **6**, 1762-1773.
128. H. Lai, J. Zhang and P. Xiao, *ACS Sustainable Chemistry & Engineering*, 2023, **11**, 16365-16406.
129. R. L. Atkinson, O. R. Monaghan, M. T. Elsmore, P. D. Topham, D. T. Toolan, M. J. Derry, V. Taresco, R. A. Stockman, D. S. De Focatiis and D. J. Irvine, *Polymer Chemistry*, 2021, **12**, 3177-3189.
130. M. A. Hillmyer and W. B. Tolman, *Accounts of Chemical Research*, 2014, **47**, 2390-2396.
131. S. E. Woods, J. D. Tinkler, N. Bensabeh, M. Palà, S. J. Martin, I. Martin-Fabiani, G. Lligadas and F. L. Hatton, *ACS Sustainable Chemistry & Engineering*, 2023, **11**, 9979-9988.
132. K. Alfonsi, J. Colberg, P. J. Dunn, T. Fevig, S. Jennings, T. A. Johnson, H. P. Kleine, C. Knight, M. A. Nagy and D. A. Perry, *Green Chemistry*, 2008, **10**, 31-36.
133. F. Coumes, M. Balarezo, J. Rieger and F. Stoffelbach, *Macromolecular Rapid Communications*, 2020, **41**, 2000002.
134. N. A. Stini, P. L. Gkizis and C. G. Kokotos, *Green Chemistry*, 2022, **24**, 6435-6449.
135. I. Zaborniak, M. Klamut, C. M. Warne, K. Kisiel, M. Niemiec, P. Błoniarz, A. Pellis, K. Matyjaszewski and P. Chmielarz, *ACS Sustainable Chemistry & Engineering*, 2024, **12**, 4933-4945.
136. A. Marathianos, E. Liarou, E. Hancox, J. L. Grace, D. W. Lester and D. M. Haddleton, *Green Chemistry*, 2020, **22**, 5833-5837.
137. J. E. Camp, *ChemSusChem*, 2018, **11**, 3048-3055.
138. T. Marino, F. Galiano, A. Molino and A. Figoli, *Journal of Membrane Science*, 2019, **580**, 224-234.
139. O. J. Harris, R. Larder, B. Jordan, I. Prior, R. El-Khoury, K. O. Sebakhy and F. Hatton, *Chemical Communications*, 2024.
140. U. Azzena, M. Carraro, L. Pisano, S. Monticelli, R. Bartolotta and V. Pace, *ChemSusChem*, 2019, **12**, 40-70.
141. V. Pace, P. Hoyos, L. Castoldi, P. Domínguez de María and A. R. Alcántara, *ChemSusChem*, 2012, **5**, 1369-1379.

142. C. S. M. Pereira, V. M. T. M. Silva and A. E. Rodrigues, *Green Chemistry*, 2011, **13**, 2658-2671.
143. A. Quintavalla, D. Carboni, C. Sepe, L. Mummolo, N. Zaccheroni and M. Lombardo, *Advanced Synthesis & Catalysis*, 2023, **365**, 252-262.
144. B. Hahn-Hägerdal, M. Galbe, M. F. Gorwa-Grauslund, G. Lidén and G. Zacchi, *Trends in Biotechnology*, 2006, **24**, 549-556.
145. A. Kumar, M. Saha, R. Vishwakarma, K. Behera and S. Trivedi, *Journal of Molecular Liquids*, 2024, **410**, 125642.
146. M. J. Earle and K. R. Seddon, *IUPAC Pure and Applied Chemistry*, 2000, **72**, 1391-1398.
147. S. Mallakpour and M. Dinari, in *Green Solvents II: Properties and Applications of Ionic Liquids*, eds. A. Mohammad and D. Inamuddin, Springer Netherlands, Dordrecht, 2012, pp. 1-32.
148. Z. Lei, B. Chen, Y.-M. Koo and D. R. MacFarlane, *ACS Publications*, 2017, **117**, 6633-6635.
149. A. Ray and B. Saruhan, *Materials*, 2021, **14**, 2942.
150. M. Hasib-ur-Rahman, M. Siaj and F. Larachi, *Chemical Engineering and Processing: Process Intensification*, 2010, **49**, 313-322.
151. N. Nasirpour, M. Mohammadpourfard and S. Zeinali Heris, *Chemical Engineering Research and Design*, 2020, **160**, 264-300.
152. S. A. Forsyth, J. M. Pringle and D. R. MacFarlane, *Australian Journal of Chemistry*, 2004, **57**, 113-119.
153. A. J. Greer, J. Jacquemin and C. Hardacre, *Molecules*, 2020, **25**, 5207.
154. H. Ohno, *Bulletin of the Chemical Society of Japan*, 2006, **79**, 1665-1680.
155. V. I. Pârvulescu and C. Hardacre, *Chemical Reviews*, 2007, **107**, 2615-2665.
156. T. Welton, *Chemical reviews*, 1999, **99**, 2071-2084.
157. Y. Lee, G. Lee, J. Cho, B. Choi, N. G. Han and D. K. Kim, *Case Studies in Thermal Engineering*, 2023, **45**, 102920.
158. D. Lovrec, R. Kalb and V. Tič, *Applied Sciences*, 2024, **14**, 2187.
159. S. Kosiński, I. Rykowska, M. Gonsior and P. Krzyżanowski, *Polymer Testing*, 2022, **112**, 107649.
160. Y. Zhou and J. Qu, *ACS Applied Materials & Interfaces*, 2017, **9**, 3209-3222.
161. T. Beyersdorff, F. Stiemke and T. Schubert, 2012.
162. M. Talebi, R. A. Patil and D. W. Armstrong, *Commercial Applications of Ionic Liquids*, 2020, 131-165.
163. B. E. Lee, L. A. DiCecco, H. Exir, A. Weck, K. N. Sask and K. Grandfield, *ChemBioChem*, 2021, **22**, 571-576.
164. D. Wei and A. Ivaska, *Analytica Chimica Acta*, 2008, **607**, 126-135.
165. A. P. Abbott, G. Frisch and K. S. Ryder, *Annual Review of Materials Research*, 2013, **43**, 335-358.
166. G. Yang, Y. Song, Q. Wang, L. Zhang and L. Deng, *Materials & Design*, 2020, **190**, 108563.
167. K. Zhang, X. Zhang, K. G. Brooks, B. Ding, S. Kinge, Y. Ding, S. Dai and M. K. Nazeeruddin, *Solar Rrl*, 2023, **7**, 2300115.
168. H. Nawaz and F. Xu, in *Encyclopedia of Ionic Liquids*, Springer, 2023, pp. 1266-1271.
169. J. Lu, F. Yan and J. Texter, *Progress in Polymer Science*, 2009, **34**, 431-448.
170. W. F. Elmobarak, F. Almomani, M. Tawalbeh, A. Al-Othman, R. Martis and K. Rasool, *Fuel*, 2023, **344**, 128102.
171. T. Christoff-Tempesta and T. H. Epps, 3rd, *ACS Macro Lett*, 2023, **12**, 1058-1070.
172. T. Abbas, G. Gonfa, K. C. Lethesh, M. I. A. Mutalib, M. b. Abai, K. Y. Cheun and E. Khan, *Fuel*, 2016, **177**, 296-303.
173. L. M. Haverhals, M. P. Foley, E. K. Brown, D. M. Fox, H. C. De Long and P. C. Trulove, in *Ionic Liquids: Science and Applications*, American Chemical Society, 2012, vol. 1117, ch. 6, pp. 145-166.

174. B. Wu, W. Liu, Y. Zhang and H. Wang, *Chemistry–A European Journal*, 2009, **15**, 1804-1810.
175. J. Fraga-Dubreuil, K. Bourahla, M. Rahmouni, J. P. Bazureau and J. Hamelin, *Catalysis Communications*, 2002, **3**, 185-190.
176. A. R. S. Santha Kumar, M. Roy and N. K. Singha, *European Polymer Journal*, 2018, **107**, 294-302.
177. R. T. Carlin, R. A. Osteryoung, J. S. Wilkes and J. Rovang, *Inorganic Chemistry*, 1990, **29**, 3003 - 3009.
178. N. K. Singha, K. Hong and J. W. Mays, in *Polymerized Ionic Liquids*, ed. A. Eftekhari, The Royal Society of Chemistry, 2017.
179. N. Winterton, *Journal of Materials Chemistry*, 2006, **16**, 4281-4293.
180. V. Strehmel, A. Laschewsky, H. Wetzel and E. Görnitz, *Macromolecules*, 2006, **39**, 923-930.
181. P. Kubisa, *European Polymer Journal*, 2020, **133**, 109778.
182. P. Kubisa, *Journal of Polymer Science Part A: Polymer Chemistry*, 2005, **43**, 4675-4683.
183. M. Zhu and Y. Yang, *Green Chemistry*, 2024, **26**, 5022 - 5102.
184. C. Liao, R. Liu, X.-s. Hou, X.-g. Sun and S. Dai, *New Carbon Materials*, 2014, **29**, 78-80.
185. J. Yuan and M. Antonietti, *Polymer*, 2011, **52**, 1469-1482.
186. R. Tamate, K. Hashimoto, T. Ueki and M. Watanabe, *Physical Chemistry Chemical Physics*, 2018, **20**, 25123-25139.
187. F. Ghorbanizamani, H. Moulahoum, F. Zihnioglu and S. Timur, *Journal of Molecular Liquids*, 2021, **323**, 115076.
188. Y. He, Z. Li, P. Simone and T. P. Lodge, *Journal of the American Chemical Society*, 2006, **128**, 2745-2750.
189. Y. He, P. G. Boswell, P. Bühlmann and T. P. Lodge, *The Journal of Physical Chemistry B*, 2007, **111**, 4645-4652.
190. T. P. Lodge and T. Ueki, *Accounts of Chemical Research*, 2016, **49**, 2107-2114.

2. Transparent dispersions of diblock copolymer nanoparticles via RAFT emulsion polymerisation in ionic liquid

2.1 Introduction

Block copolymers represent a broad class of macromolecules which are commonly researched and utilised across many fields due to their unique physical and chemical properties[1-3]. There are many examples of block copolymer structures, the simplest being an AB diblock copolymer which is comprised of two segments (or blocks) of covalently bonded monomer units linked in a linear polymer chain[1, 4, 5]. Within the literature, such block copolymers have been shown to self-assemble into nanostructures in a range of different solvents, including examples in polar and non-polar media, as well as ionic liquids[6-9].

Ionic liquids (ILs) are compounds made up entirely of ions typically with melting points below 100 °C[7, 10]. In contrast to conventional solvents, ILs have many advantageous and unique physicochemical properties including non-flammability, high conductivity, non-volatility, recyclability and good thermal stability[11]. This, combined with the vast variety of possible anion and cation combinations allows for numerous applications of ionic liquids in solvent chemistry, catalysis, and electrochemistry[12-14] as well as their additional ability to function as performance additives such as anti-static[15, 16] and dispersing agents[17, 18]. ILs serving as an environmentally friendly alternative choice to reduce the use of traditional organic solvents have become increasingly popular[19, 20], with their application also extending to the field of polymer chemistry[21-23]. Previous work has reported that polymerisation reactions in ILs occur faster, which is attributed to factors such as increased viscosity and polarity of the system which reduces the rate of termination and increases propagation, respectively[24-26]. ILs also have the potential to be recycled after multiple reactions, and have been shown to not significantly affect polymer conversion [27].

Over the past 20 years, reversible addition–fragmentation chain transfer (RAFT) polymerisation has become a widely used reversible deactivation radical polymerisation (RDRP) technique to synthesise polymers, specifically well-defined block copolymers, which can be used in a broad range of applications[28, 29]. Self-assembly of such block copolymers allows different morphologies to be obtained however, post-polymerisation processing such as solvent pH switching and film rehydration is required[8, 30]. Polymerisation-induced self-assembly (PISA) removes this requirement of additional processing steps, and enables syntheses to be conducted at higher concentrations (up to 50 w/w%) [31]. The process typically involves the chain extension of a solvophilic macromolecular chain transfer agent (macro-CTA) using a selected monomer that will form an insoluble polymer block. This promotes the *in situ* formation of a range of sterically stabilised nano-objects, mainly

spheres, worms or vesicles, due to the self-assembly of the AB diblock copolymer chains[32]. Reactions can occur via either dispersion[30, 33-40] or emulsion[41-43] polymerisation, where the added monomer is miscible or immiscible with the solvent for dispersion or emulsion PISA, respectively. Combining RAFT with PISA leads to a more versatile technique for the preparation of dispersions of block copolymer nano-objects, and RAFT-mediated PISA is frequently employed due to its high compatibility with a range of monomers, solvents (water, polar solvents or non-polar media[44]) and reaction conditions[45-47].

There are many reports of RAFT-mediated PISA in literature, however there are very few reports of PISA syntheses being conducted in ILs. Additionally, it should be noted that all reports of RAFT-mediated PISA conducted in ILs are examples of dispersion polymerisations. This type of reaction was first reported by Zhang and Zhu[39] whereby a trithiocarbonate terminated poly(ethylene glycol) (PEG) macro-CTA was chain extended using styrene (St), *n*-butyl methacrylate (BuMA) or 2-hydroxyethyl methacrylate (HEMA) in the imidazolium-based IL 1-butyl-3-methylimidazolium hexafluorophosphate, [BMIM][PF_6]. This study demonstrated the use of ILs as a solvent for RAFT dispersion PISA syntheses to form spherical nanoparticles (spherical micelles or vesicles), as confirmed by transmission electron microscopy (TEM). This was further demonstrated by Zhou[40] when focusing on the effect of solvents for the synthesis of a PEG-*b*-PSt diblock copolymer by using either [EMIM][PF_6], methanol or a methanol/water mixture. Again, TEM successfully showed the formation of spherical nano-objects (spherical and vesicular morphologies). Additionally, it was shown that using IL as a solvent increased the rate of polymerisation, with 95% monomer conversion being achieved in 12 hours, whereas syntheses in methanol and methanol/water mixtures only achieved 20% and 65%, respectively, for the same duration. Yamanaka *et al.*[38] recently reported on the first PISA formulation yielding ionogels formed from the self-assembly of ABA triblock copolymers in IL, which was studied using *in situ* small-angle X-ray scattering (SAXS) and rheology. It was demonstrated that after the initial induction period, the gelation process occurs alongside self-assembly, producing interconnected spherical domains. In addition to this, Yamanaka *et al.*[48] used terminally functionalised star PEGs to polymerise St monomers in [EMIM][PF_6] using PISA, consequently producing a gel. Hexagonally packed cylinder (HEX) and hexagonal close-packed sphere (HCP) structures were obtained from 2-arm PEG-PSt and 4/8-arm PEG-PSt, respectively[48]. Maitland *et al.*[37] have recently established the synthesis of AB diblock copolymers via RAFT dispersion PISA in ILs as a direct route to worm gels in IL, or worm ionogels, which have significant potential for use as gel electrolytes. In this prior study, a poly(2-hydroxyethyl

methacrylate) (PHEMA) macro-CTA was successfully chain extended with benzyl methacrylate (BzMA) in 1-ethyl-3-methylimidazolium dicyanamide, [EMIM][DCA], to form worm morphologies, and thus a free-standing ionogel, as confirmed using SAXS and TEM. Electrochemical studies demonstrated significant potential for use in energy storage applications since the bulk resistance of the worm ionogel formed was comparable to that of the IL alone.

This chapter focuses on emulsion polymerisations *via* RAFT-mediated PISA in ILs which generate transparent dispersions containing spherical morphologies. The refractive index of a material can be defined as a dimensionless number related to the speed of light when it passes through a dielectric medium[49]. Snell's law states that when light travels between two media with the same refractive index values, no refraction will occur[50], which results in optical transparency. The synthesis of transparent nanoparticle-containing dispersions has been explored in the literature. Examples include work conducted by György *et al.*[33], where it was found that the transparency of the resulting nanoparticle-containing solutions was dependant on different solvents at different temperatures. In addition to this, Thompson *et al.*[51] and Rymaruk *et al.*[41] have also demonstrated isorefractivity, using Pickering emulsions which contained anisotropic and spherical morphologies. The development of an emulsion-based polymerisation formulation in ILs that yields transparent solutions due to matched refractive index values demonstrates how ILs provide many advantages over traditional solvents (decreased reaction time, lower flammability and ability to form nanostructures in transparent dispersions).

Herein, we report for the first time a RAFT-mediated emulsion PISA formulation in IL. Moreover, this system yields highly transparent (≥ 95% transmittance at 700 nm) dispersions of diblock copolymer nanoparticles even when particle diameters exceed 100 nm. Specifically, poly(2-hydroxyethyl methacrylate)-*b*-poly(*n*-butyl methacrylate) (PHEMA-*b*-PBuMA) diblock copolymer nanoparticles were synthesised *via* RAFT emulsion polymerisation in 1-ethyl-3-methylimidazolium ethyl sulfate, [EMIM][$EtOSO_3$] (Scheme 1). Detailed molecular and nanoparticle characterisation was conducted using ^{1}H nuclear magnetic resonance (NMR) spectroscopy, gel permeation chromatography (GPC), dynamic light scattering (DLS), transmission electron microscopy (TEM), small-angle X-ray scattering (SAXS) and ultraviolet-visible light (UV-vis) spectroscopy.

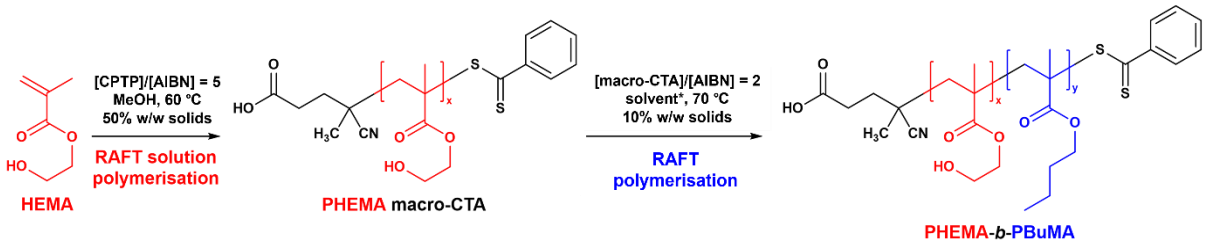

***Scheme 1**. Synthesis of poly(2-hydroxyethyl methacrylate) (PHEMA) macromolecular chain transfer agent (macro-CTA) via RAFT solution polymerisation in methanol at 60 °C, followed by RAFT polymerisation of n-butyl methacrylate (BuMA) in a range of solvents (* = 1-ethyl-3-methylimidazolium ethyl sulfate ([EMIM][EtOSO$_3$]), N,N-dimethylformamide (DMF) and an ethanol-water mixture (EtOH:H$_2$O, 4:1 w:w)) at 70 °C to yield PHEMA$_x$-b-PBuMA$_y$ diblock copolymers.*

2.2 Experimental

2.2.1 Materials

2-Hydroxyethyl methacrylate (HEMA) and *n*-butyl methacrylate (BuMA) were purchased from Sigma Aldrich and passed through a basic alumina column prior to use to remove the inhibitor. 2,2′-Azobisisobutyronitrile (AIBN) was purchased from Molekula and recrystallised from methanol prior to use. 4-Cyano-4-(phenylcarbonothioylthio) pentanoic acid (CPTP) RAFT agent and 1-ethyl-3-methylimidazolium ethyl sulfate ([EMIM][EtOSO$_3$]) were purchased from Sigma Aldrich and used as received. Reagent grade methanol, diethyl ether and *N,N*-dimethylformamide (DMF) were purchased from Fisher Scientific. Dimethyl sulfoxide-d6 (DMSO-d6), methanol-d4 (MeOD-d4), acetone-d6 ((CD$_3$)$_2$CO-d6) and chloroform-d (CDCl$_3$) for ^{1}H NMR analysis were purchased from Cambridge Isotope Laboratories.

2.2.2 ^{1}H Nuclear magnetic resonance (NMR) spectroscopy

^{1}H Nuclear magnetic resonance (NMR) spectroscopy was employed to examine the chemical structures of samples. These were prepared in MeOD-d4, CDCl$_3$, (CD$_3$)$_2$CO-d6 or DMSO-d6 solvents by dissolving approximately 15 mg of sample in 1 mL of solvent and agitating on a vortex mixer until dissolved. They were then processed using a Bruker Avance Neo 300 MHz spectrometer for 16 scans, with the subsequent spectra being analysed using TopSpin 4.2.0.

2.2.3 Gel permeation chromatography (GPC)

Gel permeation chromatography (GPC) was used to analyse the molecular weight distribution of the synthesised polymers, with the obtained traces being used to calculate the number average molar mass (M_n), weight average molar mass (M_w), and dispersity ($Đ$, M_w/M_n) of each sample. The eluent solution used was HPLC grade DMF containing a 0.10% w/v lithium bromide additive, in which samples were prepared. The Agilent Infinity II multi-detector GPC instrument was equipped with a single guard column and two PL gel mixed-C columns and was held at a constant flow rate of 1.0 mL min^{-1} and ran at a temperature of 40 °C. The system was calibrated with near monodisperse poly(methyl methacrylate) standards (M_p range = 535 – 1,591,000 g mol^{-1}) and experimental data was analysed using Agilent GPC/SEC software.

2.2.4 Differential light scattering (DLS)

Dynamic light scattering (DLS) studies were conducted using a Zetasizer Nano ZS instrument (Malvern Panalytical, UK) at a fixed scattering angle of 173°. The block copolymer dispersions were diluted in [EMIM][$EtOSO_3$] (refractive index = 1.48 as determined by A. P. Fröba *et al.*,[52] viscosity = 94.2 cP) to 0.10% w/w prior to light scattering studies at 25 °C. The polydispersity index (PDI) and average diameter (D) were calculated, and data was averaged over three sets of approximately thirteen runs each of 30 seconds duration.

2.2.5 Transmission electron microscopy (TEM)

Bright field transmission electron microscopy (TEM) imaging was conducted using a JEOL2100 microscope operating at 200 kV. Prior to analysis, block copolymer dispersions were diluted with [EMIM][$EtOSO_3$] to 0.10% w/w and 10 µL of this solution was deposited on lacey carbon coated copper grids, blotted using filter paper and allowed to dry for 4 days at ambient conditions. No staining agent was required. These images were obtained by Dr Evelina Liarou (University of Warwick).

2.2.6 Small-angle X-ray scattering (SAXS)

Small-angle X-ray scattering (SAXS) patterns were recorded for 1.0% w/w block copolymer dispersions in [EMIM][$EtOSO_3$] in 1.5 mm diameter polycarbonate capillaries at a synchrotron source (beamline B21, Diamond Light Source, UK[53]) using monochromatic X-ray radiation (X-ray wavelength λ = 0.9464 Å, sample-to-detector distance of 3.685 m corresponding to scattering vector q ranging from 0.0045 to 0.34 $Å^{-1}$) and an EigerX 4M detector (Dectris, Switzerland). Scattering data were reduced using standard protocols from the beamline and were further analysed using Irena SAS macros for Igor Pro[54]. Background-subtracted SAXS data were fitted to a spherical micelle model as detailed below. These data fits were conducted by Dr Georgia L. Maitland (Aston University).

In general, the intensity of X-rays scattered by a dispersion of nano-objects [as represented by the scattering cross-section per unit sample volume, $\frac{d\Sigma}{d\Omega}(q)$] can be expressed as:

$$\frac{d\Sigma}{d\Omega}(q) = NS(q)\int_0^\infty \dots \int_0^\infty F(q, r_{1,} \dots, r_k)^2 \Psi(r_{1,} \dots, r_k) dr_{1,} \dots, dr_k \qquad \textbf{2.1}$$

where $F(q, r_1, \dots, r_k)$ is the form factor, $r_{1,} \dots, r_k$ is a set of k parameters describing the structural morphology, $\Psi(r_{1,} \dots, r_k)$ is the distribution function, $S(q)$ is the structure factor and N is the number density of nano-objects per unit volume expressed as:

$$N = \frac{\varphi}{\int_0^\infty \dots \int_0^\infty V(r_1, \dots, r_k)\Psi(r_1, \dots, r_k) dr_1, \dots, dr_k} \qquad \textbf{2.2}$$

where $V(r_1, \dots, r_k)$ is the volume of the nano-object and φ is its volume fraction within the dispersion. It is assumed that $S(q)$ = 1 at the sufficiently low copolymer concentrations used in this study (1.0% w/w).

The spherical micelle form factor for Equation 2.1 is given by[55]:

$$F_{s_{mic}}(q) = N_s{}^2\beta_s{}^2A_s{}^2(q,R_s) + N_s\beta_c{}^2F_c(q,R_g) + N_s(N_s-1)\beta_c{}^2A_c{}^2(q) + 2N_s{}^2\beta_s\beta_cA_s(q,R_s)A_c(q) \quad \textbf{2.3}$$

where R_s is the volume-average sphere core radius and R_g is the radius of gyration of the coronal steric stabilizer block. The X-ray scattering length contrasts for the core and corona blocks are given by $\beta_s = V_s(\xi_s - \xi_{sol})$ and $\beta_c = V_c(\xi_c - \xi_{sol})$ respectively. Here, ξ_s, ξ_c and ξ_{sol} are the X-ray scattering length densities of the core block (ξ_{PBuMA}= 9.39 x 10^{10} cm^{-2}), corona block (ξ_{PHEMA}= 11.31 x 10^{10} cm^{-2}) and [EMIM][$EtOSO_3$] solvent (ξ_{sol}= 9.10 x 10^{10} cm^{-2}), respectively. V_s and V_c are the volumes of the core block (V_{PBuMA}) and the corona block (V_{PHEMA}), respectively. The sphere form factor amplitude is used for the amplitude of the core self-term:

$$A_c(q,R_s) = \Phi(qR_s)\exp\left(-\frac{q^2\sigma^2}{2}\right) \quad \textbf{2.4}$$

where $\Phi(qR_s) = \frac{3[\sin(qR_s) - qR_s\cos(qR_s)]}{(qR_s)^3}$. A sigmoidal interface between the two blocks was assumed for the spherical micelle form factor (Equation 2.3). This is described by the exponent term with a width σ accounting for a decaying scattering length density at the micellar interface. This σ value was fixed at 2.5 during fitting.

The form factor amplitude of the spherical micelle corona is:

$$A_c(q) = \frac{\int_{R_s}^{R_s+2s}\mu_c(r)\frac{\sin(qr)}{qr}r^2dr}{\int_{R_s}^{R_s+2s}\mu_c(r)r^2dr}exp\left(-\frac{q^2\sigma^2}{2}\right) \quad \textbf{2.5}$$

The radial profile, $\mu_c(r)$, can be expressed by a linear combination of two cubic b splines, with two fitting parameters s and a corresponding to the width of the profile and the weight coefficient respectively. This information can be found elsewhere[56, 57], as can the approximate integrated form of Equation 2.5. The self-correlation term for the coronal block is given by the Debye function:

$$F_c(q, R_g) = \frac{2\left[\exp\left(-q^2 {R_g}^2\right) - 1 + q^2 {R_g}^2\right]}{q^4 {R_g}^4} \quad \textit{2.6}$$

where R_g is the radius of gyration of the PHEMA coronal block.

The aggregation number, N_s, of the spherical micelle is given by:

$$N_s = (1 - x_{sol}) \frac{\frac{4}{3}\pi {R_s}^3}{V_s} \quad \textit{2.7}$$

where x_{sol} is the volume fraction of solvent within the PBuMA micelle cores, which was found to be zero in all cases. A polydispersity for one parameter (R_s) is assumed for the micelle model, which is described by a Gaussian distribution. Thus, the polydispersity function in Equation 2.1 can be represented as:

$$\Psi(r_1) = \frac{1}{\sqrt{2\pi {\sigma_{Rs}}^2}} exp\left(-\frac{(r_1 - R_s)^2}{2{\sigma_{Rs}}^2}\right) \quad \textit{2.8}$$

where σ_{Rs} is the standard deviation for R_s. In accordance with Equation 2.2, the number density per unit volume for the micelle model is expressed as:

$$N = \frac{\varphi}{\int_0^\infty V(r_1)\Psi(r_1)dr_1} \quad \textit{2.9}$$

where φ is the total volume fraction of copolymer in the spherical micelles and $V(r_1)$ is the total volume of copolymer within a spherical micelle [$V(r_1) = (V_s + V_c)N_s(r_1)$].

2.2.7 Ultraviolet visible spectroscopy

Ultraviolet-visible (UV-Vis) spectra were recorded in absorbance mode between 800 and 400 nm for 10% w/w block copolymer dispersions/solutions synthesised in [EMIM][$EtOSO_3$], DMF and EtOH/H_2O mixtures, using an Implen NanoPhotometer® C40. Reference absorption was based on the pure solvent in each case, and subsequent solutions were prepared as 10% w/w basis for all samples and analysed in single use polystyrene cuvettes.

2.2.8 Synthesis of poly(2-hydroxyethyl methacrylate) macromolecular chain transfer agent via RAFT solution polymerisation

The synthesis of a $PHEMA_{77}$ macro-CTA at 50% w/w solids was conducted as follows. A 100 mL round-bottomed flask was charged with 2-hydroxyethyl methacrylate (HEMA; 15.0 g; 115 mmol), 4-cyano-4-(phenylcarbonothioylthio)pentanoic acid (CPTP; 0.645 g; 2.31 mmol), 2,2′-azobisisobutyronitrile (AIBN; 75.7 mg; 0.461 mmol; CPTP/AIBN molar ratio = 5.0) and methanol (15.7 g). The sealed reaction flask was purged with nitrogen for 30 minutes prior to being placed in a preheated aluminium block at 60 °C and stirred for 6 hours (Scheme 2). The resulting PHEMA (HEMA conversion = 65% (Figure 2.1), M_n = 8 900 g mol^{-1}, $Đ_M$ = 1.19 (Figure 2.11)) was purified by twice precipitating into a ten-fold excess of diethyl ether and dried on a rotary evaporator until all solvent was removed as judged by ^1H NMR spectroscopy. The resulting PHEMA macro-CTA was obtained as a pink solid.

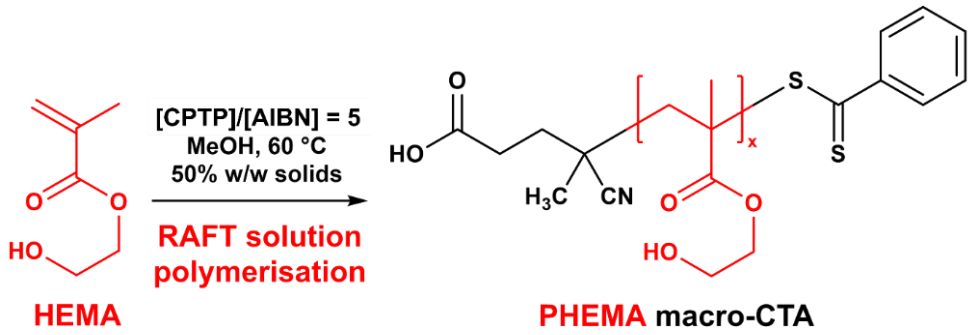

Scheme 2. *Synthesis of poly(2-hydroxyethyl methacrylate) (PHEMA) macro-CTA via RAFT solution polymerisation in methanol at 60 °C.*

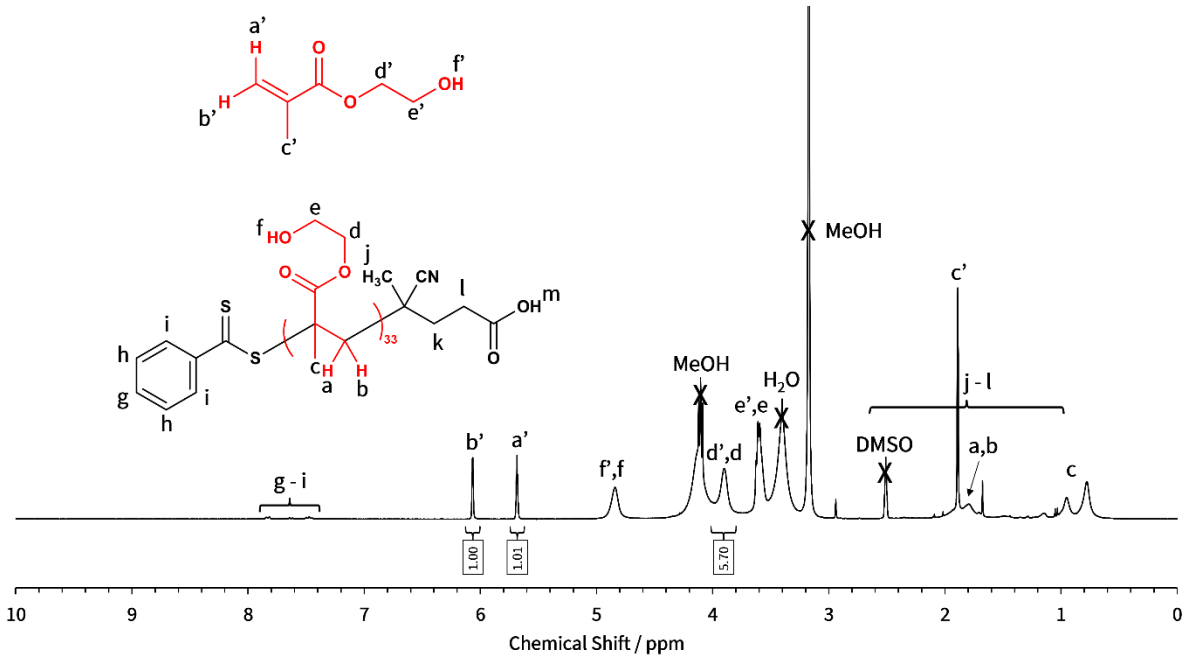

Figure 2.1. *Assigned ^{1}H NMR spectrum of crude PHEMA macro-CTA in DMSO-d6.*

$$I_p = [integral(d')] = 2H \qquad \textbf{2.10}$$

$$I_m = [integral(d)] \qquad \textbf{2.11}$$

$$conversion\ (\%) = \frac{(I_m + I_p) - 2}{I_m + I_p} \times 100 = \frac{5.70 - 2}{5.70} \times 100 = \mathbf{65\%}\ (2s.f.) \qquad \textbf{2.12}$$

The mean degree of polymerisation (DP) of this macro-CTA was calculated to be 77 using ^{1}H NMR spectroscopy by comparing the integrated signals corresponding to the five CPTP aromatic protons (g – i) at 7.2–8.0 ppm relative to the peak at 3.8–4.0 ppm (d/d') corresponding to the two oxymethylene protons of PHEMA (Figure 2.2).

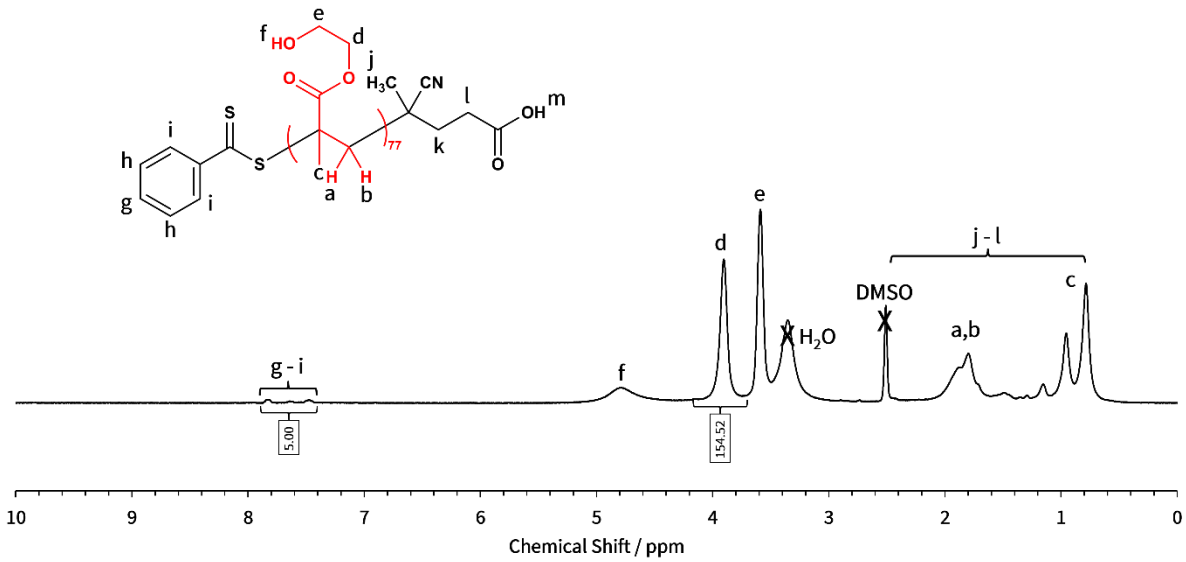

Figure 2.2. *Assigned ^{1}H NMR spectrum of purified PHEMA$_{77}$ macro-CTA in DMSO-d6.*

The DP of the PHEMA macro-CTA and the CTA efficiency was calculated using the following equations:

$$[integral(g - i)] = 5H \qquad \textbf{2.13}$$

$$PHEMA\ DP = \frac{[integral(d)]}{2} = \frac{154.2}{2} = \mathbf{77} \qquad \textbf{2.14}$$

$$\%\ CTA\ Efficiency = \frac{Target\ DP \times NMR\ conversion}{Actual\ PHEMA\ DP} \times 100 = \frac{50 \times 0.65}{77} \times 100 = \mathbf{42\%}\ (2s.f.) \qquad \textbf{2.15}$$

A PHEMA$_{21}$ macro-CTA using the same methodology was synthesised by a colleague (Dr Georgia L. Maitland [Aston University]) and kindly provided for use in this research (Figure 2.3 and Figure 2.4).

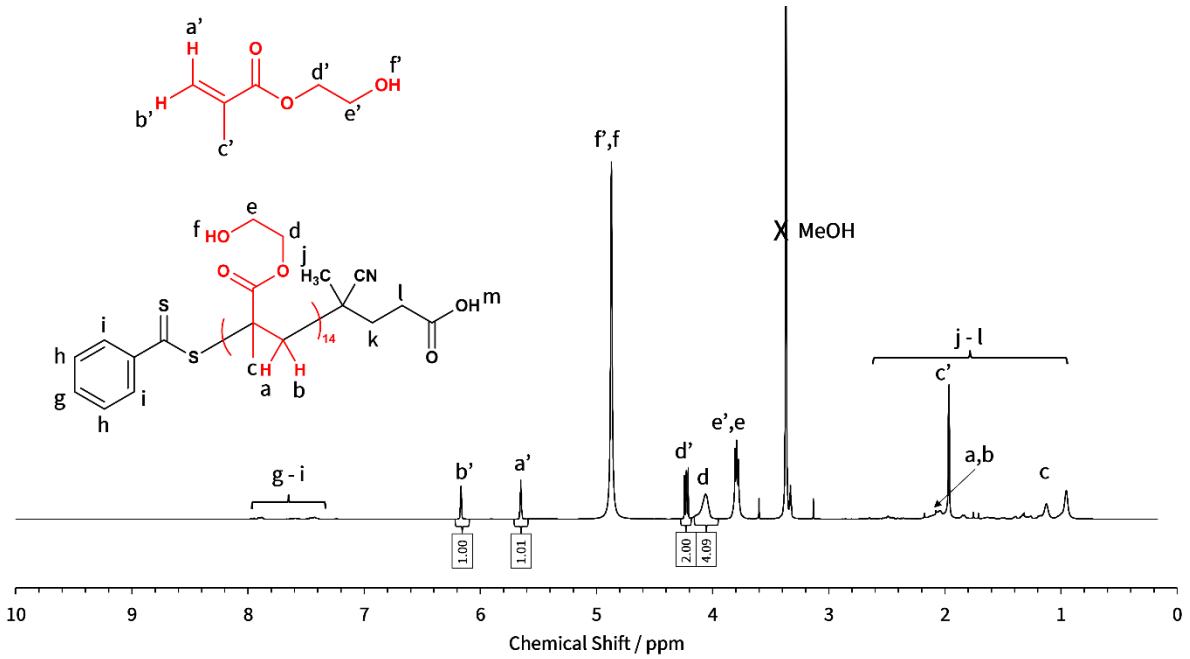

Figure 2.3. *Assigned ^{1}H NMR spectrum of crude PHEMA macro-CTA in MeOD-d4.*

$$I_p = [integral(d')] = 2H \qquad \textbf{2.16}$$

$$I_m = [integral(d)] \qquad \textbf{2.17}$$

$$conversion\ (\%) = \frac{I_p}{I_m + I_p} \times 100 = \frac{4.09}{2.00+4.09} \times 100 = \mathbf{67\%}\ (2s.f.) \qquad \textbf{2.18}$$

The mean degree of polymerisation (DP) of this macro-CTA was calculated to be 21 using ^{1}H NMR spectroscopy by comparing the integrated signals corresponding to the five CPTP aromatic protons (g – i) at 7.2–8.0 ppm relative to the peak at 4.0–4.2 ppm (d/d') corresponding to the two oxymethylene protons of PHEMA (Figure 2.4).

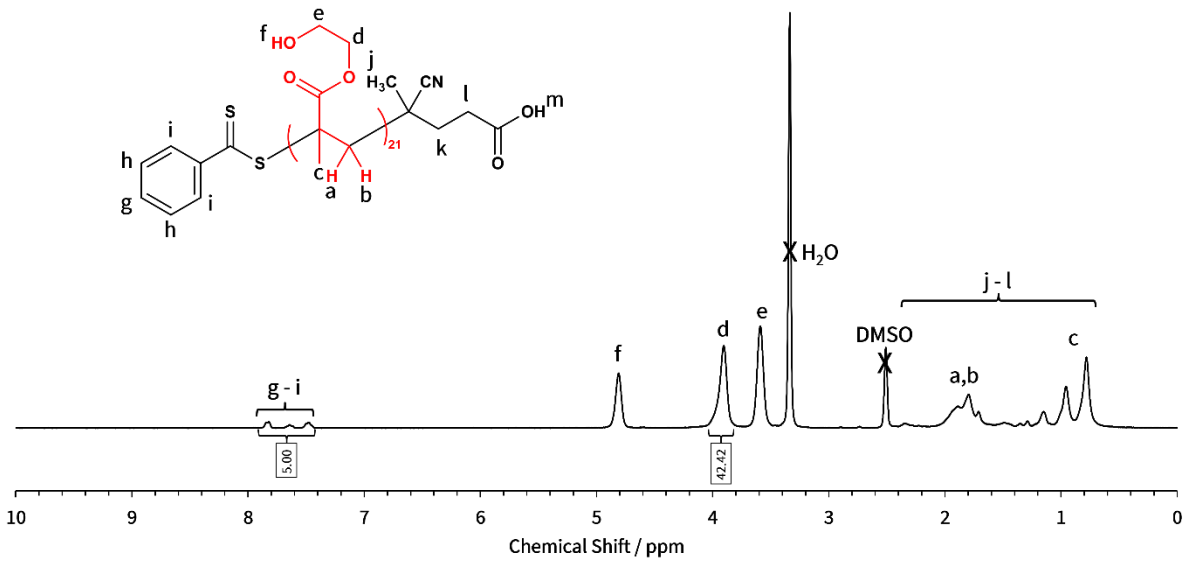

Figure 2.4. *Assigned ^{1}H NMR spectrum of purified $PHEMA_{21}$ macro-CTA in DMSO-d6.*

$$[integral(g - i)] = 5H \qquad \textbf{2.19}$$

$$PHEMA\ DP = \frac{[integral(d)]}{2} = \frac{42.42}{2} = \mathbf{21} \qquad \textbf{2.20}$$

$$\%\ CTA\ Efficiency = \frac{Target\ DP \times NMR\ conversion}{Actual\ PHEMA\ DP} \times 100 = \frac{20 \times 0.67}{21} \times 100 = \mathbf{64\%}\ (2s.f.) \qquad \textbf{2.21}$$

2.2.9 Synthesis of poly(2-hydroxyethyl methacrylate)-*block*-poly(n-butyl methacrylate) (PHEMA-*b*-PBuMA) diblock copolymers

2.2.9.1 Synthesis of poly(2-hydroxyethyl methacrylate)-block-poly(n-butyl methacrylate) (PHEMA-b-PBuMA) diblock copolymer via RAFT emulsion polymerisation in 1-ethyl-3-methylimidazolium ethyl sulfate

A typical RAFT emulsion polymerisation for the synthesis of $PHEMA_{21}$–*b*–$PBuMA_{96}$ at 10% w/w solids was conducted as follows. *n*-Butyl methacrylate (BuMA; 0.49 g; 3.45 mmol), 2,2′-azobisisobutyronitrile (AIBN; 2.8 mg; 24.3 µmol), $PHEMA_{21}$ macro-CTA (0.10 g; 34.5 µmol;

macro-CTA/initiator molar ratio = 2.0; PBuMA target DP = 100) and 1-ethyl-3-methylimidazolium ethyl sulfate ([EMIM][$EtOSO_3$]; 5.38 g) were added to a 14 mL sample vial. The sealed reaction mixture was purged with nitrogen for 30 minutes prior to being placed in a preheated aluminium block at 70 °C whilst stirring for 2 hours (BuMA conversion = 96% (Figure 2.5 and Figure 2.6); M_n = 7 000 g mol^{-1}, $Đ_M$ = 1.26).

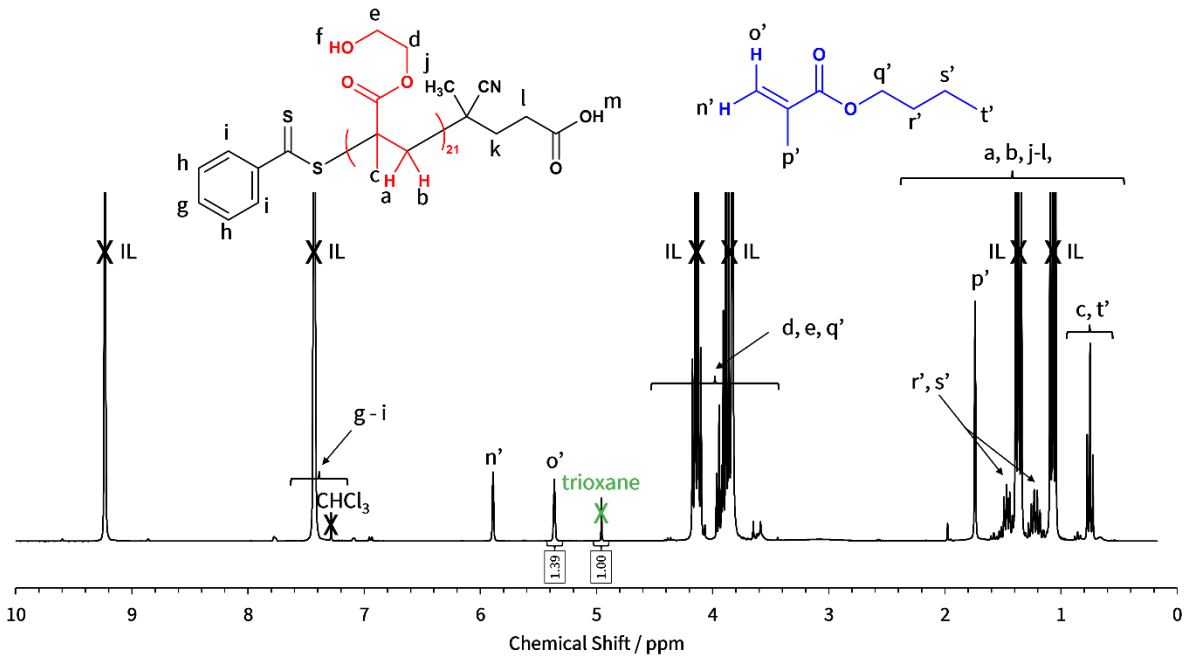

Figure 2.5. *Assigned ^{1}H NMR spectrum of target $PHEMA_{21}$-b-$PBuMA_{100}$ (with [EMIM][$EtOSO_3$] as the reaction solvent) before the polymerisation reaction. NMR solvent = $CDCl_3$, trioxane = reference peak.*

Integral(trioxane)] = Reference Peak = 1 ***2.22***

[integral(o')] = 1H = 1.39 ***2.23***

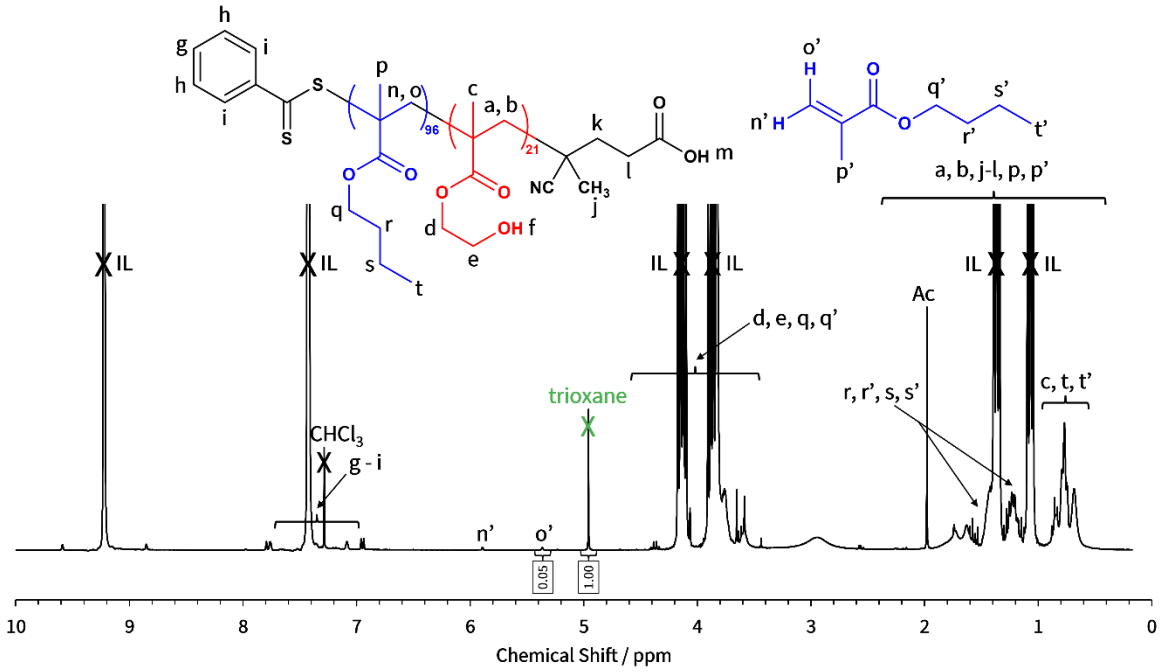

Figure 2.6. *Assigned ^{1}H NMR spectrum of target PHEMA$_{21}$-b-PBuMA$_{100}$ (with [EMIM][EtOSO$_3$] as the reaction solvent) after the polymerisation reaction. NMR solvent = $CDCl_3$, trioxane = reference peak.*

$$Integral(trioxane)] = Reference\ Peak = 1 \qquad \textbf{2.24}$$

$$[integral(o')] = 1H = 0.05 \qquad \textbf{2.25}$$

$$Conversion = 1 - \frac{[integral\ (o')]\ after\ reaction}{[integral(o')]\ before\ reaction} \times 100\% = 1 - \frac{0.05}{1.39} \times 100\% = \textbf{96\%}\ (2s.f.) \qquad \textbf{2.26}$$

2.2.9.2 *Synthesis of poly(2-hydroxyethyl methacrylate)-block-poly(n-butyl methacrylate) (PHEMA-b-PBuMA) diblock copolymer via RAFT solution polymerisation in N,N-dimethylformamide*

A typical RAFT solution polymerisation for the synthesis of PHEMA$_{21}$–*b*–PBuMA$_{87}$ at 10% w/w solids was conducted as follows. *n*-Butyl methacrylate (BuMA; 0.47 g; 3.32 mmol), 2,2'-azobisisobutyronitrile (AIBN; 2.7 mg; 16.6 µmol), PHEMA$_{21}$ macro-CTA (0.10 g; 33.2 µmol; macro-CTA/initiator molar ratio = 2.0; PBuMA target DP = 100) and *N,N*-dimethylformamide (DMF; 5.17 g) were added to a 14 mL sample vial. The sealed reaction mixture was purged with nitrogen for

30 minutes prior to being placed in a preheated aluminium block at 70 °C whilst stirring for 25 hours (BuMA conversion = 87% (Figure 2.7 and Figure 2.8); M_n = 5 900 g mol^{-1}, $Đ_M$ = 1.59).

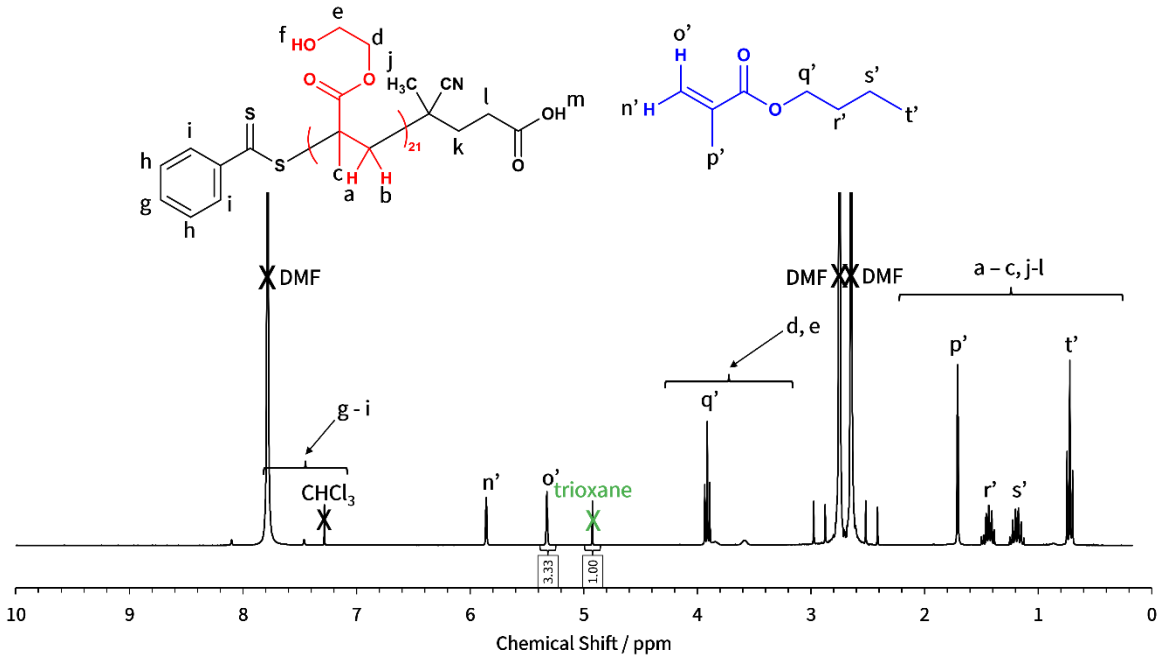

Figure 2.7. *Assigned ^{1}H NMR spectrum of target $PHEMA_{21}$-b-$PBuMA_{100}$ (with DMF as the reaction solvent) before the polymerisation reaction. NMR solvent = $CDCl_3$, trioxane = reference peak.*

Integral(trioxane)] = Reference Peak = 1 ***2.27***

[integral(o')] = 1H = 3.33 ***2.28***

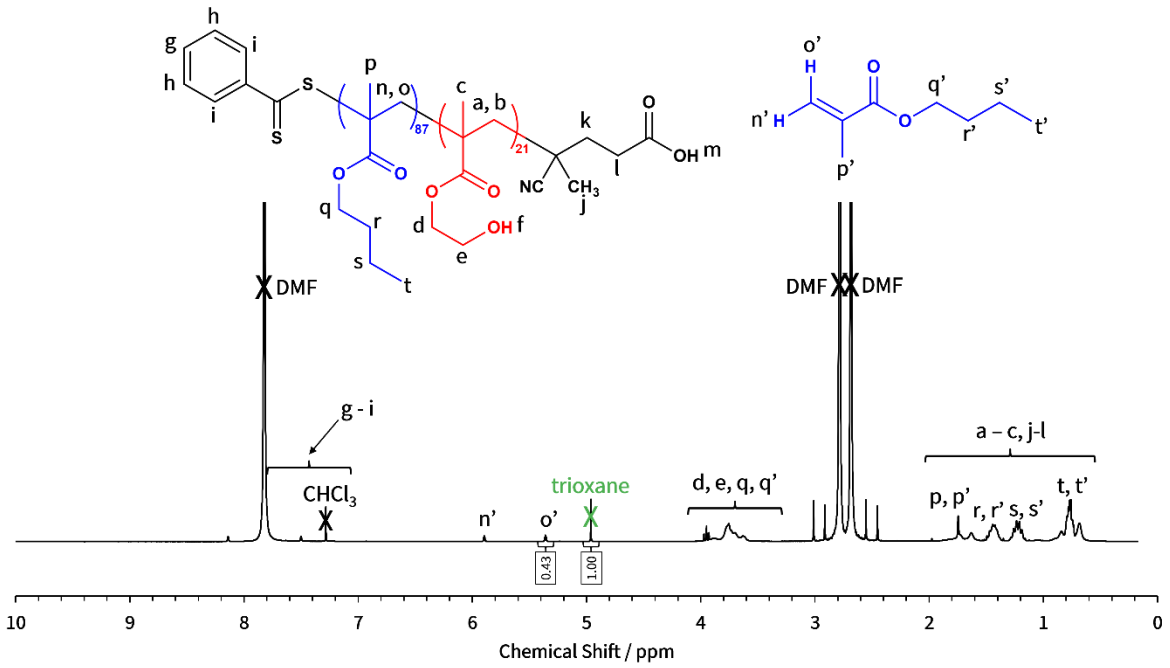

Figure 2.8. *Assigned ^{1}H NMR spectrum of target PHEMA$_{21}$-b-PBuMA$_{100}$ (with DMF as the reaction solvent) after the polymerisation reaction. NMR solvent = CDCl$_3$, trioxane = reference peak.*

$$Integral(trioxane)] = Reference\ Peak = 1 \qquad \textbf{2.29}$$

$$[integral(o')] = 1H = 0.43 \qquad \textbf{2.30}$$

$$Conversion = 1 - \frac{[integral\ (o')]after\ reaction}{[integral(o')]\ before\ reaction} \times 100\% = 1 - \frac{0.43}{1.39} \times 100\% = \textbf{87\%}\ (2s.f.) \qquad \textbf{2.31}$$

2.2.9.3 Synthesis of poly(2-hydroxyethyl methacrylate)-block-poly(n-butyl methacrylate) (PHEMA-b-PBuMA) diblock copolymer via RAFT dispersion polymerisation in an ethanol-water mixture

A typical RAFT dispersion polymerisation for the synthesis of PHEMA$_{21}$–*b*–PBuMA$_{70}$ at 10% w/w solids was conducted as follows. *n*-Butyl methacrylate (BuMA; 0.57 g; 3.98 mmol), 2,2'-azobisisobutyronitrile (AIBN; 0.7 mg; 3.98 µmol), PHEMA$_{21}$ macro-CTA (0.02 g; 7.97 µmol; macro-CTA/initiator molar ratio = 2.0; PBuMA target DP = 100), ethanol (EtOH; 4.26 g) and water (H_2O; 1.06 g) were added to a 14 mL sample vial. The sealed reaction mixture was purged with nitrogen for

30 minutes prior to being placed in a preheated aluminium block at 70 °C whilst stirring for 24 hours (BuMA conversion = 70% (Figure 2.9 and Figure 2.10); M_n = 13 800 g mol^{-1}, $Đ_M$ = 1.51).

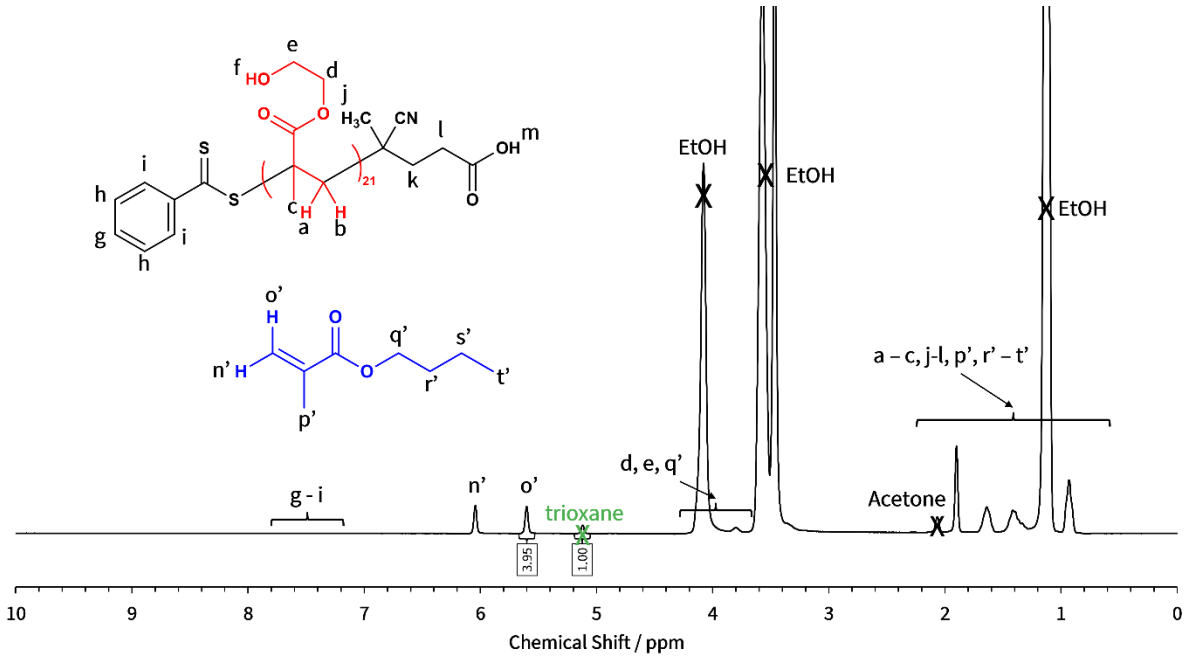

Figure 2.9. *Assigned ^{1}H NMR spectrum of target PHEMA$_{21}$-b-PBuMA$_{100}$ (with EtOH/H$_2$O as the reaction solvent) before the polymerisation reaction. NMR solvent = acetone-d6, trioxane = reference peak.*

$$Integral(trioxane)] = Reference\ Peak = 1 \qquad \textbf{2.32}$$

$$[integral(o')] = 1H = 3.95 \qquad \textbf{2.33}$$

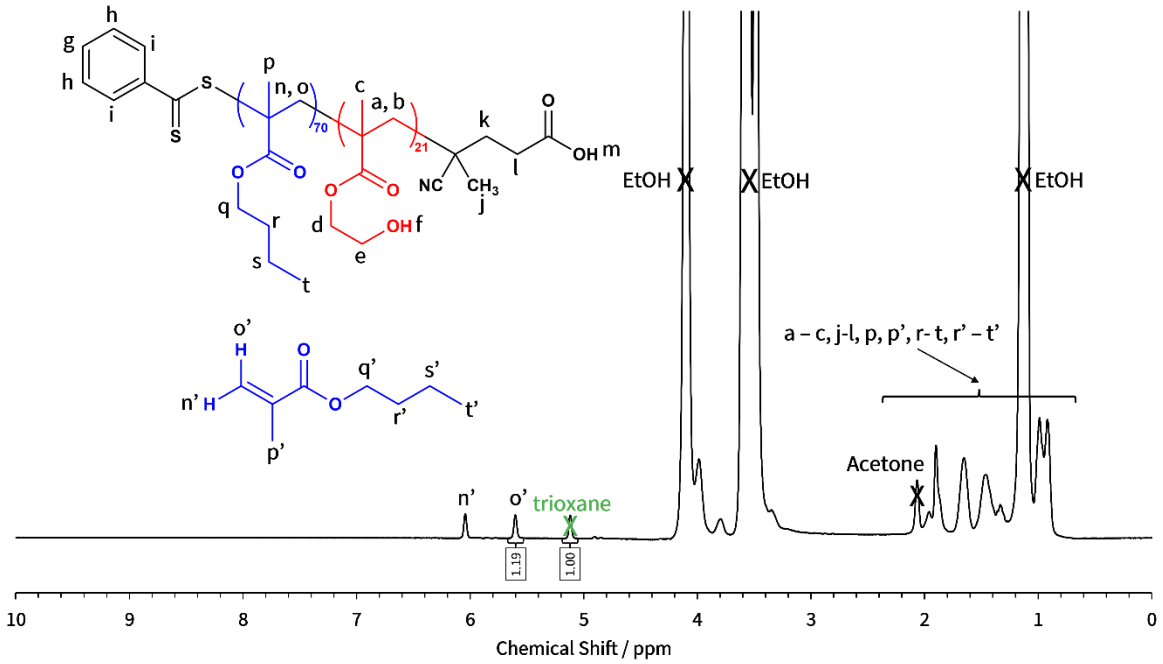

Figure 2.10. *Assigned ^{1}H NMR spectrum of target PHEMA$_{21}$-b-PBuMA$_{100}$ (with EtOH/H$_2$O as the reaction solvent) after the polymerisation reaction. NMR solvent = acetone-d6, trioxane = reference peak.*

$$Integral(trioxane)] = Reference\ Peak = 1 \qquad \textbf{2.34}$$

$$[integral(o')] = 1H = 1.19 \qquad \textbf{2.35}$$

$$Conversion = 1 - \frac{[integral\ (o')]after\ reaction}{[integral(o')]\ before\ reaction} \times 100\% = 1 - \frac{1.19}{3.95} \times 100\% = \textbf{70\%}\ (2s.f.) \qquad \textbf{2.36}$$

2.3 Results and discussion

2.3.1 Synthesis of poly(2-hydroxyethyl methacrylate) macromolecular chain transfer agent via RAFT solution polymerisation

PHEMA was deemed a suitable macromolecular chain transfer agent (macro-CTA) due to its tested solubility in a wide range of solvents including DMF, EtOH/H$_2$O mixtures and ILs, in particular [EMIM][EtOSO$_3$]. Thus, it was therefore considered a good candidate as the solvophilic stabiliser block in subsequent PISA syntheses. In preparation for these PISA reactions, the synthesis of a PHEMA macro-CTA was conducted *via* RAFT solution polymerisation in methanol at 60 °C using 4-cyano-4-(phenylcarbonothioylthio)pentanoic acid (CPTP) as a chain transfer agent. The reaction

was quenched after 6 hours, resulting in a final HEMA monomer conversion of 67%. This intermediate monomer conversion was deliberately targeted in order to preserve the end group functionality[58] and enable use of this homopolymer as a macro-CTA. ^{1}H NMR spectroscopy was used to determine the mean degree of polymerisation (DP), which was calculated to be 21. The macro-CTA was analysed using GPC to quantify the number-average molecular weight (M_n) and dispersity ($Đ_M$), which were found to be 3,800 g mol^{-1} and 1.34, respectively (Figure 2.11). It can be observed that there is a small low molecular weight shoulder at just below 18 minutes retention time, which could be due to early termination of shorter polymer chains which would appear at longer retention times. This procedure was repeated to synthesise an additional PHEMA macro-CTA, this time targeting a higher DP, resulting in PHEMA$_{77}$ as judged by ^{1}H NMR spectroscopy. For this macro-CTA, an M_n of 9500 g mol^{-1} and a $Đ_M$ of 1.30 were obtained from GPC analysis (Figure 2.12), thus confirming good control over the RAFT polymerisation. It can be observed that there is a small high molecular weight shoulder at just below 15 minutes retention time. This could be due to the HEMA monomer containing traces of ethylene glycol dimethacrylate (EGDMA), which can act as an efficient crosslinking agent, and hence result in the formation of higher molecular weight molecules[59].

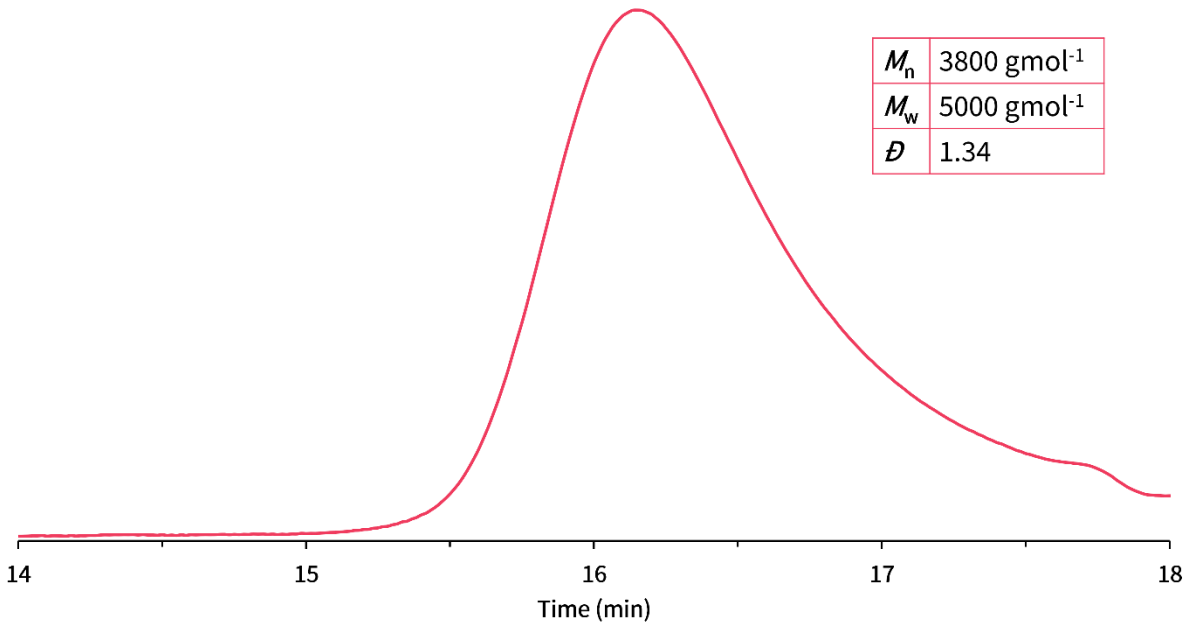

Figure 2.11. *DMF GPC chromatogram (vs. poly(methyl methacrylate) standards) obtained of poly(2-hydroxyethyl methacrylate) macromolecular chain transfer agent (PHEMA macro-CTA), with a final degree of polymerisation of 21, synthesised via the RAFT solution polymerisation of 2-hydroxyethyl methacrylate for 6 hours at 60 °C in methanol at 50% w/w solids.*

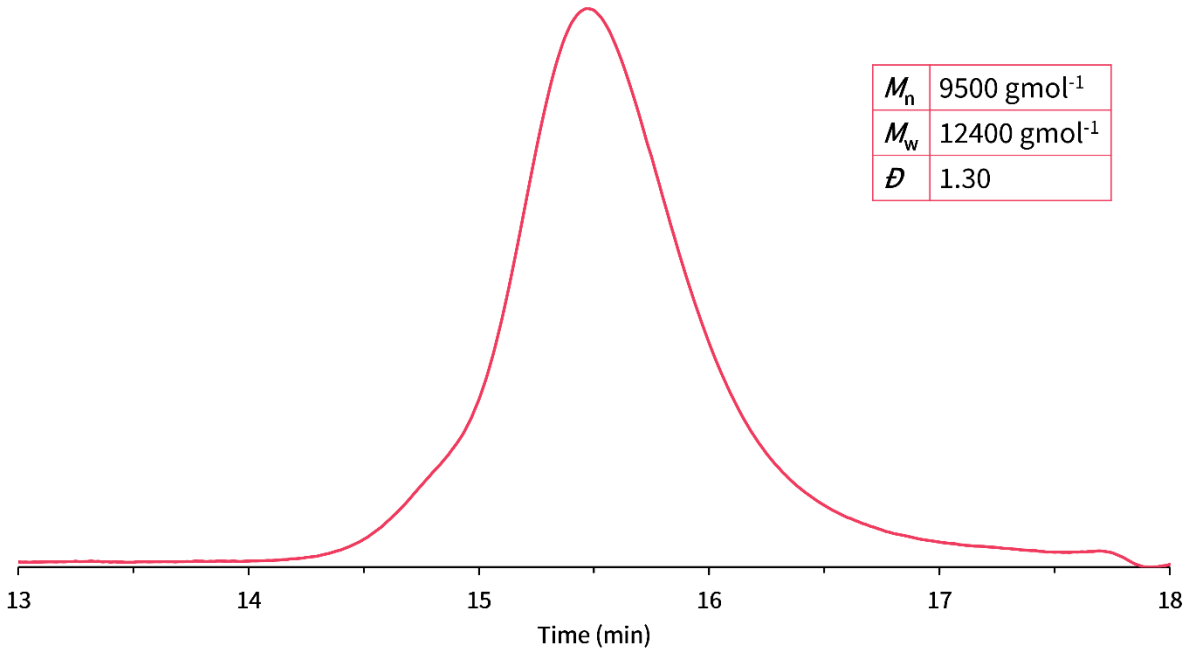

Figure 2.12. *DMF GPC chromatogram (vs. poly(methyl methacrylate) standards) obtained of poly(2-hydroxyethyl methacrylate) macromolecular chain transfer agent (PHEMA macro-CTA), with a final degree of polymerisation of 77, synthesised via the RAFT solution polymerisation of 2-hydroxyethyl methacrylate for 6 hours at 60 °C in methanol at 50% w/w solids.*

2.3.2 Synthesis of poly(2-hydroxyethyl methacrylate)-*block*-poly(n-butyl methacrylate) (PHEMA-*b*-PBuMA) diblock copolymers

Initially, the kinetics for the chain extension of the $PHEMA_{21}$ and $PHEMA_{77}$ macro-CTAs using BuMA was investigated to identify the optimum reaction duration to achieve ≥90% monomer conversion. High conversions are ideal as they would mitigate/shorten the duration of any post-polymerisation processing required to remove any unreacted monomer and obtain a purified product. The kinetic studies were conducted for 2 hours at 70 °C using [EMIM][$EtOSO_3$] as the solvent with a total solids concentration of 10% w/w, with a target PBuMA DP of 100 for the chain extension of both the $PHEMA_{21}$ (Figure 2.15) and $PHEMA_{77}$ (Figure 2.16) macro-CTAs.

Since BuMA is immiscible with [EMIM][$EtOSO_3$] and PBuMA is insoluble in this IL, this reaction proceeds as an emulsion polymerisation. Throughout the kinetic studies, samples were withdrawn every 5 minutes for the first 60 minutes, and every 10 minutes for the remaining duration of the reaction. An internal standard, 1,3,5-trioxane was used to enable monitoring of the reduction in

intensity of the BuMA vinyl proton signals in the ^{1}H NMR spectrum and thus determine monomer conversion (Figure 2.13 and Figure 2.14).

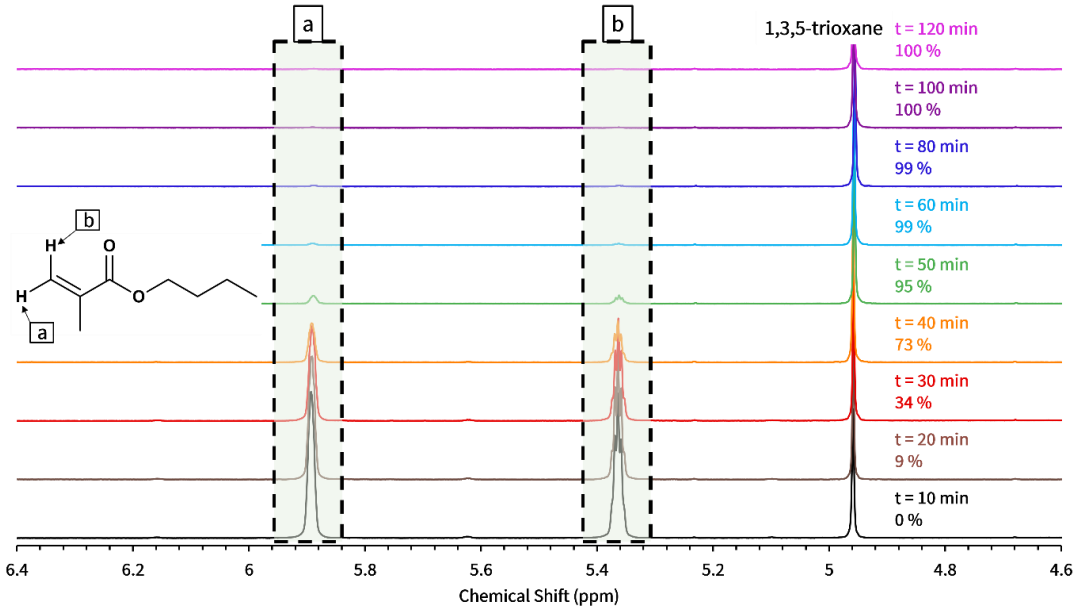

Figure 2.13. *Assigned ^{1}H NMR spectra depicting the progression of the chain extension of the $PHEMA_{21}$ macromolecular chain transfer agent with n-butyl methacrylate (BuMA) in [EMIM][$EtOSO_3$] at timed intervals (t), where the decrease in a and b represent the decrease in vinylic protons of BuMA as the polymerisation proceeds.*

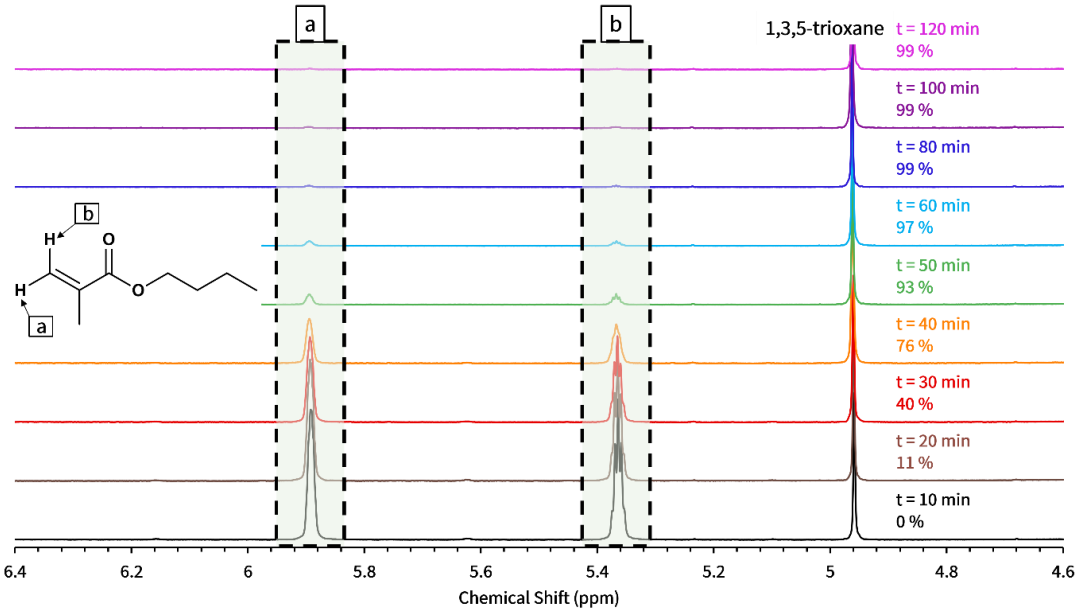

Figure 2.14. *Assigned ^{1}H NMR spectra depicting the progression of the chain extension of the $PHEMA_{77}$ macromolecular chain transfer agent with n-butyl methacrylate (BuMA) in [EMIM][$EtOSO_3$] at timed intervals (t), where the decrease in a and b represent the decrease in vinylic protons of BuMA as the polymerisation proceeds.*

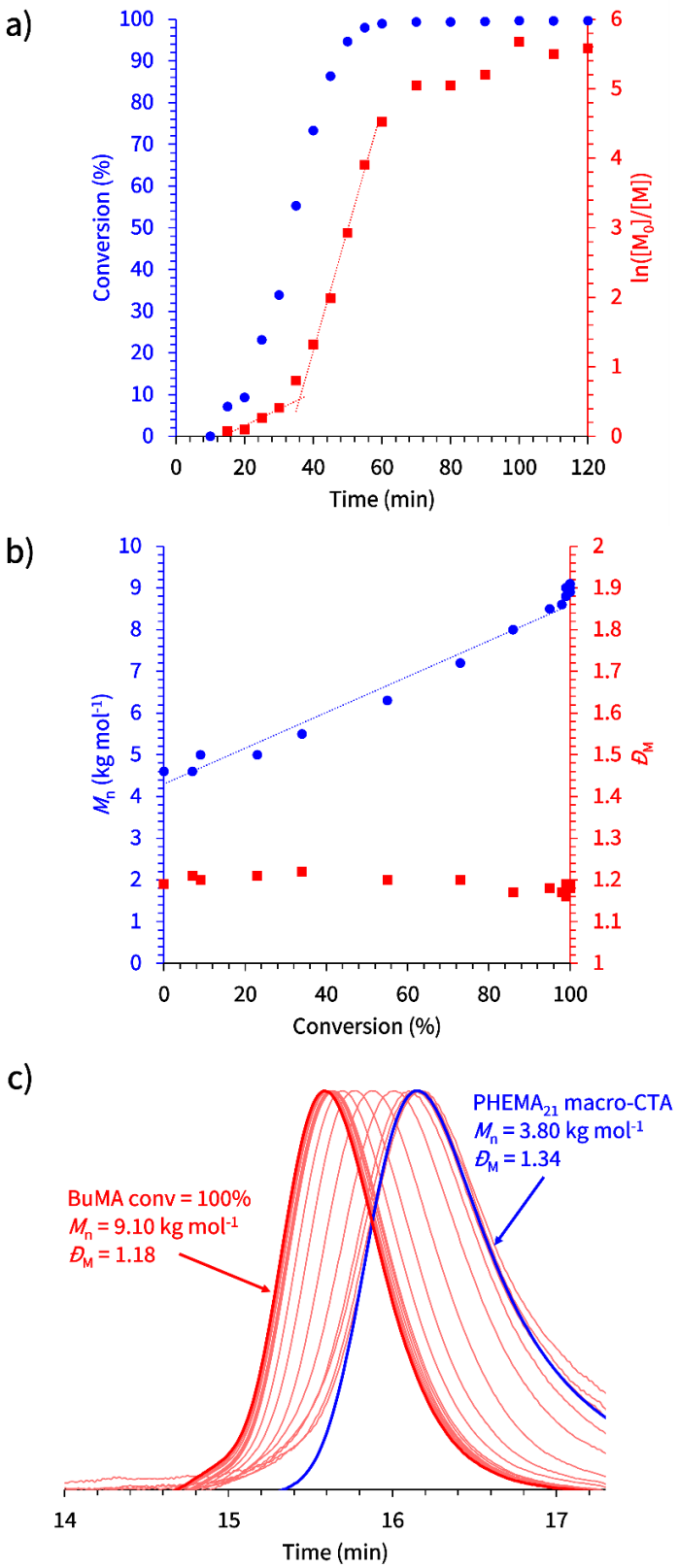

Figure 2.15. *Kinetic study for the RAFT emulsion polymerisation of BuMA (target DP = 100) in [EMIM][EtOSO$_3$] at 10% w/w solids using a PHEMA$_{21}$ macro-CTA: (a) BuMA conversion vs. time (blue circles) and semi-log kinetic (red squares); (b) M_n (blue circles) and $Đ_M$ (red squares) vs. BuMA conversion; (c) DMF GPC chromatograms (vs. poly(methyl methacrylate) standards).*

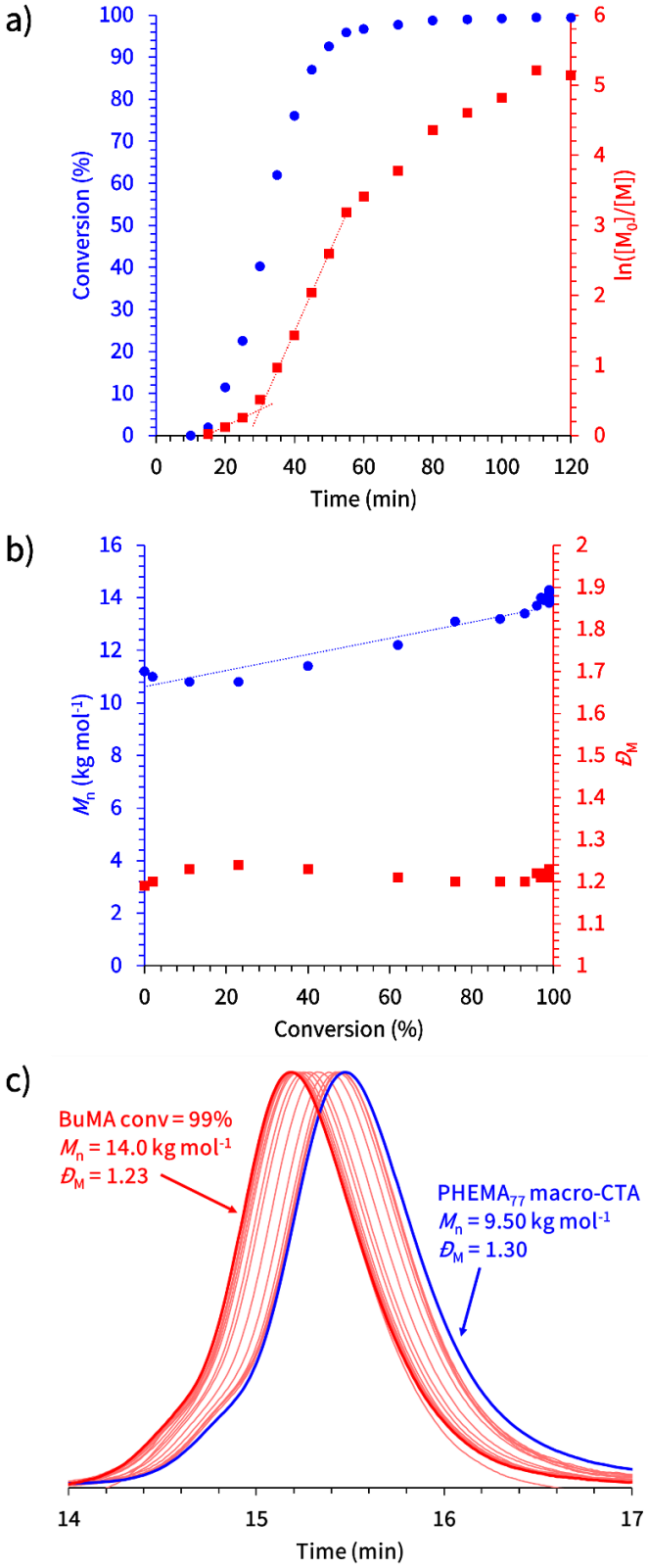

Figure 2.16. *Kinetic study for the RAFT emulsion polymerisation of BuMA (target DP = 100) in [EMIM][EtOSO$_3$] at 10% w/w solids using a PHEMA$_{77}$ macro-CTA: (a) BuMA conversion vs. time (blue circles) and semi-log kinetic (red squares); (b) M_n (blue circles) and $Đ_M$ (red squares) vs. BuMA conversion; (c) DMF GPC chromatograms (vs. poly(methyl methacrylate) standards).*

Due to difficulties arising from the two-phase nature of the emulsion system, early sample collection was found to be unreliable, and therefore kinetic data was plotted beginning from 10 minutes. For the extension of the $PHEMA_{21}$ macro-CTA, ^{1}H NMR analysis revealed that full monomer conversion was achieved at approximately 60 minutes. Furthermore, the time at which micellar nucleation occurs was observed to be approximately 36 minutes, which corresponds to a PBuMA DP of 58. This critical DP reflects the length of the PBuMA structure-directing block which triggers spontaneous self-assembly, which is observed by an approximate seven-fold increase in rate of reaction (Figure 2.15a). During the onset of nucleation, the unreacted monomer (in this case BuMA) enters the micelle cores which results in a higher local monomer concentration, therefore resulting in a sudden increase in rate of reaction. This is in agreement with literature examples from Derry *et al.*[58] and Blanazs *et al.*[60]. In addition to this, both the linear increase of M_n with monomer conversion and the maintained low dispersity values demonstrate good RAFT control of the system[37, 58] (Figure 2.15b). The success of the chain extension can be confirmed using GPC analysis, where a clear gradual shift of the distribution to the higher molecular weight is observed (Figure 2.15c). The extension of the $PHEMA_{77}$ macro-CTA, again targeting a PBuMA DP of 100, showed similar results. In this case the critical PBuMA DP for self-assembly was determined to be 40. It can be observed from Figure 2.16a that the extension of this macro-CTA had an approximate five-fold increase in rate of reaction for the onset of micellization. Based on these kinetic analyses, the optimal polymerisation time for complete monomer conversion during the RAFT emulsion polymerisation of BuMA in [EMIM][$EtOSO_3$] using both of the PHEMA macro-CTAs was identified as 2 hours. Subsequently, series of $PHEMA_x$-*b*-$PbuMA_y$ diblock copolymers with targeted PBuMA DPs varying from 50 to 1000 were synthesised using both the $PHEMA_{21}$ and $PHEMA_{77}$ macro-CTAs (Figure 2.17 and Figure 2.18).

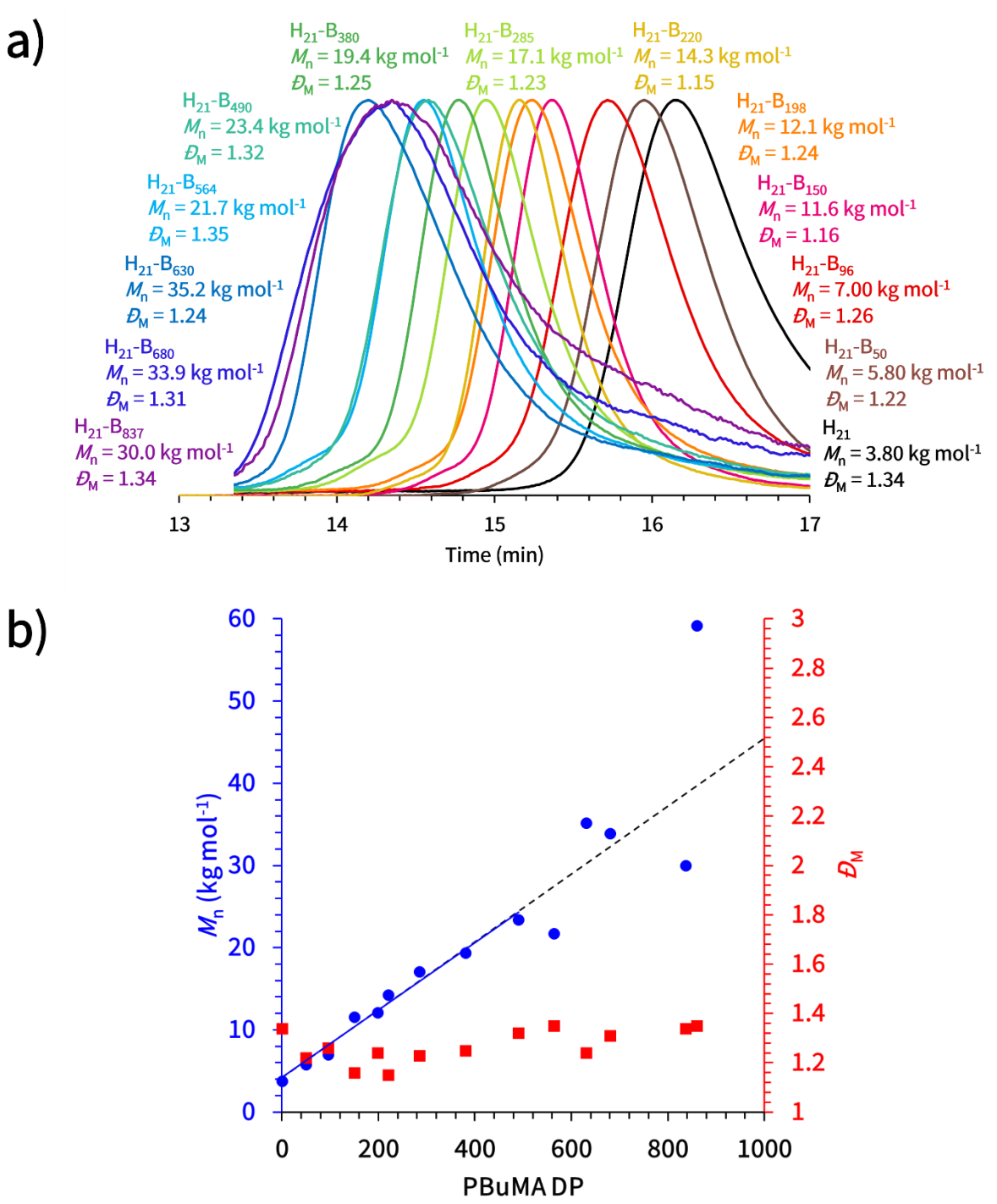

Figure 2.17. *Normalised DMF GPC data (vs. poly(methyl methacrylate) standards) obtained for $PHEMA_{21}$-b-$PbuMA_y$ block copolymers synthesised via RAFT emulsion polymerisation of n-butyl methacrylate (BuMA) in [EMIM][$EtOSO_3$] at 10% w/w solids, where PHEMA is denoted as H and PBuMA is denoted as B. Chromatograms obtained for a selection of $PHEMA_{21}$-b-$PbuMA_y$ block copolymers (a), with the corresponding plots of M_n vs. PBuMA DP (blue circles) and $Đ_M$ (red squares) vs. actual PBuMA DP (b).*

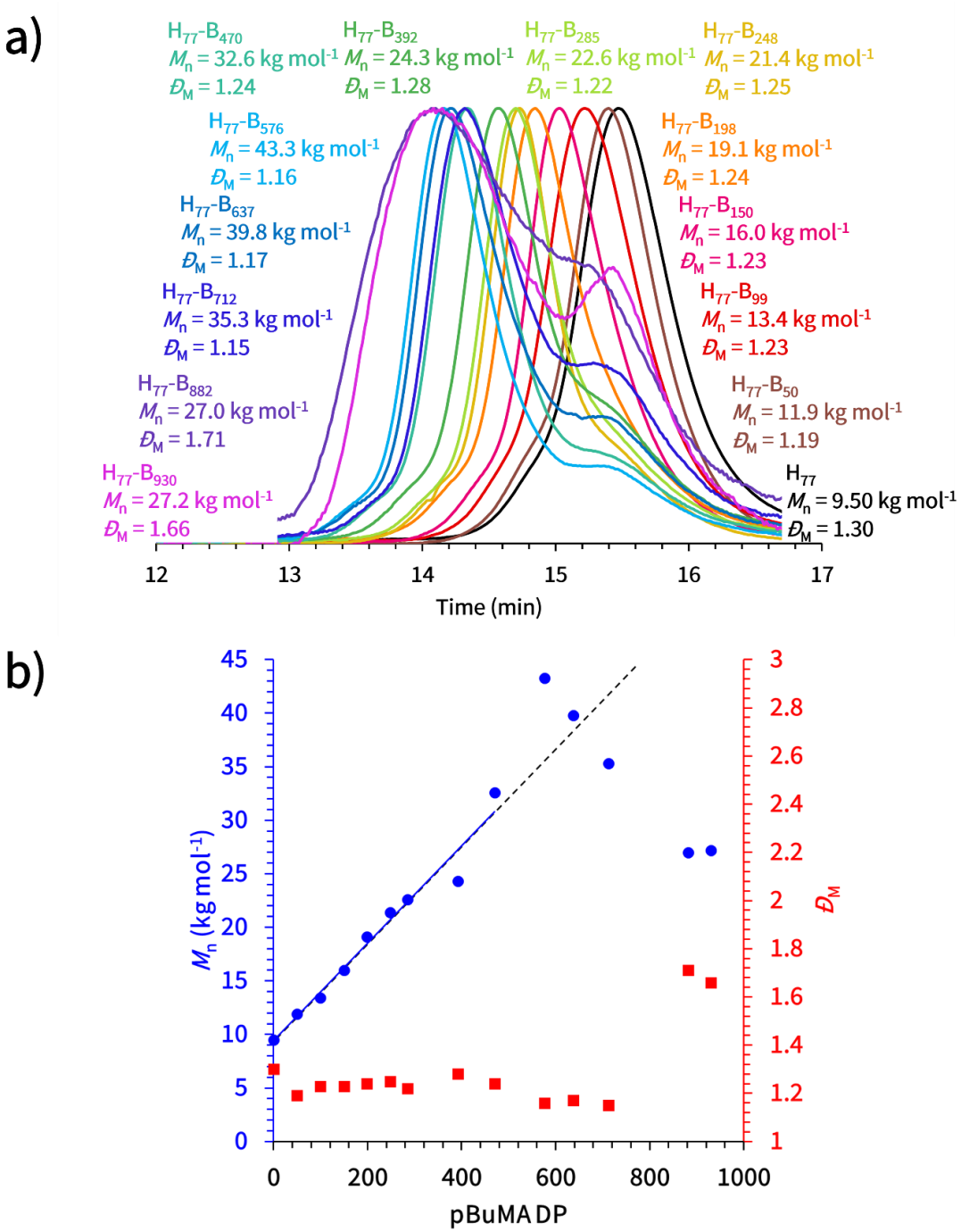

Figure 2.18. *Normalised DMF GPC data (vs. poly(methyl methacrylate) standards) obtained for PHEMA$_{77}$-b-PbuMA$_y$ block copolymers synthesised via RAFT emulsion polymerisation of n-butyl methacrylate (BuMA) in [EMIM][EtOSO$_3$] at 10% w/w solids, where PHEMA is denoted as H and PBuMA is denoted as B. Chromatograms obtained for a selection of PHEMA$_{77}$-b-PbuMA$_y$ block copolymers (a), with the corresponding plots of M_n vs. PBuMA DP (blue circles) and $Đ_M$ (red squares) vs. actual PBuMA DP (b).*

From Figure 2.17a, it can be observed that the extension of the PHEMA$_{21}$ macro-CTA resulted in a trend of polymers with increasing M_n, targeting a DP of up to 500 for PBuMA. After this point

(targeting DPs 600 to 1000), there is no trend for M_n, which also occurred when using the $PHEMA_{77}$ macro-CTA. Figure 2.18a shows the formation of a low molecular weight shoulder in the GPC traces from DP 392 of PBuMA onwards. These shoulder peaks appear at a very similar retention time to the precursor $PHEMA_{77}$ macro-CTA, implying that unreacted macro-CTA is present. When targeting a PBuMA DP of 1000 using either macro-CTA, problems arose when preparing samples for GPC analysis. The prepared solutions would not easily pass through the filter and the resulting solution that did pass through resulted in a trace displaying no peak for the $PHEMA_{21}$ series, hence its lack of presence in the above overlaid traces (Figure 2.17). Looking at Figure 2.17b and Figure 2.18b, the blue trend-line is representative of the linear growth of M_n when targeting higher PBuMA DPs. It should be noted that this trendline was terminated beyond DP 500, as any DPs past this do not follow the trend; the polymerisations appeared to be less controlled. This is confirmed by the black dashed line representing the linear line of best fit (plotted using data points up to target DP 500 for PBuMA) displaying that the data points plotted above DP 490 (for $PHEMA_{21}$) and 470 (for $PHEMA_{77}$) deviate from this line, additionally matching the trend of the starting point of changes within the GPC data. This was also observed by Parker *et al.*[36], where targeting above a structure-directing block DP of 1000 when extending a poly(stearyl methacrylate) macro-CTA with benzyl methacrylate deviated from the trendline of M_n increasing monotonically. Lower blocking efficiencies are a common occurrence for when higher DPs are targeted, this often indicates that reinitiation occurs slower, hence the need for longer reaction times required to reach higher conversions to match the lower targeted DPs. This can often be indicated from the broadening of the molecular weight distribution or the appearance of a shoulder[36, 61], which is observed in Figure 2.17a for DPs over 490 and more so in Figure 2.18a for DPs over 285. As mentioned, the appearance of this shoulder lines up with the macro-CTA GPC trace in the overlaid spectra, appearing at a very similar retention time and therefore suggesting that there is unreacted macro-CTA present in the system.

The kinetic studies for the chain extension of the $PHEMA_{21}$ and $PHEMA_{77}$ macro-CTAs using BuMA was also investigated in *N*,*N*-dimethylformamide (DMF). This reaction is a solution polymerisation due to all components (macro-CTA, BuMA and the resulting PBuMA polymer) being soluble in or miscible with the reaction solvent. These kinetic studies were conducted for 10 hours at 70 °C using DMF as the solvent with a total solids concentration of 10% w/w, with a target PBuMA DP of 100 when chain extending both the $PHEMA_{21}$ (Figure 2.21) and $PHEMA_{77}$ (Figure 2.22) macro-CTA. Throughout these kinetic studies, samples were withdrawn every 30 minutes for a total period of 10 hours. The same internal standard, 1,3,5-trioxane was used to enable monitoring of the reduction in intensity of the

BuMA vinyl proton signals in the ^{1}H NMR spectrum and thus determine monomer conversion (Figure 2.19 and Figure 2.20).

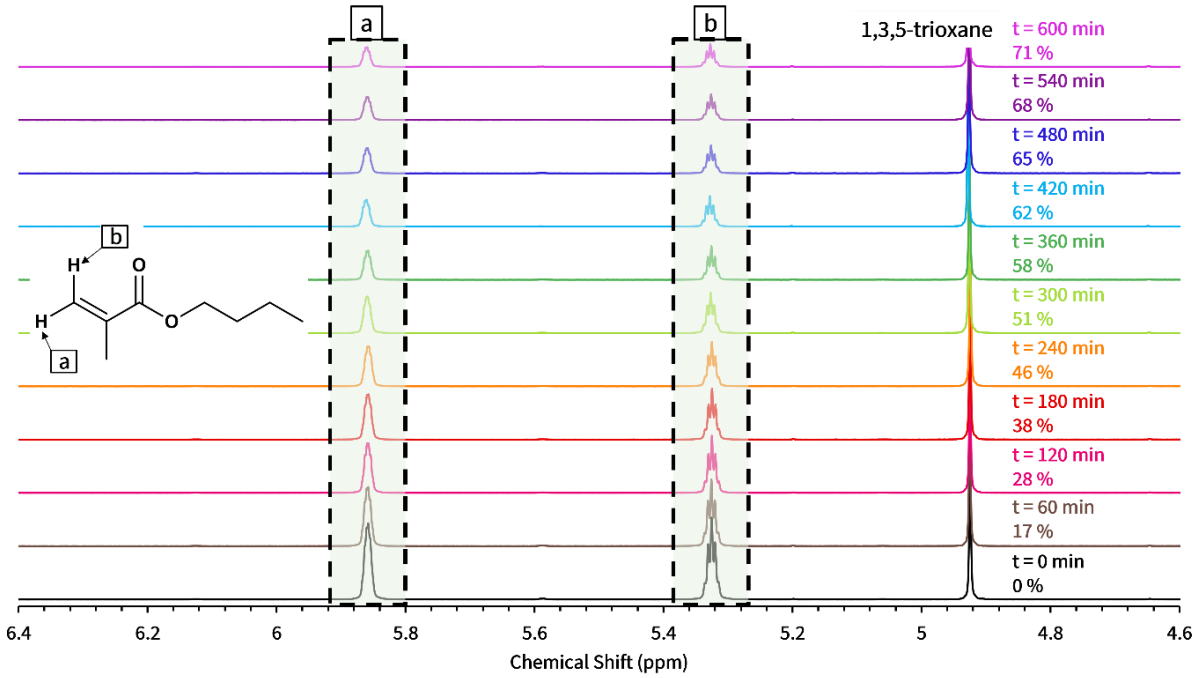

Figure 2.19. *Assigned ^{1}H NMR spectra depicting the progression of the chain extension of the $PHEMA_{21}$ macromolecular chain transfer agent with n-butyl methacrylate (BuMA) in DMF at timed intervals (t), where the decrease in a and b represent the decrease in vinylic protons of BuMA as the polymerisation proceeds.*

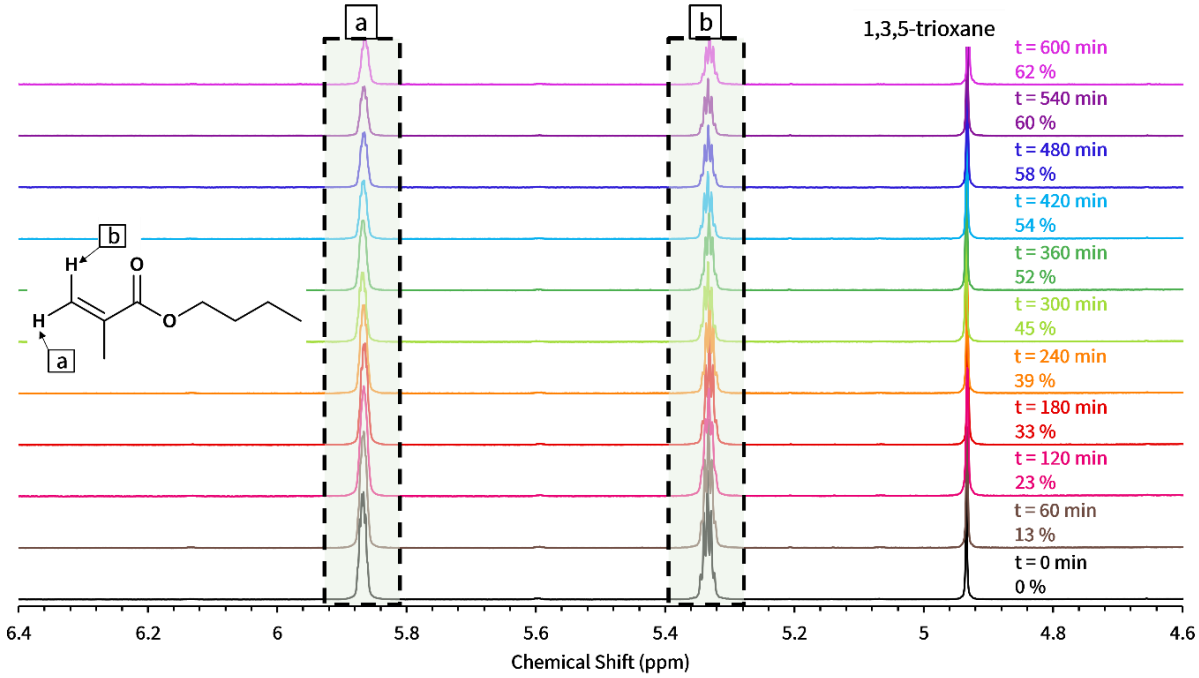

Figure 2.20. *Assigned ^{1}H NMR spectra depicting the progression of the chain extension of the $PHEMA_{77}$ macromolecular chain transfer agent with n-butyl methacrylate (BuMA) in DMF at timed intervals (t), where the decrease in a and b represent the decrease in vinylic protons of BuMA as the polymerisation proceeds.*

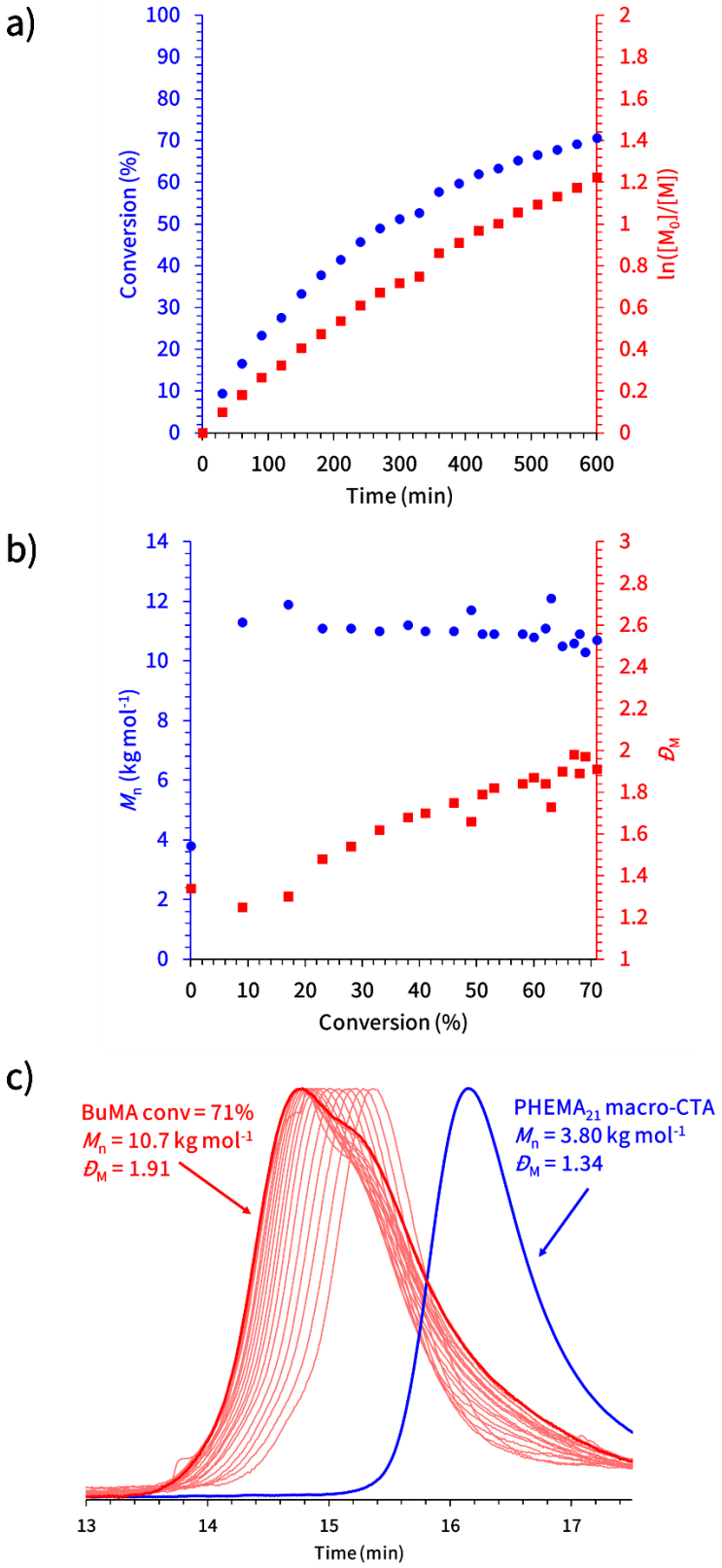

Figure 2.21. *Kinetic study for the RAFT solution polymerisation of BuMA (target DP =100) in DMF at 10% w/w solids using a $PHEMA_{21}$ macro-CTA: (a) BuMA conversion vs. time (blue circles) and semi-log kinetic (red squares); (b) M_n (blue circles) and $Đ_M$ (red squares) vs. BuMA conversion; (c) DMF GPC chromatograms (vs. poly(methyl methacrylate) standards).*

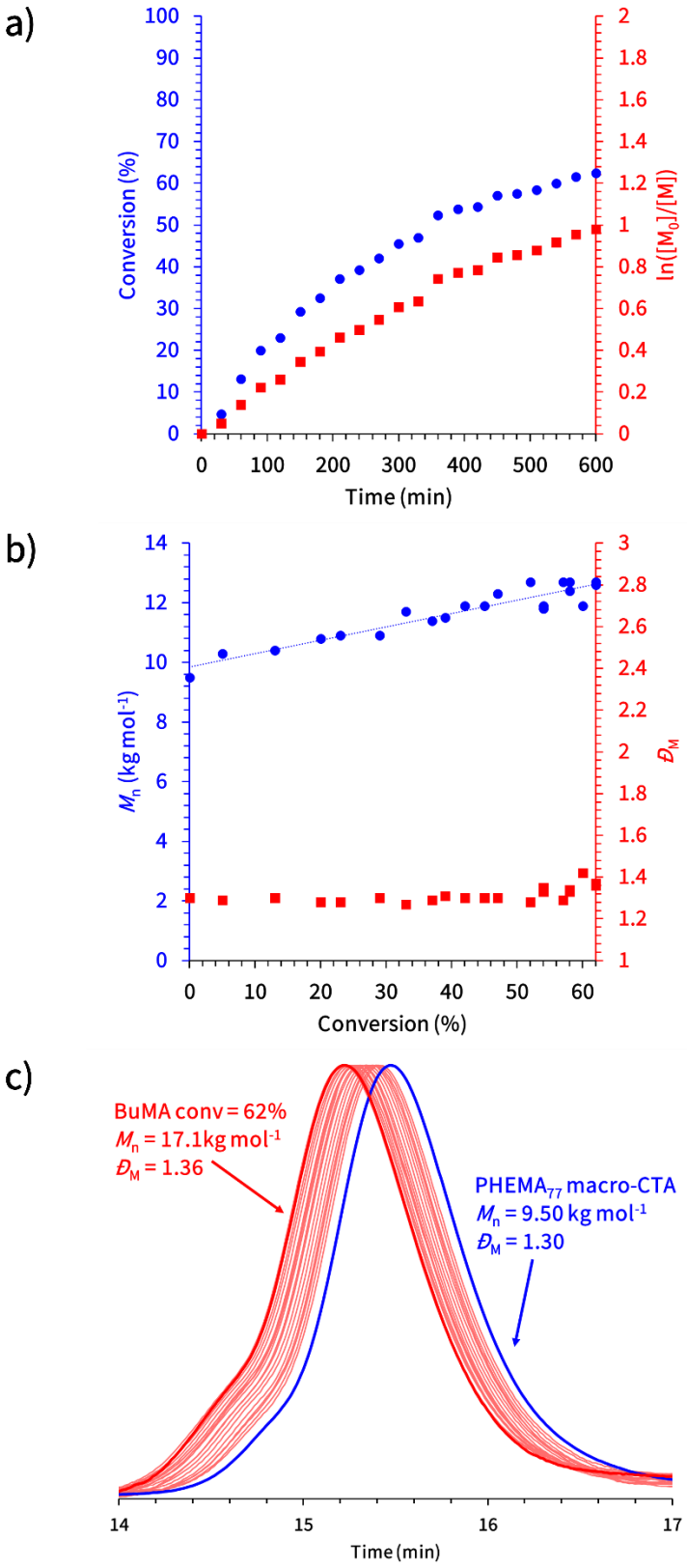

Figure 2.22. *Kinetic study for the RAFT solution polymerisation of BuMA (target DP = 100) in DMF at 10% w/w solids using a PHEMA$_{77}$ macro-CTA: (a) BuMA conversion vs. time (blue circles) and semi-log kinetic (red squares); (b) M_n (blue circles) and $Đ_M$ (red squares) vs. BuMA conversion; (c) DMF GPC chromatograms (vs. poly(methyl methacrylate) standards).*

It can be observed that with DMF as the reaction solvent, the synthesis of the desired block copolymer (PHEMA-*b*-PBuMA) proceeded much slower than when conducted in the IL, [EMIM][$EtOSO_3$]. The conversions obtained using the $PHEMA_{21}$ and $PHEMA_{77}$ macro-CTAs at the end of the 10-hour kinetic study was 71% and 62%, respectively (Figure 2.19 and Figure 2.20). In an attempt to reach full monomer conversion, the reactions were prepared again and allowed to proceed overnight after which conversions of 88% and 83% were obtained after a total period of 25 hours, for the target block copolymers $PHEMA_{21}$-*b*-$PBuMA_{100}$ and $PHEMA_{77}$-*b*-$PBuMA_{100}$, respectively. The gradual increase in conversion along with time, as seen in Figure 2.21a and Figure 2.22a, displays a common trend as observed for solution polymerisations. Although full monomer conversion was not reached during this time, the success of the chain extension was again confirmed using GPC analysis, where a clear shift of the distribution to higher molecular weight is noticeable for polymerisations using either the $PHEMA_{21}$ (Figure 2.21c) or $PHEMA_{77}$ (Figure 2.22c) macro-CTAs. However, from Figure 2.21b and Figure 2.22b, it is clear that these polymerisations did not both proceed via the same mechanism. Figure 2.21b displays an initial sharp increase in M_n, after which there is no significant change and the values remain in the same region (within range). This is often indicative of free radical polymerisations (Figure 1.3), unlike for RAFT polymerisations where the establishment of the RAFT equilibrium ensures a linear evolution of M_n with monomer conversion (as discussed in Section 1.3.2.1). This could mean that the pre-equilibrium step, during which the R-group is removed and facilitates re-initiation of BuMA, occurs inefficiently and thus hinders the RAFT polymerisation from proceeding. As previously mentioned, ILs have high viscosity and high polarity which result in a decrease in the rate of termination and an increase in the rate of propagation[24-26]. Since DMF is less viscous and less polar, this could have the reverse effects, meaning that the polymerisation would proceed much slower and also not be as controlled. This loss of control can also be observed due to the high dispersity value of 1.91 obtained after 25 hours reaction time. This is not visible for the extension of the $PHEMA_{77}$ macro-CTA, where there is a slow but steady increase of M_n with conversion and no large jump between macro-CTA and the first sample taken at 30 minutes (Figure 2.21c). Instead, this polymerisation remained relatively controlled as judged by the steady dispersity values seen in Figure 2.22c. Following these kinetic studies, a series of $PHEMA_x$-*b*-$PBuMA_y$ diblock copolymers with targeted PBuMA DPs varying from 100 to 1000 were synthesised using either the $PHEMA_{21}$ or $PHEMA_{77}$ macro-CTAs, to compare with those synthesised in [EMIM][$EtOSO_3$].

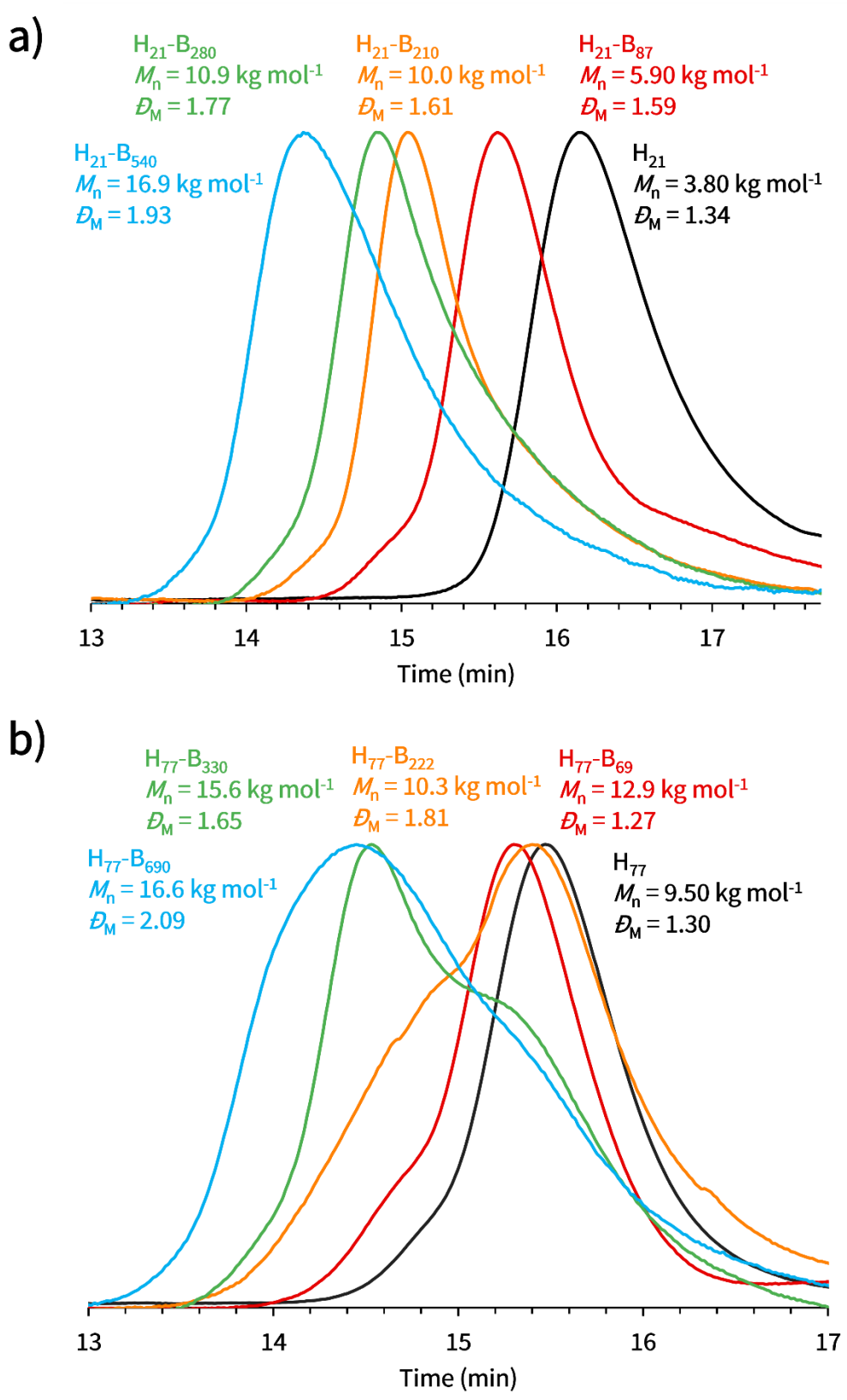

Figure 2.23. *DMF GPC data (vs. poly(methyl methacrylate) standards) obtained for: a) $PHEMA_{21}$-b-$PBuMA_y$ and b) $PHEMA_{77}$-b-$PBuMA_y$ block copolymers synthesised via RAFT solution polymerisation of n-butyl methacrylate (BuMA) in DMF at 10% w/w solids, where PHEMA is denoted as H and PBuMA is denoted as B.*

Figure 2.23 displays that successful chain extension occurred using both PHEMA macro-CTAs, due to the notable shift in molecular weight distributions to shorter retention times (and hence high molecular weight) when targeting increasing PBuMA DPs. However, it can also be observed that there is an increase in dispersity values, ranging from 1.27 to 2.09, indicating that these polymerisations proceeded to become uncontrolled. This uncontrolled nature was distinct for the data obtained from the $PHEMA_{21}$-*b*-$PBuMA_{100}$ kinetics reaction (Figure 2.21), however not for the $PHEMA_{77}$-*b*-$PBuMA_{100}$ kinetics reaction (Figure 2.22). Both $PHEMA_{21}$ and $PHEMA_{77}$ block copolymer syntheses were left overnight to run for a total time of 25 hours, whereas the kinetic study was terminated after only 10 hours. This meant that although the lack of control was not evident in either kinetic study, it was more apparent at increased reaction duration. Thus, at higher conversions there was an increasing loss of control for the extension of both macro-CTAs. Despite this, block copolymer synthesis from $PHEMA_{21}$, targeting DPs 100, 300, 500 and 1000 (Figure 2.23a) does show a trend of increasing molecular weight with increasing DP, however this is not the case for the $PHEMA_{77}$ series (Figure 2.23b) in which there is no clear trend and a large broadening of peaks.

Comparing the GPC data for block copolymers synthesised in [EMIM][$EtOSO_3$] with those synthesised in DMF, lower dispersity values ranging between 1.15 and 1.32 for $PHEMA_x$-*b*-$PBuMA_y$ were obtained for those synthesised in IL, whereas values of 1.27–2.09 were obtained in DMF (Table 2-1 and Table 2-2). It can be noted that in IL, using the $PHEMA_{21}$ macro-CTA demonstrated more efficient chain extension than the $PHEMA_{77}$ macro-CTA. This is evident from the low molecular weight shoulder present in GPC traces for $PHEMA_{77}$-*b*-$PBuMA_y$ when targeting PBuMA DPs ≥ 400, which is characteristic of unreacted macro-CTA. Despite this, the dispersity values for both series of block copolymers in IL remained low (≤ 1.32) when targeting PBuMA DPs up to 500 using the $PHEMA_{21}$ macro-CTA and up to 300 using the $PHEMA_{77}$ macro-CTA, with both sets of data exhibiting a linear evolution of M_n with increasing PBuMA DP. For targeted PBuMA DPs > 500 using the $PHEMA_{21}$ macro-CTA and DPs > 300 using the $PHEMA_{77}$ macro-CTA, a deviation from the expected trend was observed, indicating a loss of control in the synthesis. This observation is in line with several PISA formulations previously reported[45]. Also, in the RAFT emulsion polymerisations conducted in [EMIM][$EtOSO_3$], high BuMA conversions were achieved using either PHEMA macro-CTA when targeting PBuMA DPs up to 300, above which longer reaction times were required to achieve approximately 90% conversion (see Table 2-1). For comparison, synthesis of $PHEMA_x$-*b*-$PBuMA_y$ block copolymers were conducted in DMF using each of the $PHEMA_{21}$ and $PHEMA_{77}$ macro-CTAs, targeting a range of DPs 100 – 1000 with a reaction time of 25 hours, yielded monomer conversions ranging between 54 and 87%.

This indicates that not only lower BuMA monomer conversions, but much slower reaction rates were achieved in DMF compared to [EMIM][$EtOSO_3$]. This demonstrates that the synthesis of block copolymers in IL represents more than a ten-fold increase in reaction rate (based on the initial gradient of the semi-log kinetic plot for reactions in IL [Figure 2.15a], compared to the overall gradient of the semi-log kinetic plot for reactions in DMF [Figure 2.21a]), and hence is a more appropriate reaction solvent for these block copolymer syntheses.

Table 2-1: *Target copolymer composition, BuMA conversion, actual copolymer composition, theoretical M_n, GPC M_n and $Đ_M$, and transmittance at 700 nm for $PHEMA_x$-b-$PBuMA_y$ diblock copolymers prepared via RAFT emulsion polymerisation of BuMA in [EMIM][$EtOSO_3$] at 70 °C and 10% w/w using AIBN initiator ([macro-CTA]/[AIBN] molar ratio = 2.0). $PHEMA_x$-b-$PBuMA_y$ is denoted as H_x-B_y for brevity.*

	^{1}H NMR Spectroscopy			DMF GPC		UV-Vis
Target Composition	**BuMA conversion (%)**	**Actual Composition[a]**	***$M_{n,th}$*** **(g mol^{-1})[b]**	***M_n*** **(g mol^{-1})**	***Đ***	**Transmittance at 700 nm (%)**
H_{21}	-	H_{21}	-	3800	1.34	-
H_{21}-B_{50}	100	H_{21}-B_{50}	3800	5800	1.22	97
H_{21}- B_{100}	96	H_{21}- B_{96}	10910	7000	1.26	98
H_{21}- B_{150}	100	H_{21}- B_{150}	18020	11600	1.16	98
H_{21}- B_{200}	99	H_{21}- B_{198}	25130	12100	1.24	99
H_{21}- B_{250}	88	H_{21}- B_{220}	32240	14300	1.15	100
H_{21}- B_{300}	95	H_{21}- B_{285}	39350	17100	1.23	98
*H_{21}- B_{400}	95	H_{21}- B_{380}	46460	19400	1.25	97
*H_{21}- B_{500}	98	H_{21}- B_{490}	60680	23400	1.32	97
*H_{21}- B_{600}	94	H_{21}- B_{564}	74900	21700	1.35	97
**H_{21}- B_{700}	90	H_{21}- B_{630}	89120	35200	1.24	96
**H_{21}- B_{800}	85	H_{21}- B_{680}	103340	33900	1.31	98
**H_{21}- B_{900}	93	H_{21}- B_{837}	117560	30000	1.34	97
**H_{21}- B_{1000}	86	H_{21}- B_{860}	131780	59200	1.35	98
H_{77}	-	H_{77}	-	9500	1.30	-
H_{77}-B_{50}	99	H_{77}-B_{50}	16539	11900	1.19	98
H_{77}- B_{100}	99	H_{77}- B_{99}	23578	13400	1.23	98
H_{77}- B_{150}	100	H_{77}- B_{150}	30830	16000	1.23	98
H_{77}- B_{200}	99	H_{77}- B_{198}	37656	19100	1.24	98
H_{77}- B_{250}	99	H_{77}- B_{248}	44695	21400	1.25	98
H_{77}- B_{300}	95	H_{77}- B_{285}	50027	22600	1.22	97
*H_{77}- B_{400}	98	H_{77}- B_{392}	65242	24300	1.28	98
*H_{77}- B_{500}	94	H_{77}- B_{470}	76334	32600	1.24	98
*H_{77}- B_{600}	96	H_{77}- B_{576}	91407	43300	1.16	97
**H_{77}- B_{700}	91	H_{77}- B_{637}	100081	39800	1.17	99
**H_{77}- B_{800}	89	H_{77}- B_{712}	110746	35300	1.15	97
**H_{77}- B_{900}	98	H_{77}- B_{882}	134920	27000	1.71	95
**H_{77}- B_{1000}	93	H_{77}- B_{930}	141746	27200	1.66	97

[a] Calculated using conversion from ^{1}H NMR

[b] Calculated using actual composition

*All reactions targeting PBuMA degree of polymerisations between 50 and 600 were initially performed for 2 hours, however upon calculating low conversions, the polymerisations indicated with a single asterisk were conducted for a further 2 hours with the same amount of additional initiator as used for the first run (AIBN).

** All reactions targeting PBuMA degree of polymerisations between 700 and 1000 were initially performed for 6 hours, however upon calculating low conversions, the polymerisations indicated with a double asterisk were conducted for a further 6 hours with the same amount of additional initiator as used for the first run (AIBN).

Table 2-2: *Target copolymer composition, BuMA conversion, actual copolymer composition, theoretical M_n, GPC M_n and $Đ_M$, and transmittance at 700 nm, for PHEMA$_x$-b-PBuMA$_y$ diblock copolymers prepared via RAFT solution polymerisation of BuMA in DMF at 70 °C and 10% w/w for 25 hours using AIBN initiator ([macro-CTA]/[AIBN] molar ratio = 5.0). PHEMA$_x$-b-PBuMA$_y$ is denoted as H$_x$-B$_y$ for brevity.*

	^{1}H NMR Spectroscopy			DMF GPC		UV-Vis
Target Composition	**BuMA conversion (%)**	**Actual Composition[a]**	***$M_{n,th}$*** **(g mol^{-1})[b]**	***M_n*** **(g mol^{-1})**	***Đ***	**Transmittance at 700 nm (%)**
H_{21}	-	H_{21}	-	3800	1.34	-
H_{21}-B_{100}	87	H_{21}-B_{87}	16171	5900	1.59	100
H_{21}- B_{300}	70	H_{21}- B_{210}	33662	10000	1.61	100
H_{21}- B_{500}	56	H_{21}- B_{280}	43616	10900	1.77	99
H_{21}- B_{1000}	54	H_{21}- B_{540}	80588	16900	1.93	99
H_{77}	-	H_{77}	-	9500	1.30	-
H_{77}-B_{100}	69	H_{77}-B_{69}	22212	12900	1.27	99
H_{77}- B_{300}	74	H_{77}- B_{222}	43968	10300	1.81	97
H_{77}- B_{500}	66	H_{77}- B_{330}	59326	15600	1.65	99
H_{77}- B_{1000}	69	H_{77}- B_{690}	110518	16600	2.09	99

[a] Calculated using conversion from ^{1}H NMR
[b] Calculated using actual composition

2.3.3 Transparent dispersions of PHEMA-*b*-PBuMA block copolymer nanoparticles in [EMIM][EtOSO$_3$]

The vast majority of PISA formulations result in the formation of turbid dispersions due to the light scattering events caused by the presence of nanoparticles of differing refractive indices to that of the solvent. However, it was observed that all the resulting PHEMA-*b*-PBuMA dispersions in [EMIM][EtOSO$_3$] presented in this work were optically transparent (Figure 2.24), despite clear evidence for polymerisation-induced self-assembly, and thus the formation of block copolymer nanoparticles, from the kinetics studies presented earlier. This observation is particularly interesting given that initial reaction mixtures were turbid prior to syntheses being conducted, as expected for an emulsion polymerisation where the monomer is immiscible with the solvent[42]. The optical transparency of final dispersions was quantified using UV-vis spectroscopy (see values in Table 2-1), where the transmittance values were measured across the visible range (Figure 2.25 and Figure 2.26) and the transmittance at 700 nm plotted against the PBuMA DP value for each dispersion.

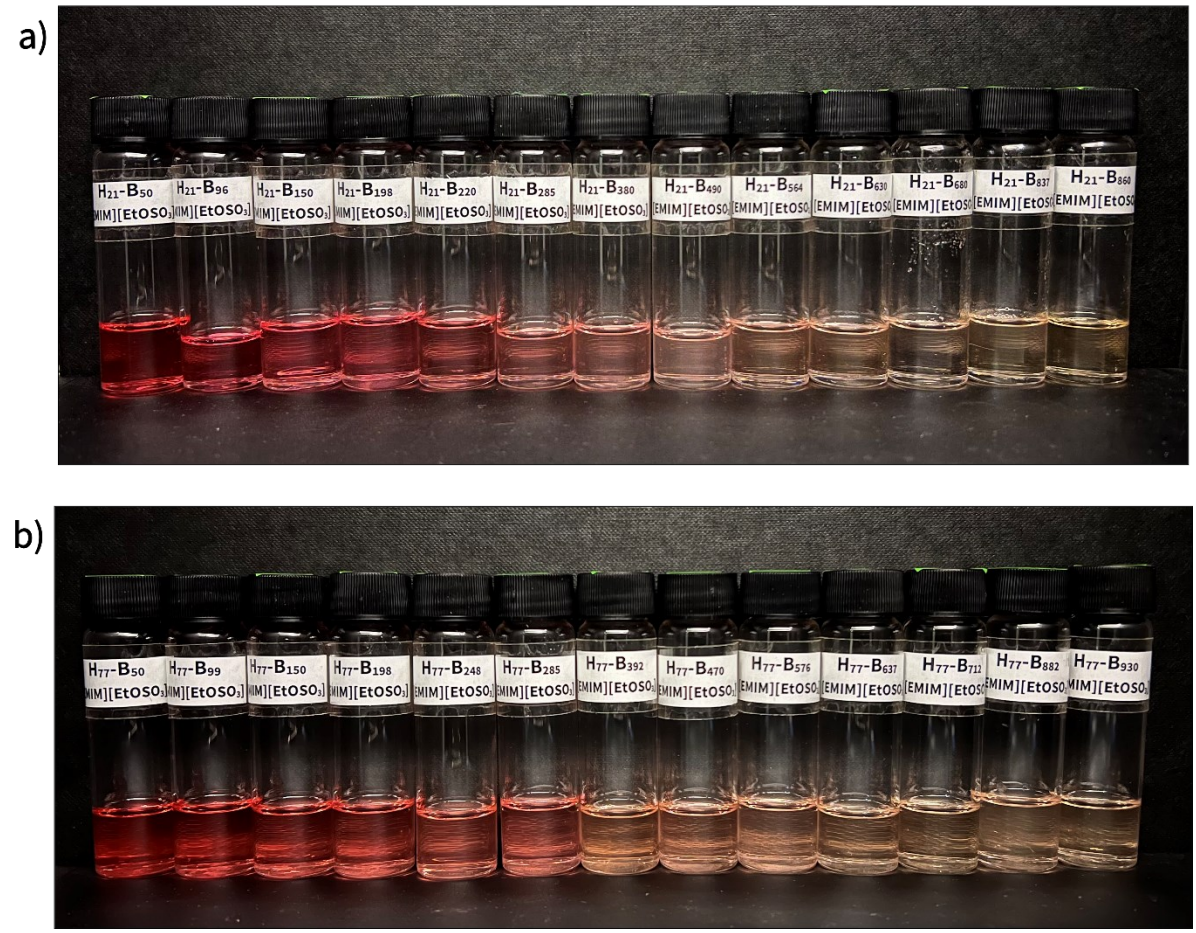

Figure 2.24. *Images showing the physical appearance and decrease in colour intensity with increasing PBuMA DP for the series of (a) $PHEMA_{21}$-b-$PBuMA_y$, and (b) $PHEMA_{77}$-b-$PBuMA_y$ block copolymer dispersions in [EMIM][$EtOSO_3$] at 10% w/w solids. $PHEMA_x$-b-$PBuMA_y$ is denoted as H_x-B_y for brevity.*

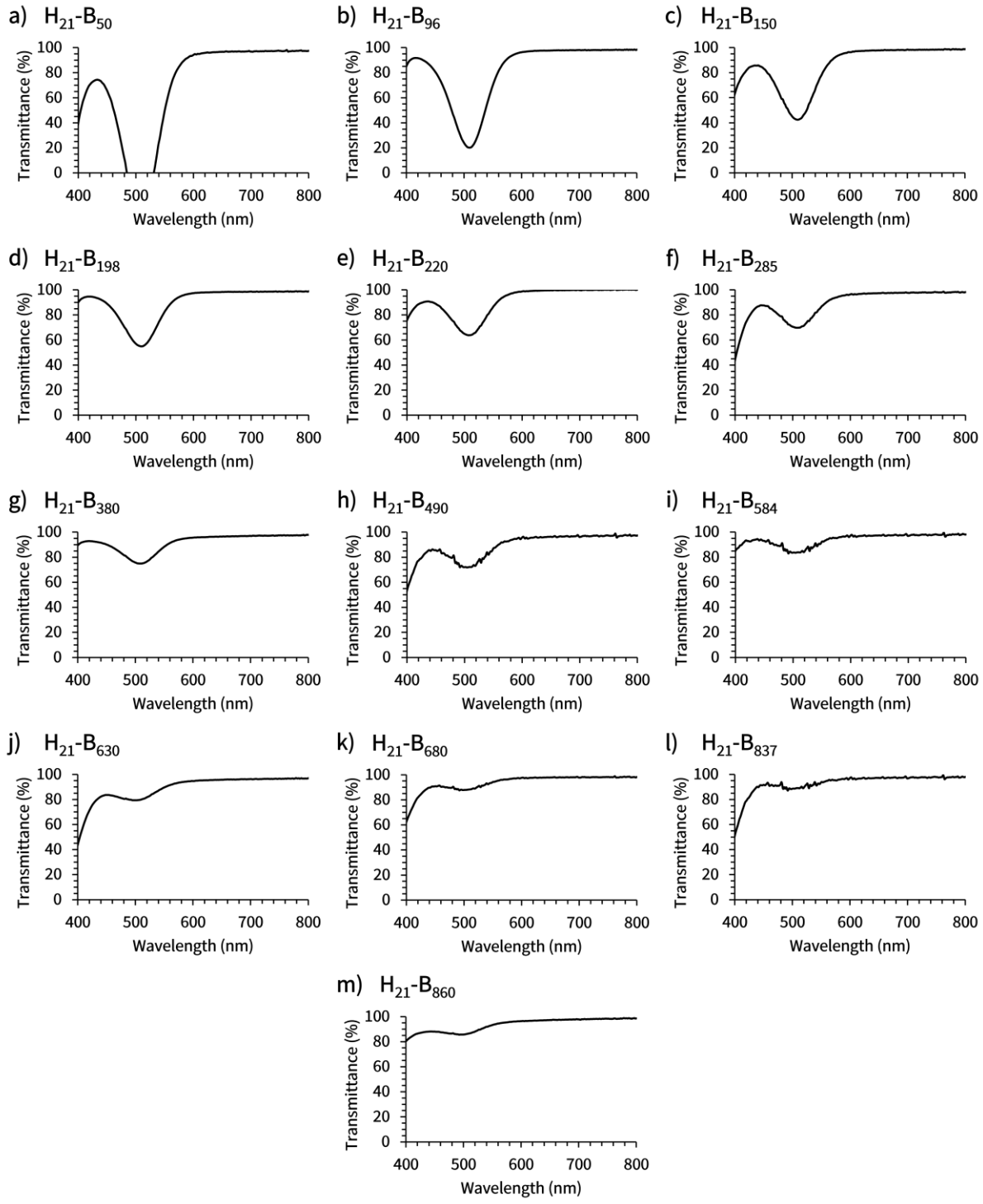

Figure 2.25. *UV-Vis spectra of transmittance against wavelength for 10% w/w dispersions of $PHEMA_{21}$-$PBuMA_y$ block copolymer nanoparticles in [EMIM][$EtOSO_3$], where the peak at ~500 nm represents the CPDT chain end which decreases in intensity with higher targeted PBuMA DPs. $PHEMA_x$-b-$PBuMA_y$ is denoted as H_x-B_y for brevity.*

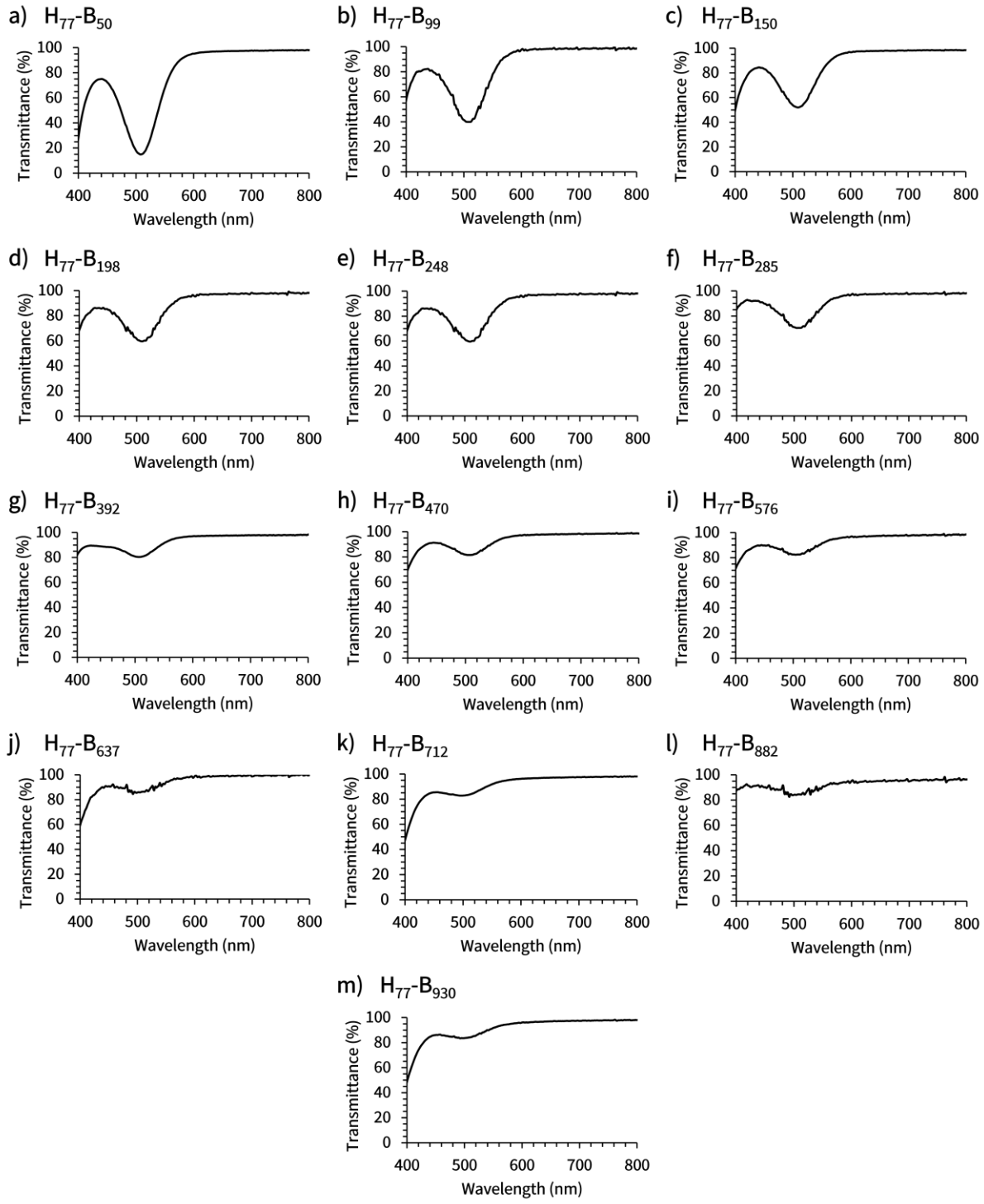

Figure 2.26. *UV-Vis spectra of transmittance against wavelength for 10% w/w dispersions of $PHEMA_{77}$-$PBuMA_y$ block copolymer nanoparticles in [EMIM][$EtOSO_3$], where the peak at ~500 nm represents the CPDT chain end which decreases in intensity with higher targeted PBuMA DPs. $PHEMA_x$-b-$PBuMA_y$ is denoted as H_x-B_y for brevity.*

Transmittance values at 700 nm were judged to be ≥95% for all dispersions, strongly suggesting the formation of near-isorefractive dispersions where the refractive index of the solvent and nanoparticle core are very similar. Indeed, this aligns with the refractive index values reported in literature for [EMIM][$EtOSO_3$] and PBuMA, which are both 1.48[52, 62, 63], explaining the solution transparency. For a direct comparison, PHEMA-*b*-PBuMA block copolymers were prepared via RAFT-PISA in an ethanol/water solvent mixture (4:1, w:w) to demonstrate the appearance of a turbid dispersion for this formulation (Figure 2.27c and d). The refractive index of this solvent system is around 1.36[64], therefore the difference in values would not result in an isorefractive solution. This solvent system was chosen as it is a good solvent in which PHEMA and BuMA are soluble, however PBuMA is insoluble. This solvent system has also been used in other PISA formulations[65, 66], including work conducted by Zhang *et al.*[66], whereby a macro-CTA comprising of methacrylic acid and poly(ethylene oxide) (50:50 %mol) was chain extended using benzyl methacrylate (BzMA) in a different solvent mixtures, including ethanol-water (ethanol–water, 95/5, v/v), to yield nanoparticles (mainly spheres and fibres).

As mentioned, since the refractive index value for the EtOH/H_2O solvent mixture has been reported to be 1.36[64], these dispersions would not provide high solution transmittance at 700 nm (Figure 2.27c and d). The actual values for transmittance at 700 nm from UV-Vis spectroscopy for these solutions were unable to be quantified due to the light scattering from the nanoparticles in solution. It can also be observed from that the extension of both PHEMA macro-CTAs in EtOH/H_2O resulted in block copolymers with high dispersity values of 1.51 and 1.61 (Figure 2.28), implying that the polymerisation in this solvent system was less well controlled than when [EMIM][$EtOSO_3$] was used as the solvent system.

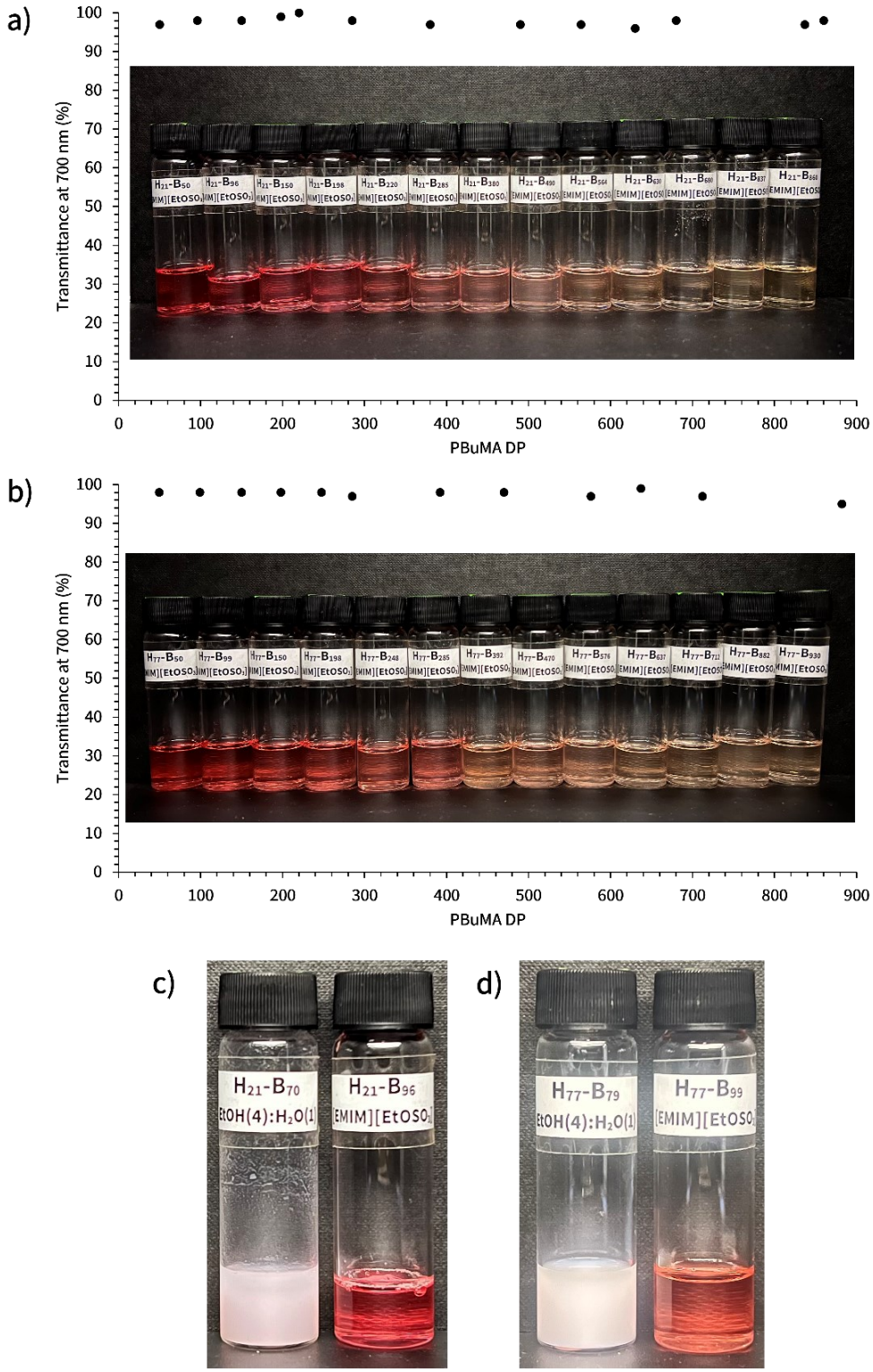

Figure 2.27. *Images showing the physical appearance of the series of (a) $PHEMA_{21}$-b-$PBuMA_y$, and (b) $PHEMA_{77}$-b-$PBuMA_y$ block copolymer dispersions in [EMIM][$EtOSO_3$] at 10% w/w solids, alongside corresponding transmittance values at 700 nm obtained from UV-vis spectroscopy. Labels on sample vials denote the actual $PHEMA_x$-b-$PBuMA_y$ composition, denoted as H_x-B_y, as determined using ^{1}H NMR spectroscopy. Images comparing the (c) $PHEMA_{21}$-b-$PBuMA_y$ and (d) $PHEMA_{21}$-b-$PBuMA_y$ dispersions prepared in an ethanol/water (4:1 w:w) solvent mixture (as a control measure) (left) and [EMIM][$EtOSO_3$] (right).*

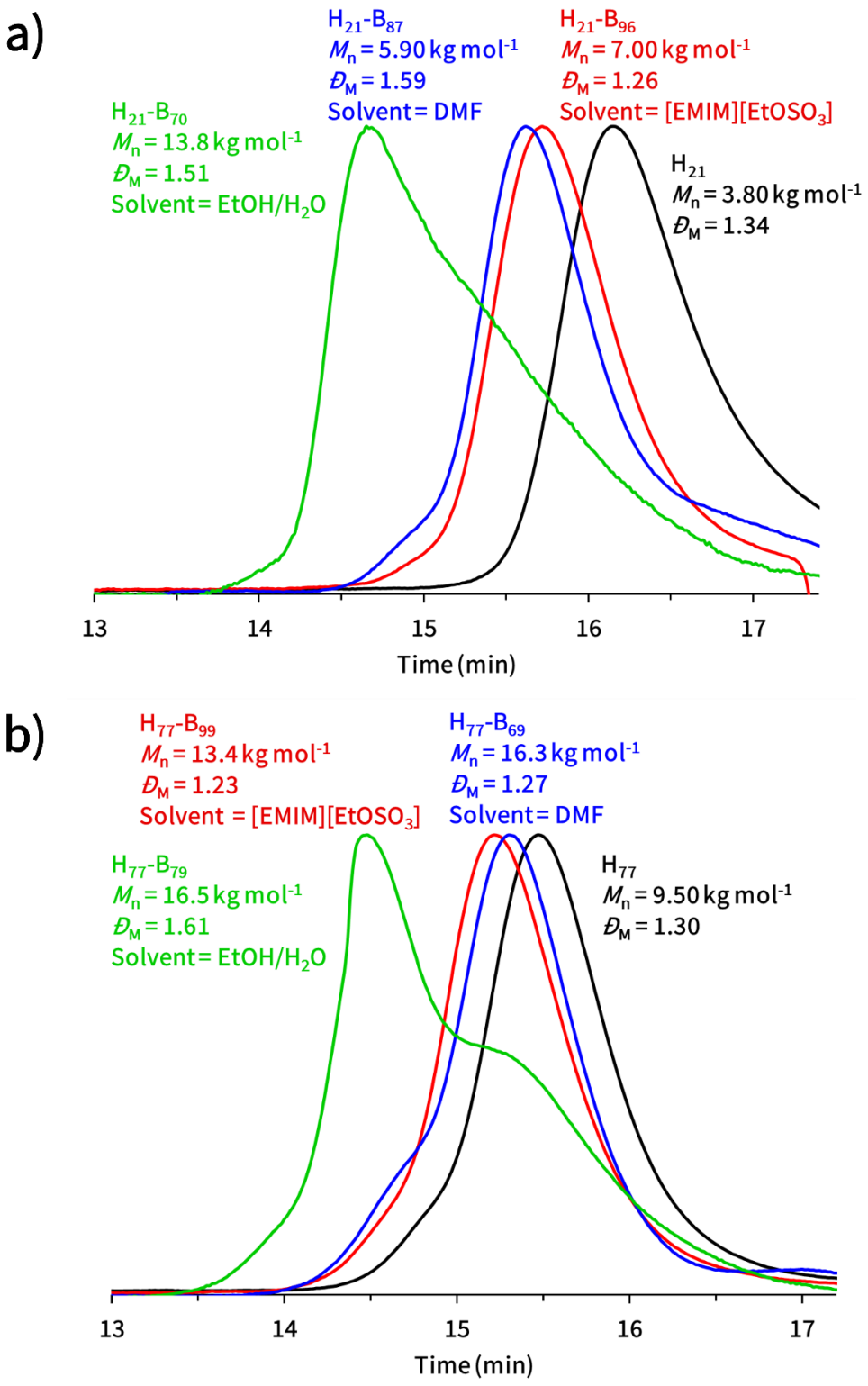

Figure 2.28. *DMF GPC data (vs. poly(methyl methacrylate) standards) obtained for the extension of a) $PHEMA_{21}$ and b) $PHEMA_{77}$ macro-CTAs with n-butyl methacrylate (BuMA), targeting a degree of polymerisation of 100, via RAFT emulsion PISA in [EMIM][$EtOSO_3$], solution polymerisation in DMF and dispersion PISA in EtOH/H_2O at 10% w/w solids, where PHEMA is denoted as H and PBuMA is denoted as B.*

2.3.4 Characterisation of PHEMA-*b*-PBuMA block copolymer nanoparticles in [EMIM][EtOSO$_3$]

A range of analytical techniques, specifically dynamic light scattering (DLS), transmission electron microscopy (TEM) and small-angle X-ray scattering (SAXS), were employed to characterise the nanoparticles present in the PHEMA$_{21}$-*b*-PBuMA$_y$ and PHEMA$_{77}$-*b*-PBuMA$_y$ block copolymer dispersions in [EMIM][EtOSO$_3$] (Table 2-3). Firstly, DLS was employed to demonstrate the presence of particles within the system, as shown in Figure 2.29. The DLS data obtained depicts a general trend of increasing diameter for increasing PBuMA DPs up to a target DP of 500, after this point, there is no clear trend present in the data. Although these results display a trend up to a certain point which aligns with other data, they must be interpreted with caution. In the case of PHEMA-*b*-PBuMA nanoparticles in [EMIM][EtOSO$_3$], the refractive index (RI) values of the nanoparticle cores (PBuMA, RI =1.483[63]) and the solvent ([EMIM][EtOSO$_3$] , RI = 1.480[52, 62]) are extremely similar and thus this formulation is isorefractive, as previously discussed in Section 2.3.3, meaning that the particles would be virtually undetectable by the equipment. Due to this, a representative correlogram of PHEMA$_{21}$-b-PBuMA$_{490}$ was obtained to show the data obtained from DLS was valid (Figure 2.30).

Table 2-3. *Actual copolymer composition, DLS diameter and PDI and SAXS measured core diameter (nm) for $PHEMA_x$-b-$PBuMA_y$ diblock copolymers prepared via RAFT emulsion polymerisation of BuMA in [EMIM][$EtOSO_3$] at 70 °C and 10% w/w using AIBN initiator ([macro-CTA]/[AIBN] molar ratio = 2.0). $PHEMA_x$-b-$PBuMA_y$ is denoted as H_x-B_y for brevity.*

	DLS		SAXS
Actual Composition	**Diameter (nm)**	**PDI**	**Core Diameter (nm)**
H_{21}	-	-	-
H_{21}-B_{50}	431	0.28	14.4*
H_{21}- B_{96}	44	0.14	21.5
H_{21}- B_{150}	57	0.22	35.1
H_{21}- B_{198}	59	0.17	41.0
H_{21}- B_{220}	70	0.16	35.3
H_{21}- B_{285}	102	0.07	61.7*
H_{21}- B_{380}	91	0.22	83.7*
H_{21}- B_{490}	86	0.14	113*
H_{21}- B_{564}	97	0.15	118*
H_{21}- B_{630}	63	0.26	139*
H_{21}- B_{680}	95	0.27	131*
H_{21}- B_{837}	132	0.13	126*
H_{21}- B_{860}	124	0.33	110*
H_{77}	-	-	-
H_{77}-B_{50}	34	0.37	10.5*
H_{77}- B_{99}	44	0.14	20.4
H_{77}- B_{150}	62	0.10	27.0
H_{77}- B_{198}	65	0.24	33.4
H_{77}- B_{248}	66	0.14	38.2
H_{77}- B_{285}	66	0.04	43.4
H_{77}- B_{392}	74	0.22	49.5
H_{77}- B_{470}	103	0.14	49.6
H_{77}- B_{576}	109	0.14	84.3*
H_{77}- B_{637}	87	0.14	71.6*
H_{77}- B_{712}	83	0.15	65.7*
H_{77}- B_{882}	123	0.13	124*
H_{77}- B_{930}	117	0.11	118*

*Estimated from the position of the peak (using core diameter = 2 * core radius = 4π/q). This was due to: 1) the q range not being sufficient and 2) some patterns show the presence of multiple populations (in this case, the particle with the largest diameter was recorded).

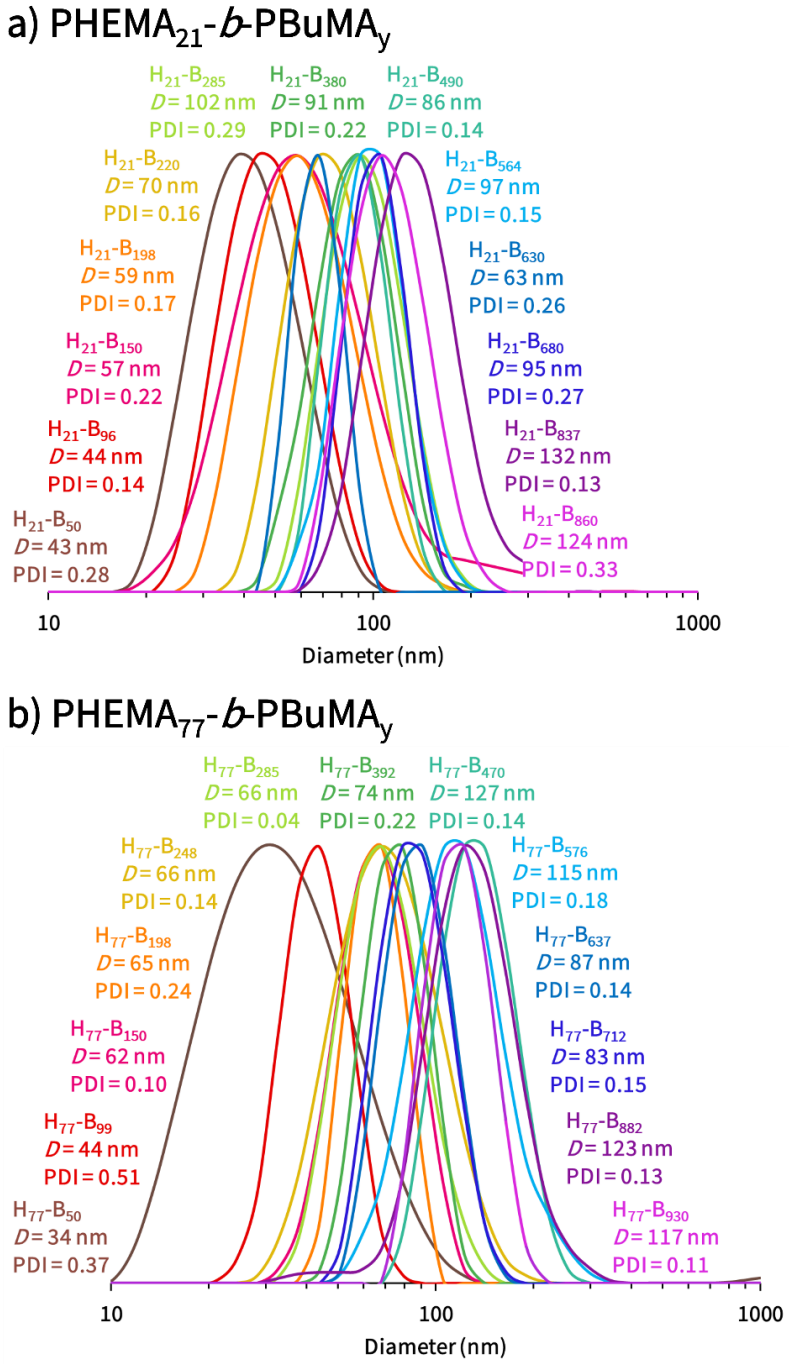

Figure 2.29. *DLS data (size vs intensity) obtained for 0.10% w/w dispersions of a) $PHEMA_{21}$-b-$PBuMA_y$ and b) $PHEMA_{77}$-b-$PBuMA_y$ block copolymers in [EMIM][$EtOSO_3$] prepared via RAFT emulsion polymerisation, where $PHEMA_x$-b-$PBuMA_y$ is denoted as H_x-B_y for brevity.*

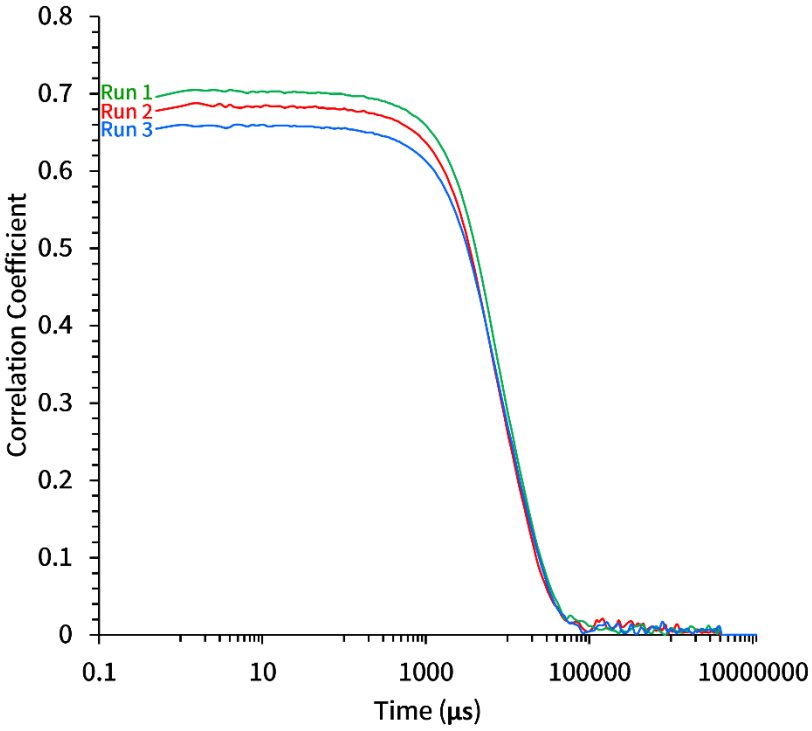

Figure 2.30. *Representative DLS correlogram (correlation coefficient vs time) for PHEMA$_{21}$-b-PBuMA$_{490}$.*

Thus, a more reliable analytical technique to determine not only the presence of particles, but also their morphology is SAXS. The SAXS data obtained for PHEMA$_{21}$-b-PBuMA$_y$ and PHEMA$_{77}$-b-PBuMA$_y$ can be seen below in Figure 2.31 and Figure 2.32.

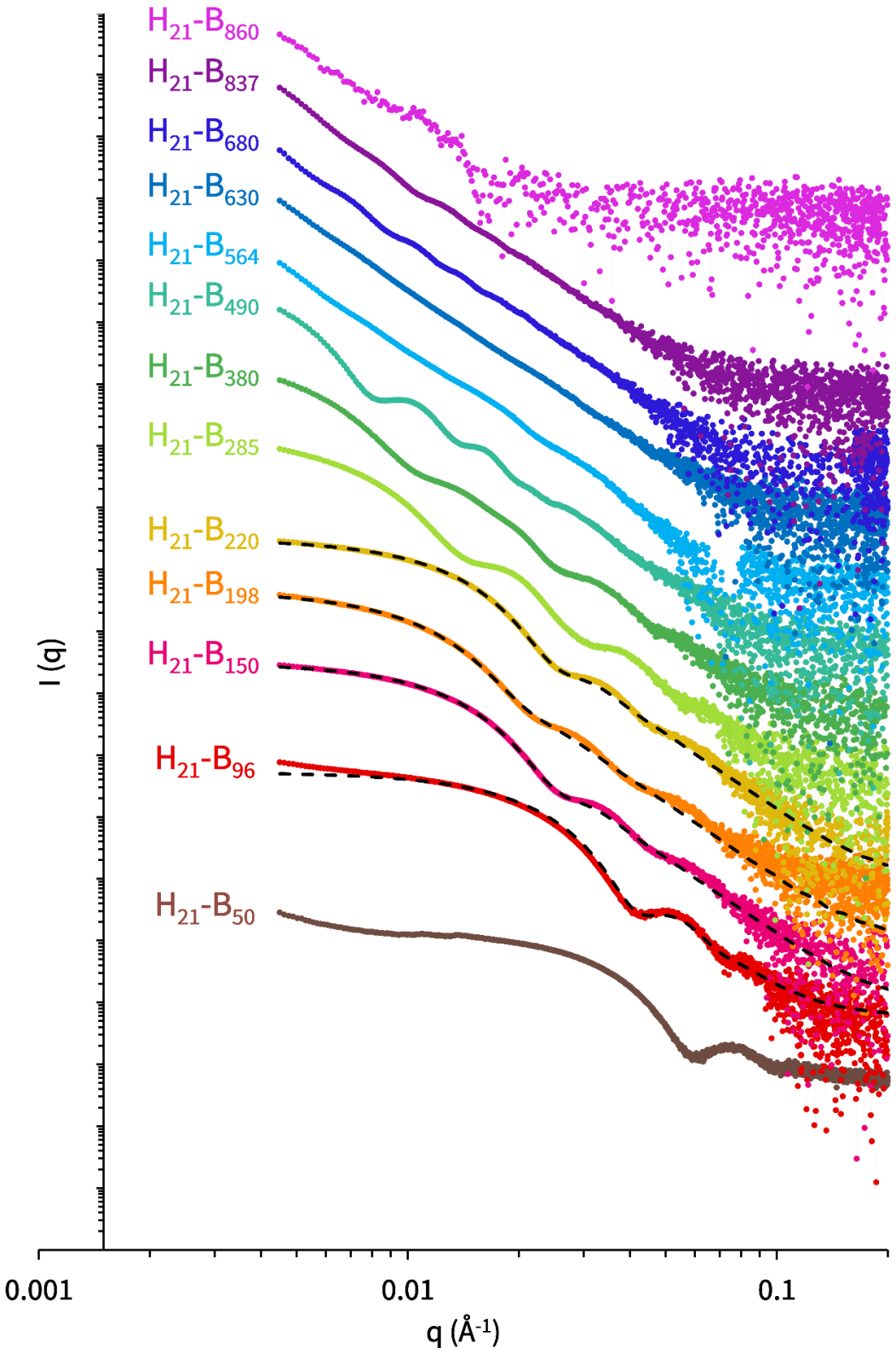

Figure 2.31. *Background-subtracted SAXS patterns recorded at 1.0% w/w for $PHEMA_{21}$-b-$PBuMA_y$ spheres (with PHEMA denoted as H and PBuMA denoted as B) prepared via RAFT emulsion polymerisation, where dashed lines represent fits to the spherical micelle model (as discussed in Section 1.6.3). For clarity, data are offset on the y-axis by a factor of 10.*

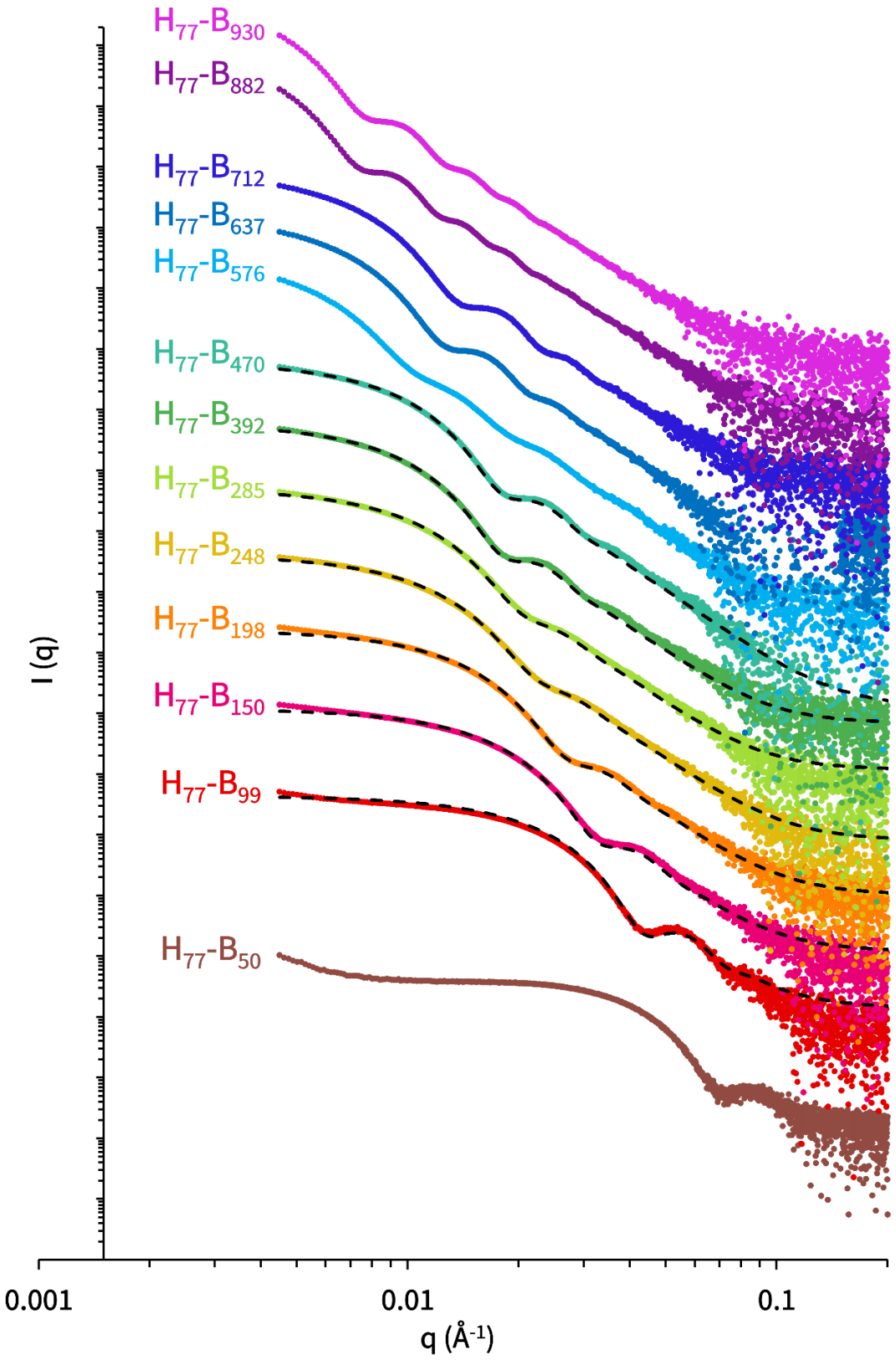

Figure 2.32. *Background-subtracted SAXS patterns recorded at 1.0% w/w for $PHEMA_{77}$-b-$PBuMA_y$ (with PHEMA denoted as H and PBuMA denoted as B) prepared via RAFT emulsion polymerisation, where dashed lines represent fits to the spherical micelle model (as discussed in Section1.6.3). For clarity, data are offset on the y-axis by a factor of 10.*

The SAXS data above (Figure 2.31 and Figure 2.32) indicates the presence of only spherical morphologies. This was determined from the plateauing of the gradient at lower q values, as a gradient of zero is indicative of spherical morphologies[67]. This is mostly clear from block copolymers H_{21}-B_{96} to H_{21}-B_{220} and H_{77}-B_{99} to H_{77}-B_{470}. The q range accessible meant that this plateauing was not visible for larger particles, however from the trend in increasing core diameter values in Table 2-3 it is implied that all morphologies present were spherical. The lowest PBuMA DP block copolymers, H_{21}-B_{50} and H_{77}-B_{50}, are not expected to have this trend as only loose aggregates would be present. From this, a spherical micelle model[55] was used to fit each background-subtracted data set, which can be observed from the black dashed line. It should be noted that although the presence of spheres for all samples was confirmed, it was not possible to fit all data sets, especially those obtained when targeting PBuMA DPs ≥ 500. Despite seeing clear evidence for the formation of nanoparticles in the SAXS patterns obtained for $PHEMA_{21}$-*b*-$PBuMA_{50}$ or $PHEMA_{77}$-*b*-$PBuMA_{50}$ dispersions, the spherical micelle model could not be used to satisfactorily fit these data. This is most likely due to the presence of a high proportion of freely dissolved polymer chains and/or the formation of loose, less well-defined aggregates. This is unsurprising since, as previously discussed, the DP at which micellization occurs was determined to be 58 when extending the $PHEMA_{21}$ macro-CTA and 40 when extending the $PHEMA_{77}$ macro-CTA. Nevertheless, the spherical micelle model was successfully applied to SAXS data obtained for $PHEMA_{21}$-*b*-$PBuMA_y$ nanoparticles with PBuMA DP values ≤ 220 and for $PHEMA_{77}$-*b*-$PBuMA_y$ nanoparticles with PBuMA DP values ≤ 470. A summary of the fitting parameters obtained in each of these fits can be found in Table 2-4 below.

Table 2-4. *Summary of parameters obtained when fitting SAXS data to the spherical micelle model with actual composition of sample and the corresponding volume fraction of spheres (φ), core radius, R_s (nm) and radius of gyration of the stabiliser chains, R_g (nm).*

Actual Composition	Volume fraction of spheres, φ	Core radius, R_s (nm)	Radius of gyration of the stabiliser chains, R_g (nm)
H_{21}-B_{96}	0.0572	10.8 ± 1.5	1.0
H_{21}-B_{150}	0.0845	17.6 ± 3.2	1.0
H_{21}-B_{198}	0.0750	20.5 ± 4.5	1.0
H_{21}-B_{220}	0.0810	17.7 ± 3.1	1.0
H_{77}-B_{99}	0.0782	10.2 ± 1.3	1.0
H_{77}-B_{150}	0.0795	13.5 ± 2.0	1.3
H_{77}-B_{198}	0.0883	16.7 ± 2.7	1.3
H_{77}-B_{248}	0.0858	19.1 ± 3.4	1.3
H_{77}-B_{285}	0.0807	21.7 ± 3.9	1.3
H_{77}-B_{392}	0.0621	24.7 ± 3.7	1.5
H_{77}-B_{470}	0.0619	24.8 ± 3.8	1.5

As mentioned, PBuMA DPs above these values, data fits were unsuccessful, this is most likely due to the q-range accessible by the B21 beamline at Diamond Light Source, which is limited to $q \geq 0.045$ nm^{-1} and thus cannot resolve larger nanoparticles. Another possibility is the presence of multiple populations of spherical micelles in the dispersion, which may arise due to the uncontrolled nature of the RAFT polymerisation when targeting higher PBuMA DPs as observed in the deviation from linearity when plotting M_n vs. PBuMA DP and in dispersity values (Figure 2.17 and Figure 2.18). From the successful spherical micelle model fittings, the relationship between actual PBuMA DP and the sphere core diameter (D) was plotted. The equation $D \sim k.DP^{\alpha}$, where k represents a constant, DP represents degree of polymerisation of PBuMA and α represents a scaling exponent (the alpha parameter), which can then be used to analyse the data further. An alpha value of 0.5 represents unperturbed chains within the micelle cores, meaning that the polymer chains behave as if under theta conditions. This behaviour results in random (Gaussian) coils which are ideal – meaning that there is an equal balance between the interactions of the polymer chains with either the solvent or other polymer chains within proximity[68, 69]. Conversely, an alpha value of 1 indicates that the polymer chain is completely stretched inside of the micelle and there is a linear relationship between core diameter and DP. The effect of shorter and longer stabiliser blocks on the alpha parameter value can be seen in Figure 2.33.

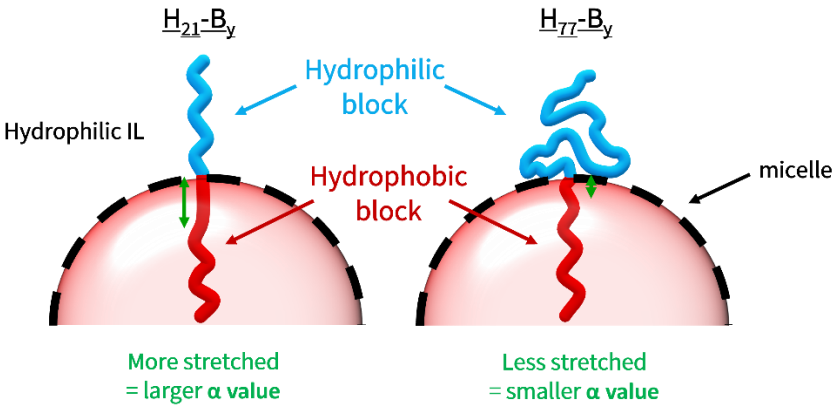

Figure 2.33. *A diagram displaying the effect of differing length stabiliser blocks (in this case $PHEMA_{21}$ and $PHEMA_{77}$) on the alpha parameter value.*

In this case (Figure 2.34), it can be observed that the series for the $PHEMA_{21}$-*b*-$PBuMA_y$ spherical nanoparticles exhibit a steeper gradient with an alpha value of 0.90, whereas the $PHEMA_{77}$-*b*-$PBuMA_y$ series exhibits a shallower gradient with a lower alpha value of 0.71. From the literature, it has been suggested that the alpha parameter for block copolymer micelles in theory should be around 0.67[69, 70], which is closer to the blue data for the $PHEMA_{77}$-*b*-$PBuMA_y$ nanoparticles, whereas the data set for the $PHEMA_{21}$-*b*-$PBuMA_y$ nanoparticles is closer to 1. Such a difference in alpha values between series of spherical micelles prepared via PISA using macro-CTAs of varying length has also been reported in the literature by both Derry *et al.*[71] for a dispersion PISA formulation and Akpinar *et al.*[72] for an emulsion PISA formulation. Both of these examples demonstrate that when preparing different block copolymer series using macro-CTAs with different DPs, the extension of longest DP macro-CTA results in a decreased alpha (α) parameter. This is also in agreement with this research, which has shown that the alpha value obtained for the extension of the $PHEMA_{77}$ macro-CTA was lower (0.71) than the extension of the shorter $PHEMA_{21}$ macro-CTA (0.90). The reasoning behind this phenomenon is due to the longer stabiliser block copolymers having weaker segregation, and therefore adapting a more coiled conformation, rather than stretched which is common for shorter stabiliser block copolymers[69, 71]. Table 2-3 shows how the $PHEMA_{77}$ polymer nanoparticles have a lower diameter compared to those of the corresponding nanoparticles yielded from the $PHEMA_{21}$ polymers, which is also in agreement with this theory and the literature[69, 71].

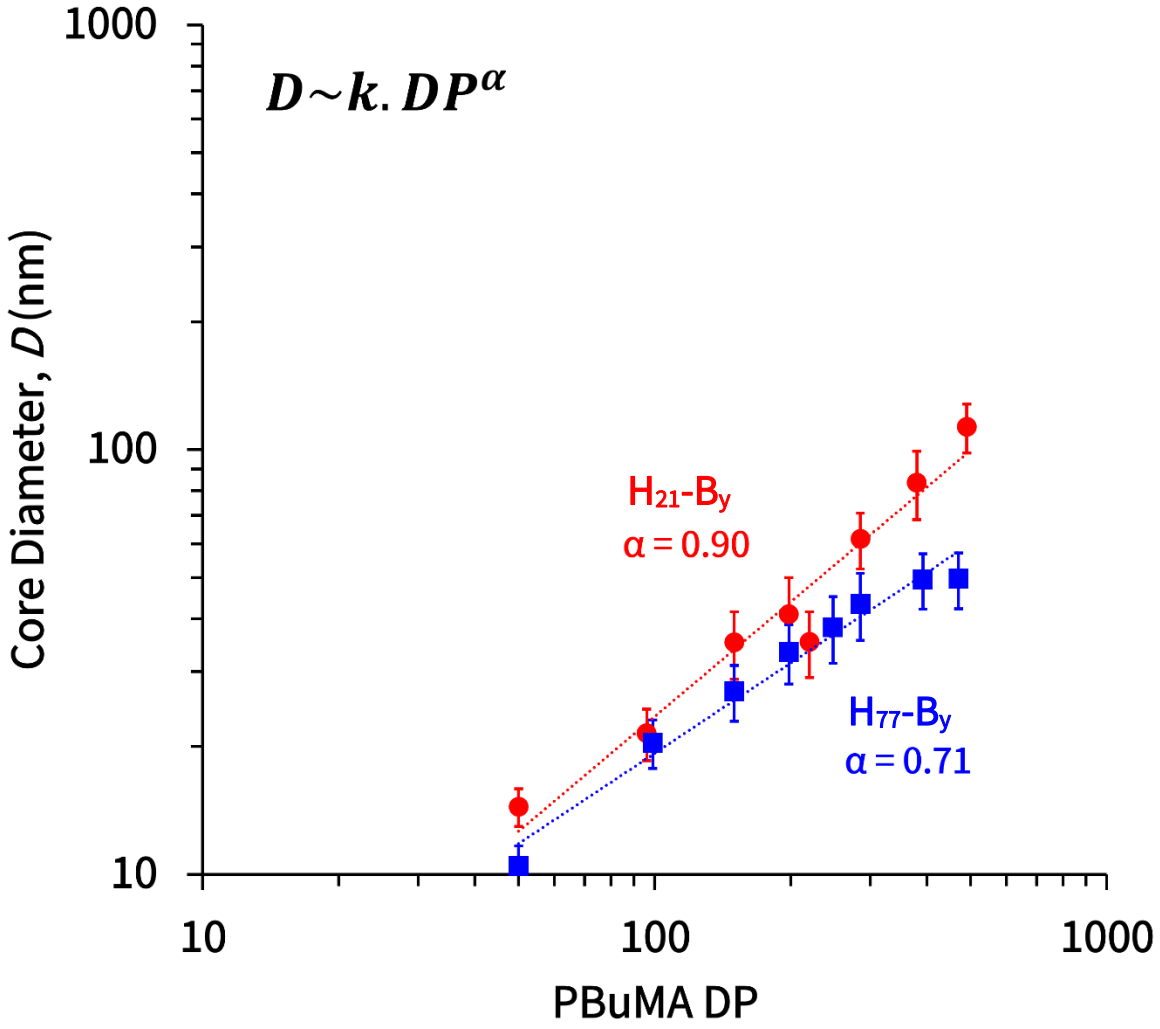

Figure 2.34. *Relationship between core radius and target DP of the PBuMA block (y) for series of $PHEMA_{21}$–b–$PBuMA_y$ (red circles) and $PHEMA_{77}$–b–$PBuMA_y$ (blue squares) diblock copolymer spheres prepared via RAFT emulsion polymerisation of BuMA in [EMIM][$EtOSO_3$] at 70 °C. The error bars represent the standard deviation of the diameter and α is the scaling factor.*

TEM was also used to characterise the synthesised nanoparticles, however the imaging proved difficult due to the presence of residual ionic liquid in the sample. This is due to the extremely low volatility of ionic liquids, which is explained by the strong ionic bonding between molecules within the fluid, resulting in extremely low vapour pressure values[73]. By contrast, traditional solvents have significantly higher vapour pressures which result in spontaneous evaporation, such as DMF which has a vapour pressures of ~1 kPa at 34 °C[74]. The exact vapour pressure value for [EMIM][$EtOSO_3$] alone specifically was not found in the literature, however a value of 0.0071 kPa at 20°C was obtained from

an online CAS DataBase list. This resulted in challenges arising in the analysis of many of the samples as the presence of residual ILs produced unclear imaging in the majority of cases.

Due to these difficulties, the TEM images seen below in Figure 2.35 were the only successful attempts at imaging these samples. Automated particle size analysis was attempted (using imageJ) with the clearest images, however the lack of high resolution meant that the diameter values for the particles were unattainable. Whilst this is not ideal, the combination of DLS, SAXS and TEM as a suite of nanoparticle characterisation techniques provides confidence that well-defined spherical nanoparticles are formed during the RAFT emulsion polymerisation of BuMA in [EMIM][$EtOSO_3$] using PHEMA macro-CTAs as steric stabilisers.

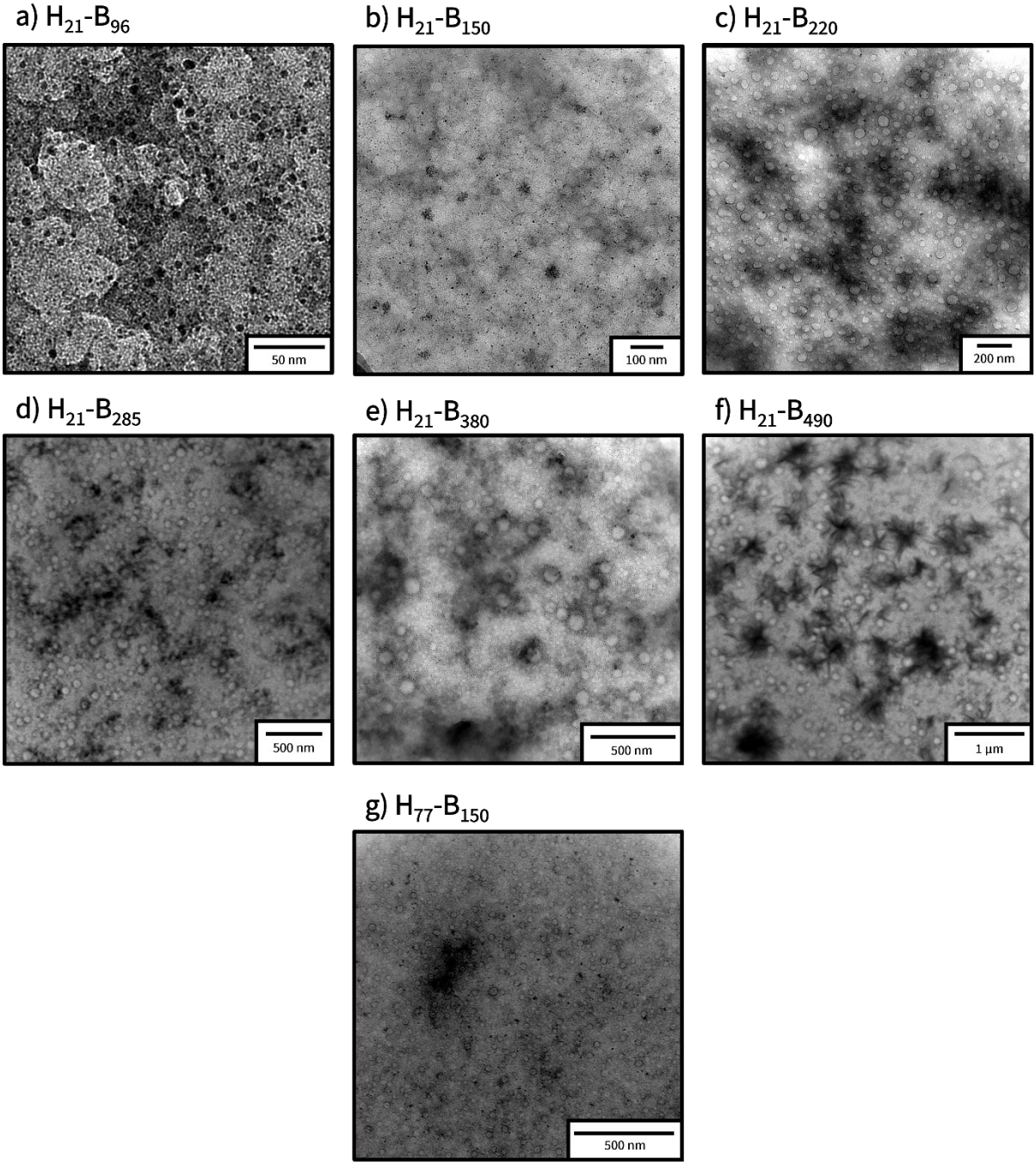

Figure 2.35. *TEM images for 0.10% w/w emulsions of $PHEMA_x$-b-$PBuMA_y$ block copolymers (with PHEMA denoted as H and PBuMA denoted as B) prepared in [EMIM][$EtOSO_3$] . Images obtained using bright-field detection.*

From the available images, it is clear that spherical morphologies were formed. These spherical nanoparticles increase in size with increasing target PBuMA DP, as suggested by DLS and SAXS analysis.

2.4 Conclusions

In summary, RAFT emulsion polymerisation was used to synthesise series of $PHEMA_{21}$-*b*-$PBuMA_y$ and $PHEMA_{77}$-*b*-$PBuMA_y$ block copolymers in [EMIM][$EtOSO_3$] at 70 °C and at 10% w/w solids. This synthesis approach enabled higher monomer conversions (86 - 99%) to be obtained in only 2 hours of reaction time, compared to lower monomer conversions (54 - 87%) obtained when conducting solution polymerisations in DMF for 25 hours. In addition to this, lower dispersity values were obtained for the block copolymers synthesis via emulsion PISA in [EMIM][$EtOSO_3$] (1.15 - 1.71) compared to solution polymerisations in DMF (1.27 - 2.09). It was also found that the block copolymer synthesised in ionic liquid followed expected trends for well controlled RAFT polymerisations, such as a linear growth in M_n with increasing PBuMA DP, however this was only observed up to a limiting target PBuMA DP of 500. This observation was in agreement with the PISA literature, which also reports the deterioration of trends when targeting higher DPs for the structure-directing block. Following the PISA synthesis of PHEMA-*b*-PBuMA nanoparticles in [EMIM][$EtOSO_3$], the resulting dispersions were discovered to be highly transparent. This was due to the closely matched refractive index values of the ionic liquid solvent, [EMIM][$EtOSO_3$], and the structure-directing polymer, poly(*n*-butyl methacrylate). The presence of spherical nanoparticles in the resulting dispersions was confirmed using a combination of DLS, SAXS and TEM analyses. The DLS data obtained indicated the presence of nano-objects, but further interpretation of results was deemed unreliable due to the fact that this technique would struggle to detect nanoparticles with similar refractive indices in the continuous phase. SAXS analysis successfully demonstrated the formation of spherical nanoparticles, and additionally highlighted the decrease in alpha parameter value with the decrease in length of stabiliser block. This indicated that smaller particles would be obtained for the $PHEMA_{77}$ synthesised block copolymers in comparison to the corresponding $PHEMA_{21}$ block copolymers, which was further proven from SAXS-obtained core diameter values. TEM was also used to visually show the formation of spheres, although there were difficulties in the preparation of TEM grids due to the inherent low vapour pressure of the ionic liquid. Overall, this work demonstrates the advantages and ability of ILs to replace traditional solvents for the efficient synthesis of block copolymers, achieving higher monomer conversions at reduced polymerisation times. Additionally, this work reports the first RAFT emulsion PISA formulation in ionic liquid, advancing the capabilities of the PISA and ionic liquid communities, as well as showcasing the advances using ionic liquids as a more sustainable solvent over traditional organic solvents.

Moreover, this new formulation yields highly transparent dispersions despite the presence of large (> 100 nm) spherical nanoparticles.

2.5 References

1. T. P. Lodge, *Macromolecular chemistry and physics*, 2003, **204**, 265-273.
2. N. Politakos and A. Avgeropoulos, *Polymers*, 2023, **15**, 2930.
3. G. E. Parkes, H. J. Hutchins-Crawford, C. Bourdin, S. Reynolds, L. J. Leslie, M. J. Derry, J. L. Harries and P. D. Topham, *Polymer Chemistry*, 2020, **11**, 2869-2882.
4. H. Feng, X. Lu, W. Wang, N. G. Kang and J. W. Mays, *Polymers (Basel)*, 2017, **9**.
5. M. Zhang, S. M. June and T. E. Long, in *Polymer Science: A Comprehensive Reference*, eds. K. Matyjaszewski and M. Möller, Elsevier, Amsterdam, 2012, pp. 7-47.
6. Y. He, Z. Li, P. Simone and T. P. Lodge, *Journal of the American Chemical Society*, 2006, **128**, 2745-2750.
7. R. Tamate, K. Hashimoto, T. Ueki and M. Watanabe, *Physical Chemistry Chemical Physics*, 2018, **20**, 25123-25139.
8. Y. Mai and A. Eisenberg, *Chemical Society Reviews*, 2012, **41**, 5969-5985.
9. L. I. Atanase and G. Riess, *Polymers*, 2018, **10**, 62.
10. Z. Lei, B. Chen, Y.-M. Koo and D. R. MacFarlane, *Chemical Reviews*, 2017, **117**, 6633-6635.
11. P. Sharma, S. Sharma and H. Kumar, *Journal of Molecular Liquids*, 2024, **393**, 123447.
12. A. J. Greer, J. Jacquemin and C. Hardacre, *Molecules*, 2020, **25**, 5207.
13. G. A. O. Tiago, I. A. S. Matias, A. P. C. Ribeiro and L. M. D. R. S. Martins, *Molecules*, 2020, **25**, 5812.
14. K. Sood, Y. Saini and K. K. Thakur, *Materials Today: Proceedings*, 2023, **81**, 739-744.
15. A. Tsurumaki, T. Iwata, M. Tokuda, H. Minami, M. A. Navarra and H. Ohno, *Electrochimica Acta*, 2019, **308**, 115-120.
16. Y. Ding, H. Tang, X. Zhang, S. Wu and R. Xiong, *European Polymer Journal*, 2008, **44**, 1247-1251.
17. C. M. Caldas, B. G. Soares, T. Indrusiak and G. M. O. Barra, *Journal of Applied Polymer Science*, 2021, **138**, 49814.
18. V. Bugatti, G. Viscusi, A. Di Bartolomeo, L. Iemmo, D. C. Zampino, V. Vittoria and G. Gorrasi, *Polymers*, 2020, **12**, 495.
19. J. R. Lim, L. S. Chua and A. A. Mustaffa, *Process Biochemistry*, 2022, **122**, 292-306.
20. Z. Yang and W. Pan, *Enzyme and Microbial Technology*, 2005, **37**, 19-28.
21. G. Durga, P. Kalra, V. Kumar Verma, K. Wangdi and A. Mishra, *Journal of Molecular Liquids*, 2021, **335**, 116540.
22. P. Kubisa, *Progress in Polymer Science*, 2009, **34**, 1333-1347.
23. N. Winterton, *Journal of Materials Chemistry*, 2006, **16**, 4281-4293.
24. P. Kubisa, *European Polymer Journal*, 2020, **133**, 109778.
25. N. K. Singha, K. Hong and J. W. Mays, in *Polymerized Ionic Liquids*, ed. A. Eftekhari, The Royal Society of Chemistry, 2017, DOI: 10.1039/9781788010535-00001, p. 0.
26. H. Nawaz and F. Xu, in *Encyclopedia of Ionic Liquids*, ed. S. Zhang, Springer Nature Singapore, Singapore, 2022, pp. 1266-1271.
27. A. R. S. Santha Kumar, M. Roy and N. K. Singha, *European Polymer Journal*, 2018, **107**, 294-302.

28. J. Chiefari, Y. K. Chong, F. Ercole, J. Krstina, J. Jeffery, T. P. T. Le, R. T. A. Mayadunne, G. F. Meijs, C. L. Moad, G. Moad, E. Rizzardo and S. H. Thang, *Macromolecules*, 1998, **31**, 5559-5562.
29. S. Perrier, *Macromolecules*, 2017, **50**, 7433-7447.
30. N. J. Warren and S. P. Armes, *Journal of the American Chemical Society*, 2014, **136**, 10174-10185.
31. M. J. Derry, L. A. Fielding and S. P. Armes, *Progress in Polymer Science*, 2016, **52**, 1-18.
32. P. J. Docherty, M. J. Derry and S. P. Armes, *Polymer Chemistry*, 2019, **10**, 603-611.
33. C. György, M. J. Derry, E. J. Cornel and S. P. Armes, *Macromolecules*, 2021, **54**, 1159-1169.
34. D. Ikkene, J.-L. Six and K. Ferji, *European Polymer Journal*, 2023, **188**, 111848.
35. E. R. Jones, O. O. Mykhaylyk, M. Semsarilar, M. Boerakker, P. Wyman and S. P. Armes, *Macromolecules*, 2016, **49**, 172-181.
36. B. R. Parker, M. J. Derry, Y. Ning and S. P. Armes, *Langmuir*, 2020, **36**, 3730-3736.
37. G. L. Maitland, M. Liu, T. J. Neal, J. Hammerton, Y. Han, S. D. Worrall, P. D. Topham and M. J. Derry, *Chemical Science*, 2024, **15**, 4416-4426.
38. R. Yamanaka, A. Sugawara-Narutaki and R. Takahashi, *Macromolecules*, 2023, **56**, 4354-4361.
39. Q. Zhang and S. Zhu, *ACS Macro Letters*, 2015, **4**, 755-758.
40. H. Zhou, C. Liu, C. Gao, Y. Qu, K. Shi and W. Zhang, *Journal of Polymer Science Part A: Polymer Chemistry*, 2016, **54**, 1517-1525.
41. M. J. Rymaruk, K. L. Thompson, M. J. Derry, N. J. Warren, L. P. D. Ratcliffe, C. N. Williams, S. L. Brown and S. P. Armes, *Nanoscale*, 2016, **8**, 14497-14506.
42. A. Takashima, Y. Maeda and S. Sugihara, *ACS Omega*, 2022, **7**, 26894-26904.
43. M. Zeng, X. Li, Y. Zhang, X. Chen, X. Sui and J. Yuan, *Polymer*, 2020, **206**, 122853.
44. C. György and S. P. Armes, *Angewandte Chemie International Edition*, 2023, **62**, e202308372.
45. S. L. Canning, G. N. Smith and S. P. Armes, *Macromolecules*, 2016, **49**, 1985-2001.
46. F. d'Agosto, J. Rieger and M. Lansalot, *Angewandte Chemie International Edition*, 2020, **59**, 8368-8392.
47. J. Wan, B. Fan and S. H. Thang, *Chemical Science*, 2022, **13**, 4192-4224.
48. R. Yamanaka, A. Sugawara-Narutaki and R. Takahashi, *ACS Macro Letters*, 2024, **13**, 1050-1055.
49. U. Rivera-Ortega, C. R. Hernández-Gómez, G. Vega-Torres and M. E. Lopez-Medina, *Measurement*, 2019, **134**, 658-661.
50. J. Ziming Sun, M. C. Erickson and J. W. Parr, *International Journal of Cosmetic Science*, 2005, **27**, 355-356.
51. K. L. Thompson, J. A. Lane, M. J. Derry and S. P. Armes, *Langmuir*, 2015, **31**, 4373-4376.
52. A. P. Fröba, H. Kremer and A. Leipertz, *The Journal of Physical Chemistry B*, 2008, **112**, 12420-12430.
53. N. P. Cowieson, C. J. Edwards-Gayle, K. Inoue, N. S. Khunti, J. Doutch, E. Williams, S. Daniels, G. Preece, N. A. Krumpa and J. P. Sutter, *Synchrotron Radiation*, 2020, **27**, 1438-1446.
54. J. Ilavsky and P. R. Jemian, *Journal of Applied Crystallography*, 2009, **42**, 347-353.
55. J. S. Pedersen, *Journal of Applied Crystallography*, 2000, **33**, 637-640.
56. J. S. Pedersen and M. C. Gerstenberg, *Colloids and Surfaces A: Physicochemical and Engineering Aspects*, 2003, **213**, 175-187.
57. J. S. Pedersen, C. Svaneborg, K. Almdal, I. W. Hamley and R. N. Young, *Macromolecules*, 2003, **36**, 416-433.
58. M. J. Derry, L. A. Fielding and S. P. Armes, *Polymer Chemistry*, 2015, **6**, 3054-3062.

59. S. Gupta and V. Raus, *Reactive and Functional Polymers*, 2023, **183**, 105509.
60. A. Blanazs, J. Madsen, G. Battaglia, A. J. Ryan and S. P. Armes, *Journal of the American Chemical Society*, 2011, **133**, 16581-16587.
61. L. A. Fielding, M. J. Derry, V. Ladmiral, J. Rosselgong, A. M. Rodrigues, L. P. Ratcliffe, S. Sugihara and S. P. Armes, *Chemical Science*, 2013, **4**, 2081-2087.
62. A. N. Soriano, B. T. Doma and M.-H. Li, *Journal of the Taiwan Institute of Chemical Engineers*, 2010, **41**, 115-121.
63. J. Stevens, D. Jackson and J. Champion, *Molecular Physics*, 1975, **29**, 1893-1905.
64. T. A. Scott Jr, *The Journal of physical chemistry*, 1946, **50**, 406-412.
65. E. R. Jones, M. Semsarilar, P. Wyman, M. Boerakker and S. P. Armes, *Polymer Chemistry*, 2016, **7**, 851-859.
66. X. Zhang, J. Rieger and B. Charleux, *Polymer Chemistry*, 2012, **3**, 1502-1509.
67. I. W. Hamley, *Small-Angle Scattering: Theory, Instrumentation, Data, and Applications*, Wiley, 2021.
68. K. S. Kontturi, L. Solhi, E. Kontturi and T. Tammelin, *Langmuir*, 2024, **40**, 568-579.
69. G. Battaglia and A. J. Ryan, *Journal of the American Chemical Society*, 2005, **127**, 8757-8764.
70. S. Förster, M. Zisenis, E. Wenz and M. Antonietti, *The Journal of chemical physics*, 1996, **104**, 9956-9970.
71. M. J. Derry, L. A. Fielding, N. J. Warren, C. J. Mable, A. J. Smith, O. O. Mykhaylyk and S. P. Armes, *Chemical Science*, 2016, **7**, 5078-5090.
72. B. Akpinar, L. A. Fielding, V. J. Cunningham, Y. Ning, O. O. Mykhaylyk, P. W. Fowler and S. P. Armes, *Macromolecules*, 2016, **49**, 5160-5171.
73. M. Bier and S. Dietrich, *Molecular Physics*, 2010, **108**, 211-214.
74. X. Cui, G. Chen and X. Han, *Journal of Chemical & Engineering Data*, 2006, **51**, 1860-1861.

3. Incorporation of photo-active moieties for UV cross-linkable polymers

3.1 Introduction

Polymers alone have almost countless uses[1-4], with their presence being almost ubiquitous in modern life. Their uses span from packaging and plastics, such as the everyday plastic bag polyethylene (PE)[5] or common drinks containers (poly(ethylene tetraphthalate) (PET))[6], to high performance engineering polymers such as polyetheretherketone (PEEK)[7] or polytetrafluoroethylene (PTFE)[8], typically used in the automotive and aerospace industries for their electrical and thermally resistant properties. Despite their breadth of use, adding functionality to polymers can enhance their usefulness for more specific applications. In particular, the addition of functional groups capable of inducing cross-linking can increase the strength, stability and durability of a polymeric material[9-13]. As mentioned previously, one of the focuses of this thesis is the incorporation of functional cross-linkable groups within the polymer that can be triggered by exposure to ultraviolet (UV) light, as opposed to thermal treatment, in an attempt to increase sustainability. Parkes *et al.*[14] previously reported the synthesis of thermally triggerable block copolymers for use as dispersants in aqueous inkjet printing formulations. A series of amphiphilic diblock copolymers comprised of 2-hydroxyethyl acrylate (HEA) and *n*-propyl methacrylate (PMA) were synthesised with a thermally triggerable *N*-hydroxymethyl acrylamide (HMAA) group incorporated within the hydrophilic stabiliser block (Figure 3.1). This block copolymer additive was formulated with a commercially available printing ink, which imparted improved adhesive properties and enhanced durability after printing onto hydrophobic substrates and subsequent thermal curing to induce covalent cross-linking. Although this work showed the successful synthesis of a cross-linkable functionalised amphiphilic diblock copolymer to be used in aqueous inkjet applications (in an attempt to move away from inks using organic solvents), the process required a heating to 150 °C for up to 3 hours and resulted in a formaldehyde by-product, all of which negatively impact the sustainability credentials of this formulation.

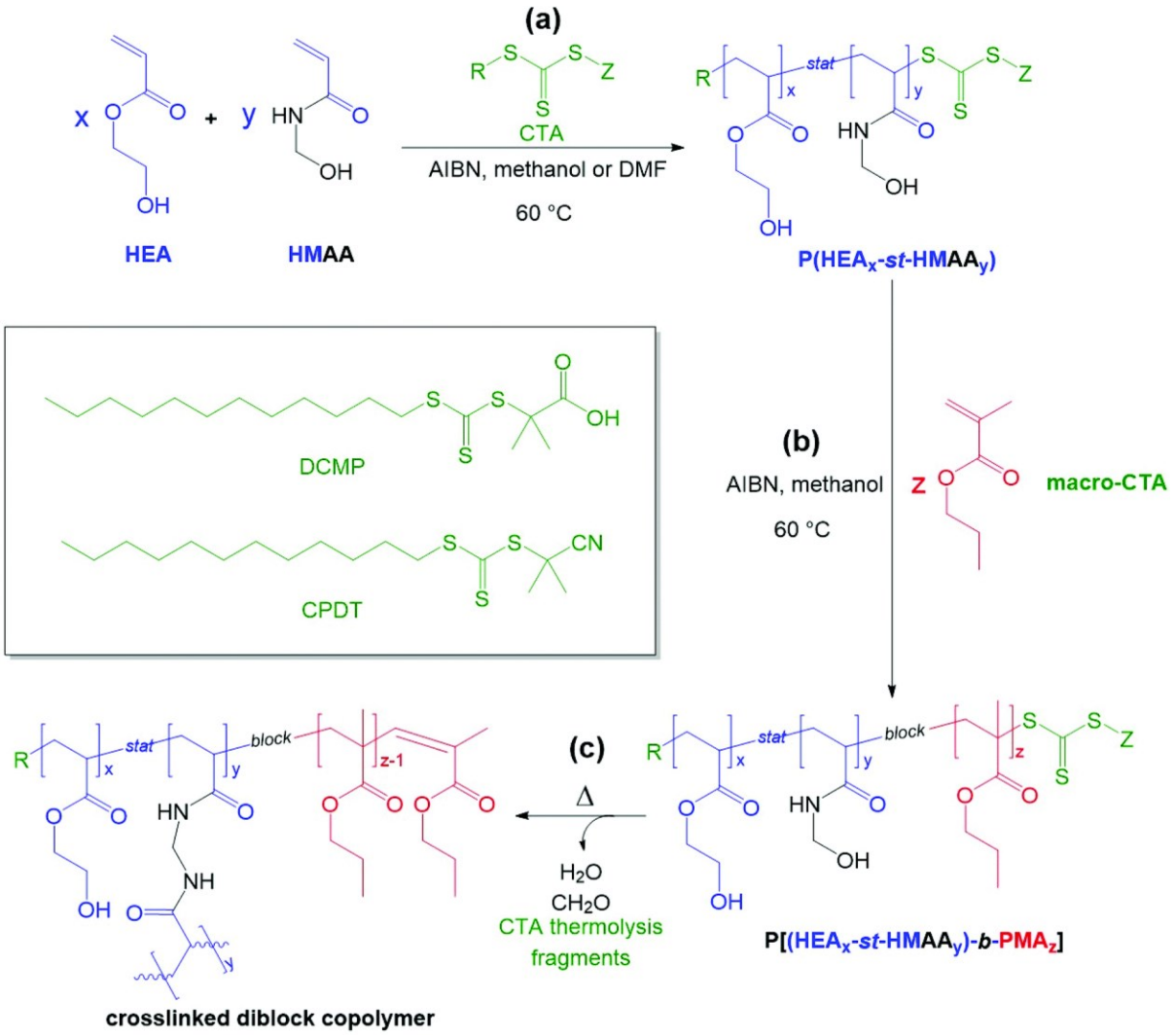

Figure 3.1. *Synthesis scheme of poly[(2-hydroxyethyl acrylate-stat-N-hydroxymethyl acrylamide)-block-propyl methacrylate] using 2-(dodecylthiocarbonothioylthio)-2-methylpropanoic acid and cyano-2-propyl dodecyl trithiocarbonate as chain transfer agents. Reproduced with permission from Parkes et al.[14].*

Using a UV-triggerable monomer would mitigate the requirement for prolonged high temperatures and remove the possibility of harmful side product formation completely. Amongst the literature, Shirai[15] has provided a list of photo-cross-linkable groups which also have shown to have degradable properties. Still focusing on sustainability, Fertier *et al.*[16] discussed molecules which can be obtained from renewable feedstocks and their use in photochemistry.

Photoactive polymers have many applications, varying from use in opto-electronic devices[17] to holographic displays[18] and also in self-cleaning surface materials (photoactive polymer films)[19]. In regard to light-mediated chemistry, photoresponsive polymerisation-induced self-assembly (PISA) has also been explored. An example of this is from Xu *et al.*[20] who used light at two different

wavelengths to both synthesise and subsequently cross-link a block copolymer. Specifically, zinc meso-tetra(*N*-methyl-4-pyridyl) porphine tetrachloride (ZnTMPyP) was used as an activator to initiate the chain extension of 2-hydroxypropyl methacrylate (HPMA) onto a pre-synthesised 4-cyano-4-[(dodecylsulfanylthiocarbonyl)sulfanyl] pentanoic acid (CDTPA)-capped poly(ethylene glycol) (PEG) macromolecular RAFT agent (PEG-CDTPA) using low energy red light exposure (595 nm, 10.2 mW cm^{-2}). This yielded a range of PEG-*b*-PHPMA block copolymer nanoparticles with spherical, worm and vesicular morphologies. A photoresponsive monomer, 7-[4-(trifluoromethyl)coumarin] methacrylamide (TCMAm), was also added into the system and was shown to not undergo cross-linking during the red light exposure, however upon exposure to ultraviolet (UV) light (365 nm, 10.2 mW cm^{-2}), cross-linking occurred.

One of the most common mechanisms by which such photo-cross-linking can occur is a via a [2+2] photocycloaddition. An example of this can be described using ethene, which can form a cyclobutane ring via a pericyclic reaction (Figure 3.2). This cyclic molecule forms as the result of the breaking of two pi (π) bonds and the forming of two sigma (σ) bonds in a single step. The correct wavelength of light is required to trigger an overlap between the highest occupied molecular orbital (HOMO) and the lowest occupied molecular orbital (LUMO) – this is the process which instigates the formation of the cyclobutane ring[21].

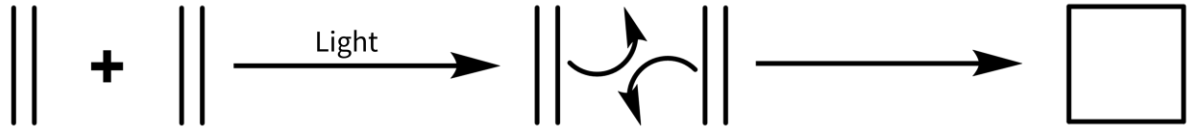

Figure 3.2. *The formation of a cyclobutane ring from the light irradiation of two ethene molecules.*

Other mechanisms by which cross-linking reactions can occur include [4+2], [6+4] and [4+4] cycloadditions, examples of these can be seen in Figure 3.3.

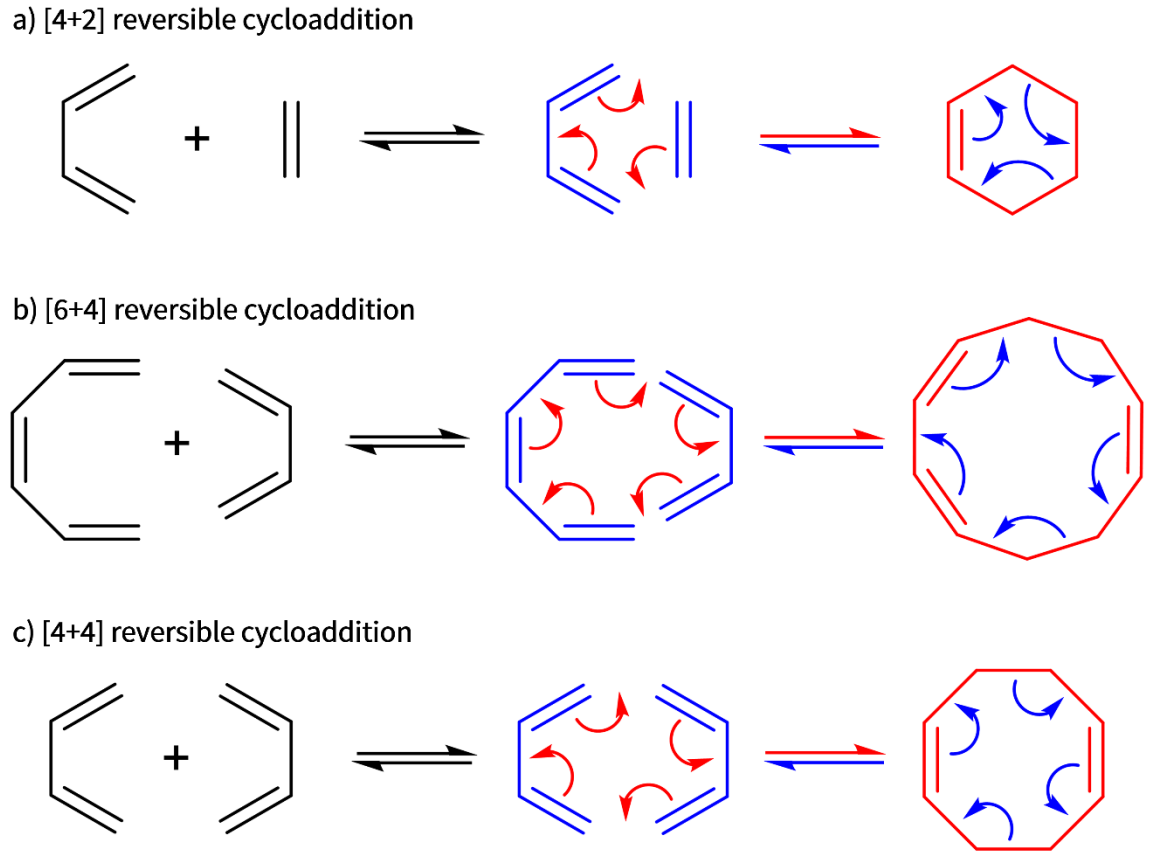

Figure 3.3. *Alternate mechanisms by which reversible cycloaddition reaction reactions can occur; a) [4+2] mechanism, b) [6+4] mechanism and c) [4+4] mechanism (where red arrows indicate the forward formation of ring structures, and blue arrows indicate the reverse reaction back to starting molecules).*

Hughes *et al.*[22] and Frisch *et al.*[23] have provided reviews discussing various precursor molecules which can undergo reversible photodimerization when exposed to specific wavelengths of light. These molecules include coumarin[24-26], cinnamic acid[27-29], and anthracene[30-32], all of which have been used in a broad range of research applications, some of which can be seen in Figure 3.4, and do not require the presence of a photo-initiator.

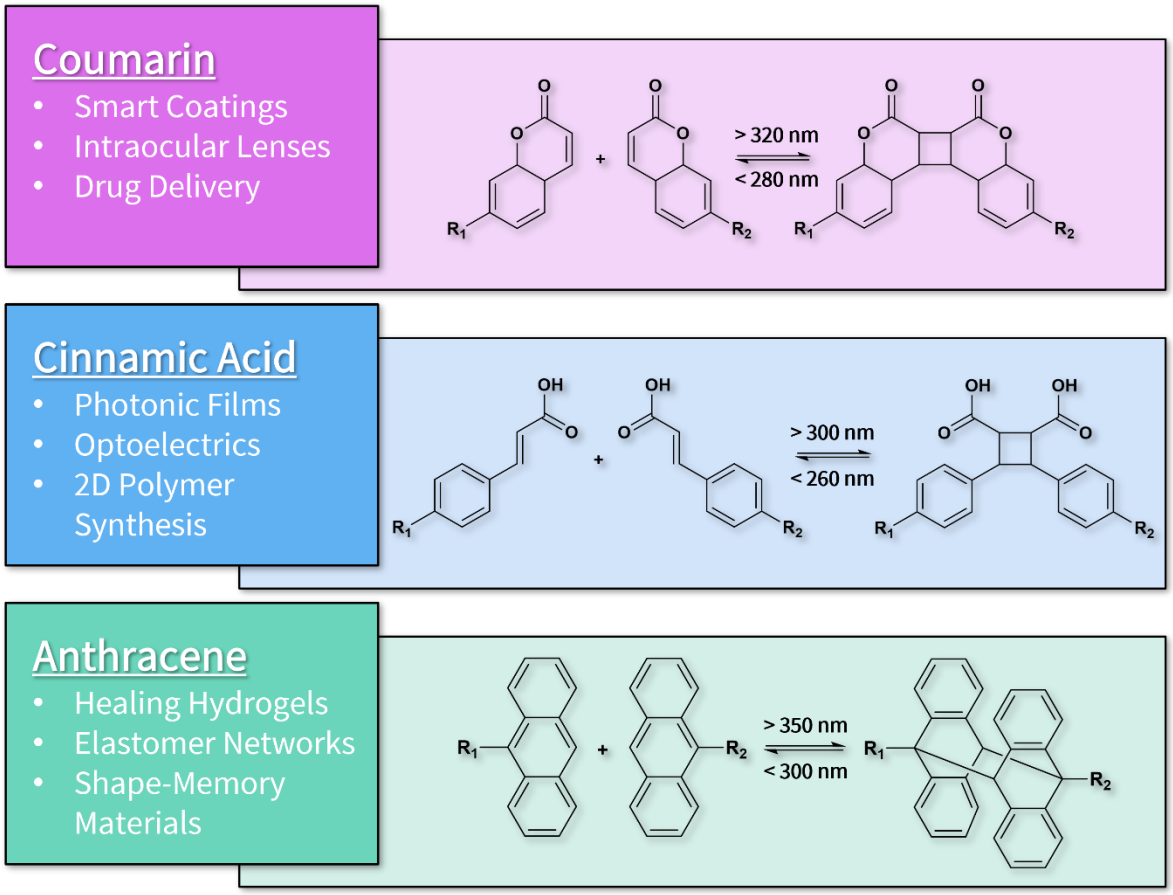

Figure 3.4. *Some of the applications in which coumarin, cinnamic acid and anthracene have been utilised and their corresponding reversible photodimerization schemes.*

4-Methylumbelliferone (4MU), also known as hymecromone, is a chemical which has medical applications, for example in the treatment of biliary spasms and research into its use as treatment for cancer/autoimmunity[33, 34]. Additionally, 4MU also has applications in self-healing materials due to its cross-linking ability. Wang *et al.*[35] synthesised a range of polyurethanes containing 4MU which displayed excellent mechanical and elastic properties, and successfully healed when exposed to 365 nm light. Coumarin-containing polyethers were synthesised by Chen *et al.*[36] and exposed to different wavelengths of light, from which results showed that the photocleavage process using 254 nm light was much faster than the photopolymerisation process using 350 nm light. Of particular interest, Patel *et al.*[37, 38] synthesised 7-acryloyloxy-4-methylcoumarin (AOMC) containing double bond functionality which could undergo polymerisation. From this, a copolymer with methyl acrylate was created via free radial polymerisation. The first report of this synthesis was from Chen *et al.*[39], and has since been explored further by other researchers[40-42].

Cinnamic acid (CA) can be naturally found in cinnamon and is often used in the food and cosmetics industries as a flavour and perfume agent, respectively[43]. It also has use in the medical research field due to its antibacterial, antiviral and antifungal properties[44-46]. Bernstein *et al.*[47] reported on the dimerization of *trans*-CA in 1943, resulting in the formation of truxillic acid. An example of this is from Shi *et al.*[48, 49], who reported a range of polymers which were grafted onto a pre-synthesised CA-functionalised copolymer, which resulted in the formation of nanoparticles that were subsequently purified via dialysis. The generated nanoparticles were then irradiated with UV light, by which cross-linking successfully occurred and therefore showed positive potential for use in drug delivery applications.

9-Anthracenecarboxylic acid (9ACA) is a derivative of anthracene, which has also been used for its cross-linking ability. An example of this in the literature is from Nasirtabrizi *et al.*[50], who modified glycidyl methacrylate using 9ACA to yield anthracene-functional cross-linkable monomers for the synthesis of polymers with improved rigidity, compared to polymers not containing the 9ACA group.

Wang *et al.*[51] demonstrated the use of furfural-based monomers, which could be polymerised using sunlight without triggering cross-linking of the C=C within the furfural. Prabhakar *et al.*[52] have also reported on the use of a furfural-based monomer with UV triggerable functionality, specifically 3-(2-furyl)acrylic acid (FAA) as a sustainable chemical building unit. In addition to this, Wang *et al.*[53] reported on the sustainable synthesis of FAA and tested its polymer cross-linking ability.

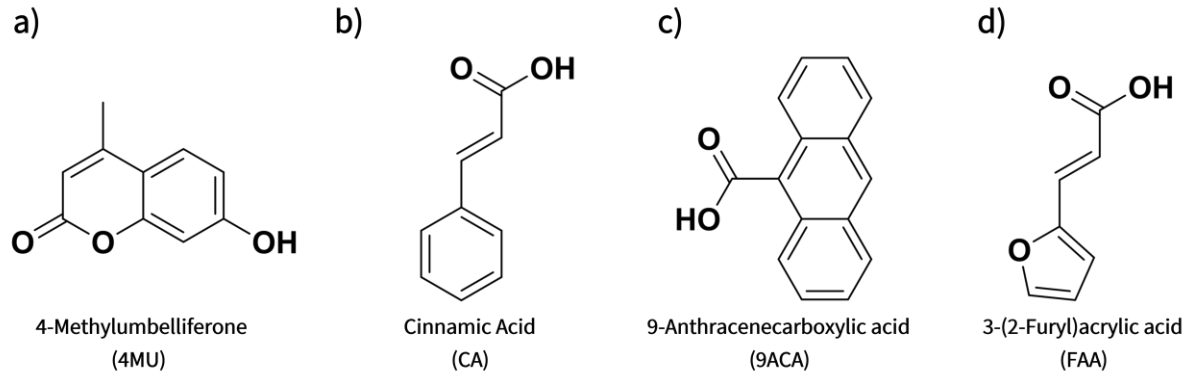

Figure 3.5. *Chemical structures of the molecules of focus: a) 4-methylumbelliferone (4MU), b) cinnamic acid (CA), c) 9-anthracenecarboxylic acid (9ACA) and d) 3-(2-furyl)acrylic acid (FAA).*

In this chapter, the testing and modification of compounds with UV triggerable functionalities is investigated. Specifically, 4MU, CA, 9ACA and FAA (Figure 3.5) were tested for their potential

dimerization properties by exposing the compound, as purchased, to the appropriate triggering UV wavelength as found in the literature. From this, the most promising compounds were taken forward to either produce monomers for use in polymer synthesis or to functionalise polymers directly. The compound with alcohol functionality (4MU) was modified via esterification to impart double-bond functionality to yield a functional monomer which could then be polymerised. On the other hand, the compounds with carboxylic acid functionality (9ACA and FAA) were assessed for their ability to be directly added onto a pre-existing polymer, again via esterification reactions, to enable subsequent UV cross-linking (Figure 3.6). CA also contains carboxylic acid functionality, however it was not functionalised due to its inability to dimerise when exposed to UV light.

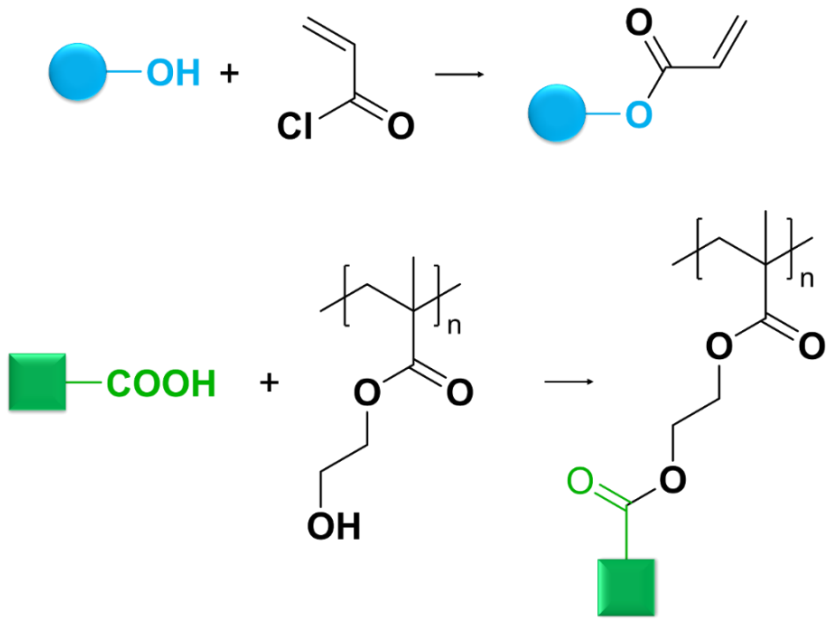

Figure 3.6. *Esterification of an alcohol containing compound (blue) and a carboxylic acid containing compound (green) using acryloyl chloride and poly(2-hydroxyethyl methacrylate) (PHEMA), respectively.*

3.2 Experimental

3.2.1 Materials

4-methylumbelliferone (4MU, 97%), acryloyl chloride (AC, 96%, stabilised with 400ppm phenothiazine), *trans*-cinnamic acid (CA, ≥99%), 3-(2-furyl)acrylic acid (FAA, 99%), *N,N'*-dicyclohexylcarbodiimide (DCC, 99%), *N,N*-dimethylformamide (DMF, ≥99%), ethanol (EtOH, analytical reagent grade, ≥99.8%), methanol (MeOH, analytical reagent grade, ≥99.9%) and tetrahydrofuran (THF, laboratory reagent grade ≥99.5%) were purchased from Fisher Scientific and

used as purchased. Sodium hydroxide (NaOH, reagent grade, ≥98%, pellets (anhydrous)), 9-anthracenecarboxylic acid (9ACA, 99%) and 4-(dimethylamino)pyridine (DMAP, ≥99%) were purchased from Sigma Aldrich and used as purchased. Azobisisobutyronitrile (AIBN) was purchased from Molekula and was recrystallised from methanol prior to use. Chloroform-d ($CDCl_3$, 99.8%), dimethyl sulfoxide-d_6 (DMSO-d_6, 99.9%) and methanol-d_4 (MeOD-d_4, 99.8%) were purchased from Cambridge Isotope Laboratories and used for ^{1}H NMR analysis as purchased.

3.2.2 ^{1}H Nuclear magnetic resonance (NMR) spectroscopy

^{1}H Nuclear magnetic resonance (NMR) spectroscopy was employed to examine the chemical structures of samples. These were prepared in acetone-d6, $CDCl_3$, DMSO-d6 or MeOD-d4 by dissolving approximately 15 mg of sample in 1 mL of solvent and agitating on a vortex mixer until dissolved. Prepared samples were then analysed using a Bruker Avance Neo 300 MHz spectrometer for 16 scans, with the subsequent spectra being analysed using TopSpin 4.2.0.

3.2.3 Gel permeation chromatography (GPC)

Gel permeation chromatography (GPC) was used to analyse the molecular weight distribution of the synthesised polymers, with the obtained traces being used to calculate the number average molar mass (M_n), weight average molar mass (M_w), and dispersity ($Đ$, M_w/M_n) of each sample. The eluent solution used was HPLC grade DMF containing a 0.10% w/v lithium bromide (LiBr) additive, in which samples were prepared. An Agilent Infinity II multi-detector GPC instrument was equipped with a single guard column and two PL gel mixed-C columns was held at a constant flow rate of 1.0 mL min^{-1} and a temperature of 40 °C. The system was calibrated with near monodisperse poly(methyl methacrylate) standards (M_p range = 535 - 1,591,000 g mol^{-1}) and experimental data was analysed using Agilent GPC/SEC software.

3.2.4 Fourier-transform infrared (FTIR) spectroscopy

Fourier-transform infrared (FTIR) spectroscopy was conducted using a Frontier Spectrometer (Perkin Elmer Ltd) in conjunction with a GladiATR attenuated total reflectance accessory (Pike Technologies) in order to analyse the chemical structure of the samples. Powder samples were

placed on the ATR crystal and compressed by a clamping arm, undergoing 16 scans at a scanning resolution of 4 cm^{-1} from 4000 cm^{-1} to 700 cm^{-1}.

3.2.5 Dimerization and cross-linking methods

UV dimerization of monomer precursors was performed using either a Solarium Model MD 1-15 lamp (Phillips) featuring 4 parallel fluorescent tubes (15 W) with UV emission wavelengths in the range of 315-400 nm or an Osram Ultra Vitalux lamp (300 W) with UV emission wavelengths in the range of 280-400 nm. Samples were prepared by manually spreading the powders/samples into a thin, even layer using a steel spatula within a polystyrene petri dish. The light source was fixed approximately 5 cm away from the samples for periods of 30 minutes during dimerization and cross-linking.

3.2.6 7-Acryloyloxy-4-methylcoumarin synthesis and homopolymerisation

3.2.6.1 7-Acryloyloxy-4-methylcoumarin synthesis

Sodium hydroxide (NaOH; 0.4 g; 10.0 mmol) was dissolved in ethanol (EtOH; 43.4 g; 942 mmol) in a 50 mL round-bottomed flask. 4MU (1.80 g; 10.0 mmol) was added to the solution and stirred at 60 °C for 45 minutes. After this duration, the mixture was cooled to between 0 and 5 °C and acryloyl chloride (AC; 1.00 g; 11.0 mmol) was added dropwise. The mixture was left to stir for a further 90 minutes, after which the product was poured over crushed ice in a 100 mL beaker. The white product obtained was filtered using vacuum filtration and recrystallized using an excess of methanol. The final purified product was dried using vacuum filtration and freeze-drying (Scheme 3).

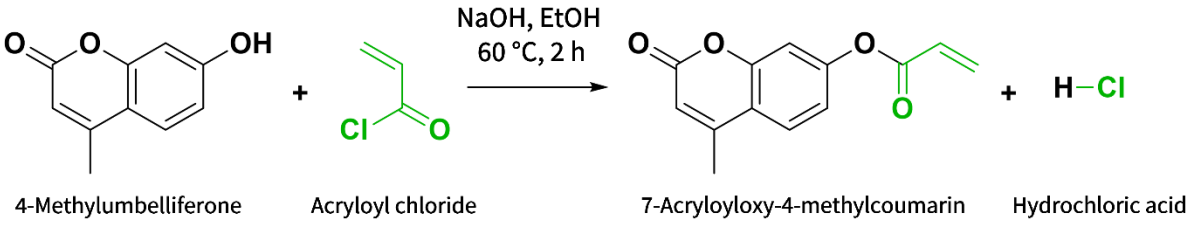

Scheme 3. *Synthesis scheme of 7-acryloyloxy-4-methylcoumarin (AOMC) monomer using 4-methylumbelliferone (4MU) and acryloyl chloride (AC) in ethanol.*

3.2.6.2 7-Acryloyloxy-4-methylcoumarin hompolymerisation via free radical polymerisation

The following method describes the homopolymerisation of AOMC using free radical polymerisation in DMF at 70 ˚C. A 25 mL round-bottomed flask was charged with AOMC (0.2 g, 0.86 mmol) and DMF (6 mL). The reaction flask was sealed using a suba-seal and parafilm, and subsequently purged with nitrogen to degas for 30 minutes. The reaction flask was then placed into a preheated aluminium block set at 70 °C for 5 hours. The polymer was purified by precipitation twice in excess methanol and dried using vacuum filtration (Scheme 4).

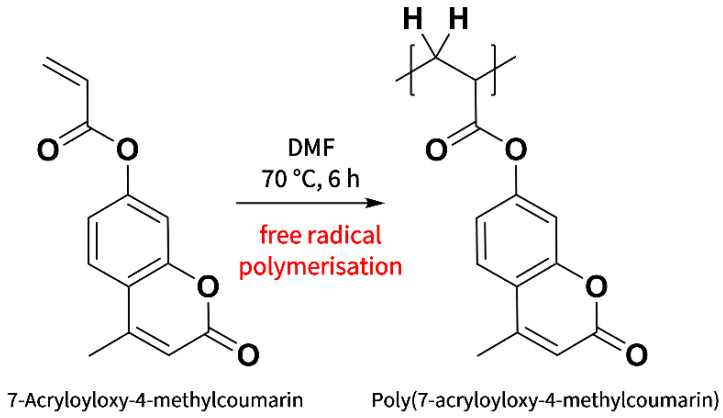

Scheme 4. *Synthesis of poly(acryloyloxy-4-methylcoumarin) (PAOMC) via free radical polymerisation in DMF at 70 °C for a duration of 6 hours.*

3.2.7 9-Anthracenecarboxylic acid esterification

The following method describes the esterification of 9ACA onto a pre-synthesised poly(2-hydroxyethyl acrylate) (PHEMA) macro-CTA. A 50 mL round-bottomed flask was charged with PHEMA (1.00 g, 78.3 µm), 9ACA (1.67 g, 7.51 mmol), dicyclohexylcarbodiimide (DCC; 1.55 g, 7.51 mmol), 4-(dimethylamino)pyridine (DMAP; 0.278 g, 2.28 mmol) and dimethylformamide (DMF; 18.1 g) along with a magnetic stirrer bar. The flask was sealed and left to stir at room temperature for 24 hours. The resulting mixture was filtered using vacuum filtration to remove the unwanted byproduct and the remaining solution was precipitated in diethyl ether three times. The purified sample was dried using rotary evaporation and a vacuum oven (Scheme 5).

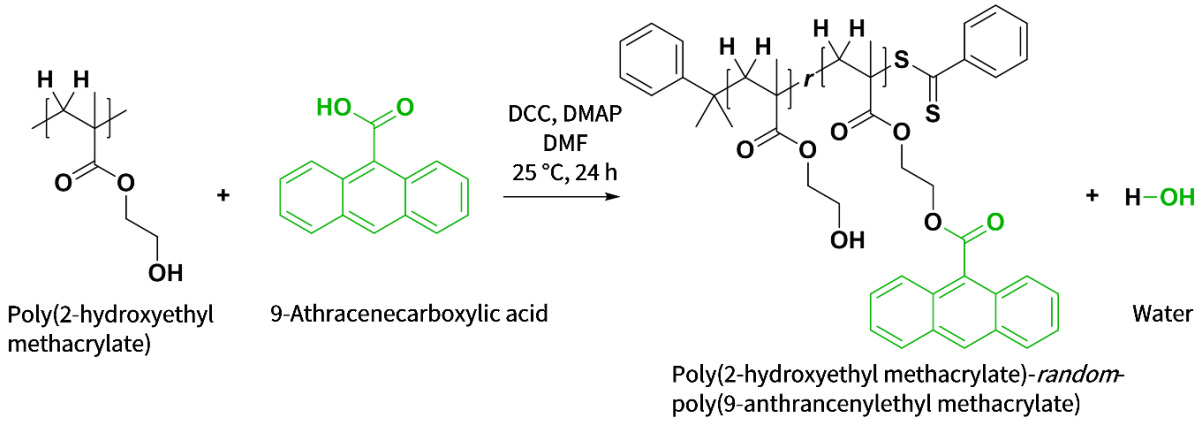

Scheme 5. *Synthesis of poly(2-hydroxyethyl methacrylate)-random-poly(9-anthrancenylethyl methacrylate) (PHEMA-r-P9AEMA) using dicyclohexylcarbodiimide (DCC) and 4-dimethylaminopyridine (DMAP) in dimethylformamide (DMF) at room temperature for 24 hours.*

3.2.8 3-(2-Furyl)acrylic acid esterification

The following method describes the esterification of FAA onto a pre-synthesised PHEMA macro-CTA. A 50 mL round-bottomed flask was charged with PHEMA (1.00 g, 78.3 µm), FAA (1.56 g, 11.3 mmol), dicyclohexylcarbodiimide (DCC; 1.56 g, 7.56 mmol), 4-(dimethylamino)pyridine (DMAP; (0.280 g, 2.29 mmol) and dimethylformamide (DMF; 15.4 g) along with a magnetic stirrer bar. The flask was sealed and left to stir at room temperature for 24 hours. The resulting mixture was filtered using vacuum filtration to remove the unwanted byproduct and the remaining solution was precipitated in diethyl ether three times. The purified sample was dried using rotary evaporation and a vacuum oven (Scheme 6).

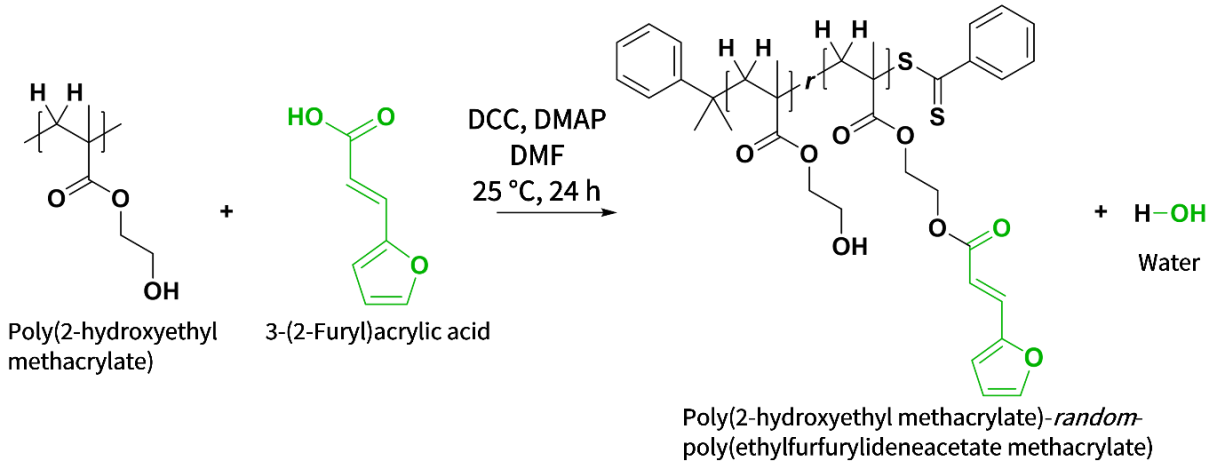

Scheme 6. *Synthesis of poly(2-hydroxyethyl methacrylate)- random-poly(ethylfurfurylideneacetate methacrylate) (PHEMA-r-PEFMA) using dicyclohexylcarbodiimide (DCC) and 4-dimethylaminopyridine (DMAP) in dimethylformamide (DMF) at room temperature for 24 hours.*

3.3 Results and discussion

3.3.1 Dimerization studies

The dimerization ability of 4MU, CA, 9ACA, and FAA were assessed using methodology as descried in Section 3.2.5. For all FTIR spectra, the C=O stretching band around 1670 cm^{-1} was used to normalise the data.

3.3.1.1 Dimerization of 4-methylumbelliferone

Coumarins undergo a [2+2] photocycloadditon reaction when exposed to specific wavelengths of light. For example, it has been reported that wavelengths above 300 nm induce the dimerization of 4MU[54, 55], therefore a UVA lamp with a wavelength range of 315-400 nm was used for irradiation of 4MU in this study (Scheme 7). The irradiated sample was then analysed using FTIR spectroscopy (Figure 3.7) and ^{1}H NMR spectroscopy (Figure 3.8).

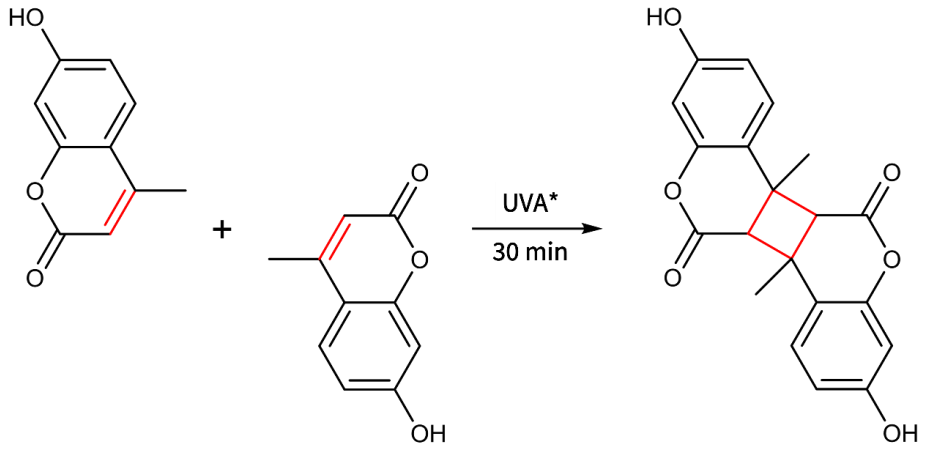

Scheme 7. *The dimerization scheme of 4-methylumbelliferone, by which the opening of the double bond to form a cyclobutane ring is highlighted in red.*
**UVA lamp with a wavelength range between 315 and 400 nm was used.*

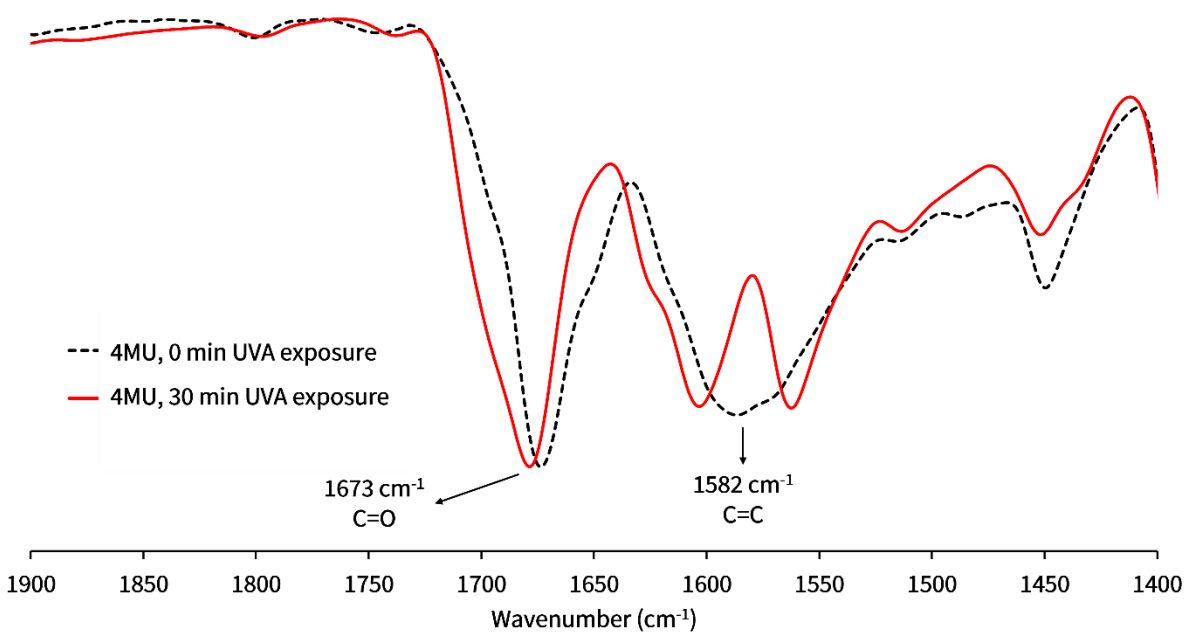

Figure 3.7. *Overlaid FTIR spectra of 4-methylumbelliferone (4-MU) before (black dashed line) and after (red line) exposure to UV irradiation, where the C=O and C=C stretches have been labelled.*

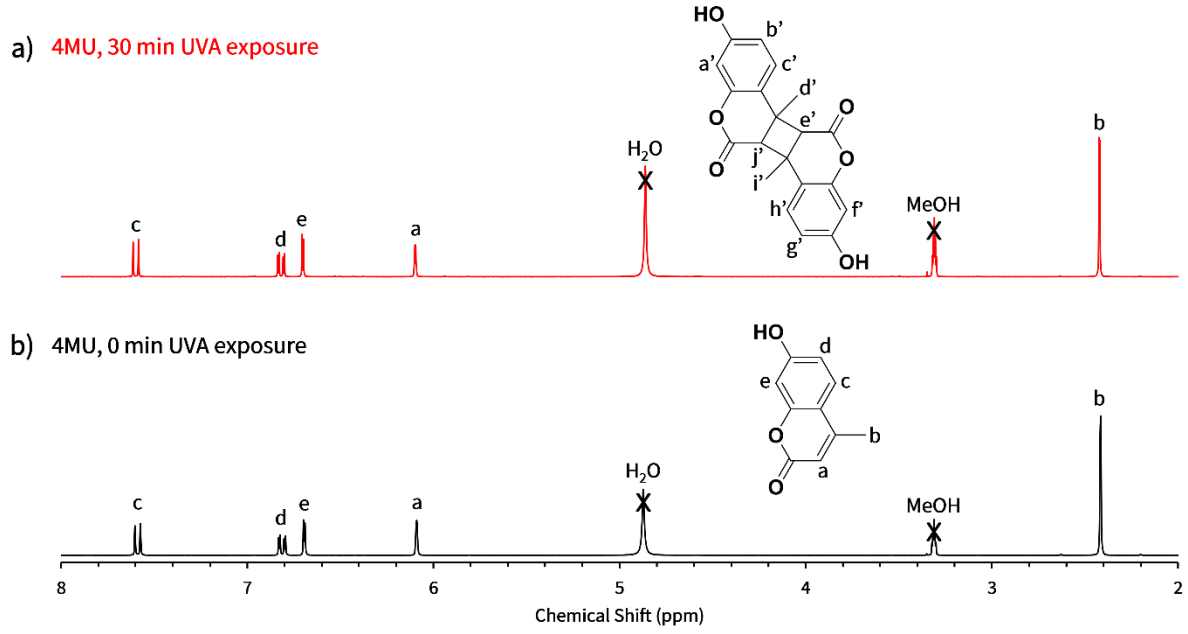

Figure 3.8. *[1]H NMR spectra of 4-methylumbelliferone a) after exposure to UV irradiation (red) and b) before exposure to UV irradiation (black). NMR solvent – MeOD-d4.*

It can be observed from Figure 3.7 that there is a slight shift to the left of the carbonyl band (C=O stretch) after irradiation compared to that of the non-irradiated sample; in the non-irradiated sample, the peak appears at 1673 cm^{-1}, whereas after irradiation the peak appears at 1680 cm^{-1}. This

suggests that dimerization has occurred as it is a common feature that the removal of conjugation of the system (in this case caused by the formation of a cyclobutane ring from two alkenes) shifts the C=O stretching band to a higher wavenumber. This is due to the loss of delocalisation of the electrons, which results in the C=O exhibiting stronger bonding, hence the shift to a higher wavenumber occurs. The relationship between energy (E) and wavenumber ($\tilde{\nu}$) can be seen below in Equation 3.1.

$$E = hc\tilde{\nu} \qquad \textit{3.1}$$

Where h represents Planck's constant and c represents the speed of light. This equation can be used to support this theory; if the C=O exhibits stronger bonding, this would result in a higher energy and since h and c are constants, would result in a higher wavenumber, which is observed. The other noticeable feature is the appearance of a single peak at 1582 cm^{-1} in the non-irradiated sample and as two peaks (1562 and 1603 cm^{-1}) in the irradiated sample. The disappearance of the single peak could be due to the removal of C=C as part of the dimerization process. Although there is no clear change in the ^{1}H NMR spectrum after irradiation (Figure 3.8), the change in the FTIR spectra gave a satisfactory result which led to the continuation of use of this compound.

3.3.1.2 Dimerization of cinnamic acid

CA typically undergoes a [2+2] photocycloadditon when exposed to wavelengths above 260 nm[56] therefore a UV lamp with a wavelength range above 280 nm was used for irradiation (Scheme 8). The irradiated sample was then analysed using FTIR spectroscopy (Figure 3.9) and ^{1}H NMR spectroscopy (Figure 3.10).

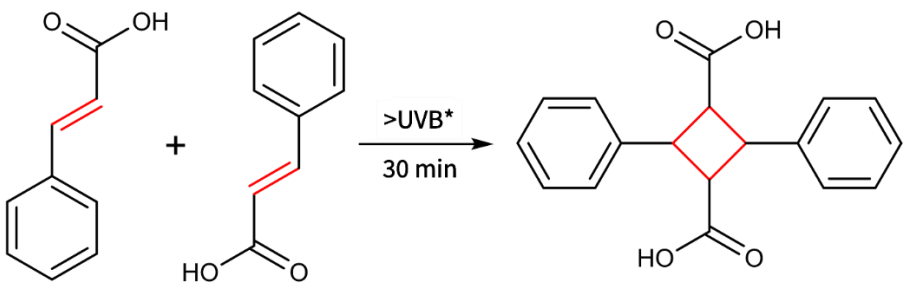

Scheme 8. *The dimerization scheme of cinnamic acid, by which the opening of the double bond to form a cyclobutane ring is highlighted in red.*
**UV lamp with a wavelength range between 280 and 400 nm was used.*

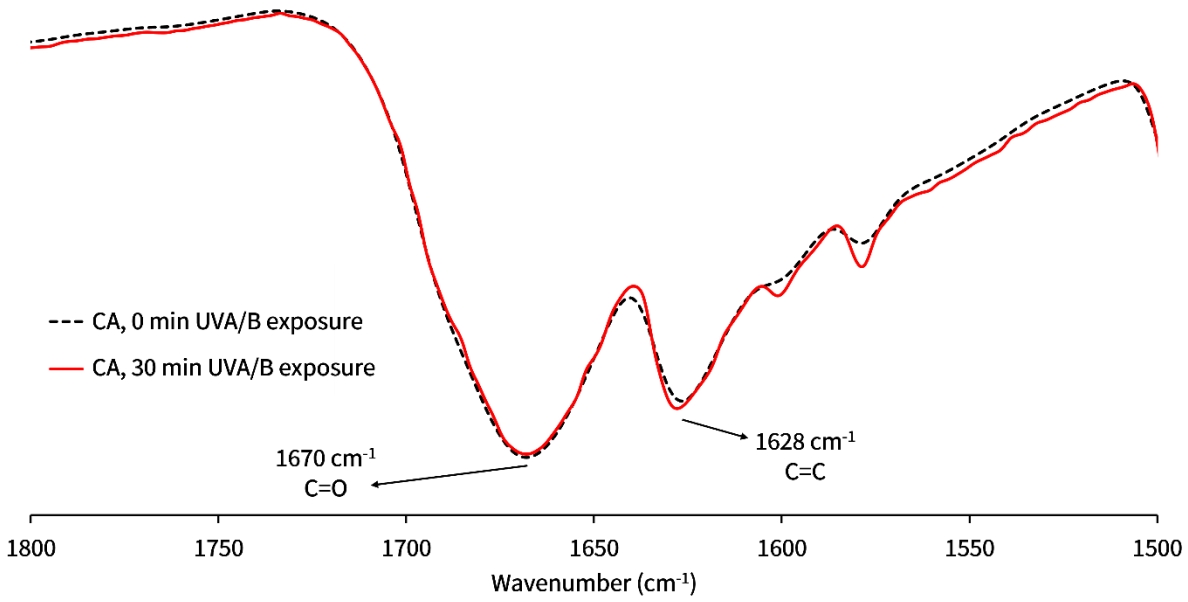

Figure 3.9. *Overlaid FTIR spectra of cinnamic acid (CA) before (black dashed line) and after (red line) exposure to UV irradiation, where the C=O and C=C stretches have been labelled.*

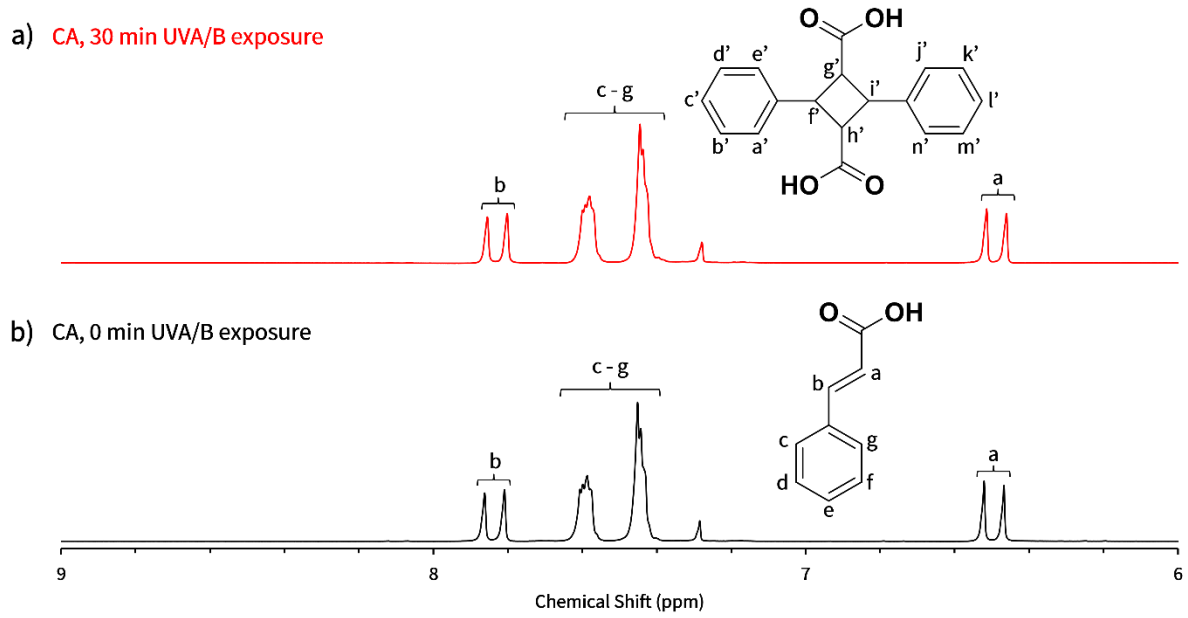

Figure 3.10. *^{1}H NMR spectra of cinnamic acid (CA) a) after exposure to UV irradiation (red) and b) before exposure to UV irradiation (black). NMR solvent – $CDCl_3$.*

It can be observed from both FTIR (Figure 3.9) and NMR (Figure 3.10) that there are no changes to the C=O stretch (1670 cm^{-1}) and C=C stretch (1628 cm^{-1}) peaks before and after irradiation. This

implies that the irradiation triggered no dimerization to occur. The CA was irradiated for a longer time period (60 minutes) and using another lamp (UVA lamp with a wavelength range between 315 and 400 nm), however the same results were obtained. Literature has shown that CA derivatives dimerize under a range of conditions, including when dissolved in cyclohexane and irradiated with 365 nm using 12 PL-L 36W/10/4P 365 nm Philips lamps[57], or when irradiated with an OSRAM Ultravitalux lamp under water-cooling (filtering wavelengths less than 280 nm)[58]. The sucessful dimerization was proven in both cases using NMR spectroscopy, where the appearance of new peaks 3.5 and 4.5 ppm were visible when using proton NMR[57]. From this, it was concluded that CA was not a suitable monomer precursor to continue with, due to its inability to dimerize under the available conditions.

3.3.1.3 Dimerization of 9-athracenecarboxylic acid

An anthracene derivative was the next molecule chosen to undergo dimerisation. From the literature it was found that 9ACA dimerises via a [4+4] photocycloaddition mechanism when exposed to wavlengths over 300 nm[59,60], therefore a UVA lamp with a wavelength range of 315-400 nm was used for irradiation (Scheme 9). The irradiated sample was then analysed using FTIR spectroscopy (Figure 3.11) and ^{1}H NMR spectroscopy (Figure 3.12).

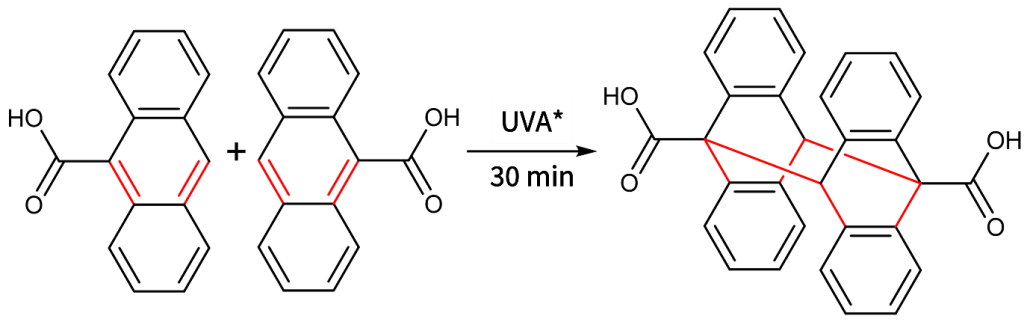

Scheme 9. *The dimerization scheme of 9-athracenecarboxylic acid, by which the opening of the double bond to form a cyclobutane ring is highlighted in red.*
**UVA lamp with a wavelength range between 315 and 400 nm was used.*

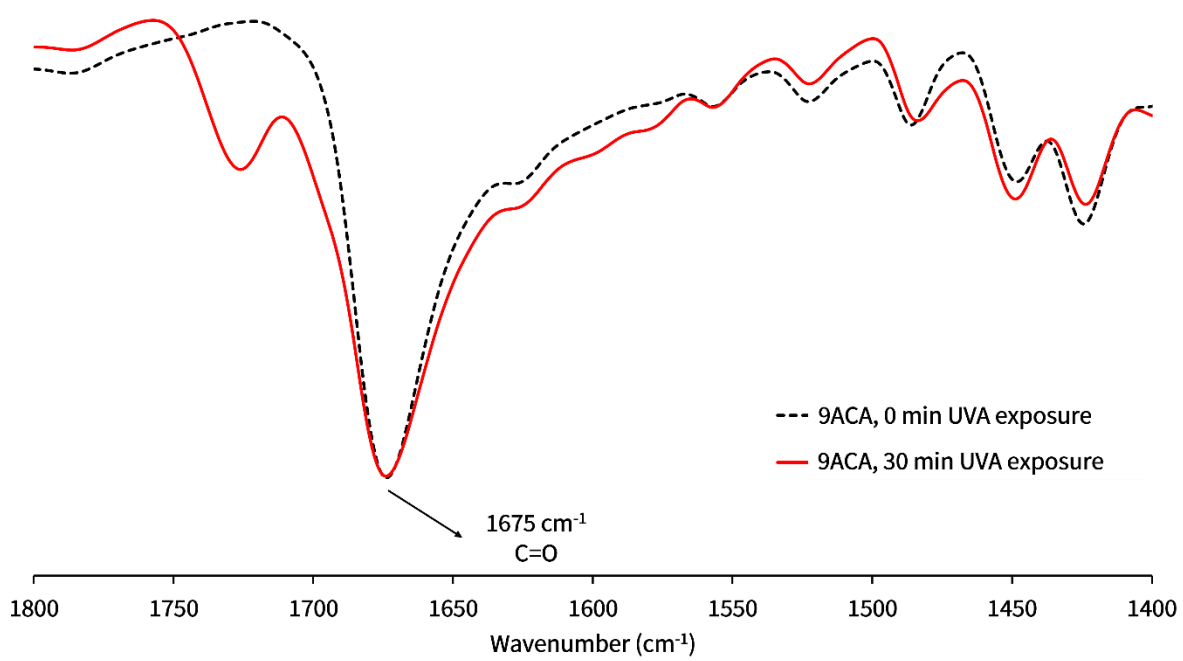

Figure 3.11. *Overlaid FTIR spectra of 9-athracenecarboxylic acid (9ACA) before (black dashed line) and after (red line) exposure to UV irradiation, where the C=O stretch has been labelled.*

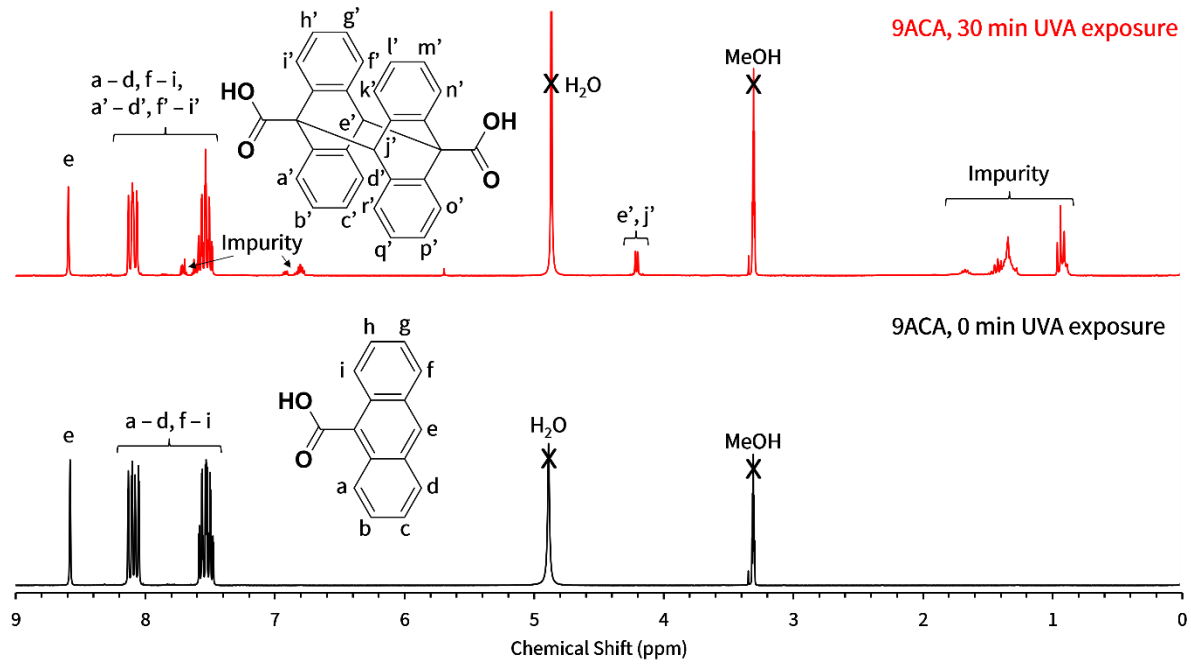

Figure 3.12. *[1]H NMR spectra of 9-athracenecarboxylic acid (9ACA) a) after exposure to UV irradiation (red) and b) before exposure to UV irradiation (black). NMR solvent – MeOD-d4.*

The FTIR data (Figure 3.11) displays that the only visible change is the appearance of a peak at 1724 cm^{-1}. This peak could also be representative of C=O stretching; as mentioned previously conjugation can affect the positioning of a carbonyl peak. Since there is a clear loss of conjugation in the system, it would be expected for there to be a shift of the C=O stretch if the dimerization was successful. Han *et al.*[59] showed the successful dimerization of 9ACA using a Spectroline Model SB-100P/FA lamp (365 nm, 100 W). ^{1}H NMR spectra also showed the formation of new peaks, however these new peaks were at 6.5 ppm, 5.5 ppm with $CDCl_3$ used as the NMR solvent. ^{1}H NMR data (Figure 3.12) for the irradiated sample also shows the appearance of new peaks, which could also indicate that the dimerization was successful, since a cyclobutane ring is formed, there would be new proton environments. The peak at 4.2 ppm represents a doublet, which before irradiation would have had aromatic properties, however after irradiation, are considered cyclic as the double bond functionality is lost. This would imply that the new proton environments would be shifted to a lower ppm in the spectrum, which can be observed. Using this peak and Equations 3.2 to 3.4, the extent of dimerization was calculated to be approximately 20%, which could potentially be improved by increasing the duration of exposure. There are also peaks formed between 0.5 and 1.5 ppm, however the origin of these peaks is unclear. Peaks in this region are typically representative of alkyl groups, where solvents such as *n*-hexane appear present, but it should be noted that no other solvents, excluding the NMR solvent, were used in the process of dimerization and therefore these peaks are attributed to contamination of some kind.

$$I_d = [integral(e')] = 0.50/2 = 0.25 \quad \textbf{3.2}$$

$$I_m = [integral(e)] = 1H \quad \textbf{3.3}$$

$$extent\ of\ dimerization\ (\%) = \frac{I_d}{I_d+I_m} \times 100 = \frac{0.25}{0.25+1} \times 100 = 20\%\ (2s.f.) \quad \textbf{3.4}$$

Taking both spectra into consideration, it was determined that 9ACA could potentially be a suitable monomer precursor as it somewhat appeared to have undergone dimerization.

3.3.1.4 Dimerization 3-(2-furyl)acrylic acid

Finally, FAA was tested for its dimerization ability when irradiated with UV light. According to literature, FAA undergoes a [2+2] photocycloadditon at wavelengths above 270 nm[61], therefore a UVA lamp with a wavelength range of 315-400 nm was used for irradiation (Scheme 10). The irradiated sample was then analysed using FTIR spectroscopy (Figure 3.13) and ^{1}H NMR spectroscopy (Figure 3.14).

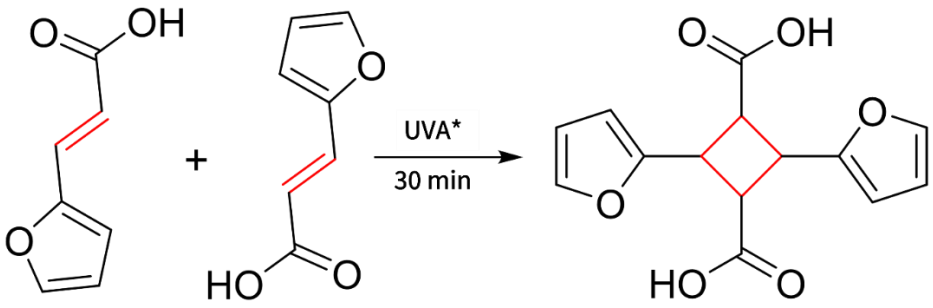

Scheme 10. *The dimerization scheme of 3-(2-furyl)acrylic acid, by which the opening of the double bond to form a cyclobutane ring is highlighted in red.*
**UVA lamp with a wavelength range between 315 and 400 nm was used.*

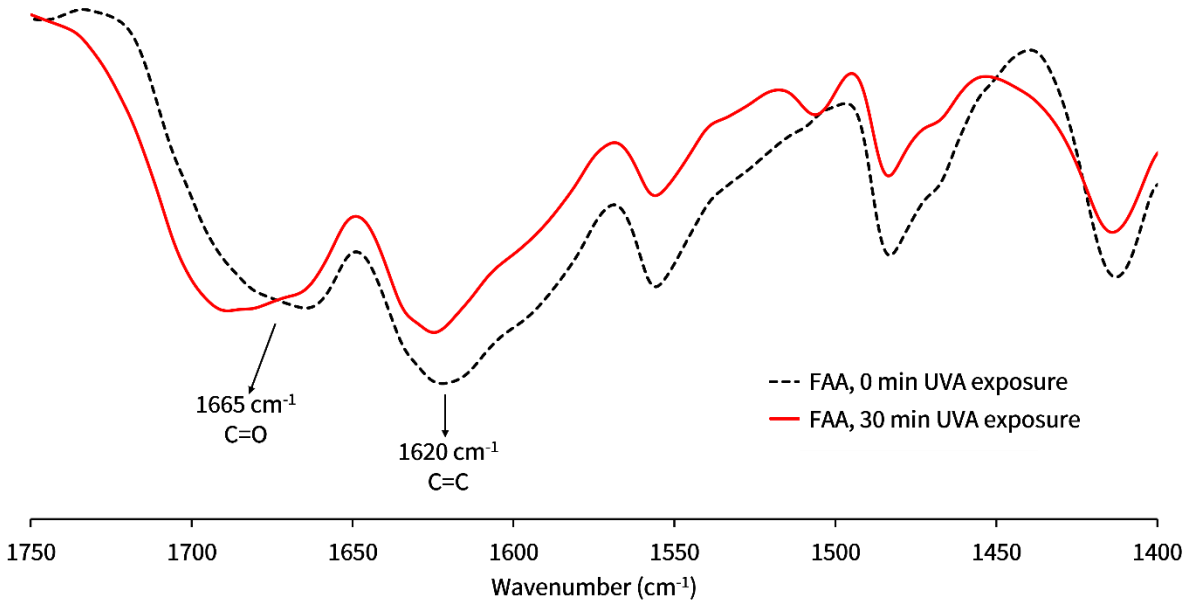

Figure 3.13. *Overlaid FTIR spectra of 3-(2-furyl)acrylic acid (FAA) before (black dashed line) and after (red line) exposure to UV irradiation, where the C=O and C=C stretches have been labelled.*

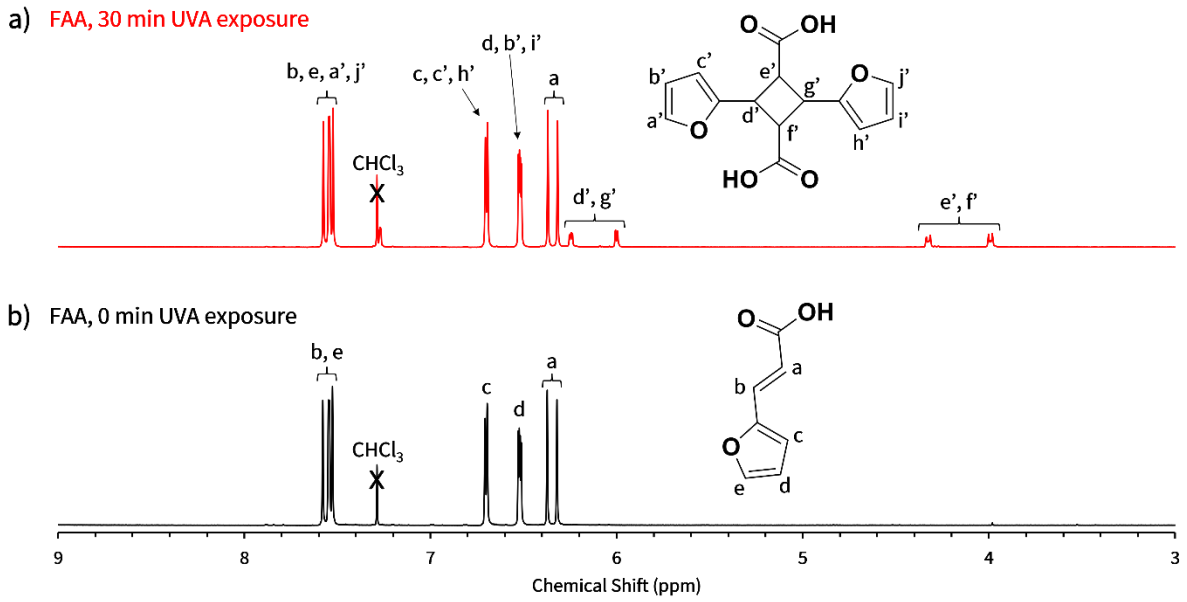

Figure 3.14. *^{1}H NMR spectra of 3-(2-furyl)acrylic acid (FAA) before (black) and after (red) exposure to UV irradiation. NMR solvent – $CDCl_3$.*

A shift in the C=O stretch is visible from the overlaid spectra obtained before and after irradiation (Figure 3.13). This observation was also present for the dimerization of 4MU and 9ACA, and is a key feature that helps to confirm the successful formation of a cyclobutane ring. In FAA, clear conjugation is present from the C=O stretching of the carboxylic end to the aromatic nature of the furan ring. This conjugation is lost as a result of the dimerization, hence resulting in a shift of the C=O stretch to a higher wavenumber (1655 cm^{-1} to 1688 cm^{-1}). In this case, the shortening in intensity of the C=C stretch at 1620 cm^{-1} can also be observed, further indicating that dimerization was successful; double bond functionality is lost when the cyclobutane ring is formed. This can also be confirmed from ^{1}H NMR spectroscopy studies (Figure 3.14), with the formation of new peaks between 4.0 and 6.4 ppm. These peaks arise from the new proton environment present at each carbon atom on the cyclobutane ring. The extent of dimerization was calculated to be 13%, which is lower than 20% observed for the dimerization of 9ACA, however as mentioned previously, this could potentially be improved in future work by increasing the exposure time to UV light.

$$I_d = [integral(e')] = 0.15 \qquad \textbf{3.5}$$

$$I_m = [integral(a)] = 1H \qquad \textbf{3.6}$$

$$extent\ of\ dimerization\ (\%) = \frac{I_d}{I_d + I_m} \times 100 = \frac{0.15}{0.15+1} \times 100 = 13\%\ (2s.f.) \quad \textbf{3.7}$$

It is clear from both spectra that dimerization had successfully occurred, therefore FAA was deemed to be a suitable monomer precursor molecule.

3.3.2 Synthesis, homopolymerisation and cross-linking of 7-acryloyloxy-4-methylcoumarin

AOMC was synthesised using a similar method to Patel *et al.*[37]. The starting reactants, 4MU and AC, and the crude and purified product (AOMC) can be seen in (Figure 3.15). The confirmation of the product can be observed from the change in peaks in the starting reagents to the final purified product. The purification of the crude product can also be confirmed form the disappearance of the peaks at around 7.46 and 6.88 ppm. It can be observed that although freeze-drying was used to remove water from the system, it had not fully been removed. The synthesis of AOMC by Patel *et al.*[37] had a high yield of 98 %, however upon repeating, a low yield of 18% was obtained (Equation 3.8). This could be due to product lost throughout the purification process (filtering and recrystalising) or insufficient reaction times which would result in a low conversion of product.

$$yield\ (\%) = \frac{Purified\ AOMC}{Crude\ AOMC} \times 100 = \frac{0.2888\ g}{1.6398\ g} \times 100 = 18\%\ (2s.f.) \quad \textbf{3.8}$$

From this, poly(AOMC) was synthesised via free radical polymerisation (FRP) using dimethylformamide (DMF) as the reaction solvent (Figure 3.16). There is a clear broadening of peaks in the poly(AOMC) spectrum, which is a strong indication that the polymerisation had occurred successfully. The original solids concentration of the reaction was 10% w/w, however, due to solubility problems encountered, a solids concentration of 0.33% w/w was used for the reaction instead. The purified polymer was also analysed using GPC, where values of 1800 g mol^{-1}, 5400 g mol^{-1} and 2.49 were obtained for M_n, M_w and $Đ$, respectively (Figure 3.17).

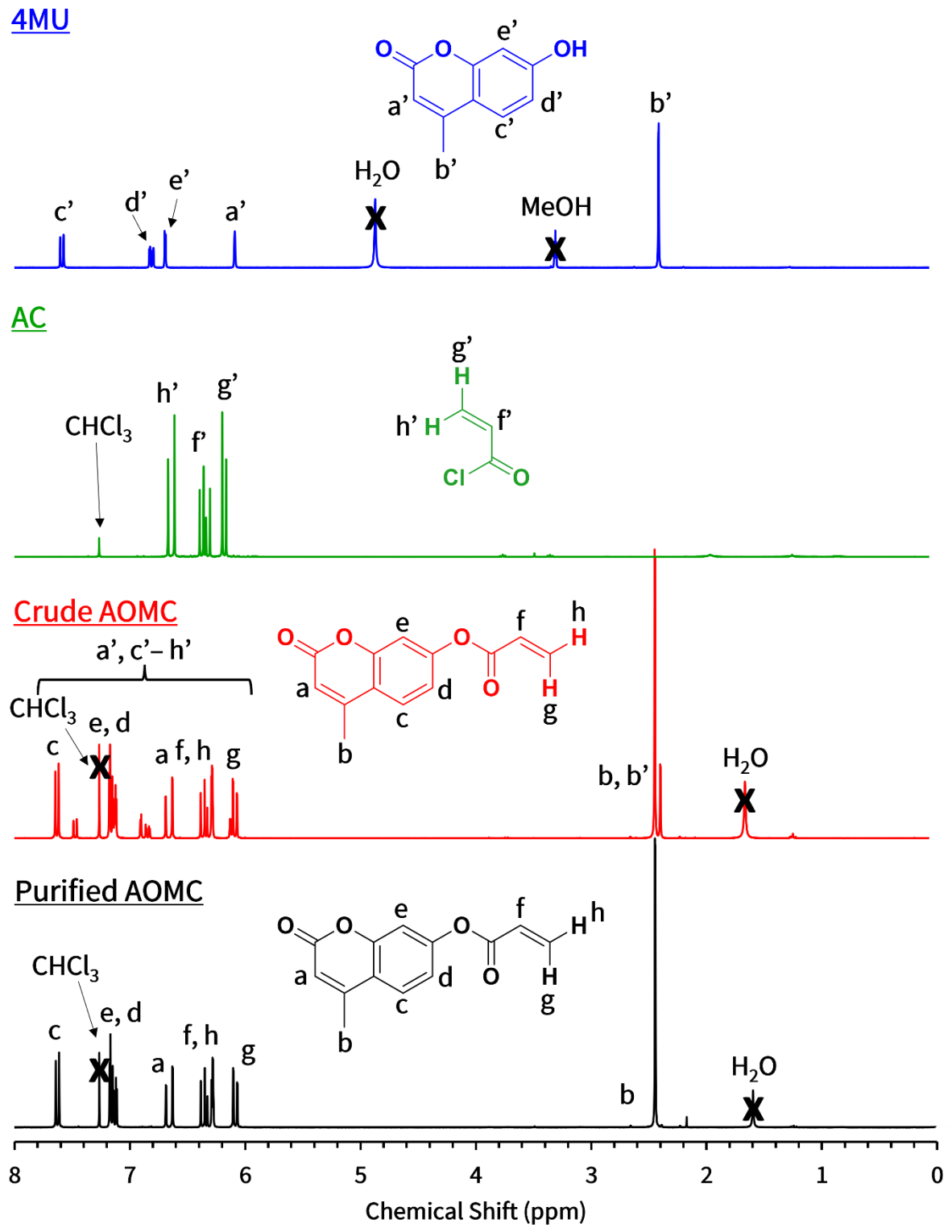

Figure 3.15. *Overlayed NMR spectra for the purified monomer, 7-acryloyloxy-4-methylcoumarin (AOMC) (black), against its crude form (red) and the starting reagents, acryloyl chloride (AC) (green) and 4-methylumbelliferone (4MU) (blue). NMR solvent – $CDCl_3$ (for AC, crude AOMC and purified AOMC) and MeOD-d4 (for 4MU).*

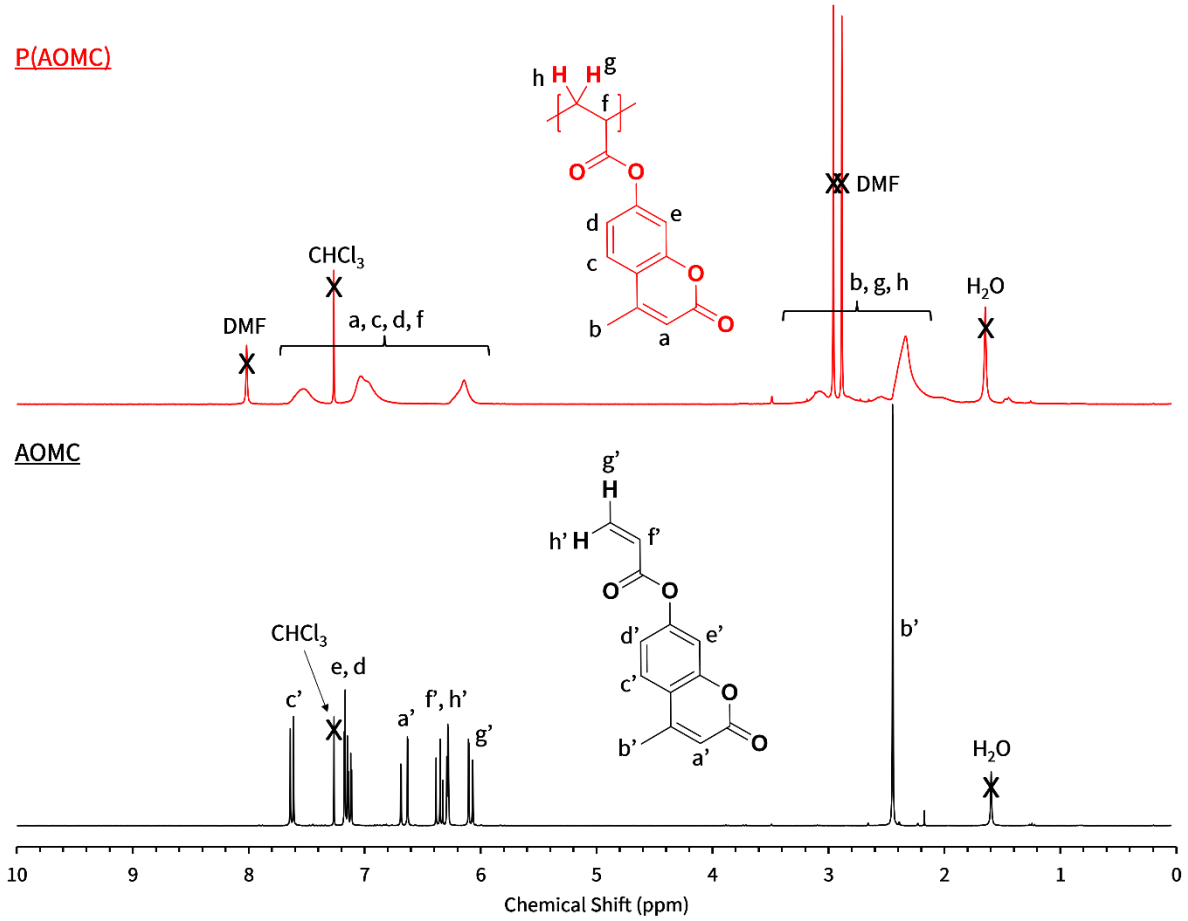

Figure 3.16. *Overlayed NMR spectra for the purified polymer, poly(7-acryloyloxy-4-methylcoumarin) (PAOMC) (black) and the synthesised monomer 7-acryloyloxy-4-methylcoumarin (AOMC). NMR solvent – $CDCl_3$.*

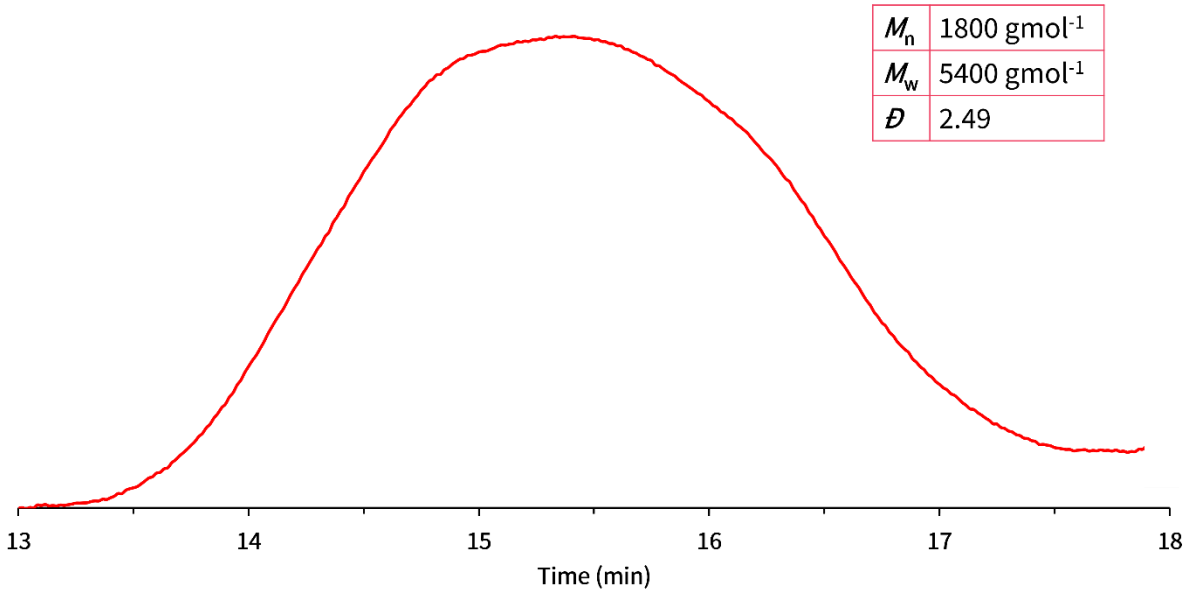

Figure 3.17. *DMF GPC chromatogram (vs. poly(methyl methacrylate) standards) obtained of poly(7-acryloyloxy-4-methylcoumarin) (PAOMC) synthesised via free radical polymerisation.*

The dispersity value obtained was large (2.49), however this was expected as an uncontrolled polymerisation technique was used. Free radical polymerisation is often used to create commercial polymers, such as poly(methyl methacrylate), however, there is limited control over the polymerisation process and due to this, there is often a broad molecular weight distribution from the different polymer chain lengths present in a given sample. There are more controlled polymerisation processes which could be used, such as reversible addition-fragmentation chain-transfer polymerisation (RAFT). The addition of a chain transfer agent (CTA) in RAFT allows for the control of the propagation process (as discussed in Section 1.3.2.1)[62], however for this purpose, the testing of the ability of the monomer to polymerise was the main concern, therefore free radical polymerisation was used before the potential progression to using other polymerisation techniques.

Since the free radical polymerisation of AOMC was successful, its ability to cross-link as a polymer was also tested (Scheme 11 and Figure 3.18).

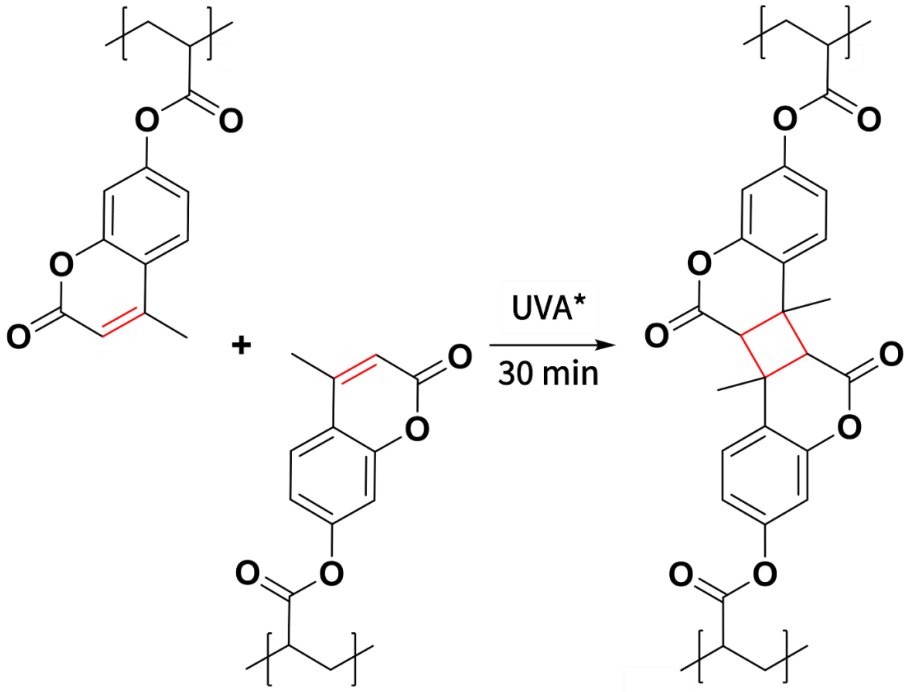

Scheme 11. *The dimerization scheme of poly(7-acryloyloxy-4-methylcoumarin) (PAOMC). *UVA lamp with a wavelength range between 315 and 400 nm.*

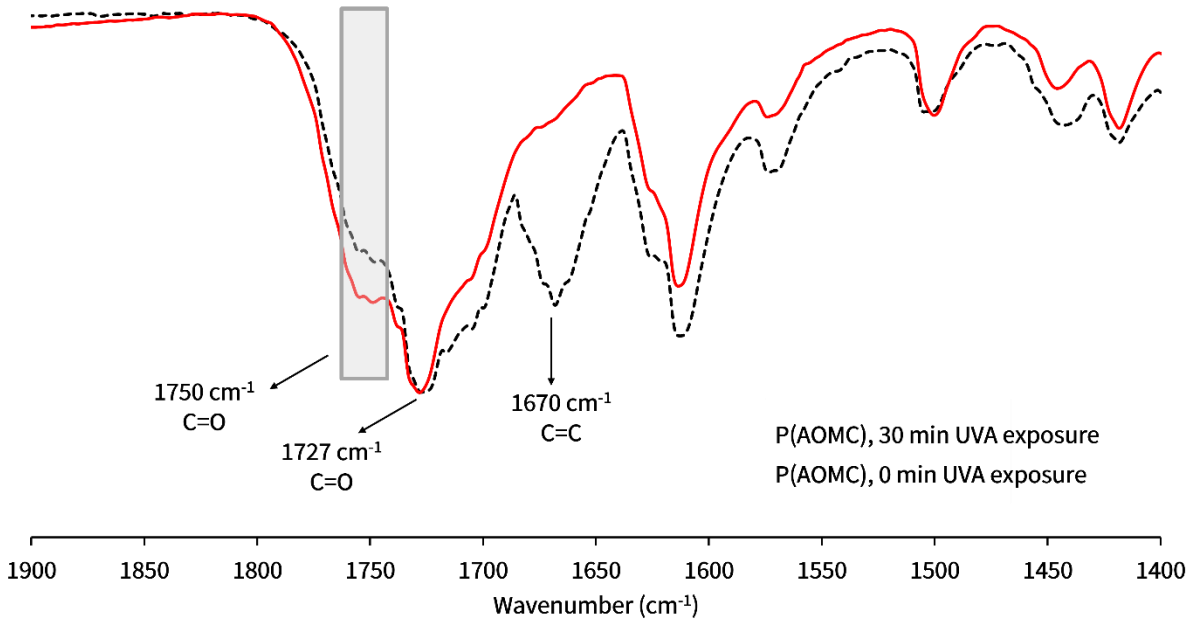

Figure 3.18. *Overlaid FTIR spectra of poly(7-acryloyloxy-4-methylcoumarin) (PAOMC) before (black dashed line) and after (red line) exposure to UV irradiation, where the C=O and C=C stretches have been labelled.*

It can be observed that there is a formation of a small peak highlighted at 1750 cm^{-1}, which could be representative of a carbonyl (C=O stretch) due to the deconjugation of the coumarin system. This potential carbonyl appearance and shift has also been observed for other synthesised coumarin derivatives[63]. The other noticeable change in the spectrum is the complete disappearance of the C=C stretch (1670 cm^{-1}), which strongly indicated that the [2+2] photocycloadditon reaction was successful and therefore the C=C double bonds had opened to form the cyclobutane ring. Additional evidence that cross-linking had successfully occurred was provided on observation that the irradiated PAOMC would not dissolve in the NMR solvent.

The synthesis of AOMC as a monomer showed promise to add cross-linkable functionality into a block copolymer. The procedure to synthesise AOMC was relatively simple, however the very low yield of 18% obtained for the purified product made the process inefficient. The literature indicates that high yields of purified AOMC (ranging between 75 and 89%)[37-39, 42] can be obtained, however upon attempts to reproducing these protocols (specifically from Patel *et al.*[37, 38]), yields herein were considerably lower. In addition to this, an unexpected large amount of solvent (up to 200 mL of methanol) was required for the recrystallization step, which would result in an unsustainable consumption of solvent if scaled up in the future. Despite this, the synthesised monomer did

successfully undergo homopolymerisation via FRP and still had the ability to cross-link, making it a potentially promising compound to be revisited in future work.

3.3.3 Esterification of 9-athracenecarboxylic acid

Unlike 4-MU, 9ACA possesses carboxylic acid functionality rather than alcohol functionality. This meant that esterification using acryloyl chloride or any other similar molecules was not possible. Instead, a poly(2-hydroxyethyl methacrylate) (PHEMA) macromolecular chain transfer agent (macro-CTA) was used, as this possesses alcohol functionality. PHEMA has already been shown to facilitate the synthesis of well-defined block copolymers in the literature. An example of this is from research conducted by Maitland *et al.*[64] who synthesised a series of poly(2-hydroxyethyl methacrylate)-*b*-poly(benzyl methacrylate) (PHEMA-b-PBzMA) block copolymer nanoparticles for potential gel electrolyte applications. Since PHEMA-containing block copolymers were successfully synthesised in Chapter 2, it was determined that demonstrating the ability to functionalise these hydroxyl-functional polymers with 9ACA via esterification would be useful. The synthesis of poly(9-anthrancenylethyl methacrylate) (P9AEMA) was conducted using DCC (*N*,*N*'-dicyclohexylcarbodiimide) and DMAP (4-dimethylaminopyridine) and a pre-synthesised PHEMA macro-CTA (Scheme 5).

The use of DCC and DMAP for the esterification reactions of carboxylic acids and alcohols is common. DCC can act as a coupling agent, which forms a reactive activated intermediate species with the carboxylic acid, which can then go forth and readily react with the alcohol to form an ester. This intermediate can result in a solid byproduct, dicyclohexylurea (DCU), which is easily removed via filtration. DMAP generates an acyl-pyridinium intermediate by reacting with the previous intermediate species (formed from DCC). From this, the alcohol-containing compound is able to more readily react and form the ester linkage between the carboxylic acid and alcohol. Relating to polymer chemistry, Liu *et al.*[65] modified poly(vinyl alcohol) (PVA) with malonic acid (MA) using these specific reagents. The PVA-MA hydrogels were successfully synthesised after a stirring period at ambient temperature for 5 days, from which the hydrogels displayed toughened and good healing characteristics. It should be noted that Scheme 5 displays the product as PHEMA-*r*-P9AEMA, this is due to the fact that the location by which the 9ACA adds onto the PHEMA polymer is unknown, therefore the resulting in a random copolymer. For this synthesis, due to the overlapping of peaks in the ^{1}H NMR spectrum, the conversion was unable to be calculated (Figure 3.19). It can be observed that the final 'purified polymer' still contained impurities, such as DCC and DMAP, even after

precipitation. An example from the literature that conducted a similar synthesis reported the use of cold diethyl ether to purify the resulting polymer, therefore this was chosen as the precipitating solvent[50]. However, the appearance of sharp peaks from the starting 9ACA, present between 9.0 and 7.5 ppm, indicate that the precipitation process in diethyl ether did not remove the excess starting reagent either. Other methods of purification, such as column chromatography, were explored as an attempt to purify the polymer, however the product remained stuck in the column. Due to the purification problems encountered at this time, the use of 9ACA to provide cross-linkablility into a block copolymer was regarded unsuitable.

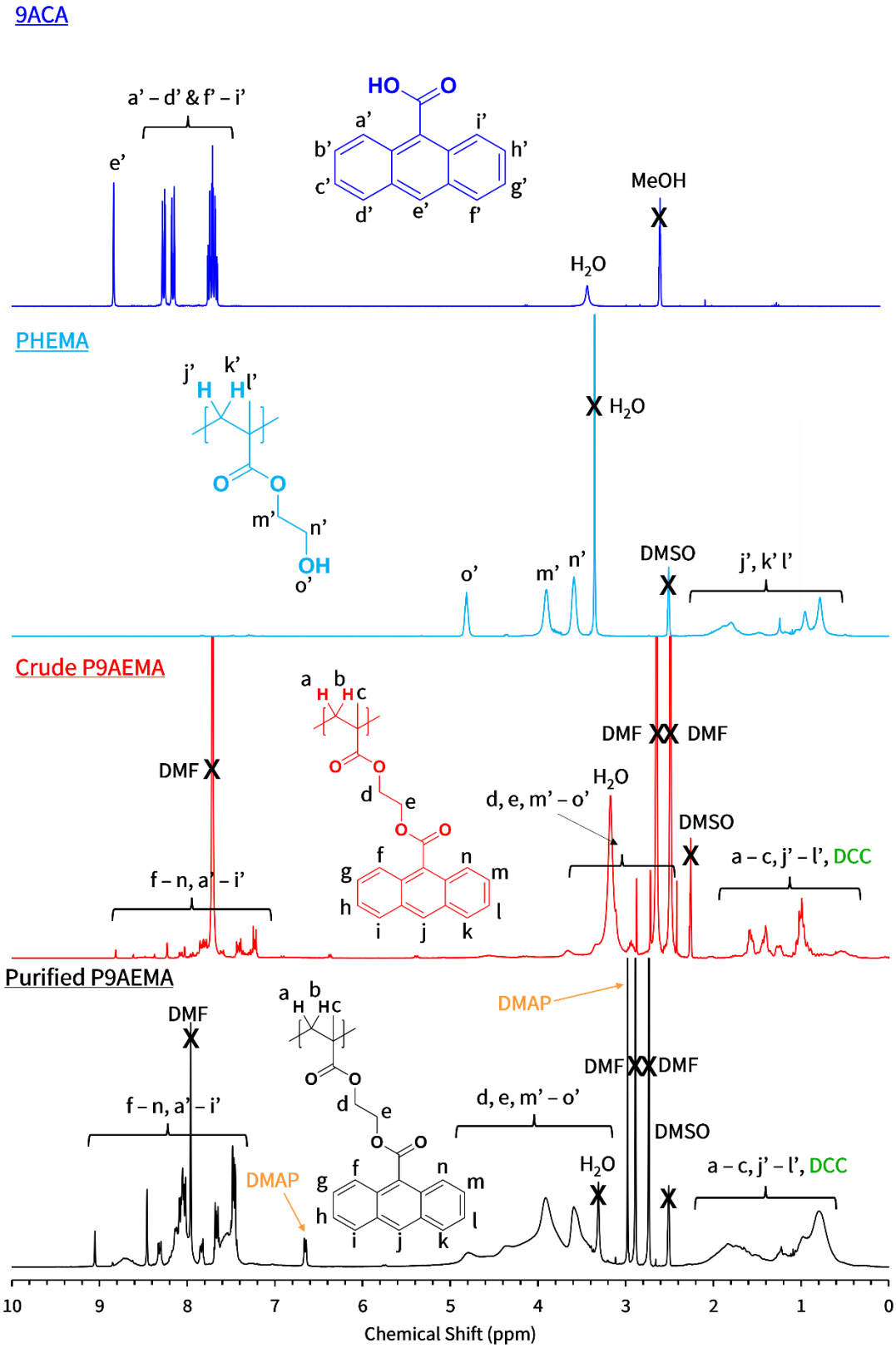

Figure 3.19. *^{1}H NMR spectra for the purified product, poly(9-anthrancenylethyl methacrylate) (P9AEMA) (black), crude product (red), poly(2-hydroxyethyl methacrylate) (PHEMA) (light blue) and 9-athracenecarboxylic acid (9ACA) (dark blue). NMR solvent – MeOD-d4 (for 9ACA) and DMSO-d6 (for PHEMA, crude P9AEMA and purified P9AEMA).*

3.3.4 Esterification and cross-linking of 3-(2-furyl)acrylic acid

Similarly to 9ACA, FAA possesses carboxylic acid functionality, therefore the same esterification reaction with PHEMA was conducted. The synthesis of poly(ethylfurfurylideneacetate methacrylate) (PEFMA) was conducted using DCC and DMAP and the same pre-synthesised PHEMA macro-CTA (Scheme 6).

The synthesis of pure PEFMA was more successful than that of P9AEMA; the purification via precipitation in diethyl ether seemed to remove the starting reagents and clear PEFMA polymer peaks were visible, suggesting a higher conversion (Figure 3.20). The actual conversion again was unable to be calculated due to the overlapping of PHEMA and PEFMA peaks. As mentioned previously and shown in Scheme 6, the resultant product can be more accurately described as PHEMA-*r*-PEFMA due to the location of the added FAA groups on PHEMA being random.

The confirmation of the successful esterification reaction arises from the peaks denoted as d and e, which are clearly shown to give a different peak compared to peak k' and j' in the PHEMA spectrum (Figure 3.20). These two new CH_2 groups represent the successful joining of the two molecules. Once precipitated, the product had a dark brown viscous appearance, which was dried using rotary evaporation and a vacuum oven to yield a dark brown solid.

Since a solid purified product was obtained, the cross-likability of the newly synthesised polymer could be tested by irradiating with UV light. This was completed to test that the [2+2] photocycloaddition reaction could still occur, post polymerisation and purification (Scheme 12 and Figure 3.21).

The transition from alcohol to ester can be observed from the strong decrease in O-H stretching, clearly visible at 3377 cm^{-1}, hence acting as further evidence that the esterification had successfully occurred. The decrease of C=C stretching at 1670 cm^{-1} is clearly observed, which is indicative that the formation of the cyclobutane ring occurred upon irradiation. The success of this reaction highlights the potential for FAA to be used as a monomer and add cross-linkability into block copolymers to enhance their functionality.

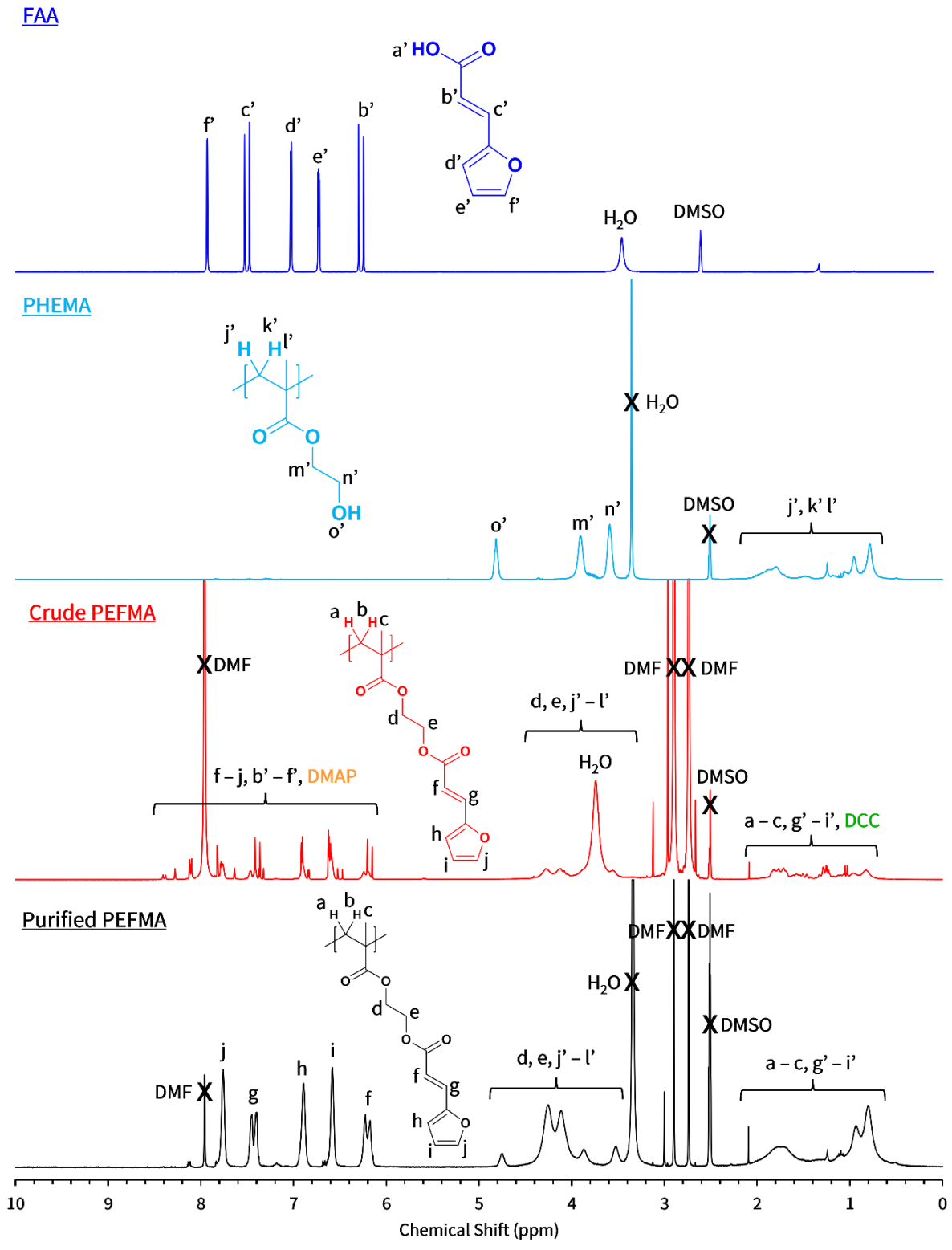

Figure 3.20. *^{1}H NMR spectra for the purified product, poly(ethylfurfurylideneacetate methacrylate) (PEFMA) (black), crude product (red), poly(2-hydroxyethyl methacrylate) (PHEMA) (light blue) and 3-(2-furyl)acrylic acid (FAA) (dark blue). NMR solvent – DMSO-d6 (for all spectra).*

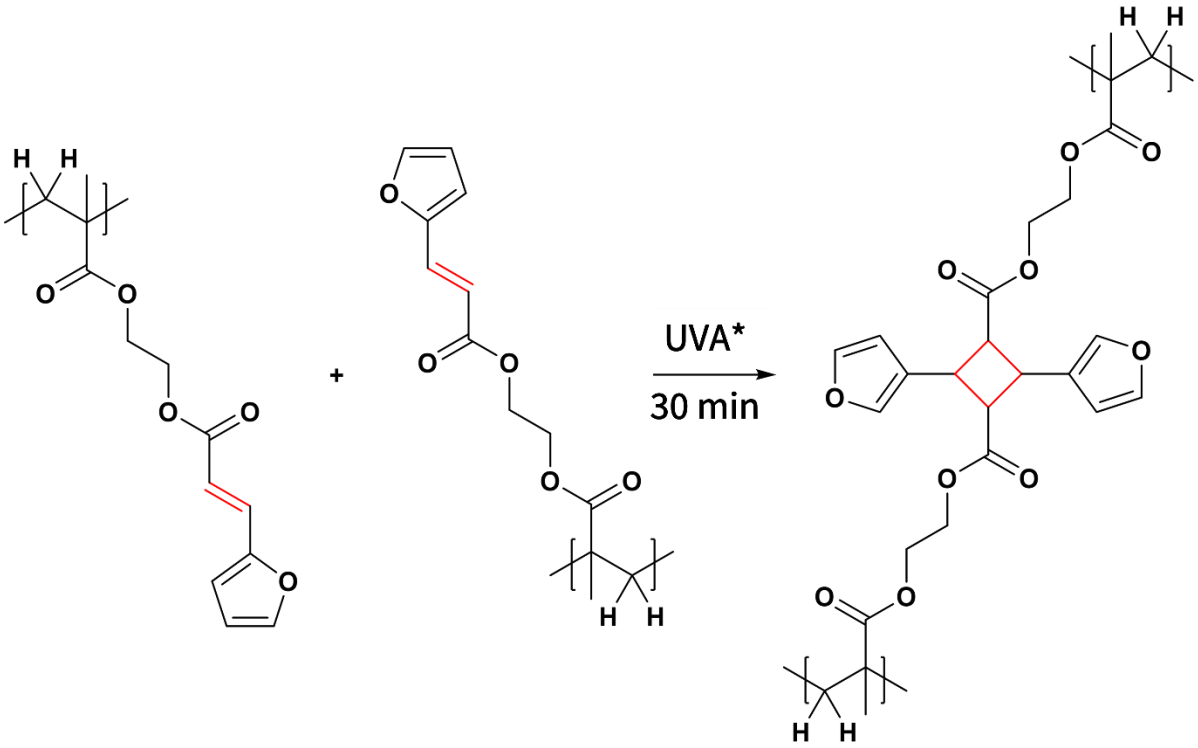

Scheme 12. *The dimerization scheme of poly(ethylfurfurylideneacetate methacrylate) (PEFMA). *UVA lamp with a wavelength range between 315 and 400 nm.*

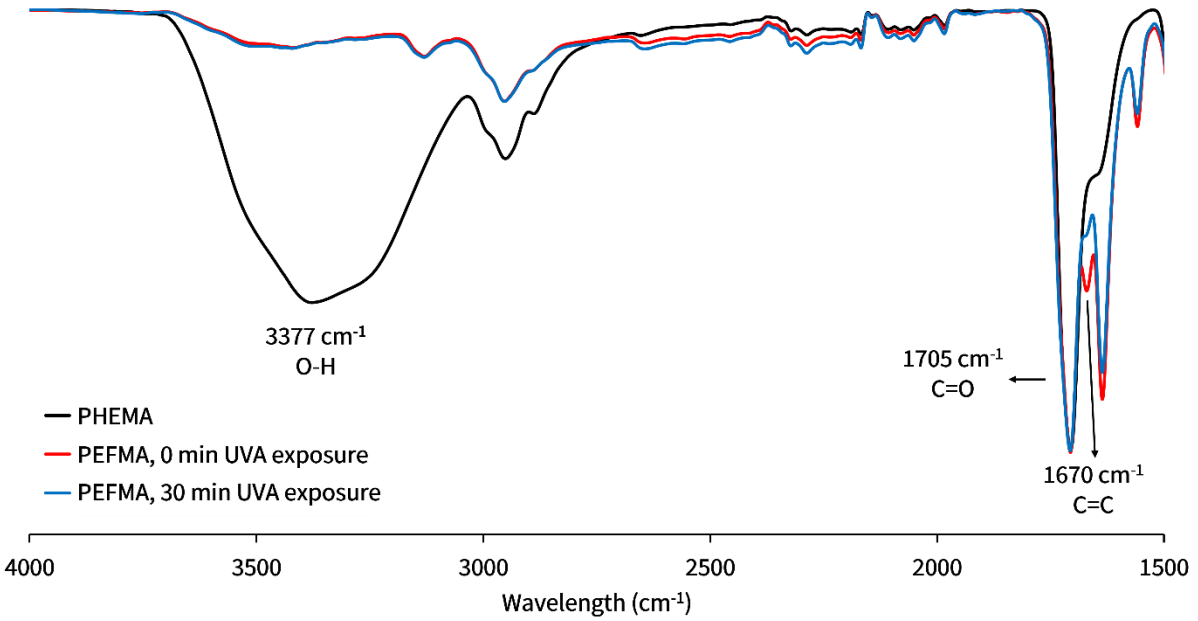

Figure 3.21. *Overlaid FTIR spectra of poly(ethylfurfurylideneacetate methacrylate) before (red line) and after (blue line) exposure to UV irradiation, and poly(2-hydroxyethyl methacrylate) for comparison (black line) , where the O-H, C=O and C=C stretches have been labelled.*

3.4 Conclusions

The dimerization of four monomer precursors, 4MU, CA, 9ACA and FAA, was assessed using irradiation from specific wavelengths of UV light (using UV lamps with emission wavelengths in the range of 315-400 and 280-400 nm) previously reported as suitable in the literature. FTIR and ^{1}H NMR spectroscopies showed that CA was the only one of these compounds that failed to dimerize under these conditions and was thus deemed unsatisfactory. 4MU and FAA successfully dimerized via a [2+2] photocylcloadditon reaction, and 9ACA via a [4+4] photocycloaddition, as proven by shifts in the C=O stretching band in the FTIR spectra due to deconjugation upon formation of the cyclobutane ring and the formation of new peaks (specifically for 9ACA and FAA).

4-MU has alcohol functionality, therefore an esterification reaction was conducted (using AC) to create a monomer with double-bond functionality (C=C) in an attempt to test its ability to undergo polymerisation. This synthesis was successful, producing AOMC as determined from ^{1}H NMR spectroscopy. AOMC was then polymerised using free radical polymerisation to yield PAOMC, which appeared as a white solid. The broadening of the peaks and decrease in monomer peaks in the ^{1}H NMR spectra were indicative that polymerisation has occurred. The final step involved irradiating the sample using the same lamp used to irradiate the molecule before modification, which displayed a distinct reduction in C=C stretching in the FTIR spectrum after irradiation, implying that the polymer had cross-linked. A failed attempt to dissolve the PAOMC in an NMR solvent provided further evidence of crosslinking. Although the monomer synthesis, polymerisation and cross-linking of the molecule was successful, the yield of the purified product (AOMC) was considerably low (18%) and used an excess of solvent in the purification steps.

9ACA and FAA both possess carboxylic acid functionality, therefore the esterification with pre-synthesised PHEMA was conducted for both molecules. The crude ^{1}H NMR spectra for both P9AEMA and PEFMA displayed a broadening of peaks, implying that the reactions had successfully occurred. However, purification of P9AEMA was unsuccessful and as a result, the final product was unable to be obtained for further testing. On the other hand, PEFMA displayed a much cleaner ^{1}H NMR spectrum after purification. The solid was obtained and used for further testing, specifically its cross-linkability. It was found that when exposed to UVA, PEFMA did have the ability to undergo a [2+2] photocylcloadditon reaction. This was proven from the reduction in the C=C stretching band after irradiation in the FTIR spectrum and its insolubility in NMR solvent.

To conclude, it was determined that although 4MU and 9ACA show promise, future work is required to improve the yield and purification process, respectively. Therefore, the use of FAA as a monomer precursor was chosen to be the most suitable from the four starting molecules.

3.5 References

1. A. Kausar, *Journal of Macromolecular Science, Part A*, 2018, **55**, 440-448.
2. R. Y. Lochhead, in *Cosmetic Nanotechnology*, American Chemical Society, 2007, vol. 961, ch. 1, pp. 3-56.
3. M. F. Maitz, *Biosurface and Biotribology*, 2015, **1**, 161-176.
4. C. Silvestre, D. Duraccio and S. Cimmino, *Progress in Polymer Science*, 2011, **36**, 1766-1782.
5. Y. Chen, A. K. Awasthi, F. Wei, Q. Tan and J. Li, *Science of The Total Environment*, 2021, **752**, 141772.
6. S. Gerassimidou, P. Lanska, J. N. Hahladakis, E. Lovat, S. Vanzetto, B. Geueke, K. J. Groh, J. Muncke, M. Maffini, O. V. Martin and E. Iacovidou, *Journal of Hazardous Materials*, 2022, **430**, 128410.
7. D. P. Jones, D. C. Leach and D. R. Moore, *Polymer*, 1985, **26**, 1385-1393.
8. E. Dhanumalayan and G. M. Joshi, *Advanced Composites and Hybrid Materials*, 2018, **1**, 247-268.
9. A. X. Chen, J. D. Hilgar, A. A. Samoylov, S. S. Pazhankave, J. A. Bunch, K. Choudhary, G. L. Esparza, A. Lim, X. Luo and H. Chen, *Advanced Materials Interfaces*, 2023, **10**, 2202053.
10. L. E. Nielsen, *Journal of Macromolecular Science, Part C*, 1969, **3**, 69-103.
11. Z. Xie, C. Wang, K. E. deKrafft and W. Lin, *Journal of the American Chemical Society*, 2011, **133**, 2056-2059.
12. J. W. Rumer and I. McCulloch, *Materials Today*, 2015, **18**, 425-435.
13. K. Mayumi, C. Liu, Y. Yasuda and K. Ito, *Gels*, 2021, **7**, 91.
14. G. E. Parkes, H. J. Hutchins-Crawford, C. Bourdin, S. Reynolds, L. J. Leslie, M. J. Derry, J. L. Harries and P. D. Topham, *Polymer Chemistry*, 2020, **11**, 2869-2882.
15. M. Shirai, *Polymer journal*, 2014, **46**, 859-865.
16. L. Fertier, H. Koleilat, M. Stemmelen, O. Giani, C. Joly-Duhamel, V. Lapinte and J.-J. Robin, *Progress in Polymer Science*, 2013, **38**, 932-962.
17. K. Mizoguchi and E. Hasegawa, *Polymers for Advanced Technologies*, 1996, **7**, 471-477.
18. N. Tsutsumi, *Polymer International*, 2017, **66**, 167-174.
19. A. H. Gelebart, D. Jan Mulder, M. Varga, A. Konya, G. Vantomme, E. Meijer, R. L. Selinger and D. J. Broer, *Nature*, 2017, **546**, 632-636.
20. S. Xu, J. Yeow and C. Boyer, *ACS Macro Letters*, 2018, **7**, 1376-1382.
21. S. Poplata, A. Tröster, Y.-Q. Zou and T. Bach, *Chemical Reviews*, 2016, **116**, 9748-9815.
22. T. Hughes, G. P. Simon and K. Saito, *Materials Horizons*, 2019, **6**, 1762-1773.
23. H. Frisch, D. E. Marschner, A. S. Goldmann and C. Barner-Kowollik, *Angewandte Chemie International Edition*, 2018, **57**, 2036-2045.
24. S. Banerjee, R. Tripathy, D. Cozzens, T. Nagy, S. Keki, M. Zsuga and R. Faust, *ACS Applied Materials & Interfaces*, 2015, **7**, 2064-2072.
25. R. Jellali, V. Bertrand, M. Alexandre, N. Rosière, M. Grauwels, M. C. De Pauw-Gillet and C. Jérôme, *Macromolecular bioscience*, 2017, **17**, 1600495.
26. H. Wang, W. Miao, F. Wang and Y. Cheng, *Biomacromolecules*, 2018, **19**, 2194-2201.

27. X. Li, J. Cui, W. Zhang, J. Huang, W. Li, C. Lin, Y. Jiang, Y. Zhang and G. Li, *Journal of Materials Chemistry*, 2011, **21**, 17953-17959.
28. K. M. Schelkle, M. Bender, S. Beck, K. F. Jeltsch, S. Stolz, J. Zimmermann, R. T. Weitz, A. Pucci, K. Müllen, M. Hamburger and U. H. F. Bunz, *Macromolecules*, 2016, **49**, 1518-1522.
29. Z. Wang, K. Randazzo, X. Hou, J. Simpson, J. Struppe, A. Ugrinov, B. Kastern, E. Wysocki and Q. R. Chu, *Macromolecules*, 2015, **48**, 2894-2900.
30. P. Froimowicz, H. Frey and K. Landfester, *Macromolecular rapid communications*, 2011, **32**, 468-473.
31. J. Manhart, S. Ayalur-Karunakaran, S. Radl, A. Oesterreicher, A. Moser, C. Ganser, C. Teichert, G. Pinter, W. Kern, T. Griesser and S. Schlögl, *Polymer*, 2016, **102**, 10-20.
32. H. Xie, M.-j. He, X.-Y. Deng, L. Du, C.-J. Fan, K.-K. Yang and Y.-Z. Wang, *ACS Applied Materials & Interfaces*, 2016, **8**, 9431-9439.
33. N. Nagy, H. F. Kuipers, A. R. Frymoyer, H. D. Ishak, J. B. Bollyky, T. N. Wight and P. L. Bollyky, *Frontiers in Immunology*, 2015, **6**.
34. I. Kakizaki, K. Kojima, K. Takagaki, M. Endo, R. Kannagi, M. Ito, Y. Maruo, H. Sato, T. Yasuda and S. Mita, *Journal of Biological Chemistry*, 2004, **279**, 33281-33289.
35. Y. Wang, Q. Liu, J. Li, L. Ling, G. Zhang, R. Sun and C.-P. Wong, *Polymer*, 2019, **172**, 187-195.
36. Y. Chen and C. S. Jean, *Journal of applied polymer science*, 1997, **64**, 1759-1768.
37. H. J. Patel, M. G. Patel, R. J. Patel, K. Patel and R. M. Patel, 2008.
38. H. Patel, M. Patel, A. Patel, K. Patel and R. Patel, *eXPRESS Polymer Letters*, 2008, **2**, 727-734.
39. Y. Chen and J.-L. Geh, *Polymer*, 1996, **37**, 4481-4486.
40. P. Vimala, *International Journal of Research and Analytical*, 1.
41. S. Venkatesan, B. Ranjithkumar, S. Rajeshkumar and K. Anver Basha, *Chinese Journal of Polymer Science*, 2014, **32**, 1373-1380.
42. R. Chitra, E. Kayalvizhy, P. Jeyanthi and P. Pazhanisamy, *Chemical Science*, 2014, **3**, 722-730.
43. R. J. M. Lubbers and R. P. de Vries, in *Encyclopedia of Mycology*, eds. Ó. Zaragoza and A. Casadevall, Elsevier, Oxford, 2021, pp. 477-488.
44. M. Sova, *Mini reviews in medicinal chemistry*, 2012, **12**, 749-767.
45. P. De, M. Baltas and F. Bedos-Belval, *Current medicinal chemistry*, 2011, **18**, 1672-1703.
46. N. Ruwizhi and B. A. Aderibigbe, *International Journal of Molecular Sciences*, 2020, **21**, 5712.
47. H. I. Bernstein and W. C. Quimby, *Journal of the American Chemical Society*, 1943, **65**, 1845-1846.
48. D. Shi, M. Matsusaki and M. Akashi, *Bioconjugate Chemistry*, 2009, **20**, 1917-1923.
49. D. Shi, M. Matsusaki and M. Akashi, *Journal of Controlled Release*, 2011, **149**, 182-189.
50. M. H. Nasirtabrizi, L. Zargin, S. Khodabandlou and S. R. Mansour, *Journal of Chemistry*, 2012, **9**, 1135-1144.
51. Z. Wang, B. Kastern, K. Randazzo, A. Ugrinov, J. Butz, D. W. Seals, M. P. Sibi and Q. R. Chu, *Green Chemistry*, 2015, **17**, 4720-4724.
52. P. S. Prabhakar and S. Dutta, *Biomass Conversion and Biorefinery*, 2023, DOI: 10.1007/s13399-023-05029-4.
53. Z. D. Wang, Q. Elliott, Z. Wang, R. A. Setien, J. Puttkammer, A. Ugrinov, J. Lee, D. C. Webster and Q. R. Chu, *ACS Sustainable Chemistry & Engineering*, 2018, **6**, 8136-8141.
54. I. Cazin, E. Rossegger, G. Guedes de la Cruz, T. Griesser and S. Schlögl, *Polymers*, 2021, **13**, 56.
55. A. Stamm, K. Schwing and M. Gerhards, *The Journal of Chemical Physics*, 2014, **141**.
56. S. D. M. Allen, M. J. Almond, J.-L. Bruneel, A. Gilbert, P. Hollins and J. Mascetti, *Spectrochimica Acta Part A: Molecular and Biomolecular Spectroscopy*, 2000, **56**, 2423-2430.

57. T. B. Nguyen and A. Al-Mourabit, *Photochemical & Photobiological Sciences*, 2016, **15**, 1115-1119.
58. I. Fonseca, S. E. Hayes, B. Blümich and M. Bertmer, *Physical Chemistry Chemical Physics*, 2008, **10**, 5898-5907.
59. D. Han, H. Lu, W. Li, Y. Li and S. Feng, *RSC advances*, 2017, **7**, 56489-56495.
60. T. Salzillo, E. Venuti, C. Femoni, R. G. Della Valle, R. Tarroni and A. Brillante, *Crystal Growth & Design*, 2017, **17**, 3361-3370.
61. L. Pezzana, G. Melilli, N. Guigo, N. Sbirrazzuoli and M. Sangermano, *Reactive and Functional Polymers*, 2023, **185**, 105540.
62. S. Perrier, *Macromolecules*, 2017, **50**, 7433-7447.
63. J. Ling, M. Z. Rong and M. Q. Zhang, *Journal of Materials Chemistry*, 2011, **21**, 18373-18380.
64. G. L. Maitland, M. Liu, T. J. Neal, J. Hammerton, Y. Han, S. D. Worrall, P. D. Topham and M. J. Derry, *Chemical Science*, 2024, **15**, 4416-4426.
65. T. Liu, X. Peng, Y. Chen, J. Zhang, C. Jiao and H. Wang, *Polymer Chemistry*, 2020, **11**, 4787-4797.

4. Conclusions and future work

The synthesis of poly(2-hydroxyethyl methacrylate)-*block*-poly(*n*-butyl methacrylate), PHEMA-*b*-PBuMA, diblock copolymers in a range of solvents and the addition of UV cross-linkable compounds has been explored in this thesis. 2-hydroxyethyl methacrylate (HEMA) and *n*-butyl methacrylate (BuMA) were selected as starting monomers as they are readily available commercially and provide hydrophilic and hydrophobic properties, respectively. Amphiphilicity is often desired for block copolymers as it enables them to be used in a wide range of applications. Specific aims of the thesis included the evaluation of the suitability of polymerisation-induced self-assembly (PISA) via reversible addition-fragmentation (RAFT) emulsion polymerisation in an ionic liquid (IL) for the synthesis of these block copolymers in comparison to traditional solvent systems, as well as identifying suitable UV cross-linker candidates for polymer functionalisation purposes. The summary of the researched systems and their success will be discussed in this section, alongside a scope of potential future work.

Firstly, the synthesis of the amphiphilic PHEMA-*b*-PBuMA diblock copolymer via the extension of a hydrophilic PHEMA macromolecular chain transfer agent (macro-CTA) with a hydrophobic BuMA monomer was conducted under RAFT conditions in various solvents. More specifically, two PHEMA macro-CTAs (with degree of polymerisation, DP, of 21 and 77) were chain extended using BuMA in 1-ethyl-3-methyl imidazolium ethyl sulfate ([EMIM][$EtOSO_3$]), *N*,*N*-dimethylformamide (DMF) and an ethanol/water (4:1 w:w) solvent mixture at 10% w/w solids concentration. All solvents successfully yielded block copolymers, with [EMIM][$EtOSO_3$] found to be the most efficient; high conversions (≥ 88%) were obtained within 2 hours when PBuMA DPs ≤ 300 were targeted, whereas the other solvent systems obtained between 54% and 87% within 25 hours. In addition to this, the molar mass dispersity values obtained when targeting a PBuMA DP of 100 when extending the $PHEMA_{21}$ macro-CTA were 1.26, 1.59 and 1.51 when using [EMIM][$EtOSO_3$], DMF and EtOH/H_2O solvent systems, respectively, indicating that the IL system provided more control than the other two traditional solvent systems. This demonstrates that IL can be successfully used to replace traditional organic solvent systems and provide enhanced monomer conversions at shorter polymerisation times. From this, the effect of other ILs on this polymerisation system could be explored and compared to [EMIM][$EtOSO_3$], which was the focus of this work, to investigate other ILs as alternative solvents. Also, as mentioned previously, sustainability is an important factor to consider and thus other green solvents could also be explored as a potential solvent system for the synthesis of this block copolymer.

Using [EMIM][$EtOSO_3$] as the reaction solvent for the preparation of PHEMA-*b*-PBuMA diblock copolymers via RAFT emulsion polymerisation yielded highly transparent (≥ 95% transmittance at

700 nm) nanoparticle dispersions as a result of the matched refractive index values of PBuMA and [EMIM][$EtOSO_3$]. To the best of our knowledge, the utilisation of ILs as the solvent for RAFT-mediated emulsion PISA has not been explored, with previous efforts being focused on RAFT-mediated dispersion PISA systems. Furthermore, this developed system in [EMIM][$EtOSO_3$] also demonstrated that transparent solutions can be obtained, which is not as typical for PISA syntheses. The obtained nanoparticles were analysed using dynamic light scattering (DLS), small-angle X-ray scattering (SAXS) and transmission electron microscopy (TEM), all of which confirmed the presence of spherical morphologies. The use of DLS was considered unreliable for these highly transparent dispersions as this analytical technique operates on the basis of light scattering. SAXS analysis confirmed the production of spheres of increasing core radius with increasing PBuMA DP up to a target PBuMA DP of 500, after which the trend was no longer observed, and the data was more difficult to fit to a spherical micelle model. TEM images also provided good evidence that nanoparticles had been formed, however, due to difficulty arising with sample preparation with IL, only a few of images were obtained with sufficient clarity. Since only spherical micelles were formed, there is a potential to explore the generation of other morphologies, such as worms and vesicles, using this IL solvent system. The synthesis of these morphologies would also affect the properties of the resulting dispersions, which could make them suitable for use in other applications. An example of this could be the possible synthesis of transparent gels resulting from obtaining worm morphologies. To obtain higher order morphologies, the volume fractions of the blocks would need to be considered, specifically the stabilising and core-forming blocks - literature has shown that the use of shorter stabiliser blocks is favourable for generating worms and vesicles. Block copolymers alone have been shown to have many uses in the literature, however the addition of different chemical functionalities can enhance their properties and make them useful for more specific applications, such as polymeric additives in inkjet printing. The addition of photo-triggerable groups was further researched for this purpose. Four compounds, 4-methylumbelliferone (4MU), cinnamic acid (CA), 9-anthracenecarboxylic acid (9ACA) and 3-(2-furyl)acrylic acid (FAA) were tested for their use as monomer precursors on the basis of their ability to dimerise/crosslink under UV light conditions. The choice of photo-triggerable groups rather than thermally-triggerable groups was made as an attempt to be more sustainable, due to the fact that thermally triggered groups have been shown to require high temperatures (>100 °C), whereas photo-triggerable compounds can be cross-linked at ambient temperature. 4MU, 9ACA and FAA all successfully dimerised when exposed to UVA wavelengths (315–400 nm), as determined form ^{1}H NMR and FTIR spectroscopy, however CA did not dimerize when exposed to wavelengths between 280 and 400 nm, despite the literature

suggesting that this is an appropriate wavelength range to promote dimerization. From this, the continuation of CA in this research was disregarded, however, future work could involve an experimental plan utilising different lamps with wavelengths in the range of UVA, UVB and UVC whilst systematically changing the distance of the sample and the duration of exposure, to see which conditions would enable the photo-triggerable dimerization of CA. Moving forwards with 4MU, 9ACA and FAA involved categorising these compounds based on their functionality. Since 4MU has alcohol functionality it was functionalised using acryloyl chloride, however 9ACA and FAA have carboxylic acid functionality and thus they were directly added onto a pre-synthesised PHEMA macro-CTA. 4MU was successfully transformed into a monomer, 7-acryloyloxy-4-methylcoumarin (AOMC), with C=C double bond functionality, meaning that it could undergo further polymerisation reactions. The newly formed AOMC was subsequently homopolymerised using free radical polymerisation, which successfully yielded polymer. From this, a small amount of purified sample was exposed to UVA, whereby it successfully cross-linked as determined from FTIR spectroscopy and from the inability for the cross-linked sample to dissolve in the same NMR solvent in which the non-cross-linked sample was soluble. Despite this success, the yield of the AOMC monomer synthesis was calculated to be around 18%, which is considerably low therefore this process was deemed to be inefficient for further use in this research. Future work around this could involve the optimisation of the synthesis of AOMC, resulting in better conversions and higher yields. This could be achieved by exploring alternative synthesis routes, different solvent systems or the possible introduction of a catalyst into the system. The chemicals used in this process, such as acryloyl chloride, are also not considered to be sustainable due to their unsafe nature (hazardous/toxic to health and the environment), therefore future work could also involve the use of 'greener' chemicals which have less of a negative impact upon the environment, as well as exploring other purification techniques which are not as wasteful in terms of solvent use. The remaining compounds, 9ACA and FAA, both underwent esterification reactions with PHEMA using dicyclohexylcarbodiimide (DCC) and 4-dimethylaminopyridine (DMAP). Both were shown to successfully esterify and add onto the PHEMA, forming P9AEMA and PEFMA, respectively, and showing promise for the addition of photo-triggerable groups into a pre-synthesised polymer. However, P9AEMA was unable to be purified, therefore further research on this system would be necessary. This could require the use of solvent screenings using mixtures of solvents, as well as exploring other purification techniques aside from precipitation and column chromatography, such as dialysis or even multi-step purification processes. On the other hand, PEFMA was successfully purified using precipitation in diethyl ether, producing a brown solid. Similarly to PAOMC, a small amount of purified PEFMA was exposed to UVA,

whereby it successfully cross-linked as determined from FTIR spectroscopy and confirmed from the inability for the cross-linked sample to dissolve in the same NMR solvent in which the non-cross-linked sample was soluble. From the experiments conducted, it was determined that FAA was the most successful as a monomer precursor as it successfully added onto a pre-synthesised polymer, from which it could be purified and cross-linked using exposure to UVA light for 30 minutes.

Despite PHEMA-*b*-PBuMA diblock copolymers being synthesised, only PHEMA was used as part of the experimental esterification with cross-linkable compounds due to difficulty in determining whether the reaction had proceeded successfully. This was because the peaks that would arise from the added cross-linkable compounds, specifically 9ACA and FAA, would overlap with the PHEMA, PBuMA and IL peaks. This means that extensive research would be required to merge both systems and result in a purified polymer. The precipitation of the PHEMA-*b*-PBuMA was tested in several solvents, including in diethyl ether and hexane, amongst others, with little success, and subsequently the synthesised block copolymers remained unpurified in solution. As mentioned previously, there are other purification techniques which could be used to obtain purified block copolymer. If successful, this would also provide the opportunity for the IL to be recycled, hence building upon the sustainability credentials of this process route. The esterification of 9ACA and FAA would therefore also require new purification systems as the PBuMA adds another component into the system, which would affect the ability of the resulting block copolymer to precipitate in diethyl ether (as previously used to precipitate PEFMA). On another note, the esterification reactions were conducted in DMF, which as a traditional organic solvent is not considered to be ‘green’, therefore future work could also involve the use of more sustainable solvent systems, such as other ionic liquids or Cyrene™.

The sustainability of the polymerisation reactions to synthesise block copolymers could also be improved. RAFT-agents are not considered to be sustainable as their synthesis involves the use of potentially harmful chemicals, such as thiols, and are very expensive to produce and thus purchase. In addition to this, a typical RAFT synthesis is conducted at high temperatures, such as 70 °C, which is due to the specific initiator utilised, namely azobisisobutyronitrile (AIBN), having a high degradation temperature required to generate radicals and thus induce polymerisation. If the temperature were to be decreased, the polymerisation would not occur due to the inability for radicals to form, thereby initiating the polymerisation process. An alternative to this could be the use of photo-active initiators, which would use readily accessible light and not require the use of such high temperatures. Literature has shown the use of specific wavelengths of light for each step

of the synthesis, an example of this is the use of red light to induce the polymerisation (620 to 750 nm) and UV light (10 to 400 nm) to induce cross-linking.

In conclusion, this work contributes to exploration of the relatively untapped potential of ionic liquids as solvents for RAFT PISA syntheses and introduces the possibility of utilising emulsion polymerisation as a novel route to optically transparent dispersions of block copolymer nanoparticles in ionic liquid. This is the first report of such a PISA formulation in ionic liquids. Though further work is required, there is clearly great promise in the use of ILs in polymerisation formulations as more efficient, greener solvents. By also identifying suitable UV cross-linker candidates with sustainable origins, this work shows there is promise for the synthesis of block copolymers containing cross-linkable compounds, for use in applications such as inkjet printing, using more sustainable conditions and reagents than currently utilised in the literature.